UNIVERSIDADE D
COIMBRA

Miguel José Simões Pereira

CONCEPTION AND DESIGN OF HIGH-PERFORMANCE STEEL-CONCRETE COMPOSITE SLABS

Tese no âmbito do Doutoramento em Construção Metálica e Mista orientada pelo Professor Doutor Rui António Duarte Simões e apresentada ao Departamento de Engenharia Civil da Faculdade de Ciências e Tecnologias da Universidade de Coimbra.

abril de 2020

The presented results were developed in the scope of the research project INOV_LAMI (Development of innovative reinforcing systems and improvement of the design models for steel-concrete composite slabs), financed by FEDER funds through the Competitivity Factors Operational Programme COMPETE 2020/Portugal 2020/UE within the scope of the research project POCI-01-0247-FEDER-003483.

Miguel José Simões Pereira

CONCEPTION AND DESIGN OF HIGH-PERFORMANCE STEEL-CONCRETE COMPOSITE SLABS

PhD Thesis in Steel and Composite Construction supervised by Professor Rui António Duarte Simões and submitted to the Department of Civil Engineering, Faculty of Sciences and Technology of the University of Coimbra

April 2020

UNIVERSIDADE D COIMBRA

I, I'm a new day rising.
I'm a brand new sky,
To hang the stars upon tonight.
I am a little divided
Do I stay or run away
And leave it all behind?

It's times like these you learn to live again
It's times like these you give and give again
It's times like these you learn to love again
It's times like these time and time again

Foo Fighters

ABSTRACT

Steel-concrete composite slabs with profiled steel sheeting represent the most common solution for floors in steel and composite buildings. In general, the main advantages of this structural system are considered to be the increase of the construction speed, the elimination of conventional replaceable shuttering and the reduction of the number of props. According to Eurocode 4, Part 1-1 (EN 1994-1-1), the real capacity of steel-concrete composite slabs could be governed by bending, vertical shear or longitudinal shear resistance. In general, the latter one is usually the most conditioning mode for slabs with the spans currently used. Due to the contribution of the profiled steel sheeting, composite slabs have a significant bending capacity but to take advantage of it higher connection degrees must be provided.

This thesis aims to develop an innovative reinforcing system to increase the longitudinal shear capacity of composite slabs. The system is constituted by a set of transversal reinforcing bars crossing the longitudinal stiffeners executed along the upper flanges of the steel sheet profiles. This type of reinforcement allows to increase the connection degree of composite slabs in order to increase their longitudinal shear capacity or even achieve their bending resistance. Transversal bars also allow to increase the ductility of the slab. Several experimental tests were carried out, including a small-scale test programme – to study the resistance provided by the reinforcing system in detail – and a full-scale test programme to test simply supported and continuous composite slabs – to assess the efficacy of the proposed reinforcing system on the global behaviour of the slabs. Based on the results of the small-scale tests, an equation to predict the resistance provided by the proposed reinforcing system was established.

In order to complement the findings from the experimental tests and verify the accuracy of the design methodologies when applied to composite slabs reinforced by the proposed reinforcing system, a numerical study was carried out using the software *Abaqus*. Numerical models were calibrated and validated according to the results experimentally obtained. After calibration and validation, the influence of several geometric and mechanical parameters in the behaviour of these slabs was studied. From the numerical results it was found that increasing the thickness of the profiled steel sheeting allows to increase significantly both the connection degree in the slab and the longitudinal shear resistance, and hence the bearing capacity of the slab.

In many cases, particularly in composite slabs with short spans or current spans but with their longitudinal shear behaviour improved by reinforcing systems, the design is governed by the vertical shear capacity, if the resistance is predicted using the design model of Eurocode 4, Part 1-1. However, the design method to predict the vertical shear resistance underestimates the shear resistance of steel-concrete composite slabs because it is based on the design model for reinforced concrete slabs stated in Eurocode 2, Part 1-1 (EN 1992-1-1), and it does not take into account adequately the contribution of the profiled steel sheeting. The results of an experimental programme, comprising 4 experimental tests on short-span steel-concrete composite slabs are then shown and discussed. In order to induce a failure by vertical shear, the composite slabs tested were reinforced by transversal bars distributed over the shear span. The results of the experimental tests were then used to validate the numerical models, which made it possible to carry out a parametric analysis. The results obtained showed that the real vertical shear resistance of a composite slab can be more than 5 times higher than its design value if predicted according to european rules. These results also showed that the profiled steel sheeting provides a significant contribution to the total resistance of the slab, particularly for composite slabs with high degrees of shear connection.

The present study allows for the conclusion that the resistance and the ductility of composite slabs using the proposed reinforcing system are significantly increased. Regarding to the vertical shear capacity of steel-concrete composite slabs, the experimental and numerical results showed that the design methodology prescribed by Eurocode 4, Part 1-1, is quite conservative as it underestimates the relevant contribution of the resistance of the profiled steel sheeting to the vertical shear capacity of the slab.

RESUMO

As lajes mistas de aço e betão representam a solução mais frequente em sistemas de pavimentos de estruturas metálicas e mistas. A redução do tempo de construção, a diminuição do número de elementos de cofragem e de escoramento e a facilidade de transporte e armazenamento das chapas perfiladas são, geralmente, as principais vantagens que permitem promover a aplicação de lajes mistas. De acordo com o Eurocódigo 4, parte 1-1 (EN 1994-1-1), a capacidade de carga de lajes mistas de aço e betão pode ser condicionada por um de três modos de rotura: flexão, esforço transverso e corte longitudinal. Habitualmente, o último modo de rotura é o mais condicionante para lajes mistas se vãos correntes. Devido à contribuição da chapa perfilada, as lajes mistas têm uma elevada capacidade de flexão, contudo para que se possa tirar partido desta é necessário garantir um elevado grau de conexão entre a chapa perfilada e o betão.

O presente documento descreve o processo de desenvolvimento de um sistema de reforço inovador para lajes mistas, que consiste na aplicação de um sistema de armadura transversal distribuído ao longo do vão a intersetar a chapa perfilada em reforços longitudinais localizados nos banzos superiores do perfil. Trata-se de um sistema de reforço que permite aumentar a capacidade de lajes mistas ao corte longitudinal, através do aumento do nível de conexão entre a chapa e o betão, e, consequentemente, tirar maior partido da elevada capacidade das lajes mistas à flexão. O sistema de reforço desenvolvido permite igualmente aumentar o nível de ductilidade do seu comportamento ao corte longitudinal. Foi levada a cabo uma campanha experimental de provetes de escala reduzida que permitiu definir a capacidade de carga em cada ponto de conexão e desenvolver uma metodologia de dimensionamento que contabilize a contribuição deste sistema de reforço. A eficácia do sistema de reforço foi comprovada pelos resultados de uma campanha experimental de ensaios de flexão a lajes mistas com armadura transversal. Em função dos resultados obtidos na campanha experimental com provetes de escala reduzida foi desenvolvida uma equação que permite definir a resistência do sistema de reforço para que possa ser considerada no dimensionamento destas lajes mistas.

Por forma a complementar os resultados experimentais e verificar o modelo de dimensionamento desenvolvido para o dimensionamento de lajes mistas com o sistema de reforço proposto foi levado a cabo um estudo numérico fazendo uso do *software*

Abaqus. Os modelos numéricos foram calibrados e validados de acordo com os resultados experimentalmente obtidos. Após a validação dos modelos numéricos, a influência de vários parâmetros geométricos e mecânicos foi estudada. A partir dos resultados numéricos foi possível observar que o aumento da espessura da chapa perfilada permite aumentar significativamente a eficácia do sistema de reforço, a resistência ao corte longitudinal e, consecutivamente, a capacidade global de lajes mistas.

Em muitos casos, particularmente em lajes mistas de vãos curtos ou vãos correntes onde o seu comportamento ao corte longitudinal é melhorado por sistemas de reforço, o dimensionamento destes elementos é condicionado pelo seu valor de resistência ao esforço transverso. Contudo, de acordo com o modelo do Eurocódigo 4, parte 1-1, o modelo de dimensionamento de lajes mistas ao esforço transverso do Eurocódigo 4 é remetido para o Eurocódigo 2, tratando estas lajes como se fossem lajes maciças de betão armado e desprezando a contribuição da chapa perfilada. Por forma a estudar o comportamento de lajes mistas ao esforço transverso foi levada a cabo uma campanha experimental a 4 lajes de vãos curtos. Por forma a provocar uma rotura por esforço transverso os provetes foram reforçados com armadura transversal distribuída ao longo do vão de corte e foram sujeitas a vãos de corte reduzidos. Os resultados experimentais permitiram validar os modelos numéricos para simular uma rotura por esforço transverso e desenvolver um estudo paramétrico de análise do comportamento de lajes mistas ao esforço transverso. Os resultados atingidos indicaram que o esforço transverso resistente de uma laje mista pode ser superior a 5 vezes o seu valor de cálculo. Estes resultados permitiram concluir que a chapa perfilada contribui significativamente para a resistência de lajes mistas ao esforço transverso, especialmente em lajes mistas com um nível de conexão elevado.

Em suma, o presente estudo permite concluir que as lajes mistas de aço e betão com o comportamento ao corte longitudinal melhorado por armadura transversal a intersetar a chapa perfilada têm uma resistência e uma ductilidade significativamente superior. Relativamente à capacidade de lajes mistas ao esforço transverso, os resultados permitiram concluir que o método de dimensionamento disponível no Eurocódigo 4, parte 1-1, é bastante conservador por não permitir ter em conta a contribuição da chapa perfilada.

KEYWORDS

composite slab

longitudinal shear

reinforcing system

vertical shear

PALAVRAS-CHAVE

laje mista

corte longitudinal

sistema de reforço

esforço transverso

ACKNOWLEDGEMENTS

The first acknowledgements are addressed to Professor Rui Simões, who supervised the developed work, for his encouragement and experienced and clever guidance in planning and carrying out the research project. Thank you for all your support, availability, guidance and professionalism as a professor and supervisor throughout these last years.

I would also like to address my acknowledgement to the steel company *O Feliz Metalomecância SA* for the collaboration in the research project and for the production of the steel test components.

To all the ISISE community I express my deeply gratitutude for the companionship showed over these years, especially to my colleagues Damjan Cekerevac, Daniel Oliveira, Filip Ljubinkovic, Francisca Santos, Helder Craveiro, João Maximino, Joel Cunha, Jocelyn Nieto, Manuela Rodrigues, Nemanja Milovanovic and Trayana Tankova. A word of recognition is also given to Professor Luís Simões da Silva, for his best effort on leading the research team. I would also like to address thanks and credits to all the technical team from the Laboratory of Structures, Structural Mechanics and Constructions of the Department of Civil Engineering of the University of Coimbra for all their work and support during the experimental campaign, namely Cláudio Martins, Ilídio Santos, João Vidal, Luís Gaspar, Miguel Queirós and Tiago Cardoso.

To all my longtime friends Adriana Lopes, Aline Oliveira, Ana Luísa Diogo, Anaïs Gonçalves, André Lima, António Soares, Catarina Medeiros, Catarina Pereira, Dani Martins, Diana Sousa, Ema Gouveia, Inês Romano, João Ramirão, Jorge Nogueira, Jorge Ribeiro, Mariana Couto, Michelle Alegre, Nuno Reis, Nuno Ramos and Vanessa Tomé, for all the leisure moments, for being always by my side and for giving me all the support and motivation that I needed.

Last but not least, I would like to express my deepest gratitude to my family. To my parents Cristina Simões and António Pereira, to my sister Rita Pereira, to my brother in law Fréderic Cordeiro and my niece Leonor Cordeiro, thank you for all the unconditional care, dedication and support that you gave me, especially over these last years.

CONTENTS

LIST OF FIGURES

LIST OF TABLES

NOTATION

Roman upper case letters

A	Area
A_0	Original area
A_c	Concrete area; concrete area under compression
A_{nom}	Nominal cross-sectional area
A_p	Area of the cross-section of the profiled steel sheeting
$A_{p,c}$	Steel sheeting area under compression
$A_{p,t}$	Steel sheeting area under tension
A_{pe}	Area of the effective cross-section of the profiled steel sheeting
$A_{pe,m}$	Area of the effective cross-section of the profiled steel sheeting per slab module
A_s	Area of the longitudinal bars placed in the concrete ribs
$A_{s,m}$	Area of the longitudinal bars placed in one concrete rib
$A_{s,-}$	Area of the hogging bending moment reinforcement
$A_{s,-,m}$	Area of hogging bending reinforcement in one slab module
$A_{sl,x}$	Area of the tensile steel cross-section with x axis direction per unit of width
$A_{sl,y}$	Area of the tensile steel cross-section with y axis direction per unit of width
C	Cost of 1 m^2 of a steel-concrete composite slab
C_{10}	Coefficient to define hyperelastic materials (*Abaqus*)
D	Damping
D_1	Structural damping; coefficient to define hyperelastic materials (*Abaqus*)
D_2	Damping due to furniture
D_3	Damping due to finishes
E	Modulus of elasticity (Young Modulus); slip Force
$E_{c,1}$	Unloading stiffness at peak strength
E_{cm}	Modulus of elasticity of concrete
E_d	Design value of the acting shear or bending moment
E_s	Modulus of elasticity of steel
F	Force
$F_{b,Rd}$	Bearing capacity of the steel sheeting
F_{ea}	Design value of the end anchorage resistance force
F_H	Horizontal forces

$F_{t,Rd}$	Bearing capacity of the steel sheeting when transversal bars are intersecting it
G_{F0}	Reference value of the fracture energy
G_F	Fracture energy
G_p	Centroidal of the profiled steel sheeting
H	Horizontal force
I	Second moment of area
I_{eq}	Second moment of area of the composite section
$I_{eq,-}$	Second moment of area of the composite section in hogging bending regions
$I_{eq,1}$	Second moment of area of the un-cracked composite section
$I_{eq,2}$	Second moment of area of the cracked composite section
I_p	Second moment of are of the profiled steel sheeting in its centroidal axis
I_y	second moment of area in *y* axis
L	Length; span
L_b	Span length under constant bending moment span
L_s	Shear span
L_{sf}	Minimum distance of a cross-section to the nearest support to be in full connection
$L_{u,\max}$	Maximum span without need of temporary supports (unpropped)
L_x	Distance from a cross-section to the nearest support
M	Bending moment; total mass of floor including finishing and a representative amount of imposed load
M_{Ed}	Design value of the bending moment acting on a member
$M_{f,Rd}$	Design value of the bending moment resistance of a cross-section consisting of the effective area of flanges only
M_{FEM}	Maximum bending moment obtained in numerical simulation
M_{Mod}	Modal mass
M_{pa}	Design value of the plastic resistance moment of the effective cross-section of the profiled steel sheeting
M_{pr}	Reduced plastic resistance moment of the profiled steel sheeting
$M_{pl,Rd}$	Design value of the plastic bending moment resistant of the composite slab with full shear connection
$M_{pl,Rd,-}$	Design value of the plastic bending moment resistance of the composite slab under hogging bending moment
M_{Rd}	Design value of the resistance moment
M_{test}	Maximum sagging bending moment measured along the span during the test
M_y	Bending moment around *y* axis
N	Normal force
N_c	Design value of the compressive normal force in the concrete
N_{cf}	Design compressive force in the concrete for full connection

N_p	Tensile force provided by the profiled steel sheeting
$N_{p,c}$	Design compressive force in the profiled steel sheeting
$N_{p,t}$	Design tensile force in the profiled steel sheeting
N_s	Design value of the plastic resistance of the steel reinforcement
$N_{s,-}$	Design value of the plastic resistance of the hogging bending reinforcement
NA_{pl}	Plastic neutral axis
P	Applied load
$P_{0.1\mathrm{mm}}$	Load causing a recorded end slip of 0.1 mm
P_{FEM}	Maximum load obtained on numerical results
P_i	Load acting on the component i
$P_{\max}$	Maximum load
$P_{pb,Rd}$	Design value of the bearing resistance of a stud
$P_{Rd,1}$	Shear resistance of the stud
$P_{Rd,2}$	Crushing resistance of the concrete due to shear connectors
$P_{Rd,3}$	Bearing resistance of the sheet due to shear connectors
P_{test}	Maximum load achieved on the test
P_u	Maximum applied load
R_d	Design value of the shear or moment resistance
S	Static moment
V	Vertical shear; coefficient of variation
V_{Ed}	Design value of the vertical shear force acting on the member
$V_{l,Rd}$	Design value of the vertical shear resistance, governed by the longitudinal shear resistance
V_{Rd}	Design value of the vertical shear resistance
V_r	Coefficient of variation
V_{rt}	Coefficient of variation
V_t	Vertical shear at the support
V_{test}	Maximum vertical shear observed during the test
$V_{v,c,Rd}$	Design value of the vertical shear resistance of the slab according to EC4
$V_{v,Rd}$	Design value of the vertical shear resistance of the slab
$V_{v,Rd,m}$	Design value of the vertical shear resistance of one slab module
$V_{Rd,w}$	Design value of the vertical shear resistance of one web of the steel sheeting
$V_{v,sum,Rd}$	Design value of the vertical shear resistance of a composite slab defined by the sum of values $V_{v,c,Rd}$ and $V_{v,p,Rd}$
$V_{v,p,Rd}$	Design value of the vertical shear resistance of the profiled steel sheeting
$V_{v,w,Rd}$	Design value of the vertical shear resistance of one web of the profile
V_X	Coefficient of variation of X
V_δ	Coefficient of variation of δ
W	Bending modulus

X_d Design value of a property X
X_k Characteristic value of a property X

Roman lower case letters

a Distance to the end of the steel sheeting
a_p Length of the loaded area for punching shear verification
b Width of the slab; mean value correction factor
b_0 Mean width of a concrete rib
b_m Width of one slab module
b_p Width of the loaded area for punching shear verification
c_c Unit cost of the concrete by m^3
c_p Critical perimeter length for punching shear verification; unit cost of the profiled steel sheeting by kg, kN or m^2
c_s Unit cost of the steel reinforcement by kg or kN
d Diameter of the bar; diameter of the shank of the stud
d_c Damage parameter in compression
$d_{c,1}$ Damage parameter at peak compression strength
d_{d0} Diameter of the weld collar
d_{max} Maximum dimension of the aggregates of the concrete
d_p Distance from the centroidal axis of the profiled steel sheeting to the upper top fibre of the composite slab in compression; effective depth of the slab
d_s Distance between the centroidal of the steel reinforcement in tension to the extreme fibre of the composite slab in compression
$d_{s,-}$ Distance from the reinforcement centroidal to the bottom flange of the steel sheet
d_t Damage parameter in tension
e Distance from the centroidal axis of the profiled steel sheeting to the extreme fibre of the composite slab in tension
e_1 Distance to the end of the steel sheeting
e_p Distance from the plastic neutral axis of profiled steel sheeting to the extreme fibre of the composite slab in tension
f Frequency
f_{bv} Shear buckling strength of the steel sheeting
f_c Compressive strength of concrete
f_{cd} Design value of the cylinder compressive strength of concrete
f_{ck} Characteristic compressive strength of concrete
$f_{ck,cube}$ Characteristic compressive cube strength of concrete
f_{cm} Mean value of concrete cylinder compressive strength

$f_{cm,cube}$	Mean value of concrete cube compressive strength
f_{ctk}	Characteristic axial tensile strength of concrete
f_{ctm}	Mean value of axial tensile strength of concrete
f_{cu}	Ultimate compression strength of concrete
f_{sd}	Design value of the yield strength of reinforcing steel
f_{sk}	Characteristic value of the yield strength of reinforcing steel
f_u	Ultimate tensile strength; ultimate strength of the material of the stud
f_{up}	Ultimate tensile strength of the steel sheeting
f_{upm}	Mean value of ultimate tensile strength of the steel sheeting
f_{yb}	Yield strength of the steel sheeting (according to EN 1993-1-3)
f_{yp}	Yield strength of the steel sheeting
$f_{yp,d}$	Design value of the yield strength of the steel sheeting
$f_{yp,m}$	Mean value of the measured yield strength of the steel sheeting
h	Overall height of the slab
h_c	Overall height of the concrete above the profiled steel sheeting; thickness of the concrete flange
h_f	Thickness of the coating layer for punching shear verification
h_p	Overall depth of the profiled steel sheeting excluding embossments
h_{pond}	Height of the slab increase due to “ponding” effect
h_{sc}	Overall nominal height of the stud
h_w	Web height between the midlines of the flanges
h_c	Height of the concrete slab above the profiled steel sheeting
k	Empirical factor for design longitudinal shear resistance (*m-k* method); statistical coefficient
k_1	Coefficient to determine the vertical shear resistance of a composite slab
k_n	Characteristic fractile factor
k_t	Coefficient influenced by the thickness t
k_τ	Coefficient to account for longitudinal stiffener
k_φ	Coefficient to determine the resistance of a shear stud
l	Length
l_0	Original length
l_b	Spacing between the transversal bars of the reinforcing system
$l_{b,min}$	Minimum anchorage length
m	Empirical factor for design longitudinal shear resistance (*m-k* method); mass of floor including finishing and a representative amount of imposed load by square meter
m_x	Mean value of the n sample results
n	Modular ratio; number of specimens; number of tests
n_m	Number of slab modules

n_w	Number of webs
n_{st}	Number of headed studs
p	Uniformly distributed load
p_c	Concrete weight per square meter
p_k	Characteristic value of the maximum load supported by the slab
q	Uniformly distributed load
r_{ei}	Experimental resistance value for specimen i
r_{ti}	Theoretical resistance value for specimen i
s	Slip
s_d	Total developed slant height of the web of the profiled steel sheeting
s_{left}	Slip measured on the left end of the specimen
s_p	Slant height of the largest plane element in the web
s_{right}	Slip measured on the right end of the specimen
s_w	Slant height of the web of the profiled steel sheeting between the midpoints of the corners
s_x	Standard deviation of n sample results
s_Δ	Standard deviation of Δ_i values
t	Thickness of the steel sheeting
t_{nom}	Nominal thickness of the steel sheeting
t_{cor}	Core thickness of the steel sheeting
w	Crack opening displacement
w_{ch}	Reference crack opening displacement
y_p	Height of the profiled steel sheeting at which the tensile force N_p acts
z	Depth; vertical distance between forces N_c and N_p
z_1	Vertical distance between forces N_c and N_p
z_2	Vertical distance between forces N_c and N_s
z_3	Vertical distance between forces N_c and $N_{s,-}$
z_{cr}	Distance between the neutral axis and the top surface of the composite slab on a cracked cross-section
$z_{cr,-}$	Distance between the neutral axis and the bottom surface of the composite slab on a cracked cross-section
z_{uncr}	Distance between the neutral axis and the top surface of the composite slab on an un-cracked cross-section
z_{pl}	Depth of the neutral axis
$z_{pl,-}$	Height of the neutral axis under hogging bending moment

Greek upper case letters

Δ_i	Logarithm of the error term δ_i
$\bar{\Delta}$	Estimated value for $E(\Delta)$

Greek lower case letters

α	Angle; coefficient
α_b	Coefficient to determine $F_{b,Rd}$
β	Coefficient
γ	Density
γ_c	Density of the concrete
γ_m	Partial safety factor (γ_m = 1.00)
γ_{M0}	Partial safety factor (γ_{M0} = 1.00)
γ_{M1}	Partial safety factor (γ_{M1} = 1.00)
γ_{M2}	Partial safety factor (γ_{M2} = 1.25)
γ_s	Density of the steel
γ_V	Partial safety factor for design shear resistance of a headed stud (γ_V = 1.25)
γ_{VS}	Partial safety factor (γ_{VS} = 1.25)
δ	Deflection; mid-span deflection
δ_i	Error term
δ_s	Deflection of steel sheeting under its own weight plus the weight of wet concrete
$\delta_{s,max}$	Limiting value of δ_s
ε	Strain
ε_0	Strain coordinate of the focal point (FP)
ε_{c1}	Compressive strain in the concrete at the peak stress
ε_{cu1}	Ultimate compressive strain in the concrete
$\varepsilon_{el,true}$	True elastic strain
$\varepsilon_{pl,true}$	True plastic strain
ε_{true}	True strain
ε_{up}	Maximum strain attained in the steel
ε_{yp}	Strain in the steel corresponding to the yield stress
$\varepsilon_{yp,60}$	Strain corresponding to the yield stress of the steel from profile LAMI 60+
$\varepsilon_{yp,120}$	Strain corresponding to the yield stress of the steel from profile LAMI 120+
η	Connection degree; calibration factor
η_d	Design value of the conversion factor
λ_w	Relative slenderness of the web
μ	Friction coefficient

v	Poisson Coefficient
ρ	Curvature
ρ_1	Total reinforcement ratio for punching shear verification
ρ_d	Ductility coefficient
ρ_{lx}	Reinforcement ratio for steel with *x* axis direction for punching shear verification
ρ_{ly}	Reinforcement ratio for steel with *y* axis direction for punching shear verification
σ	Normal stress
σ_0	Stress coordinate of the focal point (FP)
σ_c	Compression stress
σ_t	Tensile stress
σ_{true}	True stress
τ	Longitudinal shear stress
$\tau_{t,Rd}$	Design value of longitudinal shear strength of a composite slab with transversal reinforcement intersecting the profiled steel sheeting
τ_u	Value of longitudinal shear strength of a composite slab determined from testing
$\tau_{u,Rd}$	Design value of longitudinal shear strength of a composite slab
$\tau_{u,Rk}$	Characteristic value of longitudinal shear strength of a composite slab
$\upsilon_{p,Rd}$	Design value of the punching shear stress resistance stress
φ	Slope of the web relative to the flanges; curvature; reduction factor

Subscripts and superscripts

+	Positive
-	Negative
c	Concrete
e	Effective
eff	Effective
el	elastic
i	Case/specimen i
m	Slab module
max	Maximum
min	Minimum
p	Profiled steel sheeting
s	Steel; steel reinforcement
u	Ultimate
y	Around y axis
z	Around z axis

Abbreviations

CDP	Concrete Damage Plasticity
EC	Eurocode
Eq(s).	Equation(s)
et al.	*et alia* (and others)
F	Flat
FP	Focal Point
R	Ribbed
SLS	Service Limit States
ULS	Ultimate Limit States

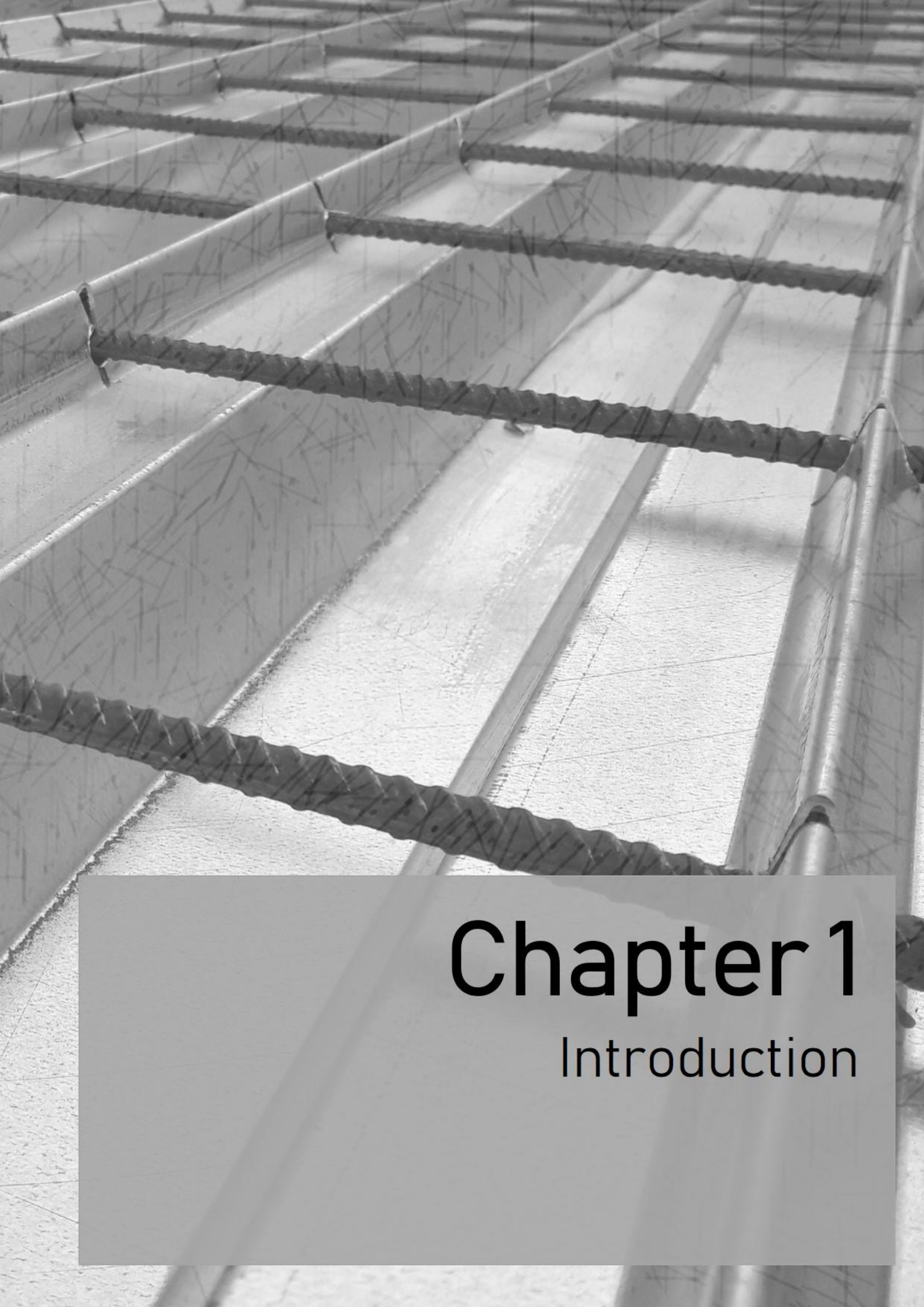

Chapter 1
Introduction

1.1 Structural performance of composite slabs

Structural members composed of two or more materials are known as composite members. Steel and concrete are materials widely combined in the conception of buildings. Their application is so common that a specific Eurocode – standard EN 1994-1-1 (CEN, 2004b) – was created to regulate the design criteria of steel-concrete composite structures. This standard addresses four main types of composite members: composite beams, composite columns, composite slabs and composite joints. The main advantage of this type of members results from the combination of the proprieties of both materials to form a single member which makes possible to compensate the weakness of each material with the strong points of the other. For example, concrete has a high resistance when subjected to compression, but shows a poor behaviour under tension (low resistance and low ductility); on the other hand, the steel has a significant resistance when subjected to tension, but its resistance is compromised by buckling phenomena under compression; taking this in consideration, the combination of both materials, i. e. to take advantage of the compression resistance of concrete and the tensile resistance of steel, offers a very efficient solution.

Floors in steel and composite buildings are usually constituted by steel-concrete composite slabs with profiled steel sheeting. Composite slabs are mainly composed by concrete and the profiled steel sheeting; typically, some reinforcement is provided to improve the distribution of the load and shear connectors to increase the longitudinal shear resistance (see Fig. 1.1). In the construction phase, profiled steel sheeting is used as shuttering and must be designed to resist the weight of the wet concrete plus additional construction loads. In the definitive phase, after curing of the concrete, the profiled steel sheeting is used to resist tension stresses while the concrete is used to resist compressive stresses. So both components are working together with different roles which is the main concept of a composite action. This multi-functional role of profiled steel sheeting leads to the main advantages of composite slabs, such as, the rapid construction process and the reduction of the formwork elements, props as temporary supports and reinforcement.

Steel-concrete composite slabs bring many economical and resistance advantages, like: (i) the profiled steel sheeting works as shuttering during the construction phase and creates a safe working platform; (ii) the profiled steel sheeting is capable of support the concrete during its cure without or almost without propping; (iii) reduction of the construction time, because it avoids the construction of additional shuttering structures for floors; (iv) reduction of the amount of reinforcement; (v) it allows to consider the diaphragm action on beams and walls lateral bracing system; (vi) high stiffness and achievement of longer spans; (vii) facilitates placing building services (like water

plumbing, communication wiring, etc.) and; (viii) allows to reduce the amount of finishing tasks in the bottom slab surface (de Andrade *et al*., 2004).

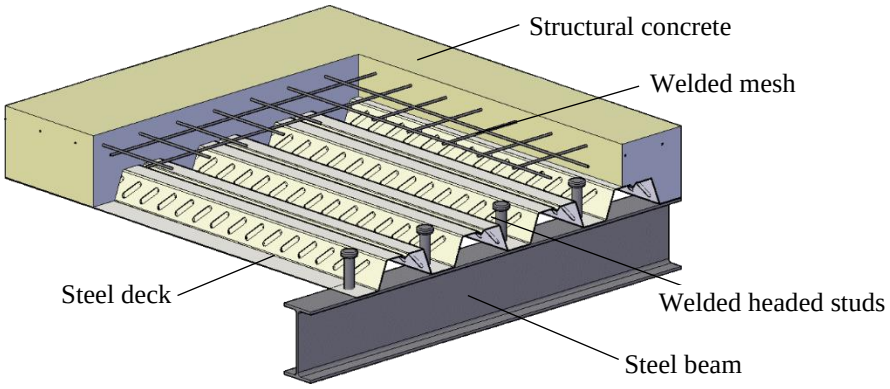

Fig. 1.1 Conventional steel-concrete composite slab

The design of composite slabs submitted to uniformly distributed loads for the ultimate limit states, as shown in Fig. 1.2, may be governed by one of three failure modes: (i) the bending moment at the mid-span cross-section, (ii) the longitudinal shear along the shear span L_s or (iii) the vertical shear in a cross-section close to the supports. These three failure modes are represented in the graph shown in Fig. 1.2, which relates the maximum load p (defined by the vertical shear at the supports V_t) with the span length (defined by the shear span L_s); the remaining symbols in Fig. 1.2 have the following meanings: b is the width of the slab; d_p is the distance from the centroidal axis of the profiled steel sheeting to the upper top fibre of the composite slab in compression; A_p is the area of the cross-section of the profiled steel sheeting on the width b; L_s is the shear span length, equal to $L/4$ for a simple supported composite slab submitted to a uniformly distributed load; m and k are constants regarding one of the methods (m-k method) given in standard EN 1994-1-1 (CEN, 2004b) to predict the longitudinal shear resistance of composite slabs.

A composite slab failure induced by vertical shear is a predictable mode but only in short span composite slabs. For current length spans between 2 and 5 m, the failure by longitudinal shear along the steel sheet-concrete interface is the most common type of failure, and consequently, the verification of the longitudinal shear resistance tends to be the governing design condition for this type of structural component. The bending moment resistance usually governs the design only in long-span slabs. The design may also be governed by the serviceability limit states, for composite slabs with low values of the relation h/L (thin slabs), where h is the thickness of the slab and L is the span length. Taking the previous assumptions into account, increasing the longitudinal shear

resistance seems to be one of the most effective ways to increase the load bearing capacity of composite slabs.

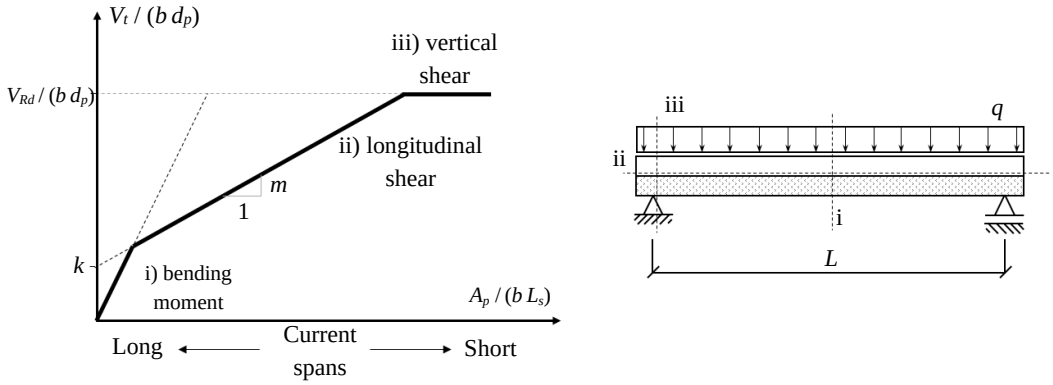

Fig. 1.2 Failure modes in steel-concrete composite slabs

As explained before, the load bearing capacity of composite slabs is usually governed by the low degree of longitudinal shear connection ensured by the sheet embossments along the steel sheet-concrete interface. The end anchorage systems constituted by stud connectors welded to the flange of the supporting steel beams if welded through the steel sheet, are one of the most used ways to increase the degree of connection between the steel and the concrete. This reinforcing system is efficient; however, it has also some constraints: the welding of the stud connectors must be executed on site, to be done through the steel sheet and the supporting beam must preferably be a steel beam.

In order to increase the longitudinal shear resistance of composite slabs or, in many cases, to achieve their bending capacity, a new reinforcing system was developed within the scope of the present thesis. The reinforcing system developed and studied in the present research comprises of a set of transversal reinforcing steel bars, distributed over the span, and placed in vertical cuts executed in the longitudinal stiffeners, for example in the inverted V-shape, located in the upper flanges of the profiled steel sheeting, as is illustrated in Fig. 1.3. The function of these bars is to prevent the relative displacement between the profiled steel sheeting and the concrete in the longitudinal direction, allowing the slab to exercise its entire bending resistance. When demands are made on the system, the shear strength of the bars and the bearing strength of the sheet are mobilized. The transference of the longitudinal shear forces is all the more effective, the greater the thickness of the steel sheets is. To prevent the bars from loosening during concreting, these are fitted into a hole-shaped cut-out located at the base of the vertical cut, whose diameter, approximately equal to the diameter of the bar, may be slightly larger than the width of the cut, thus obtaining a snap fit between the bar and the profiled sheet. This reinforcing system could be applied in two different ways: (i) as a simple reinforcing

system – consisting of just the transversal bars applied in the pre-drilled holes or (ii) as a reinforcement mesh – combining transversal and longitudinal bars. The latter could be prepared in such a way that the transversal bars, which only have a significant role in the region of the intersection with the longitudinal stiffeners, could be folded down to support the longitudinal bars and, consequently, replace the application of bar spacers. Apart from these two ways of application, other variants may be used.

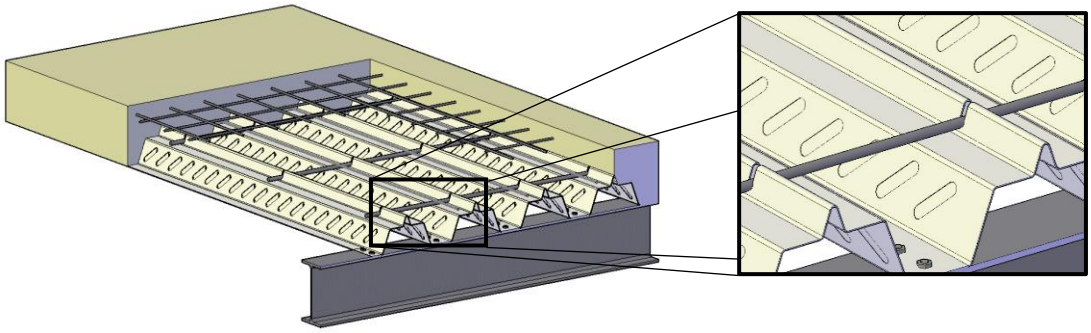

Fig. 1.3 Proposed reinforcing system

If the longitudinal shear resistance is increased by any process, the design of steel-concrete composite slabs with short and current spans tends to be governed by the vertical shear resistance. According to standard EN 1994-1-1 (CEN 2004b), the vertical shear resistance of composite slabs is mainly achieved by the concrete rib; his standard defines that the vertical shear resistance of a composite slab $V_{v,Rd}$ shall be determined in accordance with section 6.2.2 of standard EN 1992-1-1 (CEN, 2004a), in the same way as reinforced concrete slabs without required design shear reinforcement. However, this design model leads to an underestimation of the slab capacity, because the high shear capacity provided by the profiled steel sheet is not taken into account. Actually, Johnson (2018) already assumed that the Eurocode design model is conservative because it ignores the real contribution of webs of steel sheets and longitudinal reinforcing bars if any exist. The longitudinal reinforcing bars and the steel sheeting also contribute positively to the vertical shear resistance of composite slabs when the minimum anchorage conditions are guaranteed. However, the contribution of the steel sheeting is only based on its area and not on its shape. A profiled steel sheet has a significant vertical shear resistance, mainly provided by the webs of these profiles. This significant contribution is paramount in the constructive phase, when the steel sheet supports the wet concrete and constructive loads without, or with a reduced number of temporary supports. Therefore, the vertical shear design model of Eurocode 4 (CEN, 2004b) tends to be very conservative, leading in some situations to an over-dimensioning regarding composite slabs. This underestimation of slab capacity has particular influence in composite slabs with short spans, or even with the spans currently used in building construction if the longitudinal shear behaviour is

improved by some type of reinforcement system, such as end anchorage devices. The experimental and numerical studies carried out in this work intend to contribute to a future update of the vertical shear design model of composite slabs defined in standard EN 1994-1-1 (CEN, 2004b).

The work developed and presented in this thesis was conducted in the scope of the national research project INOV_LAMI – *Desenvolvimento de Sistemas de Reforço Inovadores e Aperfeiçoamento dos Modelos de Cálculo para Lajes Mistas de Aço e Betão* (Development of innovative reinforcing systems and improvement of the design models for steel-concrete composite slabs) – financed by FEDER funds through the Competitivity Factors Operational Programme – COMPETE 2020/Portugal 2020/EU and also designated as project POCI-01-0247-FEDER-003483. The reinforcing system developed has already been submitted for a patent registration.

1.2 Objectives and scope of the thesis

As was mentioned before, composite slabs are a very effective structural solution to be used in floors of steel and composite structures. However, there are still issues related to their design and structural behaviour, especially concerning the longitudinal shear behaviour and the vertical shear design model. This study was developed to overcome those issues in particular. Therefore, the main objectives of the present study were:

i. to develop a new and innovative reinforcing system, efficient in terms of structural resistance and practical application;
ii. to prove the efficiency of the proposed reinforcing system;
iii. to calibrate an analytical expression to quantify the longitudinal shear resistance of composite slabs with the reinforcing system developed;
iv. to study the vertical shear behaviour of steel-concrete composite slabs in order to improve the respective design model;
v. to verify the accuracy of the design models prescribed in standard EN 1994-1-1 (CEN, 2004b) if applied to the design of composite slabs incorporating the proposed reinforcing system.

Fig. 1.4 shows in a qualitative way the contribution of this study to the behaviour and design of steel-concrete composite slabs. On the one hand, the increase of the longitudinal shear resistance and consequently the increase of the connection between the two materials in a composite slab allows to exercise its entire bending capacity (line 3 instead of line 2). On the other hand, taking into account the resistance of profiled steel sheeting, mainly acquired by the webs of the profile, in the vertical shear resistance of composite

slabs allows for avoidance of overdesign of these structural elements (line 5 instead of line 4). As a result, the highlighted grey area A represents the positive contribution of the present study for the improvement of the structural performance of steel-concrete composite slabs.

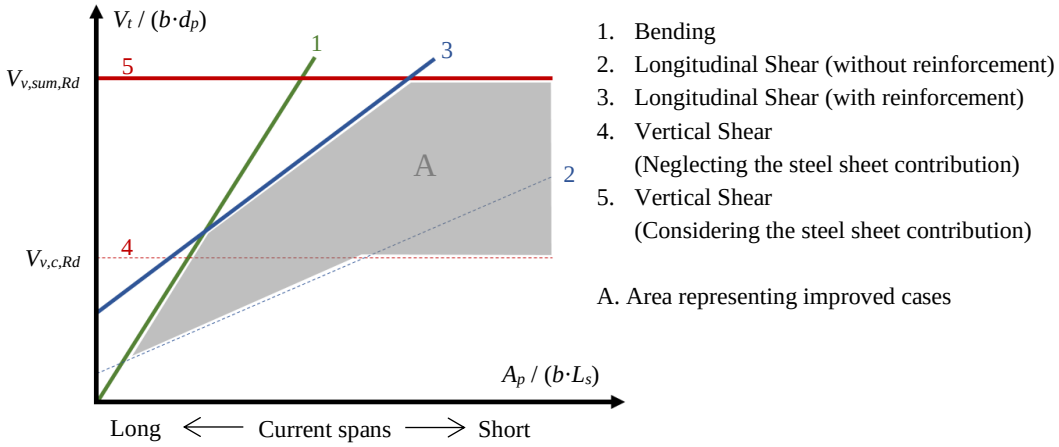

Fig. 1.4 Improvement of the structural performance of steel-concrete composite slabs

This doctoral thesis was developed on the basis of analytical, numerical and experimental results and comprises steel-concrete composite slabs with low and high profiled steel sheeting.

1.3 Main terminology

In order to avoid different understandings in the terminology of composite slabs, some terms widely used throughout this document are hereafter clarified. Some of these terms are shown in Fig. 1.5

A **composite structure** is the one comprising structural members with composite cross-sections. **Composite members** are structural members composed by concrete and structural steel, working together in terms of resistance and stiffness. In a composite member the two components are interconnected by a shear connection system in order to avoid the longitudinal slip and separation between them.

A **slab module** is the part of the slab comprised between the centres of two consecutive upper flanges with a width b_m. Since composite slabs are structural elements working mainly in their longitudinal direction (direction of the ribs), it is common to simplify their analysis considering just one module because this is transversally repeated over the total width b.

The **concrete rib** is the concrete part not included in the concrete height h_c of the slab. This part is comprised under the top flanges level and between two consecutive webs.

Additionally, two main directions can be defined in a composite slab: the **longitudinal direction** of a composite slab is the direction of the ribs and; the **transversal direction** is the horizontal one perpendicular to the longitudinal direction. Also regarding different directions, several types of reinforcement are referred along this document:

i. **Transversal bars** are the reinforcing bars distributed over the span intersecting the profiled steel sheeting in the transversal direction;
ii. **Longitudinal bars** are the longitudinal reinforcing bars usually placed in the concrete ribs. These reinforcing bars bring many advantages such as the increase of the bending and fire resistance of the slab;
iii. **Constructive reinforcement** is used to refer to the reinforcement mesh placed close to the top concrete surface to promote the load distribution. The minimum amount of constructive reinforcement in both directions is 80 mm^2/m, according to clause 9.2.1(4) of standard EN 1994-1-1 (CEN, 2004b);
iv. **Hogging bending reinforcement** refers to the longitudinal reinforcing bars required to resist the tensile forces acting in the top part of continuous slabs over the hogging bending moment regions.

Longitudinal stiffeners are folded and bended parts in the cold-formed steel sheeting profile developed to increase the effective area of the section and, consequently, its mechanical resistance.

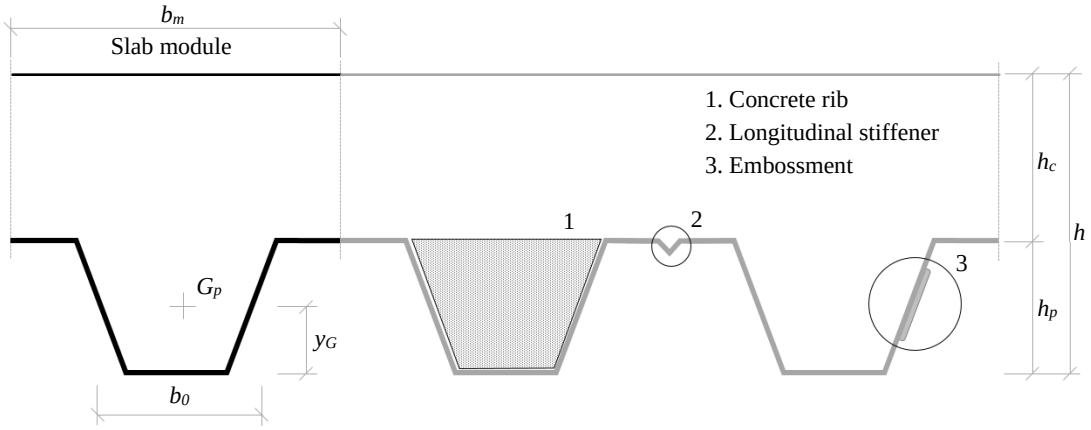

Fig. 1.5 Terminology for composite slabs

1.4 Document's outline

This thesis presents the development of an innovative reinforcing system for steel-concrete composite slabs, as well as a deep analysis to the general behaviour of this type of structural members. It is constituted by 8 main chapters and one annex:

- Chapter 1 (Introduction) presents a general introduction to the thesis. The main topics discussed and presented over the thesis and also the main objectives initially proposed are presented here. The basic terminology is also clarified in order to avoid misunderstandings in the further chapters;
- Chapter 2 (Literature review) presents the most relevant literature review on this subject. The basic concepts related to the shear connection behaviour and slip forces are firstly presented. In this chapter, several experimental approaches to study the behaviour of steel-concrete composite slabs and different systems to improve the behaviour of these members developed by other researchers are also presented, as some analytical and numerical studies and their respective conclusions. Finally, several approaches to design steel-concrete composite slabs to vertical shear are presented and compared with the design model recommended in standard EN 1994-1-1 (CEN, 2004b);
- Chapter 3 (Design of steel-concrete composite slabs) presents the general concepts and methodologies to design steel-concrete composite slabs according to standard EN 1994-1-1 (CEN, 2004b);
- Chapter 4 (Development of a new reinforcing system for composite slabs) presents the development of a new reinforcing system to improve the longitudinal shear behaviour of composite slabs, defined by transversal steel bars intersecting the profiled steel sheeting. Initially, a statistical analysis applied to the results of a small scale test campaign is presented, which allows to evaluate the reinforcing system resistance characteristic value and, consequently, to account the contribution of the reinforcing system in the design. Then, it is presented the approach and the results concerning an experimental programme carried out to study the behaviour of steel-concrete composite slabs with and without the proposed reinforcing system;
- Chapter 5 (Numeric analysis of composite slabs with transversal bars) presents the finite element modelling studies of steel-concrete composite slabs with and without the previously developed reinforcing system, performed on *Abaqus* (SIMULIA, 2015). The numerical models were calibrated and validated according to the experimental results previously obtained. Finite element models are described over this chapter, through their most relevant details and respective

adopted assumptions. Numerical models successfully validated allowed to develop parametric studies and complement the knowledge about the behaviour of steel-concrete composite slabs with transversal bars intersecting the profiled steel sheeting;

- Chapter 6 (Vertical shear capacity of composite slabs) presents the evaluation of the vertical behaviour of steel-concrete composite slabs against the respective design model advocated in standard EN 1994-1-1 (CEN, 2004b). In this chapter an experimental programme carried out to study the vertical shear behaviour of composite slabs is described. The experimental results are discussed and compared with the analytical design resistance values. Taking into consideration the main work developed in the previous chapter, a parametric study was carried out by finite element models to enlarge the amount of results concerning the vertical shear failure of composite slabs;
- Chapter 7 (Assessment of the efficiency of the reinforcing system) presents the reinforcing system efficiency. Three different analyses were carried out in terms of quantity, global cost and bearing capacity. Some examples are presented using composite slabs design tables, which are widely used in the design of these structural members and provided by the producing companies. Some practical examples are presented, showing the influence of the reinforcing system in the governing design mode and the load bearing capacity of the slab. Additionally, a parametrical study is presented to study the influence of several parameters in the reinforcing system efficiency;
- Chapter 8 (Main conclusions and future work) presents the most relevant conclusions obtained from this research and also some topics for further investigation within this research work. Moreover, some recommendations are presented for future researches about steel-concrete composite slabs in order to study and improve their behaviour.

Also in the scope of this research work, a design tool to produce the design tables for steel-concrete composite slabs incorporating the innovative aspects developed and proposed over the current thesis was developed. One annex was included at the end of this document to present the developed design tool:

- Annex A (Developed design tool for composite slabs) presents a design tool developed in the scope of the study. This annex shows the main options of the tool and some assumptions assumed;

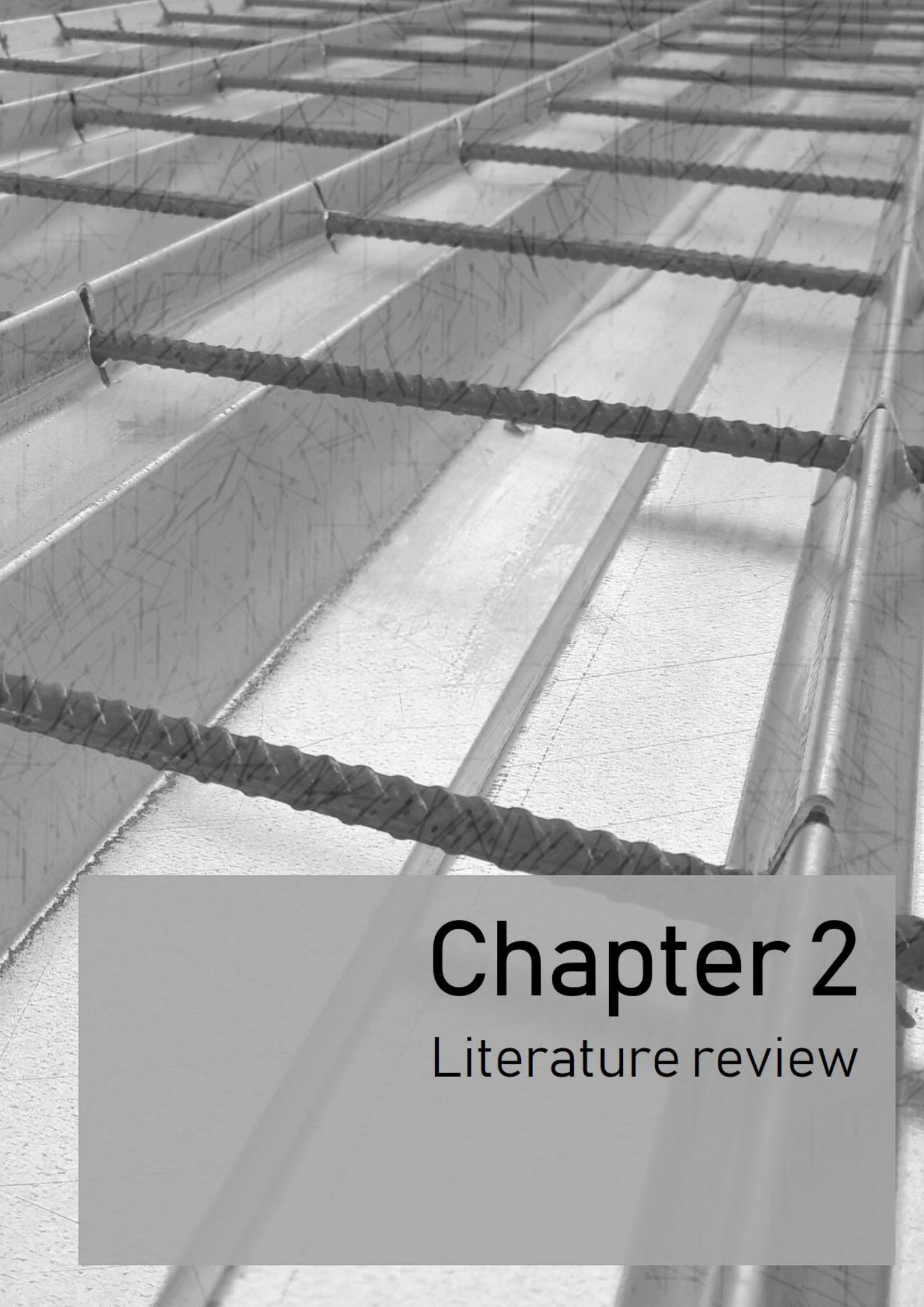

Chapter 2

Literature review

2.1 Introduction

According to Bridge and Patrick (2002), profiled steel sheeting has been used since the 1930's, originated in the USA for constructing lightweight floors. In the first applications, profiled steel sheeting only had the shuttering purpose during the concrete cure. However, two decades later researchers found that steel decks were able to increase the bearing capacity of slabs, and their contribution in tension started to be accounted to resist the loads in the definitive phase. In the 1960's profiled steel decking improved and the first profiles with embossments appeared in order to increase the connection between steel and concrete (Viest, 1997). Until nowadays the application of steel-concrete composite slabs have been increasing, due to their advantages described in the previous chapter, and it is now the most common solution in floors of steel and composite buildings.

In spite of all the advantages of using steel-concrete composite slabs referred in chapter 1, there are still some gaps that negatively influence its performance and limits their application in steel and composite structures. As it was mentioned before, composite slabs exhibit a high bending capacity due to the contribution of the profiled steel sheeting to resist the tensile forces. However, in general, this high resistance is not used because the steel-concrete connection is not strong enough to achieve the bending capacity.

For the analysis of a composite member in bending, the shear connection between concrete and steel components can be classified as the following: null connection, full connection or partial connection. Fig. 2.1 shows the normal stresses diagram in a composite beam under all the three conditions. When full connection is considered, the connection is rigid and so the longitudinal shear capacity corresponds to the bending resistance of the cross-section. If null connection is considered, both components should be considered separately. In partial connection the longitudinal shear resistance, according to the normal stress diagram, should be defined as a ratio of the bending capacity.

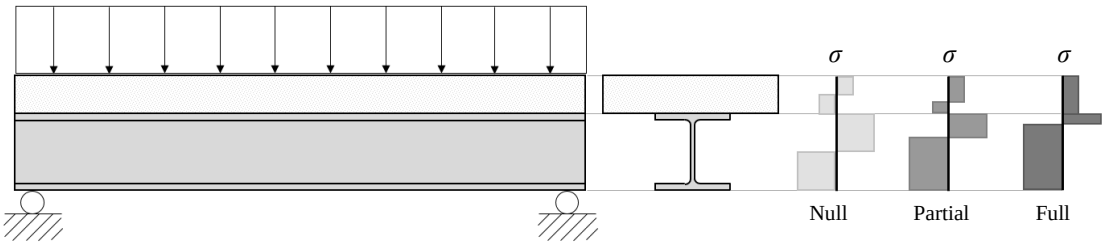

Fig. 2.1 Effect of shear connection on normal stresses σ

Standard EN 1994-1-1 (CEN, 2004b), in order to avoid a null connection situation in composite slabs, requires that the profiled steel sheeting should be capable of transmiting longitudinal shear on its contact surface with the concrete component by at least one of four types of interlock mechanisms. However, these mechanisms are not strong enough to increase the longitudinal shear degree of steel-concrete composite slabs until its bending capacity. To increase the longitudinal shear capacity of composite slabs, several reinforcing systems have been developed by the scientific community. The main ones are described along this chapter. Since the longitudinal shear resistance of composite slabs must be defined according to methods which require parameters that should be obtained experimentally, some researchers have also developed and validated methods to predict the slip behaviour of composite slabs, which are also presented and discussed in this chapter.

The development and the revision of the Eurocodes show how the research community have been trying to standardize design models (Crisinel and Marimon, 2004). However, Eurocodes still present some contradictions in the design of identical structural members. Crisinel and Marimon (2004) presented a revision based in one comparison example: the authors compared the design principals of composite slabs and composite beams, because both are members that bend mainly in one direction. Although the design principles for the bending resistance are identical, those concerning the evaluation of the vertical shear resistance are almost the opposite: in composite slabs, only the concrete cross-section is accounted for their vertical shear resistance; on the contrary, for composite beams the vertical shear resistance essentially takes into account the resistance of the steel cross-section. The longitudinal shear design model is also based on different procedures: in composite slabs full scale tests are required while in composite beams the shear resistance of the connectors is obtained by push-out tests (small-scale specimens).

2.2 Improvement of the longitudinal performance of steel-concrete composite slabs

2.2.1 Introduction

In Europe, the design of composite slabs is regulated by the standard EN 1994-1-1 (CEN, 2004b), which states that the profiled steel sheeting must be capable of transmitting horizontal shear at the interface between itself and the concrete to ensure the composite behaviour. The composite behaviour between the two components (steel sheeting and concrete layer) must be ensured by one or more interlocking systems. As shown in Fig. 2.2, standard EN 1994-1-1 (CEN, 2004b) predicts 4 types of interlocking systems to be

applied: (i) a mechanical interlock provided by indentations or embossments in the profile; (ii) a frictional interlock; (iii) an end anchorage provided by welded studs or another type of local connection between the concrete and the profiled steel sheeting, in combination with the previous ones; (iv) an end anchorage system by deformation of the ribs at the end of the sheeting, which must be combined with a frictional interlock.

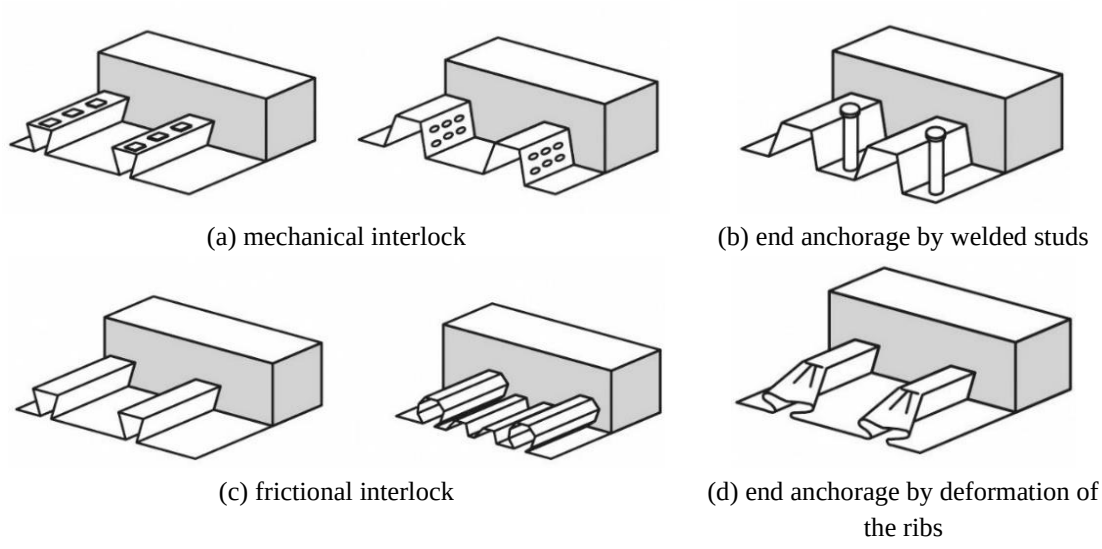

(a) mechanical interlock (b) end anchorage by welded studs

(c) frictional interlock (d) end anchorage by deformation of the ribs

Fig. 2.2 Forms of interlock in composite slabs (CEN, 2004b)

2.2.2 Experimental evaluation of composite slabs

Over the past decades, the effort to develop innovative systems to improve the longitudinal shear behaviour of steel-concrete composite slabs and increase their bearing capacity has been evident. This effort is crucial to promote the application of steel-concrete composite slabs, regarding their many advantages. However, the development of new reinforcing systems requires research activity by means of extensive experimental tests to prove their efficiency. Experimental tests are useful to understand the real behaviour of steel-concrete composite slabs under specific conditions. Two main types of experimental tests are usually carried out: (i) full-scale tests – to study the global behaviour of composite slabs with current dimensions; (ii) small-scale tests – to evaluate the longitudinal shear resistance of composite slabs with a specific profile steel sheeting or reinforcing system.

(i) Full-scale tests

Full-scale tests are bending tests to study and evaluate the capacity of steel-concrete composite slabs with dimensions typically adopted in real conditions of steel and composite buildings.

For a specific steel sheeting profile, standard EN 1994-1-1 (CEN, 2004b) requires a full-scale testing campaign to define the longitudinal shear resistance parameters, like *m* and *k* – to design composite slabs for longitudinal shear using the *m-k* method – and the design value of the shear stress resistant $\tau_{u,Rd}$ – to design composite slabs for longitudinal shear using the partial connection method. Fig. 2.3 shows the conditions required in the referred standard for the experimental layout. Steel-concrete composite slabs must be supported as simply supported members. Two linear loads must be applied at a distance of *L*/4 from the supports, where *L* is the span length. Between the loading structure and the slab, neoprene bands should be placed over the width of the slab, with a maximum width of 100 mm. Under the slab, between the slab and the supports, bearing plates with a minimum thickness of 10 mm and maximum width of 100 mm should be placed. The distance between the ends of the slab and the centre line of the supports must be less than 100 mm.

Standard EN 1994-1-1 (CEN, 2004b) requires a cyclic load stage in the beginning of the test and before reaching the ultimate load, varying the applied load between $0.2P_u$ and $0.6P_u$, where P_u is the maximum expected applied load. The cyclic load has the main purpose of eliminating the chemical bond between the concrete and the steel. Several researchers have been publishing results that show that cyclic loading has no significant influence on the maximum load achieved (Hedaoo *et al.*, 2012; Hedaoo *et al.*, 2015; Lauwens *et al.*, 2018), however, some of these authors observed a lower deflection on specimens where no cyclic load was applied.

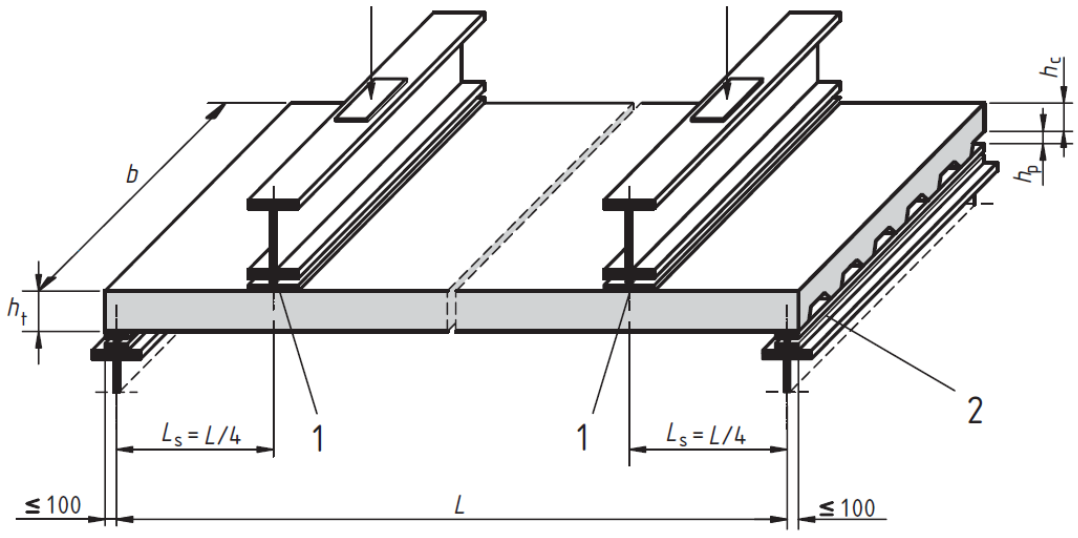

1 · Neoprene pad or equivalent ≤ 100 mm x *b*
2 · Support bearing plate ≤ 100 mm x *b* x 10 mm (min)

Fig. 2.3 Test set-up according to standard EN 1994-1-1 (CEN, 2004b)

Several research studies about the behaviour of steel-concrete continuous composite slabs have also been carried out (Abas *et al.*, 2013; Chen, 2003; Gholamhoseini, 2018; Gholamhoseini *et al.*, 2016). Continuous composite slabs are tested to study the behaviour of these elements in the hogging moment region, where the profiled steel sheeting is mainly under compression. Usually, tests to continuous slabs comprise 4 linear loads applied over the 2 spans – 2 linear loads in each span, and 3 supports. Fig. 2.4 shows the experimental campaign carried out by Gholamhoseini (2018).

Fig. 2.4 Bending test to continuous composite slabs (Gholamhoseini, 2018)

(ii) Small-scale tests

In order to study the behaviour of steel-concrete composite slabs and the resistance of developed reinforcing systems, small-scale test programmes are usually carried out. Small-scale test is the term assigned to experimental tests on specimens with reduced dimensions – usually just one rib/module – compared with full scale tests. This type of tests is useful to reduce the time necessary to produce the specimens, their storage space or the experimental campaign costs – aspects which usually discourage the research on steel-concrete composite slabs. The main limitation of small-scale tests is that they only allow to evaluate the longitudinal shear behaviour of composite slabs. Small-scale tests are appropriate to study the resistance of the shear bond of composite slabs and to study very specific/local effects on it. There are three main types of small-scale tests: slip-block; pull-out and; push-out.

Slip-block tests were developed by Patrick (1993) and Patrick and Bridge (1993, 1994). This is a test performed in a small specimen to simulate the conditions of a longitudinal shear failure. The specimen of a slip-block test typically comprises just one module of a composite slab and a length of 300 mm. Slip-block tests allow to obtain the friction coefficient μ and the ultimate shear stress τ_u by application of a constant vertical force V, perpendicular to the ribs direction, and one horizontal force H, in the direction of the ribs,

which increases until the failure of the specimen, as illustrated on Fig. 2.5(a). Fig. 2.5(b) shows the equipment and layout adopted by Ganesh *et al.* (2005) to evaluate the shear bond capacity of composite slabs by slip-block tests. Holomek *et al.* (2016) studied the effect of the way of application of the clamping force and recommended some values for the minimum loading speed: 0.2 mm/min until 2.5 mm of displacement, 0.8 mm/min until 10 mm of displacement and 5.0 mm/min until the end of the test (Holomek *et al.*, 2012; Holomek *et al.*, 2017; Holomek *et al.*, 2016).

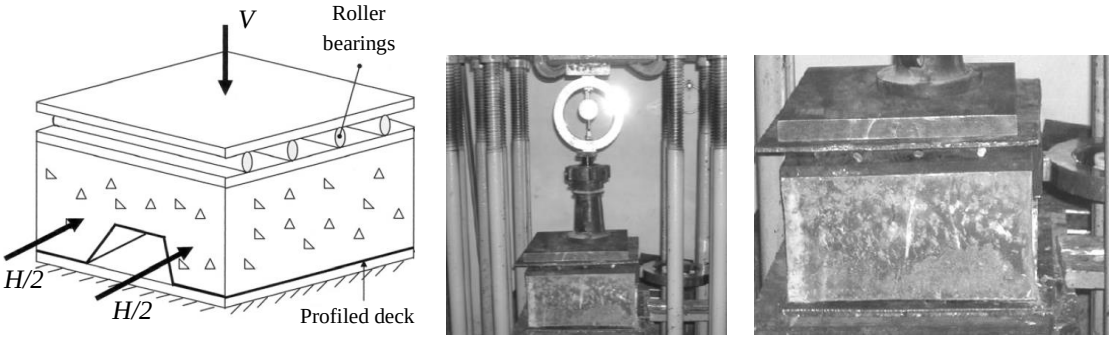

(a) layout test (b) equipment (c) specimen

Fig. 2.5 Slip-block tests carried out by Ganesh *et al.* (2005)

The pull-out test was developed by Daniels (1990) and makes it possible to obtain the stress-slip *τ-s* curve for each type of profiled steel sheet to define the connection between the steel sheeting and the concrete. Specimens for these tests comprise one module of two profile steel sheeting, placed back-to-back and bolted to a steel plate placed between them, and a concrete part connected to each sheeting (Fig. 2.6(a)). The test starts with the application of a lateral force *F* on the concrete blocks to prevent them from completely separating from the sheet and to simulate a normal force at the interface. Then, a tensile force *P* is applied to the sheeting. The main output of this test is the load-slip *P-s* curve, being the experimental layout described in Fig. 2.6(b).

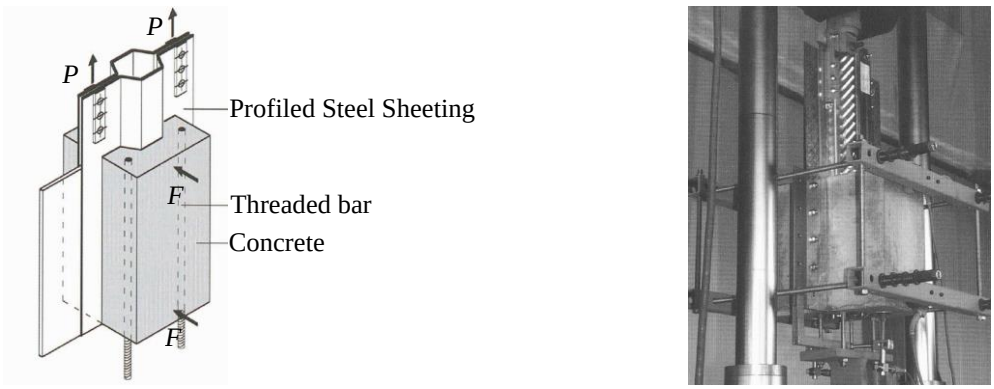

(a) pull-out specimen (b) experimental layout

Fig. 2.6 Pull-out test (Crisinel *et al.*, 2002)

Push-out tests are defined by two profiled steel decks connected to a concrete block. The length of steel decks is higher than the concrete length so it can be possible to push the concrete over the steel sheeting. The specimens are supported just in the profiled steel decking and the load is longitudinally applied in the concrete top surface, so all forces can be transferred from the concrete to the profiled steel decking. No lateral forces are applied in this type of test. According to Burnet and Oehlers (2001), push-out tests without lateral loads applied would be more efficient. Fig. 2.7 shows some examples of experimental layouts that have been adopted in push-out test without lateral forces acting on the profiled steel sheeting. Burnet and Oehlers (2001), based on the experimental layout developed by Porter and Ekberg (1978), carried out an experimental program of 33 push-out tests of this type. Push-out test allows to define the main parameters to characterize the chemical and mechanical bond between steel and concrete.

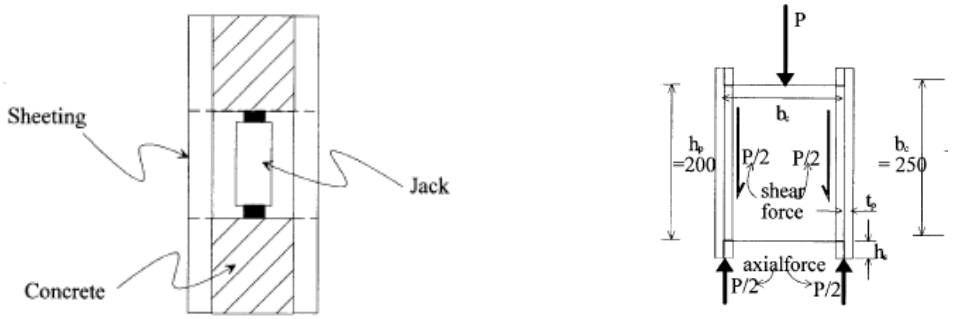

(a) Porter and Ekberg (1978) (b) Burnet and Oehlers (2001)

Fig. 2.7 Push-out tests without lateral forces

2.2.3 Developed reinforcing systems

As it was said before, the behaviour of composite slabs needs to be enhanced by some type of interlock system to prevent the separation on the steel-concrete interface. The most used systems to improve the longitudinal shear behaviour are the embossments pattern rolled on the profiled steel sheeting (mechanical interlock) and headed studs welded in the supports through the profiled steel sheeting. To take better advantage of the high bending capacity of composite slabs, several researchers have been studying these mechanisms and developing new ones to improve the longitudinal shear behaviour of steel-concrete composite slabs, the main ones being reviewed in the following paragraphs.

Porter and Greimann (1984) carried out one of the first experimental studies to analyse the influence of end anchorage systems on steel-concrete composite slab resistance. These authors carried out an experimental programme comprising 15 prototypes of composite slabs with or without end anchorage devices constituted by end-span studs, in order to

determine the percentage of load increase by comparing the prototypes without studs with the prototypes with studs. The test results showed that the inclusion of end studs increased the bearing load capacity of those composite slabs by 8 to 33%.

Later, Jolly and Lawson (1992) carried out an experimental study to evaluate the influence of end anchorage device in the capacity of composite slabs. The applied device was provided by headed studs welded through the profiled steel sheeting in the supporting beams. The authors carried out an experimental programme composed by composite slabs with and without end anchorage reinforcement. The obtained experimental results allowed to observe the following: composite slabs with end anchorage system achieved a capacity 2 times higher than composite slabs without it; the acquired stiffness provided by the embossments in the profiled steel sheeting was higher than acquired stiffness provided by studs. So, these researchers proposed that only half of the resistance of the studs would be accounted in the design.

Calixto *et al.* (1998) presented an experimental investigation on the behaviour of simply-supported composite slabs. The authors tested composite slab specimens with different types of profiled steel decking, including different embossment patterns. The authors also studied the effect of headed studs as end anchorage. The experimental results showed that the headed studs welded at the supports improved significantly the composite slab behaviour. The role of the embossments on the profiled steel sheeting was found to be relevant for the longitudinal shear capacity; according to Calixto *et al.* (1998), the contribution of each type of interlock mechanism makes a contribution to the global capacity and behaviour of the slab.

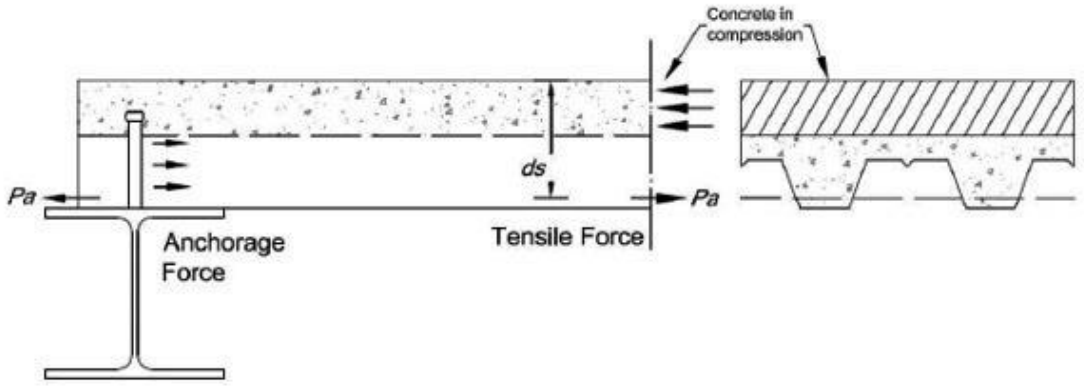

Fig. 2.8 End anchorage in composite slabs

Chen (2003) tested 7 simply supported one-span and 2 continuous composite slabs – Fig. 2.9 – with different end restraints to evaluate the influence of the shear bond action on the composite behaviour. The results obtained showed that the slabs with end anchorage

were found to have a higher longitudinal shear bond resistance than the slabs without end anchorage. The author also noticed that the composite slabs without end anchorage devices showed a brittle behaviour, unlike those with end anchorage systems that showed a ductile behaviour.

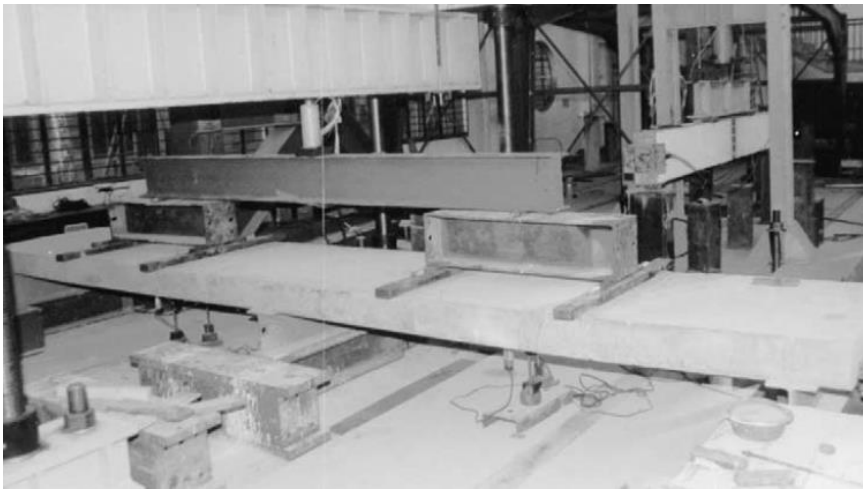

Fig. 2.9 Bending test to a continuous composite slab (Chen, 2003)

Several papers were published to present the behaviour of steel-concrete composite slabs based on experimental and numerical results (Crisinel *et al.*, 2006; Ferrer and Crisinel, 2005; Ferrer *et al.*, 2006; Ferrer *et al.*, 2004; Ferrer *et al.*, 2005). Ferrer *et al.* (2005) carried out experimental and numerical studies to understand the effect of several geometrical parameters on the shear bond resistance, such as: the embossing slope, the thickness of the sheet, the embossment depth, the profiling angle and the embossment inclination, illustrated on Fig. 2.10. Numerical models were validated by the experimental results of a programme composed by pull-out and full-scale bending tests. The parametric study made it possible to optimize the behaviour of the slab and to develop a new steel-sheet design method.

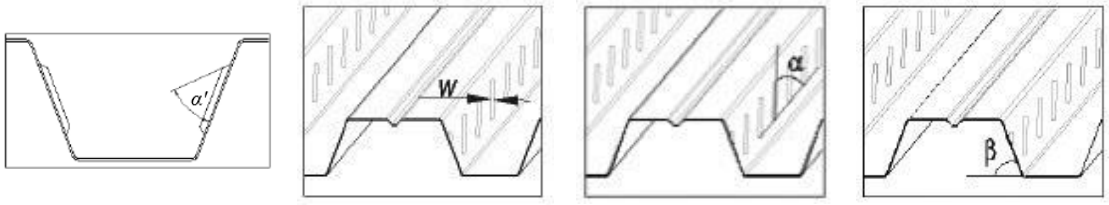

(a) embossment slope α' (b) embossment width w (c) embossment slope α (b) web slope β

Fig. 2.10 Parameters evaluated by Ferrer *et al.* (2005)

Numerical results obtained from the research studies referred in the previous paragraph are shown in Fig. 2.11. These results allowed to conclude that the longitudinal shear

capacity increases when: (i) the slope between the web plane and the embossment α' is higher; (ii) the embossments width w is higher; (iii) higher angles of the embossments with the horizontal plane α; the slope of the web β is increased. However, if the embossments slope α' is overly increased the ductility of the slab could be lost and the slab could collapse in a brittle way. Furthermore, if the embossment slope α is too high, then more energy would be necessary in the fabrication process. The authors also evaluated the influence of the embossments direction. The results obtained showed that alternated embossing is more effective, since shear resistance becomes similar in both directions and so the sliding effect becomes more uniform and higher.

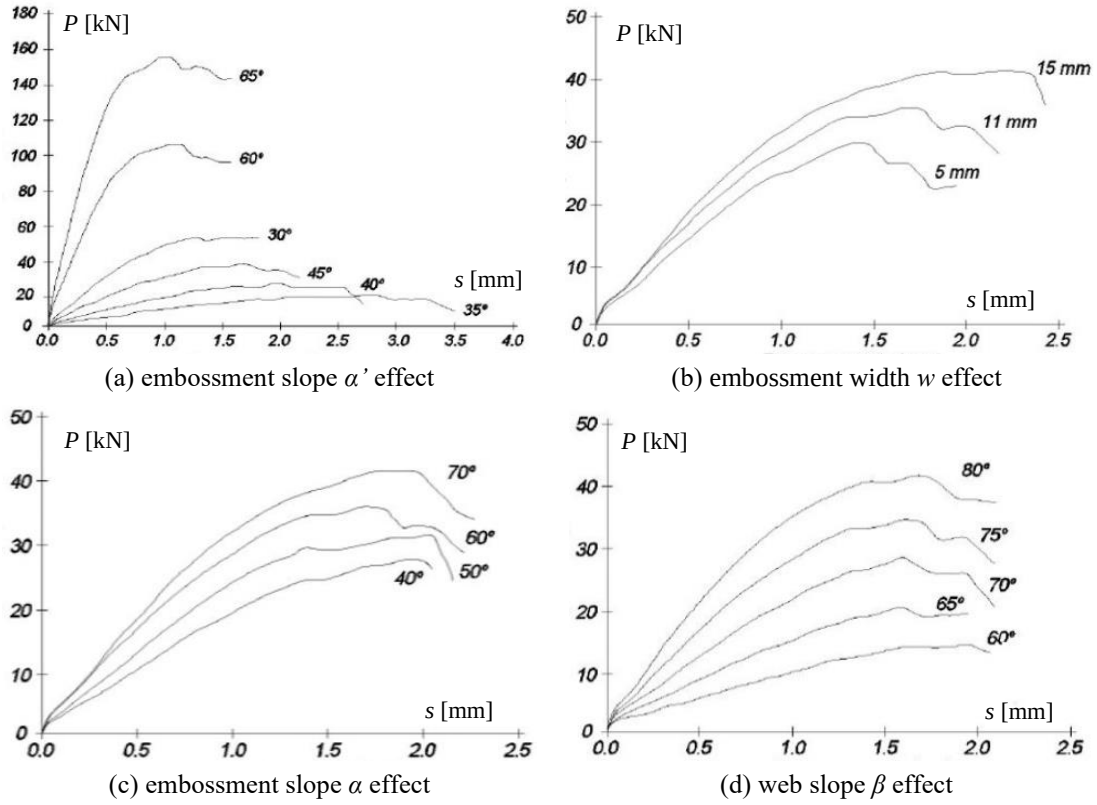

(a) embossment slope α' effect (b) embossment width w effect

(c) embossment slope α effect (d) web slope β effect

Fig. 2.11 Experimental results obtained by Ferrer *et al.* (2005)

Chuan *et al.* (2008) performed an experimental programme to test composite slabs using shear screws in order to improve their longitudinal shear resistance (see Fig. 2.12). The authors carried out an experimental programme composed by 12 bending tests on composite slabs with and without shear screws. The obtained results showed that the shear screws increased the load carrying capacity and the ductility of the slab. The obtained results also allowed to conclude that the reinforcing system is more effective for slender slabs and shear screws did not influence the stiffness of the slab. El-sayed *et al.* (2015) also carried out an experimental programme composed by 14 push-out tests to study the effect of self-drilling screw as shear connectors and has found similar conclusions.

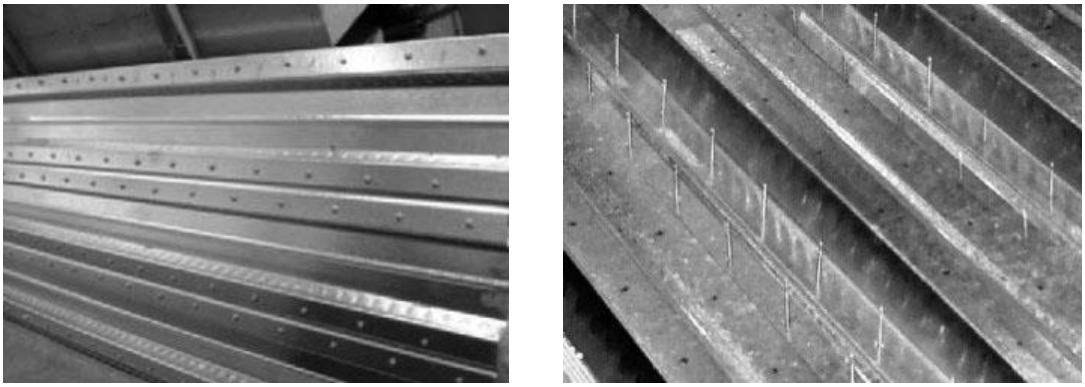

Fig. 2.12 Composite slabs with shear screws (Chuan *et al.*, 2008)

Some other researchers (Ahmed *et al.*, 2019; Salonikios *et al.*, 2012; Saravanan *et al.*, 2012) have been carrying out experimental programmes in accordance with standard EN 1994-1-1 (CEN, 2004b) to evaluate the longitudinal shear resistance of composite slabs with specific steel sheet profiles. These authors tested 6 composite slabs for each profile to obtain the *m* and *k* values to allow the design of composite slabs for longitudinal shear using the *m*-*k* method in accordance with standard EN 1994-1-1 (CEN, 2004b).

Chen *et al.* (2011) carried out an experimental program of 13 simply-supported composite slabs to study the influence of: the span length, the height of the slab, the shear span and the headed studs resistance. All slabs collapsed by longitudinal shear. The authors observed the behaviour of those slabs during the tests and noticed that the slip between the profiled steel sheeting and the concrete grew after the first cracks formed in the bottom region of the concrete. Chen *et al.* (2011) also observed that the longitudinal shear stress τ_u is not constant over the span. The longitudinal shear stress is significantly higher in the shear spans. Taking this phenomenon in consideration, they concluded that the main resistance to the longitudinal shear stress is provided in the shear span. Later, Chen *et al.* (2014) complemented the previous study with a numerical study founding the same conclusions and validating the numerical model previously proposed.

Some studies also have been developed to evaluate the behaviour and resistance of steel-concrete composite slabs reinforced by steel fibres (Abas *et al*., 2013; Ackermann and Schnell, 2008; Altoubat *et al.*, 2015; Gholamhoseini *et al*., 2016; Li, Zheng *et al.*, 2019). Abas *et al.* (2013) studied the effect of steel fibre reinforcing concrete on continuous composite slabs with deep trapezoidal steel sheeting. The authors carried out an experimental programme composed by 8 tests of two-span continuous composite slabs with or without steel fibres to study the influence of the quantity of steel fibre on the developed cracks, on the redistribution of the bending moments, on the end slip and on the bearing capacity. 7 point bending tests were performed by application of 2 linear loads

in each span at a distance of 1135 mm from the supports, as it is illustrated on Fig. 2.13. The slabs were supported by two external roller supports and a pinned intermediate support. Three different dosages of steel fibres with 60 mm long were loaded (20, 30 and 40 kg/m^3) and also one slab with 30 kg/m^3 of steel fibres with 35 mm long was tested. The authors concluded that the presence of steel fibres in those composite slabs allowed to increase the slip load and the peak load. The authors observed that the slabs with a 20 kg/m^3 steel fibre density reached a slip load, peak load and ratio of slip load to peak load 59, 34 and 75%, respectively, higher compared with the slabs without steel fibre reinforced concrete. Yet, authors also observed that the increase of the steel fibres density did not influence significantly the behaviour and the resistance of the slab.

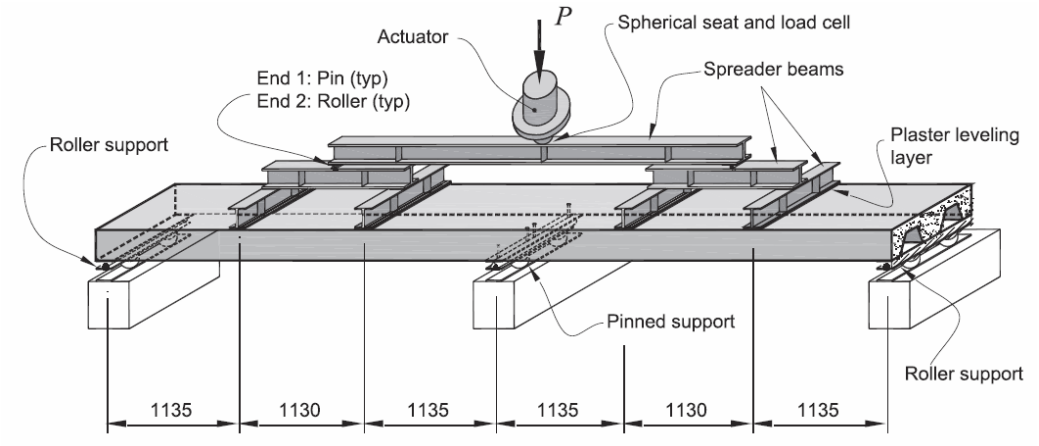

Fig. 2.13 Experimental layout (Abas *et al.*, 2013)

Altoubat *et al.* (2015) evaluated the influence of fibres and welded-wire mesh reinforcements on the diaphragm behaviour of steel-concrete composite slabs. A set of twelve tests was carried out consisting on the application of a horizontal load on cantilever composite slabs, as it is shown on Fig. 2.14. The slabs were supported by rollers on the bottom side and the load was applied and fixed to a supporting steel beam on the top side. The specimens had different types of secondary reinforcement: varying the type (synthetic or steel) and dosage of the fibres or the type of the weld-wire mesh. The orientation of the specimens was also studied: eight slabs with the ribs perpendicular to the main beam and four slabs with ribs parallel to the main beam (strong and weak orientation, respectively, according to the authors). Two of the specimens (one for each direction) did not contain any type of secondary reinforcement in order to be considered as a reference. The authors observed that slabs tested with a strong orientation developed a diagonal cracking pattern, while those with a weak orientation developed cracking in the thinner parts of the slab and achieved lower ultimate loads. The authors concluded that fibres increased the in-plane shear capacity by up to 50 %, when compared to slabs without secondary reinforcement.

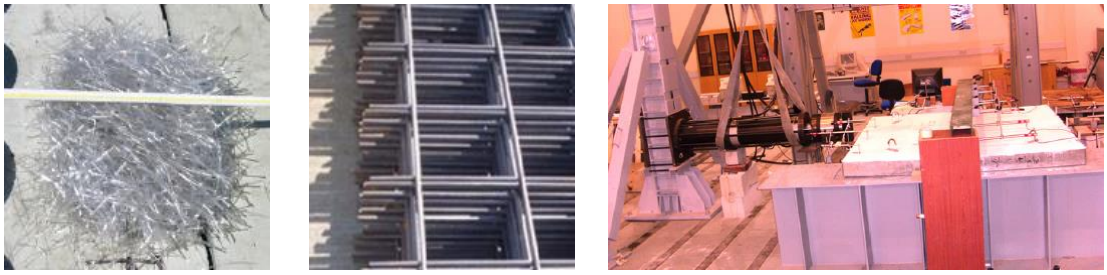

(a) synthetic macro-fibres (b) weld-wire mesh (c) experimental layout

Fig. 2.14 influence of fibres and welded-wire mesh in composite slabs (Altoubat *et al.*, 2015)

In the University of Coimbra, Fonseca *et al.* (2015), based on the study started by Carmona *et al.* (2009), improved the longitudinal shear resistance of composite slabs using transversal bars crossing the profiled steel sheeting at the middle height of the webs in the support cross-sections; this system behaves in a similar way to an end anchorage device constituted by welded studs (see Fig. 2.15(a)-(b)).

The authors performed two experimental programmes: one small-scale specimen experimental programme to develop an equation to determine the resistance provided by the new end anchorage system and one full-scale specimen experimental programme to analyse its influence on the behaviour of simply supported composite slabs. The second experimental programme comprised 8 tests of composite slabs with or without transversal bars in the support cross-sections and longitudinal bars on the concrete ribs. Each type of specimen with cross-sections illustrated on Fig. 2.16 was repeated two times. The failure mode of the specimens containing the end anchorage system was the bearing of the steel sheeting, as shown in Fig. 2.15(c). The achieved results showed that the proposed alternative end anchorage system increased the capacity and ductility of the slab. However, the authors noted that the production of the steel sheet and the erection on site would be the main disadvantages of the system.

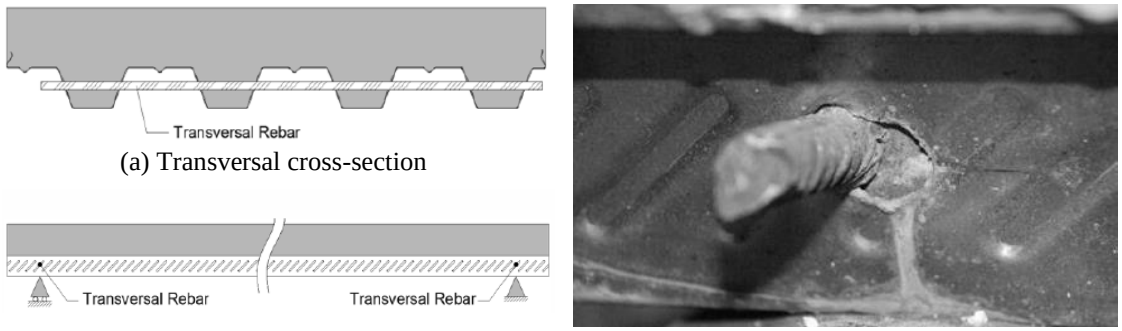

(a) Transversal cross-section

(b) Side view (c) Bearing of the steel sheeting

Fig. 2.15 End anchorage using transversal bars (Fonseca *et al.*, 2015)

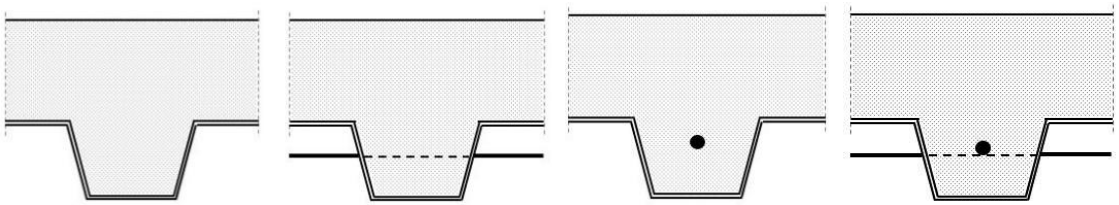

(a) A_{11} & A_{12} (b) A_{21} & A_{22} (c) A_{31} & A_{32} (b) A_{41} & A_{42}

Fig. 2.16 Cross-section in different specimens

Regarding the development of the equation to take into account the resistance provided by the end anchorage system, this research comprised a statistical analysis comparing the theoretical resistance of each contact point with the experimental results obtained in the first experimental programme.

This reinforcing system could fail by two different modes: the shear failure of the reinforcing bar and the bearing capacity of the profiled steel sheeting. According to the authors, the shear resistance of the bar would be given in the same way as the bearing capacity of a bolt loaded in shear in a bolted joint, in accordance with Table 3.4 of standard EN 1993-1-8 (CEN, 2005c). The bearing capacity of the steel sheeting $F_{b,Rd}$ when a screw is loaded in shear is given in Table 8.2 of standard EN 1993-1-3 (CEN, 2006a). For current applications – profiled steel sheeting thickness between 0.7 and 1.5 mm and bar diameter higher than 8 mm – the reinforcing system is influenced by the bearing capacity of the steel sheeting. So, comparing the experimental results of the first experimental programme comprised by small-scale specimens under compression with the theoretical resistance values defined by the bearing capacity of the steel sheeting $F_{b,Rd}$ and; applying statistical method (a) available on Annex D of standard EN 1990 (CEN, 2002a), the authors obtained the design value of the resistance of one contact point in the end anchorage system, which is expressed in Eq. (2.1). The design resistance value of the end anchorage system could be used in the partial connection method increasing the horizontal compression force in concrete N_c, according to clause 9.7.4(2) of standard EN 1994-1-1 (CEN, 2004b).

$$F_{b,Rd} = 0.5784 \frac{2.5\alpha_b k_t f_u dt}{\gamma_{M2}} \tag{2.1}$$

where:

- α_b is the minimum value between 1.0 and $e_1/(3d)$;
- e_1 is the distance of the bar to the end of the steel sheeting;
- d is the bar diameter;
- k_t is a coefficient influenced by the thickness t;
- f_u is the ultimate strength of the profiled steel sheeting;

t is the thickness of the steel sheeting;

γ_{M2} is the partial safety factor, such that $\gamma_{M2} = 1.25$.

Several studies have been developed comprising experimental and numerical studies to analyse the behaviour of composite slabs with headed studs (Johnson and Yuan, 1998; Kim *et al.*, 2001; Lloyd and Wright, 1990; Qureshi and Lam, 2012; Rana *et al.*, 2015; Swaminathan *et al.*, 2016). These studies have been allowed to conclude that the strength of the concrete and the thickness of the profiled steel sheeting significantly influence the capacity of composite slabs. The obtained experimental results also showed that the shear-bond capacity of the composite slab is mainly governed by the shear-bond stress-slip between the two materials and less by the resistance of the studs.

Also Bezerra *et al.* (2018) tried to improve the longitudinal shear capacity of composite members. These researchers developed a new V-shaped shear connector as an alternative to headed studs (see Fig. 2.17). It was designed to be used in steel-concrete composite beams. However, in the same way as headed studs, they could also be used in composite slabs, being welded through the profiled steel sheeting with a stud-welding equipment. According to the authors, the new shear connector developed provides a larger frontal contact area and is easier to install. The efficiency of this connector was validated by the results of an experimental campaign of push-out tests and a numerical study. A design model was also developed to allow designers to take their contribution in consideration in the design. According to the obtained results, it was concluded that V-shaped connectors allowed to reduce the concentration of stresses around the connector and increase the longitudinal shear capacity.

(a) Connector dimensions (b) V-shaped connector (c) Numerical model

Fig. 2.17 V-shaped connectors (Bezerra *et al.*, 2018)

More recently, Ferrer *et al.* (2018) presented an innovative full-connection bonding mechanism, defined by small crown-shaped cuttings bands produced in the webs of the profiled steel sheeting as a replacement of the embossments, named as UPC-System and shown on Fig. 2.18. The researchers carried out an experimental campaign comprising several tests of composite slabs with three different commercial trapezoidal profiles, from

60 to 80 mm height, having the UPC-System or embossments on the webs of the profile. The authors also tested different densities of punching (low, medium or high) and two different steel sheet thickness. The results allowed to observe that those slabs with the UPC-System achieved the full connection between the steel sheeting and concrete until the final failure without significant slip. The UPC-System also allowed to increase the ultimate load.

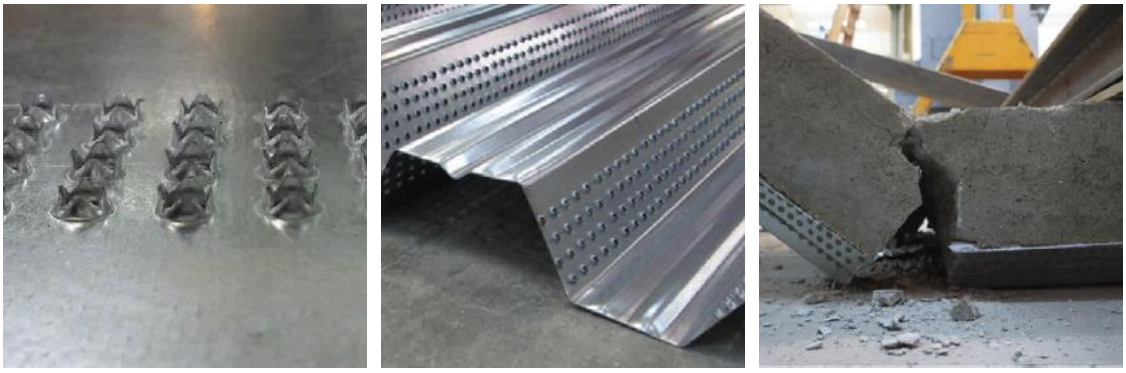

(a) Crown-shaped cuttings (b) Punched profile (c) Bending failure

Fig. 2.18 UPC System (Ferrer *et al*., 2018)

Perfobond shear connectors are also a type of reinforcing system usually applied to improve the longitudinal shear behaviour of composite members, but mainly in steel-concrete composite beams. Nevertheless, Yang *et al.* (2018) studied the behaviour of steel-concrete composite slabs with flat horizontal steel sheeting and perfobond shear connectors – see Fig. 2.19. Flat steel sheeting saves money in moulding equipment and is easier to transport but also requires a greater thickness to compensate for the loss of bending stiffness when compared to profiled ones. Yang *et al.* (2018) tested two series of three composite slabs, both with flat steel sheeting and perfobond shear connectors. A thickness of 6 mm was used for the steel plates. The authors tested composite slabs with two different spans (3400 and 2400 mm for series 1 and 2, respectively) and three different amounts of transversal bars. All slabs failed by bending with yielding of the steel plate and the connectors. The authors concluded that full connection was achieved because no significant slip occurred between the steel plate and connectors and the concrete. The authors established a calculation approach based on the experimental results and validated it.

Xu *et al.* (2018) also studied the effect perforated steel ribs in composite slabs under negative bending moments. The authors carried out an experimental programme composed by 6 tests to composite slabs with different shear connectors and amount of steel reinforcing bars. Bended bars, perforated flat ribs and perforated L-shaped ribs were welded to the profiled steel plate, as is shown on Fig. 2.20. The specimens were supported

in the middle section (rib region) and in one of the ends; a linear descending load was applied in the non-supported end. The experimental results allowed to conclude that perforated L-shaped ribs reduce the shear crack risk and increase the load-carrying capacity of composite slabs compared to flat perforated ribs.

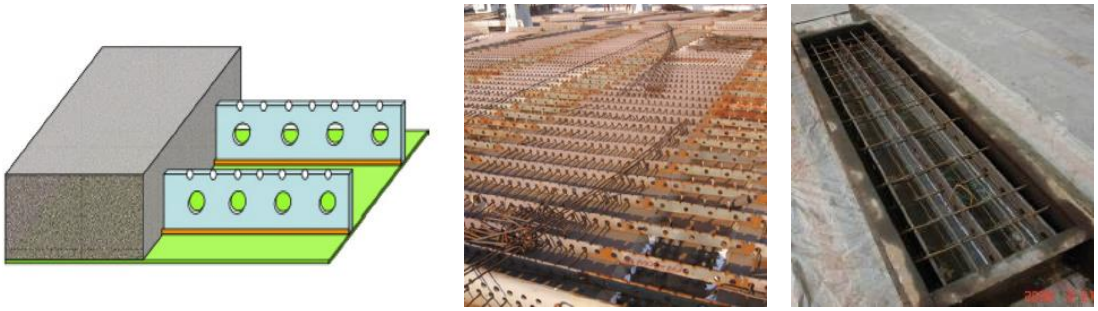

(a) Perfobond connectors in composite slabs (b) Application in Donping bridge (c) Specimen – steel part

Fig. 2.19 Perfobond connectors in composite slabs with flat steel sheeting (Yang *et al*., 2018)

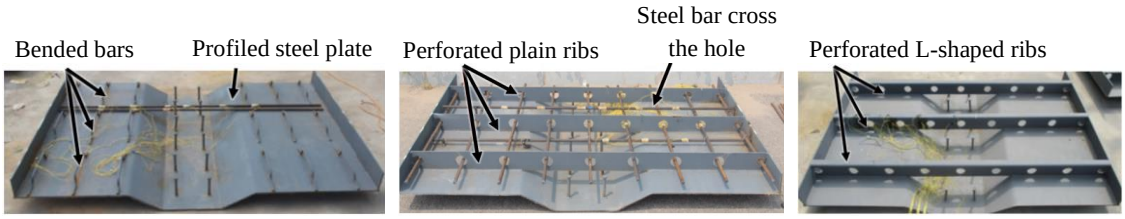

(a) Bended bars (b) Perforated plain plate (c) Perforated L-shaped plate

Fig. 2.20 Contribution of perforated reinforcing elements for composite slabs under negative bending (Xu *et al*., 2018)

Xu *et al*. (2018), for this type of reinforcement, also proposed a method to account the contribution of these elements in bending and shear strength of composite slabs: the bending resistance of the composite slab M_{Rd} could be defined according to Eq. (2.2) and the vertical shear resistance of the slab V_{Rd} can be defined according to Eq. (2.3).

$$M_{Rd} = M_{RC} + M_{Steel} \tag{2.2}$$

$$V_{Rd} = V_{cr} + V_{rib} \tag{2.3}$$

$$V_{cr} = \sqrt{f_c'}bh_0 / 6 \tag{2.4}$$

where:

M_{Rd} is the design ultimate sectional bending moment of the concrete slab according to the Chinese design code for reinforced concrete member (MHURCPRC, 2015);

M_{Steel} is the ultimate sectional bending moment of steel member defined as $f_y W_{pl}$;

V_{cr} is the vertical shear resistance of the concrete part.

In the Polytechnic University of Catalonia some researchers developed a study to evaluate the behaviour of composite slabs with ferritic stainless steel to understand the effect of this type of steel (Arrayago *et al.*, 2018; Arrayago *et al.*, 2019; Lauwens *et al.*, 2018). Stainless steel decks are not frequently applied on steel-concrete composite slabs, yet their mechanical properties, corrosion resistance and emissivity make them a good alternative to regular galvanized steel decks.

Arrayago *et al.* (2019) carried out an experimental programme to test ferritic stainless steel trapezoidal decks under different loading and supporting conditions (Fig. 2.21(a)). The experimental results were compared with: (i) the predicted loads defined according to standard EN 1993-1-4 (CEN, 2006b); (ii) previous experimental results obtained by Blaβ and Saal (2006) on galvanized carbon steel profiled steel sheeting with similar cross-section and; (iii) the resistance values according to standard EN 1993-1-3 (CEN, 2006a). The experimental results showed that the design formulas from standard EN 1993-1-3 (CEN, 2006a) could be applicable, with a few changes, to predict the ultimate load of ferritic stainless steel trapezoidal decks. The authors also compared these results with previous results from tests to galvanized carbon steel decks and found similar values for the capacity of both types of steel.

Arrayago *et al.* (2018) executed an experimental campaign comprised by short and long span composite slabs to obtain the parameters of the longitudinal shear resistance of steel-concrete composite slabs with ferritic stainless steel (Fig. 2.21(b)). These authors developed the bending tests according to EN 1994-1-1 (CEN, 2004b) in order to obtain m, k and $\tau_{u,Rd}$ parameters and compare the behaviour observed with the one of steel-concrete composite slabs with galvanized carbon profiled steel sheeting. The obtained results showed that he ultimate load does not vary significantly by changing the type of deck to a ferritic stainless steel, but the slip start occur earlier, because stainless steel present less roughness on its surface.

Lauwens *et al.* (2018) focused their research in the longitudinal shear failure of steel-concrete composite slabs (Fig. 2.21(c)). Composite slabs testes were composed by ferritic stainless steel decks. The authors performed an experimental campaign according to standard EN 1994-1-1 (CEN, 2004b) to obtain the $\tau_{u,Rd}$ parameter which allows to design composite slabs to longitudinal shear with partial connection method. This research allowed to conclude that the capacity of composite slabs with ferritic stainless steel decks is similar to capacity of composite slabs with galvanized profiled steel sheeting. So, this research allowed to observe that it is possible to combine concrete with stainless steel sheeting in the same structural element and this should be considered as an alternative.

(a) Continuous deck test (Arrayago *et al.*, 2019)

(b) Experimental setup (Arrayago *et al.*, 2018)

(c) Longitudinal shear failure (Lauwens *et al.*, 2018)

Fig. 2.21 Experimental tests on composite slabs with ferritic stainless steel decks

2.3 Design methodologies for steel-concrete composite slabs

End-anchorage devices, especially when combined with other reinforcing systems that provide the shear stress transfer, are crucial to define the longitudinal shear resistance, ductility and stiffness of composite members. Over the years, some studies have been carried out to develop design methodologies for steel-concrete composite slabs with end anchorage systems (Degtyarev, 2014a, 2014b).

For example, Crisinel and Edder (2006), Crisinel and Marimon (2004) and Crisinel *et al.* (2002) developed an analytical simplified method based on the moment-curvature M-φ at the most critical section of composite slabs. The simplified method was developed based on the experimental results of pull-out tests campaign. Lopes and Simões (2008) also validated this new method according to an experimental programme carried out. According to the authors, this method can be used to check the safety at ULS in a simple, safe and economical way. The Fig. 2.22(a) shows the M-φ curve predicted using the method which is defined by 3 main phases:

- Phase I – linear elastic behaviour without concrete cracking and without slip (total interaction);
- Phase II – elastic or elasto-plastic behaviour with concrete cracking and without slip (total interaction);
- Phase III – non-linear elasto-plastic behaviour with concrete cracking and slip (partial interaction).

The three phases are limited by 3 characteristic points:

- Point 1 – start the concrete cracking;

- Point 2 – initiation of the slip between the profiled steel sheeting and the concrete; the maximum shear stress due to chemical interlock is achieved; for steel-concrete composite slabs with a brittle behaviour this point represents the collapse moment;
- Point 3 – the bending moment resistance is achieved, based on the longitudinal shear stress resistance provided by the reinforcing systems.

Fig. 2.22(b) shows the comparison between experimental and analytical results for a steel-concrete composite slabs with a longitudinal shear ductile behaviour. The authors also made the same comparison for composite slabs showing a brittle behaviour and in both situations the results provided by the simplified method seemed to be very accurate. These method was also validated by experimental results obtained from full-scale bending tests.

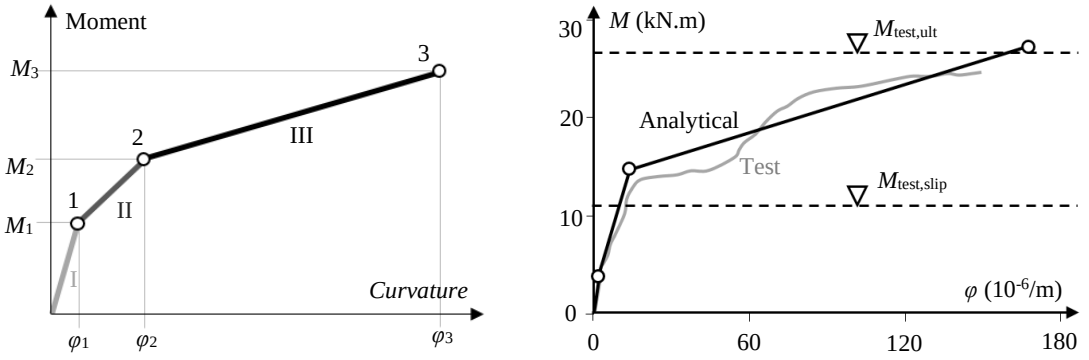

(a) M-φ curve (adapted from Crisinel and Edder, 2006)

(b) comparison between experimental and analytical results for ductile behaviour (adapted from Crisinel and Marimon, 2004)

Fig. 2.22 New method to predict the M-φ behaviour of composite slabs

Abdullah and Easterling (2009) developed and proposed a new method to model the horizontal shear connection between the profiled steel sheeting and the concrete for composite slabs. This method was based in one developed by An (1993), but without fixing the moment arm and the block bending test. This method was called Force Equilibrium Method and allowed to predict the curve load-slip in bending tests of steel-concrete composite slabs. These authors carried out and experimental campaign comprised by 30 specimens divided in 15 types to validate the proposed method. Force Equilibrium Method is based on Eq. (2.5), which defines the shear bond force F. The ultimate longitudinal stress resistance obtained from the experimental results according to partial connection method τ_u was compared with the one obtained from Force Equilibrium Method. The comparison showed that Force Equilibrium Method allows to predict accurate results in the conditions tested.

$$F = T = \frac{\frac{P}{2} L_s - M_r}{z} \tag{2.5}$$

where:

- T is the axial force in the steel deck;
- P is the total applied load;
- L_s is the shear span;
- M_r is the remaining bending resistance in the steel deck given by Eq. (2.6);
- z is the moment arm between tension and compression force;
- δ_1,δ_2 are the vertical displacement values in the loading points (Fig. 2.23);
- E_s is the modulus of elasticity of the steel;
- I_p is the moment of inertia of the profiled steel sheeting.

$$M_{ri} = \frac{\delta_1 + \delta_2}{L_s (L - 2L_{s)}} E_s I_p \tag{2.6}$$

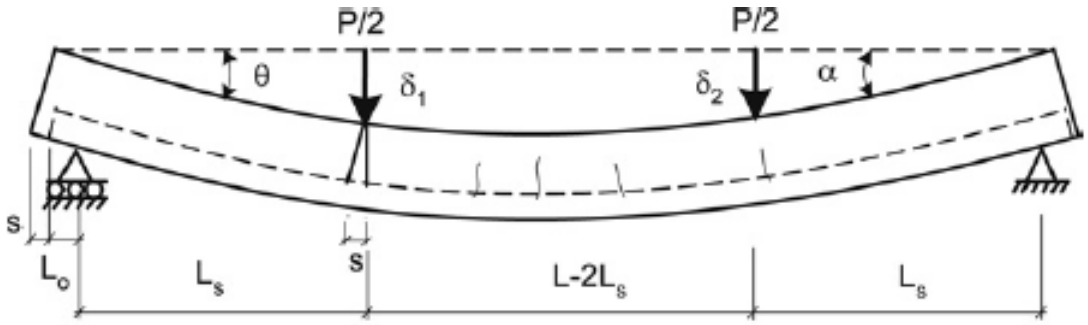

Fig. 2.23 Slab under cracking at cracking mode (Abdullah and Easterling, 2009)

Recently, Ahmed *et al.* (2019) developed a new approach to design steel-concrete composite slabs for longitudinal shear. The new method was inspired on *m*-*k* method and authors called it as *λ*-*q* method. According to the experimental results obtained by these authors, the longitudinal shear resistance can be over-estimated because of the friction between the concrete and the profiled steel sheeting.

According to these authors, *λ*-*q* method can lead to a new approach taking into account the contribution of embossments, shear connectors, slip and the shape factor on the longitudinal shear capacity of composite slabs.

2.4 Vertical shear behaviour and design of composite slabs

2.4.1 Previous studies

According to standard EN 1994-1-1 (CEN, 2004b), the vertical shear resistance of composite slabs is mainly provided from the concrete rib. However, Johnson (2018) assumes that the Eurocode design model is conservative because, in general, it ignores the real contribution of the webs of the steel sheeting. The profiled steel sheeting just contributes positively to the vertical shear resistance of composite slabs when they act in tensile and extend more than $l_{b,\min} + d_p$ beyond the section considered. However, the contribution of the steel sheeting is based only on its area and not on its shape. A profiled steel sheet has a significant vertical shear resistance, mainly provided by the webs of the profile. This significant contribution is the only one in the constructive phase, when the steel sheet supports the wet concrete and constructive loads without, or with a reduced number of temporary supports. Therefore, the vertical shear resistance model of Eurocode 4 (CEN, 2004b) tends to be very conservative, leading, in some situations, to an over-dimensioning of composite slabs.

Standard EN 1994-1-1 (CEN, 2004b) defines that the vertical shear sectional resistance of a composite slab module is mainly defined by the resistance of the rectangle with a width equal to the average width of the rib b_0 and a height defined between the centroidal axis of the steel sheet and the top fibres of the slab d_p, as it is illustrated in Fig. 2.24.

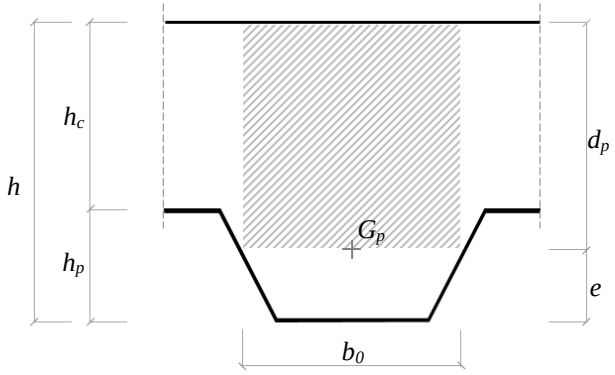

Fig. 2.24 Concrete area considered for the vertical shear resistance of composite slabs according to Eurocode 4

Patrick (1993) has carried out a large group of tests for steel-concrete composite slabs subjected to a vertical linear load placed at a distance of $1.5d_p$ from the support, where d_p

is the effective height of the slab defined by the distance between the centroidal axis of the profiled steel sheeting and the top fibres of the composite slab in compression (see Fig. 2.25). Patrick (1993) noticed that these composite slabs did not achieve the vertical shear resistance before its full plastic bending capacity. Liang (2015) supplied different methodologies for the calculation of the vertical shear resistance of a composite slab, including the one prescribed in Eurocode 4 (CEN, 2004b), but without any type of comparison between them. Therefore, Liang (2015) presented the vertical shear resistance of a cross-section of a simply supported composite slab φV_{uc} defined according to the design moment capacity of the composite slab φM_u where the load is applied, as expressed in Eq. (2.7).

$$\varphi V_u = \frac{\varphi M_u}{1.5\left(d_p - y_p\right)} \tag{2.7}$$

where:

φ is the capacity reduction factor, such that $\varphi = 0.8$;

y_p is the height of the profiled steel sheeting at which the tensile force N_p ($A_p \cdot f_{yp}$) acts.

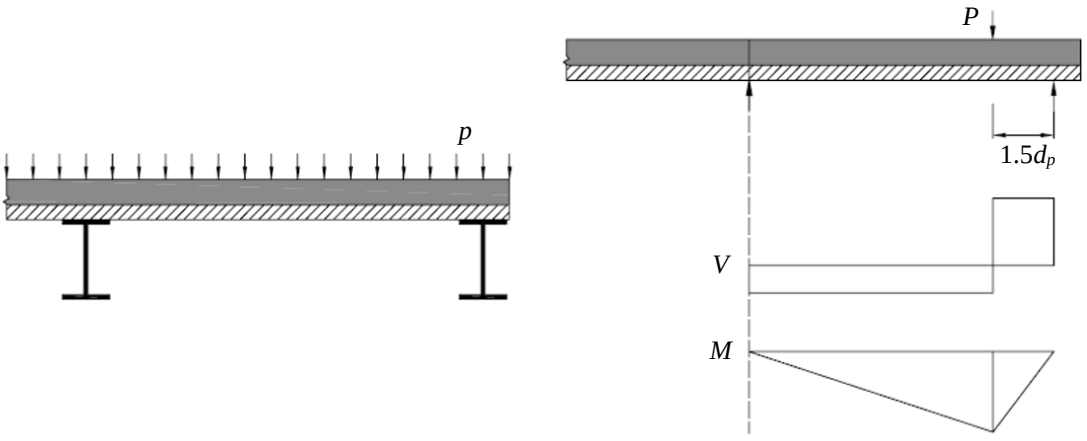

(a) continuous composite slab (b) hypothetical simply supported composite slab

Fig. 2.25 Vertical shear capacity of composite slabs (Liang, 2015)

Bruedern *et al.* (2012) carried out an experimental programme to study the behaviour of composite slabs with lightweight concrete. The authors developed a pumpable self-compacting lightweight aggregate concrete for application on composite slabs. The experimental programme carried out comprised four-point bending tests to study the longitudinal shear resistance of those specimens with the type of concrete developed. However, the failure mode observed was a combination between vertical and longitudinal shear, which motivated Hartmeyer and Kurz (2013) to develop an experimental campaign to study the vertical shear behaviour of steel-concrete composite slabs using re-entrant

sheets with embossments. The research study comprised the comparison between the experimental results and the respective design values, to develop design formulas for steel-concrete composite slabs with normal and lightweight concrete. The tested specimens collapsed due to their longitudinal shear resistance, so, it was possible to get some conclusions about the behaviour of composite slabs with low levels of shear connection. According to these authors, the design value of the vertical shear resistance of steel-concrete composite slabs V_{Rd} could be defined by the sum of the characteristic values of the shear resistance of the profiled steel sheeting $V_{p,Rk}$, the transverse force component of the uncracked compression zone $V_{c,cz}$ and the local aggregate interlock $V_{c,ct}$, divided by the partial safety factor γ_V, as it is expressed by Eq. (2.8), and illustrated in Fig. 2.26. So, authors considered the contribution of the profiled steel sheeting in the total vertical shear capacity of a composite slab. The study carried out also included a statistical analysis and found that a partial safety factor γ_V of 1.35 would be necessary. Schmeckebier and Kurz (2019) presented the same design model referring that this is going to be included in the next generation of codes.

$$V_{Rd} = \frac{1}{\gamma_V}\left(V_{0,Rk} + V_{c,ct}\right) = \frac{1}{\gamma_V}\left(V_{p,Rk} + V_{c,cz} + V_{c,ct}\right) \tag{2.8}$$

$$V_{c,cz} = \int_0^{x_m}\int_0^{b_w} \tau_{xz}(z)\cdot dy \cdot dz = \frac{2}{3} x_m b_w f_{ctm} \tag{2.9}$$

$$V_{c,ct} = 0.12 l_{ch} b_w f_{ctm} = 0.12 \frac{G_F E_{cm}}{f_{ctm}^2} b_w f_{ctm} \tag{2.10}$$

$$l_{ch} = \frac{G_F E_{cm}}{f_{ctm}^2} \tag{2.11}$$

where:

- γ_V is the partial safety factor, such that $\gamma_V = 1.35$;
- $V_{p,Rk}$ is the characteristic value of vertical shear capacity of the profiled steel sheeting;
- $V_{c,cz}$ is the transverse force component of the uncracked compression zone;
- $V_{c,ct}$ is the local aggregate interlock, defined by Eq. (2.10);
- τ_{xz} is the horizontal stress;
- x_m is the depth of the neutral axis;
- b_w is the width of the slab;
- l_{ch} is the characteristic length of the crack;
- f_{ctm} is the tensile resistance of the concrete;
- E_{cm} is the modulus of elasticity of the concrete;
- G_F is the fracture energy of the concrete.

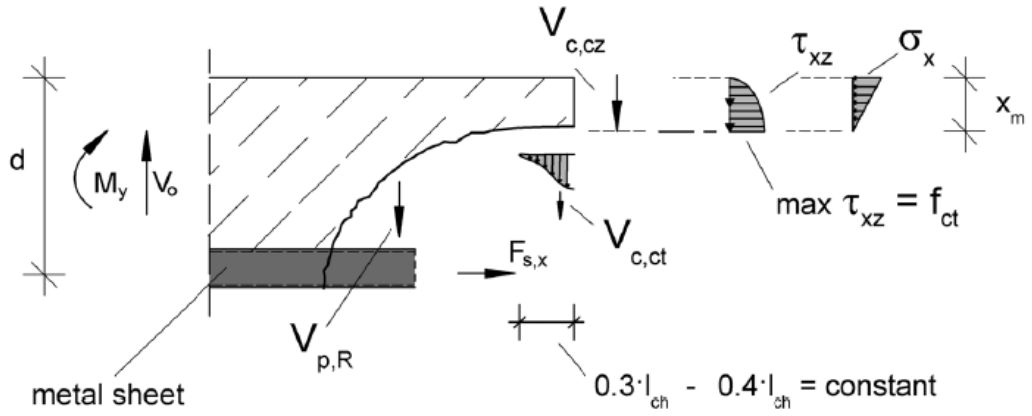

Fig. 2.26 Stress distribution for vertical shear behaviour of composite slabs (Hartmeyer and Kurz, 2013)

According to the results of the preliminary tests carried out at the University of Coimbra (Pereira *et al.*, 2017), the real vertical shear resistance of a steel-concrete composite slab can reach a value 5 times higher than its design value when evaluated according to Eurocode 4 (CEN, 2004b). This fact allowed to conclude that this design model is too conservative and consequently can lead to the conception of non-economical structural solutions.

More recently, Abspoel *et al*. (2018) carried out an experimental programme of two series of specimens of two-spans continuous composite slabs with the steel decking profiles ComFlor 210 and ComFlor 75, shown in Fig. 2.27, produced by Tata Steel Panels. Experimental tests were developed to evaluate the influence of the vertical shear on the hogging bending moment resistance of composite slabs with those profiles. The specimens collapsed in a bending mode; however, the authors observed that the sum of the vertical shear resistance of the decking profile and the vertical shear resistance of the concrete rib evaluated through the design models of Eurocode 4 (CEN 2004b) was lower than the maximum load achieved in those tests. Experimental results obtained from specimens with ComFlor75 showed also that the vertical shear force did not influence the hogging bending moment resistance for slabs with this profile.

Molkens *et al.* (2019) presented a study about the behaviour of steel-concrete composite decks composed by thick steel plate under a layer of concrete and headed studs welded over the span to increase the longitudinal shear capacity. The authors carried out an experimental programme of four-point bending tests of specimens with a steel plate and a concrete layer of, approximately, 30 mm and 150 mm, respectively, and 2 m of span. For these specimens the bending capacity and stiffness were defined. The authors also presented the vertical shear capacity of these specimens but considering the contribution of both components (steel and concrete). The authors considered that the contribution of each component to the vertical shear resistance would be proportional to its bending

stiffness. So, the vertical shear resistance of the composite section $V_{v,Rd}$, according to this approach, would be defined according to Eq. (2.12). The bending stiffness could be determined for both crack and uncracked situations. When the composite action should be considered, the uncracked bending stiffness is applied.

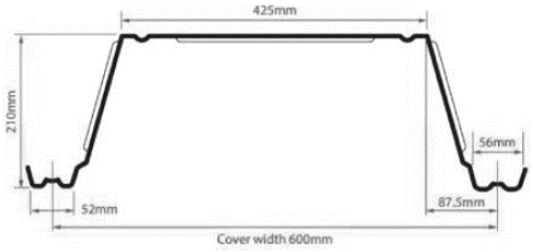

(a) ComFlor 210 geometry

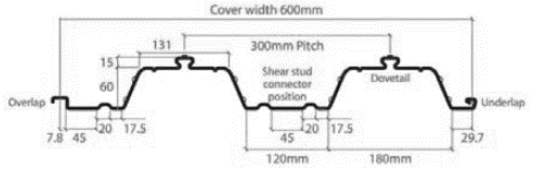

(b) ComFlor 75 geometry

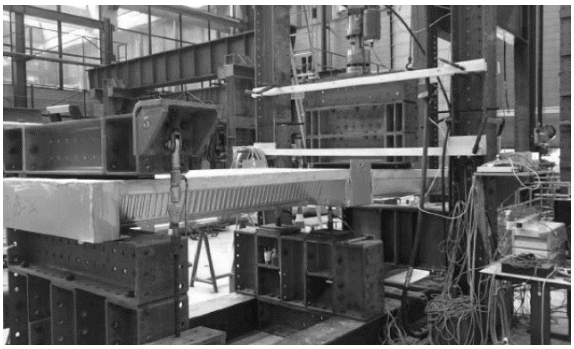

(c) Experimental layout

Fig. 2.27 Experimental tests on continuous composite slabs with ComFlor profiles (Abspoel *et al.*, 2018)

$$V_{v,Rd} = V_{v,c,Rd}\frac{(EI)_t}{(EI)_c} = V_{v,c,Rd}\frac{(EI)_c + (EI)_s}{(EI)_c} \tag{2.12}$$

where:

$V_{v,c,Rd}$ is the vertical shear resistance of the concrete layer, defined according to standard EN 1992-1-1 (CEN, 2004a);

$(EI)_c$ is the bending stiffness of the concrete layer;

$(EI)_s$ is the bending stiffness of the steel plate;

$(EI)_t$ is the bending stiffness of the composite section.

2.4.2 Non-European standard methods

Some non-european standards contain different approaches for the vertical shear design steel-concrete composite slabs. Two of them, the American standard and the Brazilian standard, are described below.

(i) American Standard ANSI

According to the American National Standards Institute and the Steel Deck Institute (ANSI and SDI 2012), the vertical shear resistance of a composite slab φV_n is defined by:

$$\varphi V_n = \varphi_v V_c + \varphi_s V_D \leq \varphi_v 0.172\sqrt{f'_c}A_c \tag{2.13}$$

where:

V_D is the vertical shear resistance of the steel sheet according to AISI S100 (ANSI, 2007);

V_c is the vertical shear resistance of the concrete part according to Eq. (2.14);

f'_c is the concrete compressive strength, never lower than 21 MPa;

A_c is the concrete area considered to resist vertical shear forces, shown in Fig. 2.28;

λ is a coefficient to take into account the density of the concrete and is defined as 1.0 for $\rho_c > 2100$ kg/m^3 and 0.75 for $\rho_c \leq 2100$ kg/m^3;

φ_v is the safety coefficient for the steel part defined as 0.75;

φ_s is the safety coefficient for the concrete part defined as 0.85

$$V_c = 0.086\lambda\sqrt{f'_c}A_c \tag{2.14}$$

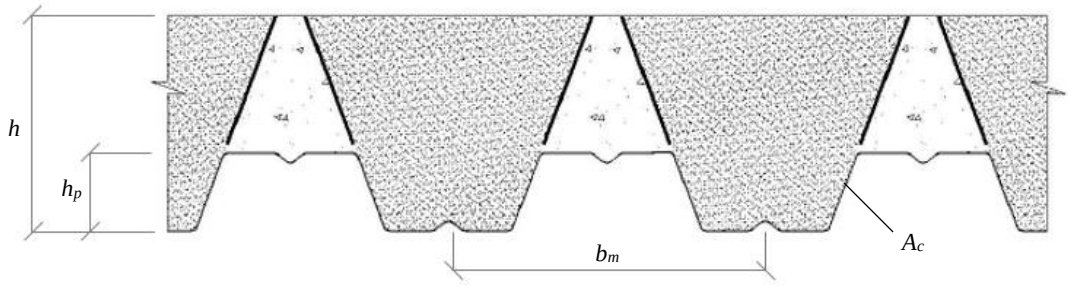

Fig. 2.28 Concrete area considered for the vertical shear resistance of composite slabs according to SDI (ANSI and SDI, 2012)

(ii) Brazilian Standard ABNT NBR 8800

The Brazilian standard ABNT NBR 8800 (ABNT, 2008) also defines a different model from the one of Eurocode to calculate the vertical shear resistance of a composite slabs, but it is similar to the American one. Composite slabs are designed according to Annex Q of standard ABNT NBR 8800 (ABNT, 2008). Section Q.3.1.3 of this standard establishes the vertical shear resistance of a composite slab $V_{v,Rd}$ as:

$$V_{v,Rd} = V_{v,F,Rd} + V_{v,c,Rd} \leq V_{\max} \tag{2.15}$$

where:

$V_{v,F,Rd}$ is the vertical shear resistance of the profiled steel sheeting, according to ABNT NBR 14762 (ABNT, 2010);

$V_{v,c,Rd}$ is the vertical shear resistance of the concrete part;

$V_{\max}$ is the upper limit of the vertical shear resistance of the slab.

The geometry of the concrete part considered for the vertical shear resistance of each concrete rib $V_{v,c,Rd}$, according to the Brazilian standard, is shown in Fig. 2.29. These concrete areas are bigger than the ones considered according to European standards.

According to Eurocode 2 a rectangular area with a width b_0 and height d_p is considered. In addition to considering a larger concrete area, standard ABNT NBR 8800 (ABNT, 2008) also considers the contribution of the vertical shear resistance of the steel sheet to the vertical shear resistance of the concrete slab. Considering that profiled steel sheets have a significant vertical shear resistance, which contributes to the shear resistance during the constructive phase, disregarding this contribution to the definite phase may lead to an over-dimensioned slab.

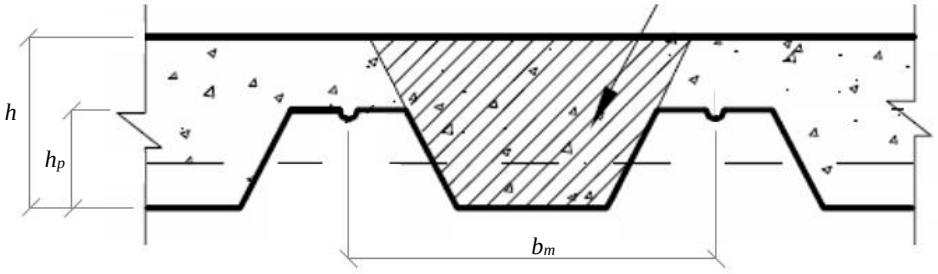

Fig. 2.29 Concrete area considered for the vertical shear resistance of composite slabs according to ABNT NBR 8800 for re-entrant profiles (ABNT, 2008)

In conclusion, American and Brazilian standards allow structural engineers to consider both contributions to the vertical shear resistance, from both the concrete slab and the steel sheet, in the total vertical shear resistance of a composite slab. On the contrary, the present version of EN 1994-1-1 (CEN, 2004b) only takes the concrete resistance into account, in some cases with a small contribution from the steel sheeting.

2.5 Final remarks

Over the last sections, the state of the art concerning the improvement of the structural performance of steel-concrete composite slabs was presented. It was shown that several researches have been developing new reinforcing systems for steel-concrete composite slabs. The main purposes of these reinforcing systems were to increase the longitudinal shear resistance and to achieve the bending capacity of composite slabs. However, it was observed that existing reinforcing systems: do not allow to achieve the full connection of composite slabs or; no methods were provided to take them into account in the design of composite slabs and so no advantage can be taken from these in the design of composite slabs. To overtake these issues, a new reinforcing system was developed and a design formula was calibrated to take its contribution into account in the design of composite slabs containing it.

A revision of different approaches to design steel-concrete composite slabs was also presented. Some researchers have already concluded that the vertical shear design model prescribed on standard EN 1994-1-1 (CEN, 2004b) is conservative. Some different approaches to design steel-concrete composite slabs for the vertical shear incorportating the contribution of the profiled steel sheeting were presented. With the main objectives of expanding these results and broadening the present knowledge concerning the real behaviour of steel-concrete composite slabs, additional experimental tests and numerical studies were carried out for the purpose of the present study.

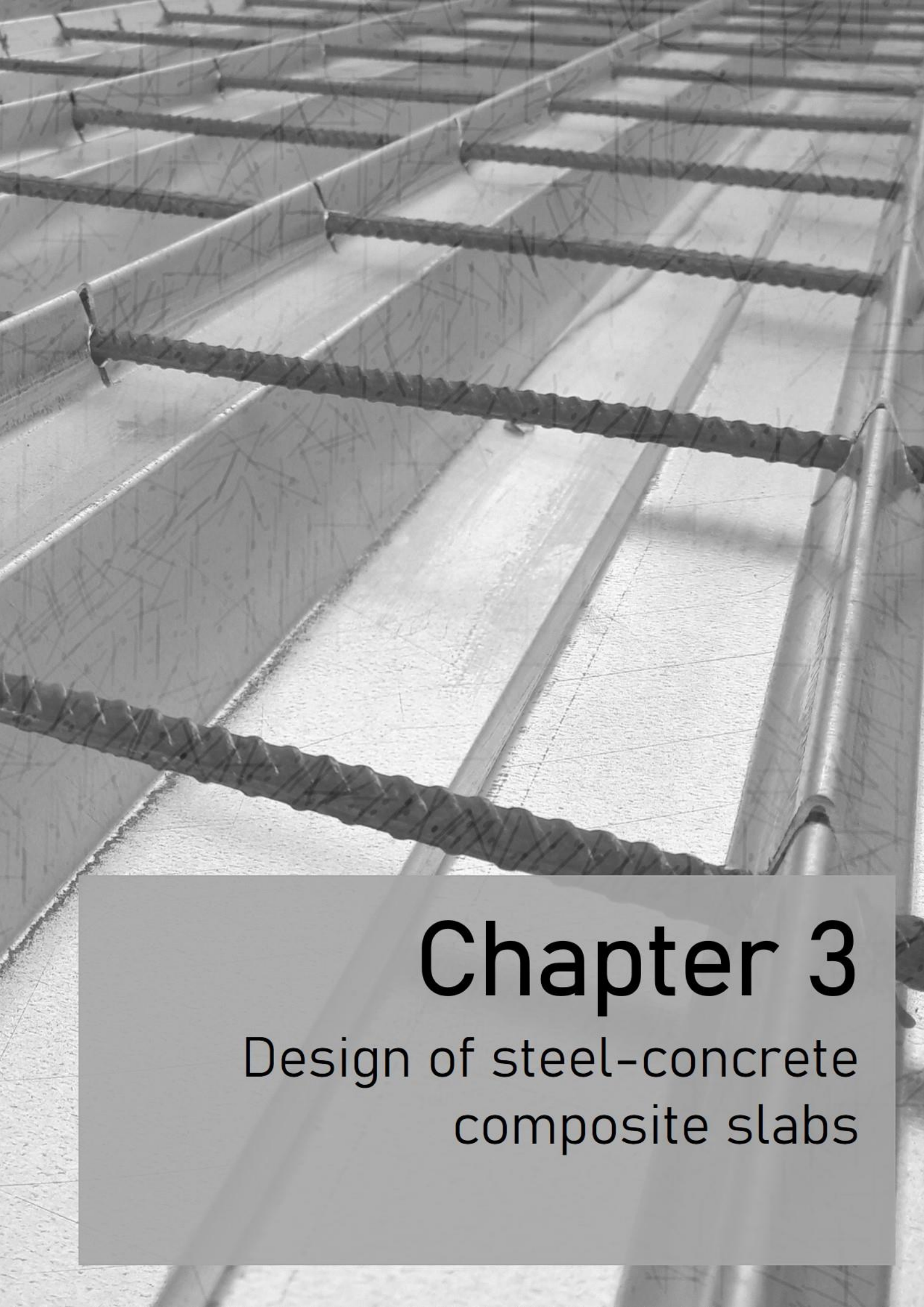

Chapter 3

Design of steel-concrete composite slabs

3.1 Introduction

3.1.1 Initial concepts

The resistance of a steel-concrete composite slab is defined along its longitudinal direction, on the direction of the ribs. Therefore, the design of composite slabs is similar to the design of composite beams. In current situations, composite slabs are supported by secondary beams, which transfer the loads to the main beams. So, the longitudinal direction of these slabs is typically perpendicular to the secondary beams direction and, consequently, parallel to the main beams longitudinal direction. In cases where the steel sheeting is flat (often applied on box-girder bridges), the two-way spanning occurs and the element is known as composite plate.

A steel-concrete composite slab must be analysed and designed in two different phases, such as for steel-concrete composite members: (i) constructive phase – during the construction stage, until the end of the concrete cure, profiled steel sheeting must be designed to support the wet concrete, reinforcing bars and other construction loads, with or without temporary supports; (ii) definitive phase – after the cure of the concrete the different components are working together and composite slab must be designed to support the use and service loads.

In this chapter, the main concepts in the design of steel-concrete composite slabs according to standard EN 1994-1-1 (CEN, 2004b) are presented.

3.1.2 Shear connection

The degree of connection between the concrete and steel components plays a fundamental role on the design of a composite member. This type of connection is mainly requested to resist to longitudinal shear stresses. In general, as the natural connection between the concrete and the steel is not strong enough to ensure the composite action, additional shear connection mechanisms must be provided.

Since 2008 the Technical Committee (TC) 11 of ECCS has been improving the understanding of the behaviour and design of shear connection for flexural members subjected to static or dynamic loads (Johnson, 2018).

In conventional steel-concrete composite beams the behaviour of the connection between the steel and the concrete components is already well known; however, for other types of composite flexural members, such as composite slabs, this topic still needs further

developments (Leskelä, 2017). In flexural members the connection can be classified as rigid or flexible: when the connection is rigid the slip in the connection interface is so small that influence the flexural behaviour and the theory of elasticity if valid for the all section; when the connection is flexible the slipping influences the bending behaviour and so the theory of elasticity is just valid for each component alone.

As it was mentioned before, the connection degree influences significantly the bending resistance of a composite member. The connection degree depends on the resistance of the interlock mechanism and the quantity of elements provided to improve (see Fig. 3.1). The connection can be classified in three different types: null connection; partial connection or; full connection. According to standard EN 1994-1-1 (CEN, 2004b), the full shear connection is achieved when the increase of the number of shear connectors does not lead to an increase of the bending resistance of the member. The null connection is verified when no interlock mechanisms are provided to ensure the shear transfer in the interface between the steel and the concrete. The partial connection is an intermediate situation between these conditions: the interlock mechanism allow the shear transfer in the interface between both materials, but is not strong enough to achieve the full bending resistance of the member.

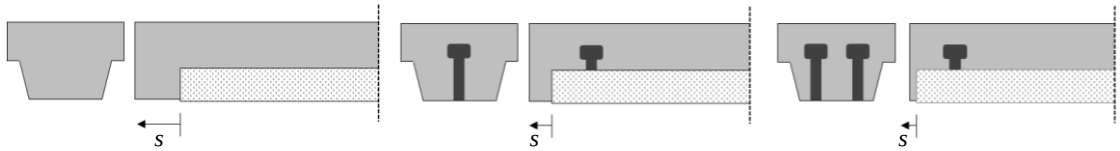

(a) Null connection (b) Partial connection (c) Full connection

Fig. 3.1 The influence of the connection degree

3.1.3 Slip Force

When a member constituted by two parts is subjected to vertical shear, V, that means that it is also subjected to bending moment variation along its longitudinal axis, since $V = dM/dx$, and slip forces along the interface between the constituent parts are developed. For exemplification, a prismatic bar with an infinitesimal length dx is considered and illustrated on Fig. 3.2. A uniformly distributed load q is applied on this member and so the member is subjected to a vertical shear V_z and a bending moment M_y. The interface between the two parts is defined by a horizontal plane at a z depth that cuts longitudinally this member.

Equilibrium conditions allow to define the relationship between the applied load q, the vertical shear V_z and the bending moment M_y, as it is defined in Eq. (3.1).

$$\begin{cases} \sum F_z = 0 \\ \sum M_y = 0 \end{cases} \rightarrow \begin{cases} q = -\dfrac{dV_z}{dx} \\ V = \dfrac{dM_y}{dx} \end{cases} \tag{3.1}$$

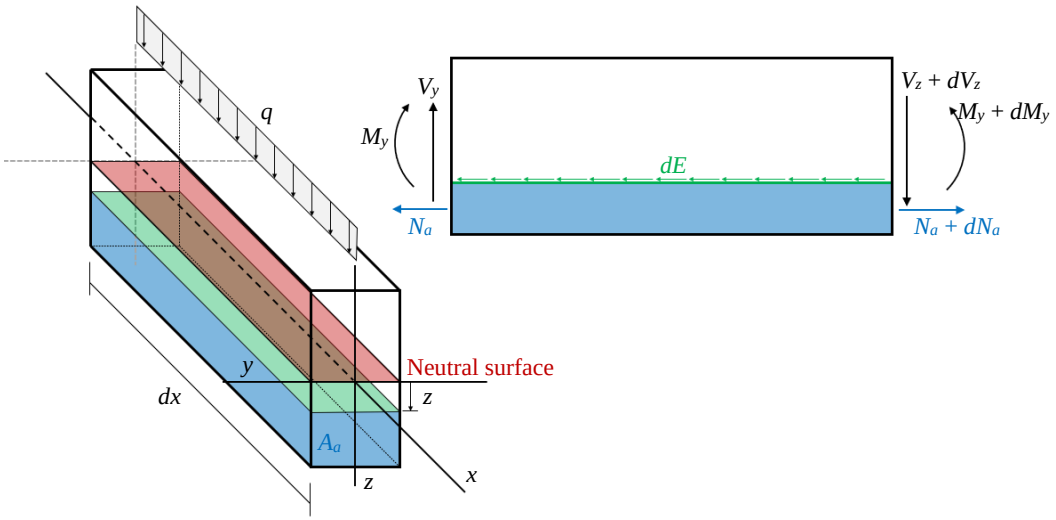

Fig. 3.2 Slip forces on a prismatic member submitted to vertical shear

Considering the force equilibrium in the longitudinal direction x, the lower member with a cross-section area A_a is subjected to a normal stress σ, which is generally defined in Eq. (3.2). The resultant normal forces acting on both ends of the infinitesimal member are then defined according to the equation system (3.3).

$$\sigma = \frac{M_y z}{I_y} \tag{3.2}$$

$$\begin{cases} N_a = \int_{A_a} \sigma \cdot dA_a = \dfrac{M_y}{I_y} \int_{A_a} z \cdot dA_a = \dfrac{M_y S}{I_y} \\ N_a + dN_a = \dfrac{M_y + dM_y}{I_y} \int_{A_a} z \cdot dA_a = \dfrac{M_y S}{I_y} + \dfrac{S dM_y}{I_y} \end{cases} \tag{3.3}$$

where S is the static moment of the section with A_a area in relation to the neutral axis, defined by Eq. (3.4).

$$S = \int_{A_a} z \cdot dA_a \tag{3.4}$$

The longitudinal equilibrium between the horizontal forces N_a and $N_a + dN_a$ is then established by the slip force dE acting on the contact surface between the two parts. Taking this in consideration, the slip force dE can be defined according to Eq. (3.5). This

equation allows to conclude that the maximum slip happens where the static moment *S* is also maximum, which corresponds to the neutral surface.

$$dE = N_a + dN_a - N_a = \frac{S \cdot dM_y}{I_y} = \frac{V_z \cdot S}{I_y} \cdot dz \tag{3.5}$$

Fig. 3.3(a) shows an example of a composite beam to illustrate the effect of the slip stress along the interface between the steel and the concrete. If the contact surface between the two different materials does not exhibit any resistance to the slip, as it can be observed on Fig. 3.3(b), then the two components will bend individually and a slip between them arise. For this case, the maximum stress in each component *i* at the fixed end section $\sigma^b_{i,\max}$ would be defined according to Eq. (3.6). Consequently, the curvature in the same section would be defined according to Eq. (3.7). On the other hand, if the contact surface between the steel and concrete exhibits total resistance to avoid the slip between them, as it can be observed on Fig. 3.3(c), then the two components will behave as just one member. For this latter case, the maximum stress at the fixed end section $\sigma^c_{\max}$ would be defined according to Eq. (3.8) and the curvature according to Eq. (3.9).

Considering the conditions expressed on Eq. (3.10) and comparing Eqs. (3.6) and (3.8), it can be verified that the higher the resistance in the contact surface between the two components the higher would be the bending stiffness of the member and, consequently, its bearing capacity.

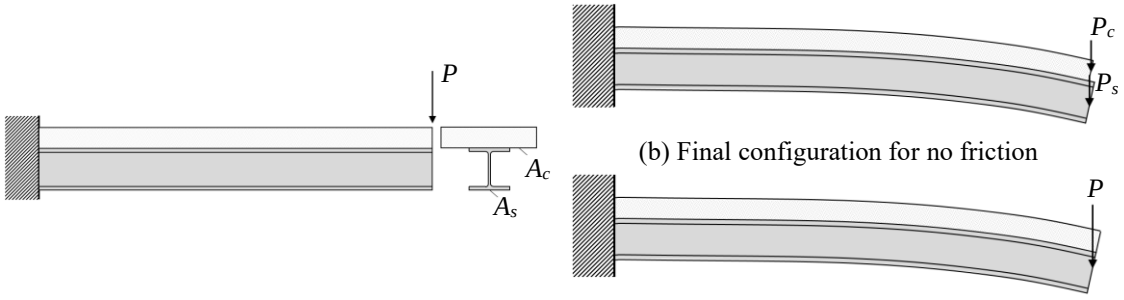

Fig. 3.3 Slip forces in a composite member

$$\sigma^b_{i,\max} = \frac{M_y}{I_{y,i} / v_i} = \frac{P_i L}{W_{y,i}} \tag{3.6}$$

$$\frac{1}{\rho_b} = \frac{M_y}{EI_{y,i}} = \frac{P_i L}{EI_{y,i}} \tag{3.7}$$

$$\sigma^{c}_{\max} = \frac{M_y}{I_y / v} = \frac{P \cdot L}{W_y} \tag{3.8}$$

$$\frac{1}{\rho_c} = \frac{M_y}{EI_y} = \frac{PL}{EI_y} \tag{3.9}$$

$$\begin{aligned} I_{y,i} &< I_y \\ W_{y,i} &< W_y \end{aligned} \tag{3.10}$$

where:

- $\sigma^{b}_{i,\max}$ is the maximum normal stress in the component *i* for case (b);
- $\sigma^{c}_{\max}$ is the maximum normal stress in the cross-section for case (c);
- $1/\rho_b$ is the curvature for case (b);
- $1/\rho_c$ is the curvature for case (c);
- $I_{y,i}$ is the moment of inertia of the component *i*;
- I_y is the moment of inertia of the total cross-section;
- $W_{y,i}$ is the bending modulus of the component *i*;
- W_y is the bending modulus of the composite section;
- P_i is the load acting on the component *i*;
- P is the total applied load;
- L is the length of the member.

3.2 Constructive phase

3.2.1 Introduction

Profiled steel sheets are usually very thin, with thickness values between 0.8 mm and 1.2 mm, for economic reasons. In order to ensure corrosion resistance, steel sheets are hot-dip galvanized and, as a consequence, its thickness increases about 0.04 mm (0.02 mm each side). So, according to section 3.2.4 of standard EN 1993-1-3 (CEN, 2006b), the design thickness of a profiled steel sheeting is defined by the steel core thickness t_{cor}. The nominal thickness t_{nom} is a target average thickness including zinc and other metallic coating layers so it needs to be reduced to the steel core thickness t_{cor} (nominal thickness minus zinc and other metallic coating). The steel sheets are produced by pressing and cold rolling processes.

The design for the constructive phase comprises the design of the profiled steel sheeting for ultimate and service limit states according to standard EN 1993-1-3 (CEN, 2006a). Usually, profiled steel sheeting are slender members, so it could be necessary to take into

consideration the local buckling in the top or bottom flanges, for sagging or hogging bending moment regions, respectively; typically, elastic analysis and design are used. For the constructive phase, profiled steel sheeting could be governed by its (i) bending resistance (ULS), (ii) vertical shear resistance (ULS), (iii) deflection limit state (SLS). If the safety in the construction phase is not verified, the number of props or the thickness of the steel sheeting should be increased until the safety of the profiled steel sheeting is successful checked. In order to reduce the cost of propping profiled steel sheets during the construction, the industry has developed deeper profiles with higher stiffness and bending capacity.

3.2.2 Loads acting on the profiled steel sheeting

According to section 9.3.2 of standard EN 1994-1-1 (CEN, 2004b), the safety check of the profiled steel sheeting during the constructive phase should be performed taking into account (i) the self-weight of the profiled steel sheeting, (ii) the weight of the wet concrete, (iii) construction loads, (iv) storage load, in case it exists, and (v) the "ponding" effect.

The weight of the profiled steel sheeting is usually provided in the catalogues supplied by the profile producers; for the density of the steel γ_s, it should be considered a value comprised between 77.0 kN/m^3 and 78.5 kN/m^3, according to Annex A of standard EN 1991-1-1 (CEN, 2002b). The weight of the concrete should be based on a density γ_c of 26.0 kN/m^3 – 24 kN/m^3 relative to the nominal density of the concrete plus 1 kN/m^3 for the reinforcing bars and 1 kN/m^3 for the wet concrete, in accordance with standard EN 1991-1-1 (CEN, 2002b).

The construction loads must be defined according to section 4.11 of standard EN 1991-1-6 (CEN, 2005a). Clause 4.11.2(1) defines the recommended characteristic values of actions due to construction loads during casting of concrete in function of the concrete weight p_c as it is illustrated on Fig. 3.4. A uniformly distributed load of 10% of the concrete weight p_c must be considered in the working area comprised by a central square area of 3 m length (or the span length if is less than 3 m), but not less than 0.75 kN/m^2 and not more than 1.50 kN/m^2. Outside the working area, a uniformly distributed load of 0.75 kN/m^2 must be considered. Fig. 3.4 illustrates the options that could lead to different load scenarios, depending on the concrete weight p_c (in kN/m^2) and the span length L.

When composite slabs are designed as simply-supported, deflections may govern design. According to Johnson (2018), the maximum acceptable deflection is more relevant for the client than for the designer. However, if the predicted deflection is too large, extra weight of concrete must be taken in consideration to account the "ponding" effect. This

effect is mainly caused by the deflection of the profiled steel sheeting during the cure of the concrete. According to clause 9.3.2(2) of standard EN 1994-1-1 (CEN, 2004b), when the maximum deflection δ of the profiled steel sheeting caused by its own weight and the wet concrete weight, calculated for serviceability, is less than 10% of the slab height h the "ponding" effect may be ignored. Otherwise, if $\delta > 0.1h$, this effect must be taken into account assuming in the design that the nominal thickness of the concrete is increased over the whole span by h_{pond} defined as 0.7δ, as it is illustrated on Fig. 3.5. Since this represents an artificial addition of material, the "ponding" effect must be considered as a dead load in the design of the profiled steel sheeting for the ultimate limit states.

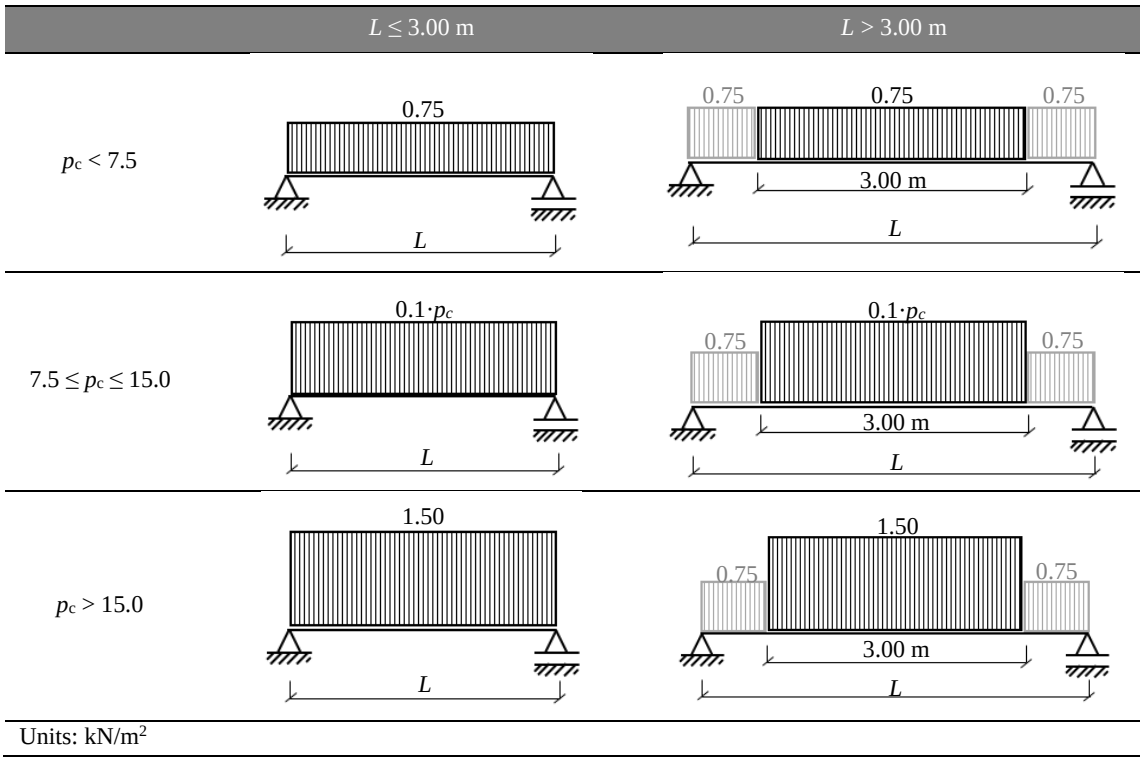

Fig. 3.4 Construction loads to consider in steel decking

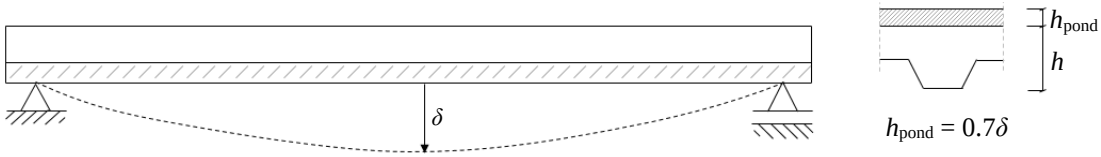

Fig. 3.5 "ponding" effect

3.2.3 ULS design

3.2.3.1 Introduction

Typically, profiled steel sheeting are slender members, so possible buckling phenomena must be taken into account considering a reduced bending stiffness. The global analysis of profiled steel sheeting should be done considering a linear elastic analysis. For continuous profiled steel sheeting it is considered that the bending stiffness is constant over the span.

Usually, the sagging bending stiffness of profiled steel sheets is higher when compared to their hogging bending stiffness. The maximum sagging bending moment in a simply supported member, $pL^2/8$, is equal to the absolute value of the maximum hogging bending moment in a continuous member, where p is the uniformly distributed load value and L is the span length. So, it can be concluded that the bearing capacity of simply-supported steel sheets is higher than continuous steel sheets.

According to clause 9.4.1(2) the plastic redistribution of bending moments is not allowed when temporary supports are used. However, for continuous composite slabs the bending moment redistribution is allowed for the definitive supports. Experimental results obtained by Nethercot (2004) and Stark and Brekelmans (1990) allowed to conclude that it is possible to consider a redistribution of moments in the global analysis of a continuous profiled steel sheeting. Johnson and Anderson (2004), in the same way as standard BS 5950-4 (BSi, 1994), indicated that the redistribution must be comprised between 5 and 15%; for a redistribution higher than 10%, additional experimental tests must be developed. Lee *et al.* (2001), based on experimental results obtained from their study, concluded that a redistribution limit of 30% may be adequate if the service limit states are satisfied without the moment redistribution.

As it was mentioned before, profiled steel sheets are thin walled members which makes, typically, the constructive phase the most conditioning in the design of profiled steel sheeting. The resistance of these cold-formed profiles must be checked according to standard EN 1993-1-3 (CEN, 2006a) rules. The ULS check comprises the verification of the resistance to (i) bending moment, (ii) vertical shear and (iii) combined vertical shear and bending moment (when is necessary). The ultimate limit states check must ensure the following condition:

$$E_d \leq R_d \tag{3.11}$$

where: E_d is the design value of the acting shear or moment and R_d is the design value of the shear or moment resistance.

Standard EN 1993-1-3 (CEN, 2006a) uses, to represent the yield strength of the profiled steel sheeting, the symbol f_{yb} (basic yield strength). However, in this document, this meaning was represented by f_{yp} as it is used in standard EN 1994-1-1 (CEN, 2004b). Other symbols often used in standard EN 1993-1-3 (CEN, 2006a) were changed to the ones adopted in standard EN 1994-1-1 (CEN, 2004b).

3.2.3.2 Bending moment

The bending of a profiled steel sheeting is successfully checked when the design value of the maximum bending moment in the member M_{Ed} is not higher than the design value of the bending resistance of a steel sheet M_{Rd}, as expressed in Eq. (3.12).

$$M_{Ed} \leq M_{Rd} \tag{3.12}$$

Profiled steel sheets are thin walled members so, usually, their cross-section is classified as class 4 cross-section. Class 4 cross-sections, according to clause 5.5.2(1) of standard EN 1993-1-1 (CEN, 2005b) are those in which local buckling will occur before the attainment of yield stress in one or more parts of the cross-section. In Class 4 cross-sections flanges and webs should be reduced to their effective widths due to the effects of local buckling. So, the design bending moment resistance of a cross-section M_{Rd} is determined by Eq. (3.13).

$$M_{Rd} = \frac{W_{eff,\min} f_{yp}}{\gamma_{M0}} \tag{3.13}$$

where:

$W_{eff,\min}$	is the effective section modulus;
f_{yp}	is the yield strength of the profiled steel sheeting;
γ_{M0}	is the partial safety factor, such that $\gamma_{M0} = 1.0$.

3.2.3.3 Vertical shear

The vertical shear resistance of a profiled steel sheeting is successfully checked when the design value of the maximum vertical shear in the member V_{Ed} is not higher than the design value of the vertical shear resistance of a steel sheet $V_{v,p,Rd}$, as expressed in Eq. (3.14).

$$V_{Ed} \leq V_{v,p,Rd} \tag{3.14}$$

The design value of the vertical shear resistance of a steel sheet $V_{v,p,Rd}$, according to section 6.1.5 of standard EN 1993-1-3 (CEN 2006), is defined according to the contribution of the webs of the profile. The design value of the vertical shear resistance of one web of the profile $V_{v,w,Rd}$ is given by Eq. (3.15).

$$V_{v,w,Rd} = \frac{\frac{h_w}{\sin\varphi} t f_{bv}}{\gamma_{M0}} \tag{3.15}$$

where:

h_w is the web height between the midlines of the flanges;

φ is the slope of the web relative to the flanges, see Fig. 3.6;

t is the thickness of the profiled steel sheeting;

f_{bv} is the shear buckling strength, defined according to Table 3.1;

γ_{M0} is the partial safety factor;

$\bar{\lambda}_w$ is the relative slenderness of the web, defined according to clause 6.1.5(2) of standard EN 1993-1-3 (CEN, 2006a).

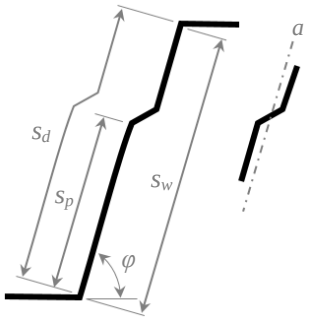

Fig. 3.6 Geometry of a longitudinally stiffened web

Table 3.1 Shear buckling strength f_{bv}

Relative web slenderness	Web without stiffening at the support	Web with stiffening at the support[(1)]
$\bar{\lambda}_w < 0.83$	$0.58\, f_{yp}$	$0.58\, f_{yp}$
$0.83 \leq \bar{\lambda}_w \leq 1.40$	$0.48\, f_{yp} / \bar{\lambda}_w$	$0.48\, f_{yp} / \bar{\lambda}_w$
$\bar{\lambda}_w > 1.40$	$0.67\, f_{yp} / \bar{\lambda}_w^2$	$0.48\, f_{yp} / \bar{\lambda}_w$

[(1)] Stiffening at the support, such as cleats, arranged to prevent distortion of the web and designed to resist the support reaction

3.2.3.4 Combined vertical shear and bending moment

According to section 6.1.10 of standard EN 1993-1-3 (CEN 2006), if the design value of the vertical shear acting on the profiled steel sheeting V_{Ed} is higher than 50% of the design value of the vertical shear resistance $V_{v,p,Rd}$, the following condition should be satisfied:

$$\frac{M_{Ed}}{M_{Rd}} + \left(1 - \frac{M_{f,Rd}}{M_{pl,Rd}}\right)\left(\frac{2V_{Ed}}{V_{v,p,Rd}} - 1\right)^2 \leq 1.0 \tag{3.16}$$

where:

$M_{f,Rd}$ is the bending moment of resistance of a cross-section consisting of the effective area of flanges only, defined according to standard EN 1993-1-5 (CEN, 2006c);

$M_{pl,Rd}$ is the plastic moment of resistance of the cross-section defined according to standard EN 1993-1-5 (CEN, 2006c);

V_{Ed} is the design value of the vertical shear;

$V_{v,p,Rd}$ is the shear force resistance.

3.2.4 SLS design

For the service limit states, the designer should ensure that, after the concrete cure, the deflection of the profiled steel sheeting does not compromise the behaviour of the slab. So, the deflection limit state should be well predicted and designed for this stage.

According to clause 9.8.2(2) of standard EN 1994-1-1 (CEN, 2004b), deflections in the construction phase should be calculated in accordance with section 7 of standard EN 1993-1-3 (CEN, 2006a) and section 7 of standard EN 1993-1-1 (CEN, 2005b). Standard EN 1993-1-1 (CEN, 2005b) establishes that limits for the service limit states section A1.4 of annex A of standard EN 1990 (CEN, 2002a) should be applied.

According to clause 9.6(2) of standard EN 1994-1-1 (CEN, 2004b) the maximum deflection δ_s (see Fig. 3.7) of the profiled steel sheeting under its own weight and the weight of wet concrete should not exceed $\delta_{s,max}$. The same clause also recommends a limit of $L/180$ for $\delta_{s,max}$, where L is the length of the span between the supports/props.

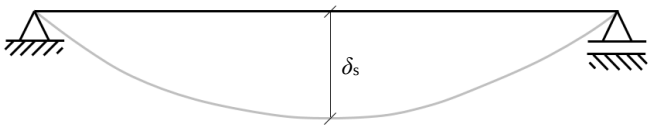

Fig. 3.7 Vertical deflections for sheeting

3.3 Composite phase

3.3.1 Initial concepts

This section presents current Eurocode 4 (CEN, 2004b) rules and some concepts that designers could take into account on the design and optimization of the structural design of composite slabs. Johnson (2018) assumed that is expected that the future edition of this

standard will incorporate some changes: (i) longitudinal reinforcing bars in the ribs will be considered in the bending resistance equations; (ii) *m-k* method will be removed, leaving only the partial connection method to design composite slabs for longitudinal shear. Therefore, although both *m-k* and partial connection methods are presented in this section, in the next chapters only partial connection method will be used to calculate resistance and design values.

Standard EN 1994-1-1 (CEN, 2004b) covers steel-concrete composite slabs with re-entrant and trapezoidal profiles. Trapezoidal profiles are the most common; therefore, the design procedure presented along this thesis is particularly focused on composite slabs with trapezoidal decking.

Simply-supported composite slabs behaves essentially under sagging bending and then the sheeting in longitudinal tension. So, the plastic theory can be used to find the bending resistance of composite slabs. However, according to clause 9.4.2(1) of standard EN 1994-1-1 (CEN, 2004b), other methods of analysis may be used for ULS: (i) linear elastic analysis with or without redistribution; (ii) rigid plastic global analysis provided that it is shown that sections where plastic rotations are required have sufficient rotation capacity; (iii) elastic-plastic analysis, taking into account the non-linear material properties. For serviceability limit states, linear method of analysis should be used.

Steel-concrete composite slabs must be designed for their ultimate limit states, which can be governed by one of the followings collapse modes: (i) vertical shear; (ii) longitudinal shear and; (iii) bending moment. When slabs are subjected to point loads they also must be designed to resist to punching shear. The longitudinal shear resistance can be defined by two different methods already mentioned: (i) *m-k* method and (ii) partial connection method. Concerning the service limit states, composite slabs must be designed for their cracking, deflection and vibration limit states.

Fig. 3.8 shows the 3 main collapse modes and the critical sections location, described as follow:

i. near the supports (**section I**), the **vertical shear** behaviour may limit the capacity of composite slabs. Usually, the design of steel-concrete composite slabs is governed by the vertical shear capacity for slabs with short spans or current length spans with reinforcing systems to improve the longitudinal shear resistance;
ii. for current spans the capacity is governed by the **longitudinal shear** resistance of the slab, which means that the connection between the profiled steel sheeting and the concrete is not enough to ensure a required connection degree. This collapse

mode occurs along the contact surface (**section II**) between the steel and the concrete components;

iii. when the full connection is achieved and usually for long spans, composite slabs tends to achieve their bending resistance, typically compromised in the mid-span cross-section (**section III**).

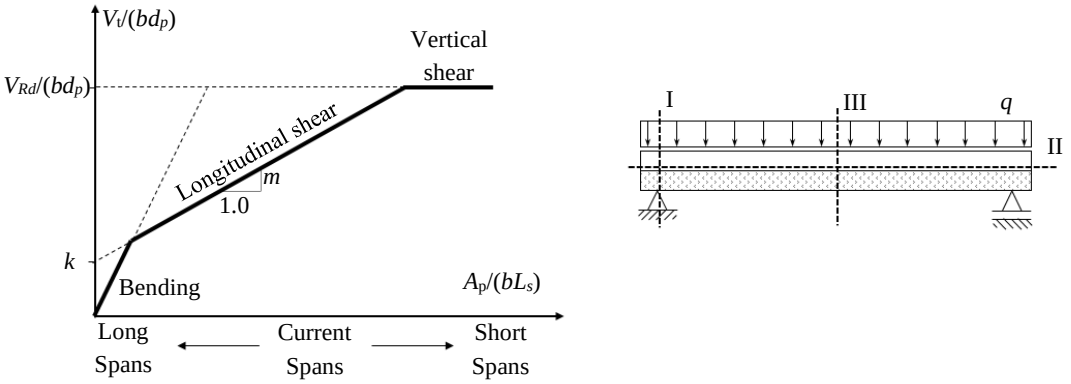

Fig. 3.8 Critical sections and failure modes

As it was mentioned before, the connection between the profiled steel sheeting and the concrete component can be classified in three different ways: (i) null connection – each component works by itself and there is no transfer of longitudinal stresses between them; (ii) partial connection – components are working together but without a total transfer; (iii) full connection – when the composite section is working as a just one component section. According to standard EN 1994-1-1 (CEN, 2004b), full shear connection exists when increasing the resistance of the longitudinal shear connection does not increase the design bending resistance. Otherwise, the shear connection is partial.

3.3.2 Loads acting on the composite slab

According to section 9.3.3 of standard EN 1994-1-1 (CEN, 2004b), the actions to be considered in the design of composite slabs should be in accordance with standard EN 1991-1-1 (CEN, 2002b). This comprises (i) the self-weight of the profiled steel sheeting, (ii) the weight of the dry concrete and (iii) other actions predicted due to the normal use of the building.

3.3.3 ULS Design

3.3.3.1 Bending moment

3.3.3.1.1 Basic assumptions

The bending moment resistance of a steel-concrete composite slab should be determined according to section 9.7.2 of standard EN 1994-1-1 (CEN, 2004b), based on the experimental results of a campaign carried out by Stark and Brekelmans (1990). The design value of the plastic resistance moment of the composite slab $M_{pl,Rd}$ is obtained based on the following assumptions:

i. there is full interaction between structural steel, reinforcement, and concrete;
ii. the concrete under compression resists to a stress of 0,85 f_{cd}, constant over the depth between the plastic neutral axis and the most compressed fibre of the concrete, where f_{cd} is the design value of the cylinder compressive strength of the concrete;
iii. the tensile resistance of concrete is neglected;
iv. the longitudinal reinforcement is stressed to their design yield strength f_{sd} in tension or compression. Alternatively, reinforcement in compression in a concrete slab may be neglected;
v. profiled steel sheeting in tension included within the effective section should be assumed to be stressed to its design yield strength $f_{yp,d}$;
vi. the contribution of the profiled steel sheeting under compression is neglected (this contribution only can be taken into account when the profiled steel sheeting is continuous and no redistribution of moments was used in the construction phase design).

When the profiled steel sheeting is in tension, the area of the embossments should be neglected in the effective area A_{pe}, as it is shown in Fig. 3.9.

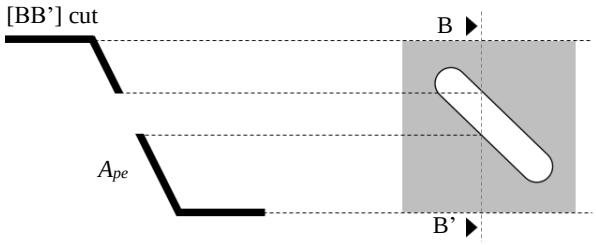

Fig. 3.9 Effective area A_{pe} without the embossments width

3.3.3.1.2 Sagging bending moment

For sagging bending moment two different positions of the plastic neutral axis NA_{pl} can occur: (i) NA_{pl} above the profiled steel sheeting ($z_{pl} < h_c$) and; (ii) NA_{pl} intersecting the profiled steel sheeting ($z_{pl} \geq h_c$).

(i) Plastic neutral axis above the steel sheeting

The stress distribution in this case is presented on Fig. 3.10 for just one slab module. Taking in consideration the horizontal equilibrium, the depth of the neutral axis is given by Eq. (3.17). Therefore, if $z_{pl} < h_c$, the same distribution should be considered to obtain the bending resistance.

$$\sum F_H = 0 \rightarrow N_{cf} = N_p \rightarrow z_{pl} b_m 0.85 f_{cd} = N_p \rightarrow z_{pl} = \frac{N_p}{b_m 0.85 f_{cd}} \tag{3.17}$$

where:

- N_{cf} is the design compressive force in the concrete for full connection;
- N_p is the tensile force provided by the profiled steel sheeting, defined by $A_{pe} f_{yp,d}$;
- z_{pl} is the depth of the neutral axis;
- b_m is the width of one slab module;
- f_{cd} is the design value of the compressive strength of the concrete ($f_{cd} = f_{ck}/1.50$);
- $f_{yp,d}$ is the design yield strength of the sheeting;
- A_{pe} is the effective cross-section of profiled steel sheeting, neglecting the coating layers and the width of the embossments.

Then, the design plastic moment resistance to sagging bending $M_{pl,Rd}$ is given by:

$$M_{pl,Rd} = N_{cf} z = N_{cf} \left(h - \frac{z_{pl}}{2} - e \right) \tag{3.18}$$

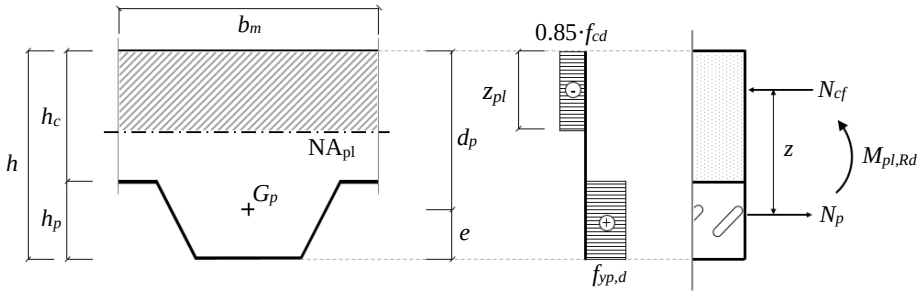

Fig. 3.10 Sagging bending moment resistance (NA above steel sheeting)

(ii) Plastic neutral axis intersecting the steel sheeting

Otherwise, if $z_{pl} \geq h_c$, it must be considered that NA_{pl} intersects the steel sheeting and the stress distribution should be different (Fig. 3.11). If the compression force over all concrete height above the profiled steel sheeting N_{cf} is lower than the profiled steel sheeting tensile force N_p, then the neutral axis will intersect the sheeting and the stress distribution for this case is shown in Fig. 3.11. In this situation, the depth of the neutral axis z_{pl} is the solution for the horizontal equilibrium expressed in Eq. (3.19).

$$\sum F_H = 0 \rightarrow N_{cf} + N_{p,c} = N_{p,t} \tag{3.19}$$

where:

N_{cf} is the design compressive force in the concrete for full connection, given by $A_c \cdot 0.85 f_{cd}$;

$N_{p,c}$ is the design compressive force in the profiled steel sheeting, given by $A_{p,c} f_{yp,d}$;

$N_{p,t}$ is the design tensile force in the profiled steel sheeting, given by $A_{p,t} f_{yp,d}$;

A_c is the concrete area under compression;

$A_{p,c}$ is the steel sheeting area under compression;

$A_{p,t}$ is the steel sheeting area under tension;

So, the design plastic moment resistance to sagging bending $M_{pl,Rd}$ is given by:

$$M_{pl,Rd} = \left(N_{p,t} z_{p,t}\right) - \left(N_{cf} z_c + N_{p,c} z_{p,c}\right) \tag{3.20}$$

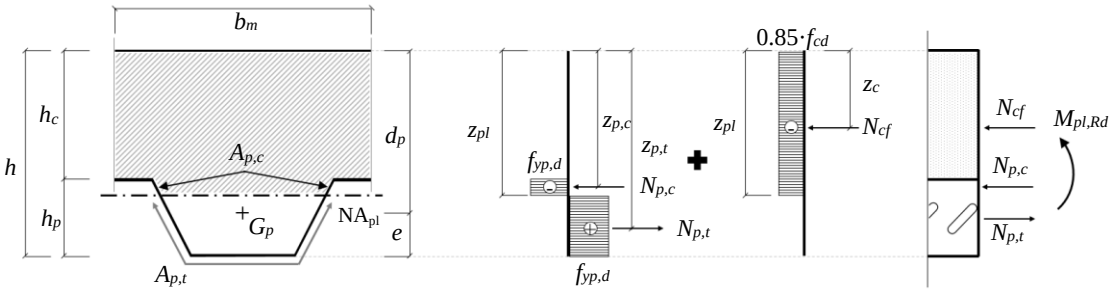

Fig. 3.11 Sagging bending moment resistance (NA intersecting steel sheeting)

This procedure leads to a complex analysis because the determination of the depth of the neutral axis requires an iterative process. However, standard EN 1994-1-1 (CEN, 2004b) provides a simplified method to calculate the design value of the bending moment resistant $M_{pl,Rd}$ for this case which gives an accurate solution. The stress distribution recommended by standard EN 1994-1-1 (CEN, 2004b) is shown in Fig. 3.12, where the contribution of the concrete under compression inside the ribs is neglected. This approach was proposed by Stark and Brekelmans (1990). This approach comprises the division of

the stress distribution in two different diagrams: one for the equilibrium between the concrete under compression and part of the profiled steel sheeting under tension; another for the reduced plastic resistance moment of the profiled steel sheeting M_{pr}, defined according to Eq. (3.21).

$$M_{pr} = 1.25 M_{pa}\left(1 - \frac{N_c}{A_{pe} f_{yp,d}}\right) \le M_{pa} \tag{3.21}$$

where:

M_{pa} is the design value of the plastic resistance moment of the effective cross-section of the profiled steel sheeting, given by $W_{pe,pl} f_{yp,d}$;

$W_{pe,pl}$ is the plastic bending modulus of the profiled steel sheeting.

The horizontal equilibrium should be satisfied according to Eq. (3.22):

$$\sum F_H = 0 \rightarrow N_p = N_{cf} = 0.85 f_{cd} b h_c \tag{3.22}$$

So, the design plastic moment resistance to sagging bending $M_{pl,Rd}$ is given by:

$$M_{pl,Rd} = N_{cf} z + M_{pr} \tag{3.23}$$

where:

z is the vertical distance between the forces N_c and N_p defined according to Eq. (3.24)

h is the total height of the slab;

h_c is the height of concrete above the profiled steel sheeting;

e_p is the distance from the plastic neutral axis of profiled steel sheeting to the extreme fibre of the composite slab in tension;

e is the distance from the centroidal axis of profiled steel sheeting to the extreme fibre of the composite slab in tension.

$$z = h - \frac{h_c}{2} - e_p + (e_p - e)\frac{N_{cf}}{A_{pe} f_{yp,d}} \tag{3.24}$$

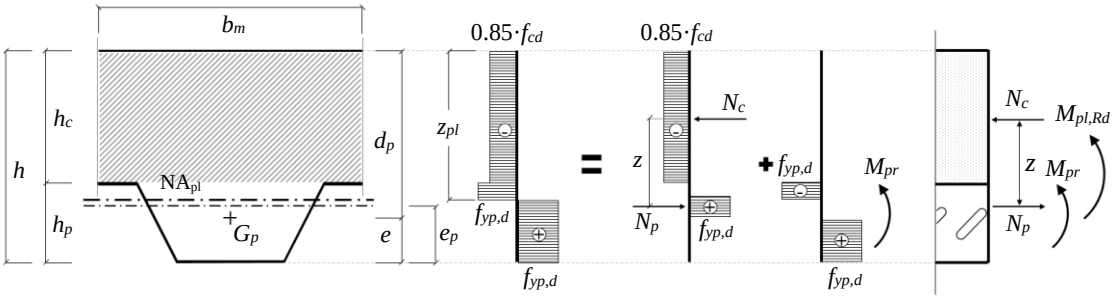

Fig. 3.12 Sagging bending moment resistance (NA intersecting steel sheeting) – simplified model

(iii) Composite slabs with longitudinal reinforcement

Johnson and Shepherd (2013) carried out an experimental programme on composite slabs with trapezoidal profiled steel sheeting and longitudinal reinforcing bars on the ribs. Usually, longitudinal reinforcing bars are placed in the ribs of steel-concrete composite slabs to improve their fire resistance. However, it is possible to take into account their contribution in "cold" design conditions. The authors observed that longitudinal reinforcing bars increase significantly the bending and longitudinal shear capacity of composite slabs. To take into account the additional resistance provided by the reinforcing bars, these researches developed and presented a methodology to design steel-concrete composite slabs with longitudinal reinforcing bars placed in the concrete ribs.

Once again, for sagging bending moment, the plastic neutral axis could be above the profiled steel sheeting, if $N_c > N_p + N_s$, or intersecting it, if $N_c \leq N_p + N_s$.

The first case is shown in Fig. 3.13, where the depth of the neutral axis is now given by Eq. (3.25) and the design value of the plastic bending moment resistant to sagging bending $M_{pl,Rd}$ by Eq. (3.26).

$$z_{pl} = \frac{N_p + N_s}{b_m 0.85 f_{cd}} \tag{3.25}$$

$$M_{pl,Rd} = N_p z_1 + N_s z_2 \tag{3.26}$$

where:

N_s is the design value of the plastic resistance of the steel reinforcement given by $N_s = A_s f_{sd}$;

z_1 is the vertical distance between forces N_c and N_p given by $z_1 = d_p - z_{pl}/2$;

z_2 is the vertical distance between forces N_c and N_s given by $z_2 = d_s - z_{pl}/2$;

d_p is the effective height of the slab given by $d_p = h - e$;

d_s is the distance between the centroidal of the steel reinforcement in tension to the extreme fibre of the composite slab in compression.

When the neutral axis intersects the profiled steel sheeting on composite slabs with longitudinal reinforcing bars in the ribs (see Fig. 3.14), the design plastic moment resistance to sagging bending $M_{pl,Rd}$ is given by Eq. (3.27).

$$M_{pl,Rd} = N_c z_1 + N_s z_2 + M_{pr} \tag{3.27}$$

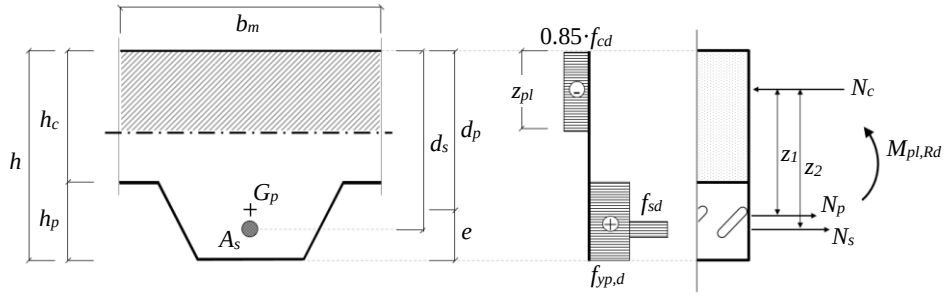

Fig. 3.13 Sagging bending moment resistance (NA above steel sheeting) – with longitudinal reinforcement

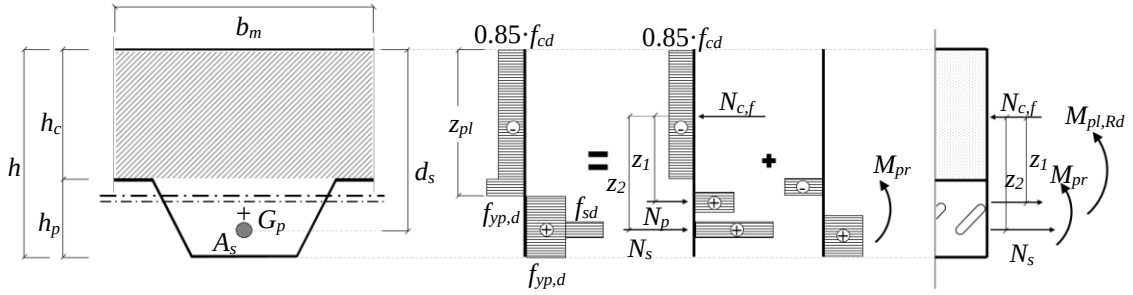

Fig. 3.14 Sagging bending moment resistance (NA intersecting steel sheeting) – with longitudinal reinforcement

3.3.3.1.3 Hogging bending moment

When continuous slabs are considered, the design to ensure negative bending moment capacity is necessary. Clause 9.4.2(5) of standard EN 1994-1-1 (CEN, 2004b) allows to design continuous composite slabs as a series of simply supported slabs. However, this is a simplification that could lead to an overdesigned solution. Over the supports, the concrete is continuous and the sheets may be as well. So standard EN 1994-1-1 (CEN, 2004b) allows to design as continuous and reduce the bending moments at internal supports if the effects of cracking of concrete are neglected in the analysis for ULS. Hogging bending moments can be then reduced by up to 30% and corresponding increases must be made to the sagging bending moments in the adjacent spans.

Usually, where composite slabs are subjected to hogging bending moment, the neutral axis intersects the profiled steel sheeting, so the contribution of the profiled steel sheeting is not taken into account on the total resistance. This contribution is not taken into account because the profiled steel sheeting is mostly or totally under compression and also because it is a small contribution compared to the one of the concrete under compression on the ribs. Fig. 3.15(a) shows the stress distribution considered to design steel-concrete

composite slabs in a negative bending moment situation. Once again, the concrete tensile resistance is ignored. For simplification, the concrete part in compression is considered with a constant width equal to the mean width of the rib b_0, as it is illustrated on Fig. 3.15(b).

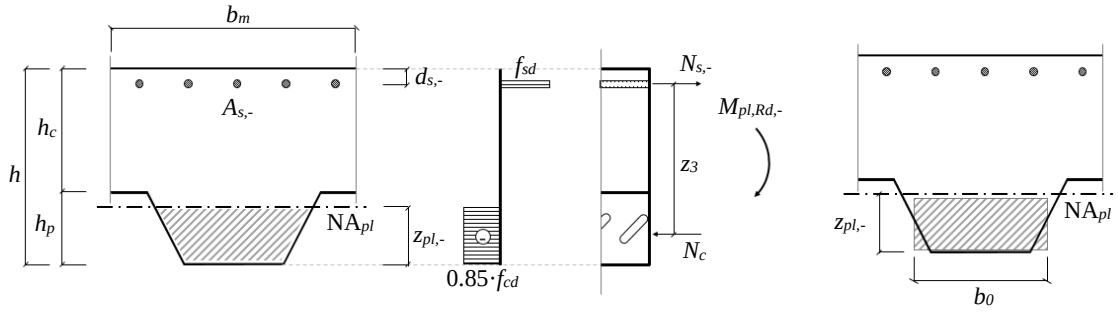

(a) stress distribution (b) compression area

Fig. 3.15 Hogging bending moment resistance

The negative plastic bending moment resistance of a composite slab $M_{pl,Rd,-}$ is given by (3.28), considering that the height of the plastic neutral axis $z_{pl,-}$ should be determined by equilibrium of the horizontal forces in just one composite slab module, as it is expressed by Eq. (3.29).

$$M_{pl,Rd,-} = N_{s,-} z_3 \tag{3.28}$$

$$\sum F_H = 0 \rightarrow N_{s,-} = N_c \rightarrow A_{s,-,m} f_{sd} = 0.85 f_{cd} b_0 z_{pl,-} \rightarrow z_{pl,-} = \frac{A_{s,-,m} f_{sd}}{0.85 f_{cd} b_0} \tag{3.29}$$

$$N_{s,-} = A_s f_{sd} \tag{3.30}$$

$$z_3 = h - \frac{z_{pl,-}}{2} - d_{s,-} \tag{3.31}$$

where:

$N_{s,-}$ is the design value of the plastic resistance of the steel reinforcement;
$A_{s,-}$ is the cross-sectional area of reinforcement to resist to negative bending;
$A_{s,-,m}$ is the cross-sectional area of reinforcement in one slab module;
f_{sd} is the design value of the yield strength of reinforcing steel;
b_0 is the mean width of a concrete rib;
z_3 is the vertical distance between forces N_c and $N_{s,-}$ given by $z_3 = h - d_{s,-} - e$;
$d_{s,-}$ is the distance from the steel reinforcement in tension to the extreme fibre of the composite slab in tension.

3.3.3.2 Longitudinal shear

3.3.3.2.1 Initial concepts

The longitudinal shear behaviour of steel-concrete composite slabs can be classified as (i) brittle or (ii) ductile. Fig. 3.16 shows the typical shapes of *P*-*δ* and *P*-*s* curves for each type of behaviour, where *P* is the applied load, *δ* the mid-span deflection and *s* the slip between the steel and the concrete. According to clause 9.7.3(3) of standard EN 1994-1-1 (CEN, 2004b) the behaviour may be considered as ductile if the maximum load P_{max} exceeds the load causing a recorded end slip of 0.1 mm $P_{0.1mm}$ by more than 10%.

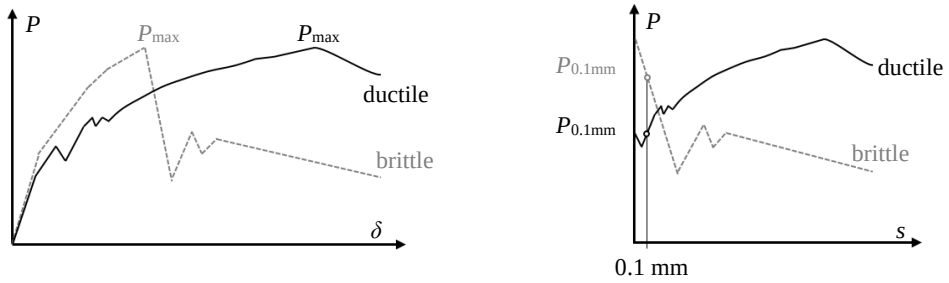

(a) Typical *P*-*δ* curves (b) Typical *P*-*s* curves

Fig. 3.16 Comparison between brittle and ductile behaviour

According to standard EN 1994-1-1 (CEN, 2004b), the longitudinal shear resistance of a composite slab can be predicted by one of two methods: (i) the *m*-*k* method or (ii) the partial connection method. In general, the *m*-*k* method is quite conservative, as it was concluded by Cifuentes and Medina (2013); it is based on empirical parameters obtained from slab tests meeting the basic requirements of the method and is valid for slabs with a brittle or ductile behaviour of the structural element. Actually, the *m*-*k* method is established for composite slabs with embossed steel sheets and it does not allow to account for different reinforcing systems implemented to increase the longitudinal shear resistance (Nagy and Szatmári, 1998). The partial connection method is also based on parameters obtained from tests but it allows us to take into account the contribution of any additional reinforcing system (e.g. end anchorage) or longitudinal reinforcing bars; however, its application is restricted to composite slabs with ductile behaviour.

According to the *m*-*k* method, the design value of the vertical shear force V_{Ed} must not be higher than the design value of the vertical shear resistance, governed by the longitudinal shear resistance, $V_{l,Rd}$. This method is conservative because it assumes that the longitudinal shear behaviour is always brittle and it does not allow to take into consideration the contribution of reinforcing systems to improve the longitudinal shear capacity of the slab; this method will be removed from the next edition of Eurocode 4 as

it was stated by Johnson (2018). According to the partial connection method, the design value of the bending moment M_{Ed} must not be higher than the design value of the bending moment resistance M_{Rd}.

3.3.3.2.2 *m-k* method

Standard EN 1994-1-1 (CEN, 2004b) provides the *m-k* method to design composite slabs for longitudinal shear. This method was developed based on the experimental programme carried out by Porter and Ekberg (1976) at the University of Iowa in United States of America. This method requires the determination of two parameters that define the linear regression line to limit the design values for each type of profile, *m* and *k*, as shown in Fig. 3.17. These parameters should be obtained by experimental tests in accordance with Annex B of Standard EN 1994-1-1 (CEN, 2004b). Clause 9.7.3(4) defines the design value of the vertical shear resistance, governed by the longitudinal shear resistance, $V_{l,Rd}$ as:

$$V_{l,Rd} = \frac{bd_p}{\gamma_{VS}}\left(m\frac{A_{pe}}{bL_s} + k\right) \tag{3.32}$$

where:

- b is the width of the slab;
- d_p is the effective height of the slab;
- γ_{VS} is the partial safety factor for the ultimate limit state, such that $\gamma_{VS} = 1.25$;
- A_{pe} is the nominal cross-sectional area of the profiled steel sheeting;
- L_s is the shear span which can be defined according to Eq. (3.33)

$$L_s = \frac{M_{Ed}}{V_{Ed}} \tag{3.33}$$

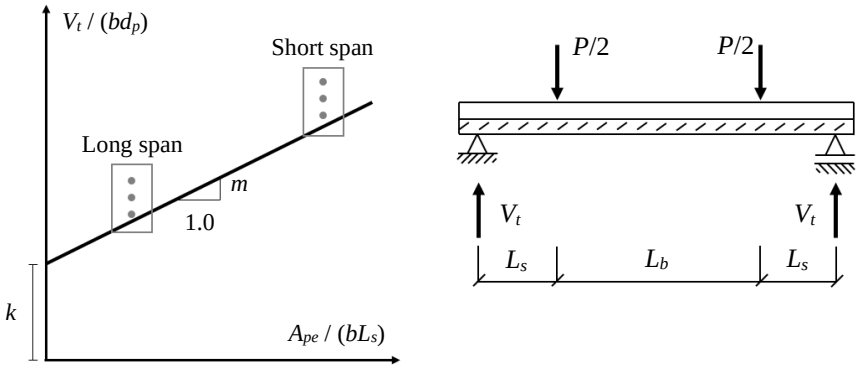

Fig. 3.17 Longitudinal shear resistance of composite slabs according to *m-k* method

Clause 9.7.3(5) of standard EN 1994-1-1 (CEN, 2004b) defines the shear span L_s according to the distribution of loading; it is defined that the shear span can be determined by the maximum moment M_{Ed} divided by the maximum vertical shear force V_{Ed} adjacent to the supports for the span considered. This definition can be applied to any case and covers the situation of a simply supported composite slab subjected to a uniformly distributed load where $L_s = L/4$. However, for continuous composite slabs, clause 9.7.3(6) of standard EN 1994-1-1 (CEN, 2004b) defines the shear span L_s of internal and external spans as 80% and 90%, respectively, of $L/4$. For composite slabs designed as continuous and subjected to uniformly distributed load these values could be conservative. For example, Table 3.2 presents for slabs with one, two and three spans (i) the maximum bending moment M_{Ed}, (ii) the maximum vertical shear next to the supports, (iii) the quotient between these values and (iv) the direct values given in standard EN 1994-1-1 (CEN, 2004b) for the shear span L_s. As it is possible to observe from Eq. (3.32), the higher the shear span L_s, the lower and, consequently, more conservative the design shear resistance $V_{l,Rd}$. So, for continuous composite slabs worth to define the shear span L_s by the quotient M_{Ed}/V_{Ed}.

Table 3.2 Shear span values for application on *m-k* method

		M_{Ed}	V_{Ed}	M_{Ed}/V_{Ed}	L_s
1 span		$\frac{pL^2}{8}$	$\frac{pL}{2}$	$\frac{L}{4}=0.25L$	$\frac{L}{4}=0.25L$
2 spans	External spans	$\frac{9pL^2}{128}$	$\frac{5pL}{8}$	$\frac{9L}{80}=0.1125L$	$0.9\frac{L}{4}=0.225L$
3 spans	Internal spans	$\frac{pL^2}{40}$	$\frac{pL}{2}$	$\frac{L}{20}=0.05L$	$0.8\frac{L}{4}=0.2L$
	External spans	$\frac{2pL^2}{25}$	$\frac{3pL}{5}$	$\frac{2L}{15}\approx 0.133L$	$0.9\frac{L}{4}=0.225L$

3.3.3.2.3Partial connection method

(i) Introduction

The partial connection method (PCM) can be used to obtain the design value of the bending moment resistant M_{Rd}, taking into account the longitudinal shear capacity of the composite slab. This method only can be used for composite slabs with a ductile behaviour ($P_{\max} \geq 1.10P_{0.1\text{mm}}$), which can be proved, for instance, by experimental campaign regulated by Annex B of standard EN 1994-1-1 (CEN, 2004b). This method is based on the design value of longitudinal shear strength of a composite slab $\tau_{u,Rd}$ mainly acquired by the embossments of the profiled steel sheeting.

According to clause B.3.2(7) of standard EN 1994-1-1 (CEN, 2004b), not less than four tests should be carried out to evaluate $\tau_{u,Rd}$ value for each type of steel sheet. Specimens must have the same height h and must not have any additional reinforcement or end anchorage. Three tests must have a span as long as possible, while still providing failure by longitudinal shear, and in the remaining one test as short as possible, while still providing failure by longitudinal shear. Shortest specimen, with a span length higher than 3h, is only used to classify the longitudinal shear behaviour of the profiled steel sheeting.

(ii) Composite slabs without end anchorage system

The partial connection method should be applied to analyse the section subjected to the maximum bending moment and it is considered that this section achieves its plastic capacity. To avoid a sudden collapse, profiled steel sheeting should provide a ductile behaviour. Usually, composite slabs with flat steel sheeting does not achieve a load higher than the one relative to the initial slip (brittle behaviour). This type of slabs should be analysed using the *m-k* method.

Section B.3.6 of standard EN 1994-1-1 (CEN, 2004b) defines that the design value of the bending moment resistance of a composite slab M_{Rd} is mainly influenced by its connection degree η, which is defined by Eq. (3.34).

$$\eta = \frac{N_c}{N_{cf}} \tag{3.34}$$

$$N_c = \tau_{u,Rd} b L_x \leq N_{cf} \tag{3.35}$$

where:

N_c is the design value of the compressive normal force in the concrete;

N_{cf} is the design value of the compressive normal force in the concrete in full shear connection;

$\tau_{u,Rd}$ is the design value of longitudinal shear strength of the composite slab;

b is the width of slab;

L_x is the distance from a cross-section to the nearest support.

Along the span (L_x) three cases can be found, regarding the nature of the connection degree η. These cases, represented by points A, B and C, are represented in Fig. 3.18, where:

A. $N_c = 0 \rightarrow \eta = 0 \rightarrow$ Null shear connection;
B. $0 < N_c < N_{cf} \rightarrow 0 < \eta < 1 \rightarrow$ Partial shear connection;
C. $N_c = N_{cf} \rightarrow \eta = 1 \rightarrow$ Full shear connection.

The point C corresponds to full connection conditions, which represents the plastic bending moment resistance. That is why clause 6.1.1(7) of standard EN 1994-1-1 (CEN, 2004b) states that a span has full shear connection when increase in the number of shear connectors would not increase the design bending resistance of the member. Otherwise, the shear connection is partial.

So, the design value of the compressive normal force in the concrete with full shear connections N_{cf} should be obtained in the same way as it was in the bending moment resistance:

$$N_{cf} = \min\left\{0.85 f_{cd} h_c b; A_{pe} f_{yp,d}\right\} \tag{3.36}$$

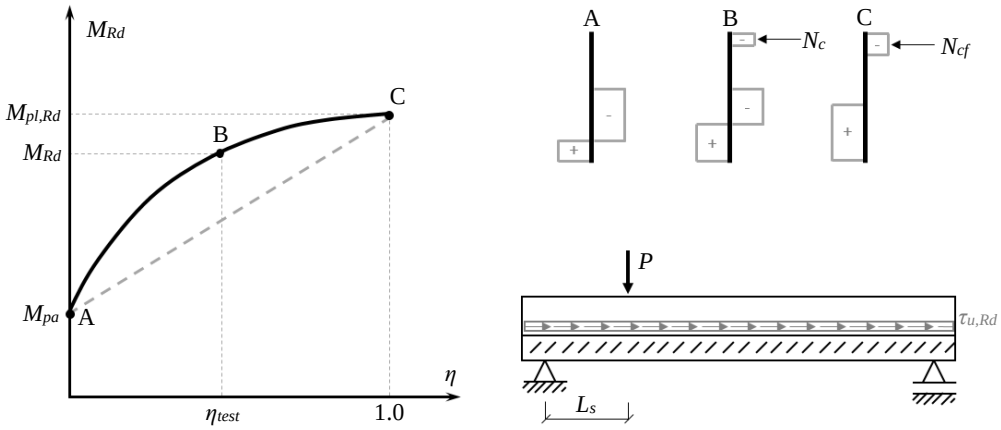

Fig. 3.18 Bending moment resistance M_{Rd} vs. connection degree η

The stress distribution is identical to the one considered for the bending moment capacity, but the design value of the resistance moment M_{Rd} is defined replacing N_{cf} value by N_c, as expressed by Eq. (3.37).

$$M_{Rd} = N_c z + M_{pr} \tag{3.37}$$

where:

$$z = h - 0.5 z_{pl,+} - e_p + (e_p - e)\frac{N_c}{A_{pe} f_{yp,d}} \tag{3.38}$$

Eq. (3.39) defines the minimum distance L_{sf} of a cross-section to the nearest support to be in full connection. For example, in simply-supported composite slabs, the slab just achieves the full connection in cross-sections where the condition $L_x \geq L_{sf}$ is verified. If the cross-section where the maximum bending moment occurs verifies this condition, this means that the bending capacity of the slab is achieved and the longitudinal shear failure is avoided.

$$\eta = 1.0 \rightarrow N_c = N_{cf} \rightarrow L_{sf} = \frac{N_{cf}}{\tau_{u,Rd} b} \tag{3.39}$$

Fig. 3.19 presents a qualitative representation of the span length influence in the connection degree at failure. Four different examples of simply-supported composite slabs subjected to uniformly distributed load are show:

A. $L_A < L_{sf} \rightarrow$ The minimum distance of a cross-section to the nearest support to be in full connection L_{sf} is higher than the total span length $L_A \rightarrow$ Longitudinal shear failure;
B. $L_B/2 < L_{sf} \rightarrow$ The minimum distance of a cross-section to the nearest support to be in full connection L_{sf} is higher than half of the total span length $L_B \rightarrow$ Longitudinal shear failure, but $M_{Rd,B} > M_{Rd,A}$;
C. $L_C/2 = L_{sf} \rightarrow$ The minimum distance of a cross-section to the nearest support to be in full connection L_{sf} is equal to half of the total span length $L_C \rightarrow$ Bending capacity is achieved and $M_{pl,Rd} = M_{Rd,C} > M_{Rd,B}$;
D. $L_D/2 > L_{sf} \rightarrow$ The minimum distance of a cross-section to the nearest support to be in full connection L_{sf} is lower than half of the total span length $L_D \rightarrow$ Bending capacity is achieved but not higher than C example, so $M_{pl,Rd} = M_{Rd,D} = M_{Rd,C}$.

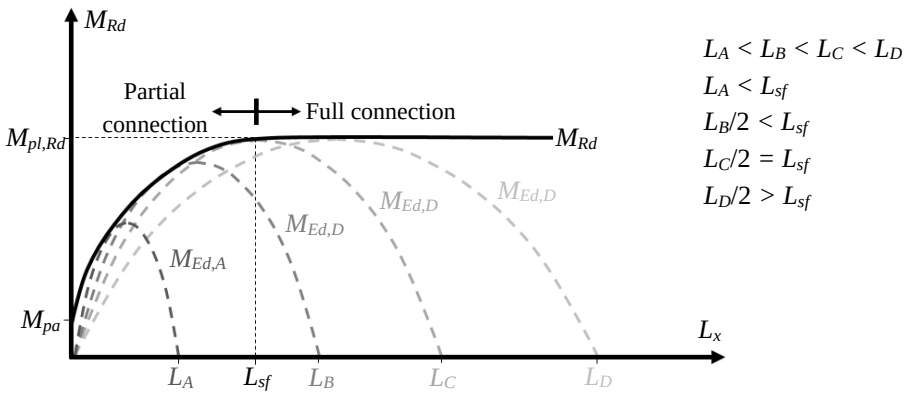

Fig. 3.19 Longitudinal shear resistance for different span lengths

(iii) Composite slabs with end anchorage devices

The partial connection method allows to take into account the contribution of reinforcing systems in the longitudinal shear resistance of composite slabs with ductile behaviour. According to clause 9.7.4(2) the design longitudinal shear resistance of slabs with end anchorage provided by welded studs or deformation of the ribs may be defined by the partial connection method with N_c increased by the design resistance of the end anchorage F_{ea}.

So the design value of the resistance moment M_{Rd} is determined by Eq. (3.40).

$$M_{Rd} = N_c z + M_{pr} \tag{3.40}$$

where:

$$N_c = \tau_{u,Rd} b L_x + F_{ea} \leq N_{cf} \tag{3.41}$$

For steel-concrete composite slabs where the longitudinal shear resistance is improved by headed studs welded to the supporting beams through the profiled steel sheeting the end anchorage F_{ea} is given by the design resistance $P_{pb,Rd}$ of a headed stud times the number of studs n_{st} over a width b, as expressed by Eq. (3.42). According to clause 9.7.4(3) of standard EN 1994-1-1 (CEN, 2004b) the design resistance $P_{pb,Rd}$ of a headed stud used for end anchorage should be taken as the minimum value between: (i) the shear resistance of the stud $P_{Rd,1}$; (ii) the crushing resistance of the concrete $P_{Rd,2}$ and; (iii) the bearing resistance of the sheet $P_{Rd,3}$.

$$F_{ea} = n_{st} P_{pb,Rd} \tag{3.42}$$

$$P_{pb,Rd} = \min\left\{P_{Rd,1}; P_{Rd,2}; P_{Rd,3}\right\} \tag{3.43}$$

with:

$$P_{Rd,1} = \frac{0.8 f_u \pi d^2 / 4}{\gamma_V} \tag{3.44}$$

$$P_{Rd,2} = \frac{0.29 \alpha d^2 \sqrt{f_{ck} E_{cm}}}{\gamma_V} \tag{3.45}$$

$$P_{Rd,3} = k_\varphi d_{d0} t f_{yp,d} \tag{3.46}$$

where:

f_u is the is the specified ultimate tensile strength of the material of the stud but not greater than 500 N/mm^2;

d is the diameter of the shank of the stud, 16 mm ≤ d ≤ 25 mm;

h_{sc} is the overall nominal height of the stud;

d_{do} is the diameter of the weld collar which may be taken as 1.1d;

a is the distance from the centre of the stud to the end of the sheeting, to be not less than 1.5·d_{d0};

t is the thickness of the sheeting;

$f_{yp,d}$ is the design value of the yield strength of profiled steel sheeting;

f_{ck} is the characteristic compressive strength of the concrete;

E_{cm} is the modulus of elasticity of concrete;

γ_V is the partial factor for design shear resistance of a headed stud, such that $\gamma_V = 1.25$;
α is given by Eq. (3.47);
k_φ is given by Eq. (3.48).

$$\alpha = \begin{cases} 0.2\left(\frac{h_{sc}}{d}+1\right), \text{ for } 3 \le h_{sc}/d \le 4 \\ 1.0, \text{ for } h_{sc}/d > 4 \end{cases} \tag{3.47}$$

$$k_\varphi = 1 + \frac{a}{d_{d0}} \tag{3.48}$$

Fig. 3.20 shows the effect of end anchorage systems on the resistance bending moment M_{Rd} diagram. End anchorage systems allows to increase the longitudinal shear resistance of composite slabs, especially close to the supports. No effect is produced where the full connection is achieved, since this type of systems does not increase the bending resistance. So, end anchorage devices allow to: (i) increase the bending moment resistant M_{Rd}; (ii) decrease the minimum distance of a cross-section to the nearest support to be in full connection L_{sf} and; (iii) increase the connection degree η.

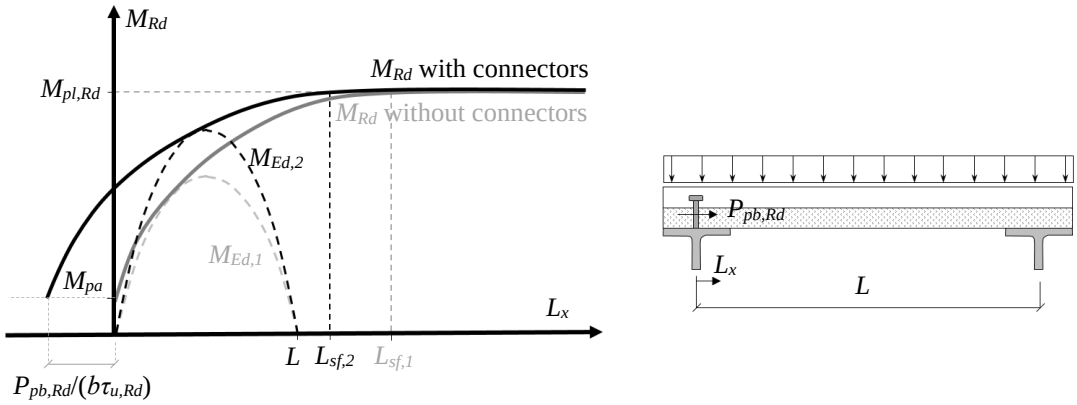

Fig. 3.20 Longitudinal shear resistance M_{Rd} of composite slabs with end anchorage devices

3.3.3.3 Vertical shear

According to standard EN 1994-1-1 (CEN 2004b), the vertical shear resistance of composite slabs is mainly acquired from the concrete rib because standard EN 1994-1-1 (CEN, 2004b) propose to evaluate the vertical shear resistance of a composite slab $V_{v,Rd}$ in accordance with section 6.2.2 of standard EN 1992-1-1 (CEN, 2004a).

According to standard EN 1992-1-1 (CEN, 2004a), the vertical shear resistance V_{Rd} of reinforced concrete members with a constant height over the span must be defined as:

$$V_{Rd} = V_{Rd,s} \leq V_{Rd,\max} \tag{3.49}$$

where $V_{Rd,s}$ is the design value of the shear force which can be sustained by the yielding shear reinforcement and $V_{Rd,\max}$ is the design value of the maximum shear force which can be sustained by the member, limited by the crushing of the compression struts.

For members where $V_{Ed} \leq V_{Rd,c}$, where $V_{Rd,c}$ is the design shear resistance of the concrete part, it is not necessary to design shear reinforcement and V_{Rd} must be defined as:

$$V_{Rd} = V_{Rd,c} \leq V_{Rd,\max} \tag{3.50}$$

Section 6.2.2 of standard EN 1992-1-1 (CEN, 2004a) predicts the design value for the shear resistance $V_{Rd,c}$ for members where is not required design shear reinforcement as:

$$V_{Rd,c} = \left[C_{Rd,c} k \left(100 \rho_1 f_{ck}\right)^{1/3} + k_1 \sigma_{cp} \right] b_w d \tag{3.51}$$

with a minimum of:

$$V_{Rd,c} = \left[v_{\min} + k_1 \sigma_{cp} \right] b_w d \tag{3.52}$$

where:

$C_{Rd,c}$ is defined as $0.18 / \gamma_c$;
γ_c is the partial safety factor for concrete such that $\gamma_c = 1.50$;
k is the coefficient defined according to Eq. (3.53);
ρ_1 is the coefficient defined according to Eq. (3.54);
b_w is the smallest width of the cross-section in the tensile area;
d is the effective height;
f_{ck} is the characteristic compressive strength of the concrete;
A_{sl} is the area of the tensile reinforcement extended more than $l_{b,\min}+d$;
$l_{b,\min}$ is the minimum design anchorage length according to section 8.4.4 of standard EN 1992-1-1 (CEN, 2004a);
$v_{\min}$ is de minimum value for v, defined according to Eq. (3.55);
k_1 is a coefficient such that $k_1 = 0.15$;
σ_{cp} is the average compression stress on the concrete cross-section.

$$k = 1 + \sqrt{200 / d} \tag{3.53}$$

$$\rho_1 = \frac{A_{sl}}{b_w d} \leq 0.02 \tag{3.54}$$

$$v_{\min} = 0.035 \cdot k^{3/2} \cdot f_{ck}^{1/2} \tag{3.55}$$

So, the vertical shear resistance of a composite slab $V_{v,Rd}$ can be defined as the product between the number of modules n in a width b and the vertical shear resistance of one

module $V_{v,Rd,m}$, as given by Eq. (3.56). The width of a module b_m is the distance between the centres of two consecutive upper flanges, as shown in Fig. 3.21. Thus, the vertical shear resistance of a composite slab module $V_{v,Rd,m}$ is evaluated by Eq. (3.57), based on Eq. (3.51), but replacing the dimensions b_w and d by the mean width of a concrete rib b_0 and the effective height of the composite slab d_p, defined as the distance between the centroidal axis of the profiled steel sheeting and the extreme fibre of the composite slab in compression, respectively. Typically, the beneficial effect of the compression in the concrete slab is not accounted, for composite slabs are usually analysed as simply supported elements, and so $\sigma_{cp} = 0$.

$$V_{v,Rd} = \frac{b}{b_m} V_{v,Rd,m} = n V_{v,Rd,m} \tag{3.56}$$

$$V_{v,Rd,m} = \max\left\{ C_{Rd,c} k \left(100 \rho_1 f_{ck}\right)^{1/3} ; \upsilon_{\min} \right\} \times b_0 d_p \tag{3.57}$$

The contribution of the profiled steel sheeting is accounted by replacing the area of the profiled steel sheeting in the A_{sl} value to define the coefficient ρ_1, when the minimum conditions of anchorage are satisfied. Accounting the contribution of the profiled steel sheeting just based on its area instead of its shape, leads to a conservative design. The webs of the profiled steel sheeting resist the vertical shear during unpropped construction and, so make a permanent contribution during the definitive phase.

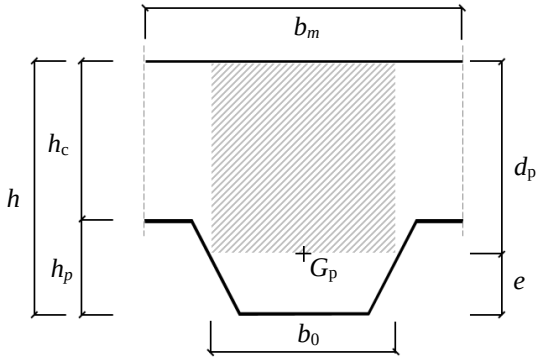

Fig. 3.21 Concrete area considered for the vertical shear resistance of composite slabs according to Eurocode 4

3.3.3.4 Punching shear

A steel-concrete composite slab subjected to significant concentrated loads may reach failure by punching shear. Also for punching shear, steel-concrete composite slabs must be designed in the same way as reinforced concrete slabs. Section 9.7.6 of standard EN 1994-1-1 (CEN, 2004b) refers that the punching shear design of composite slabs must be done in accordance with section 6.4.4 of standard EN 1992-1-1 (CEN, 2004a). The

contact surface area of the applied load influences significantly the resistance to punching shear, instead of the load application position. The larger the area of the load application, the more distributed this would be and the lower the risk of a punching shear failure. For composite slabs, the punching shear failure happens in a critical perimeter of length c_p influenced by the concrete part height h_c, in the transversal direction, and by the effective height d_p, in the longitudinal direction, as shown in Fig. 3.22. The critical perimeter length c_p for a loaded area a_p by b_p is then defined according to Eq. (3.58), where all dimensions are illustrated in Fig. 3.22.

$$c_p = 2\pi h_c + 2\left(b_p + 2h_f\right) + 2\left(a_p + 2h_f + 2d_p - 2h_c\right) \tag{3.58}$$

Section 6.4.4 of standard EN 1992-1-1 (CEN, 2004a) defines the resistance stress to punching shear $v_{p,Rd}$ according to Eq. (3.59).

$$v_{p,Rd} = C_{Rd,c}k\left(100\rho_1 f_{ck}\right)^{1/3} + k_1\sigma_{cp} \geq v_{\min} + k_1\sigma_{cp} \tag{3.59}$$

where:

ρ_1 is the total reinforcement ratio defined according to Eq. (3.60);

ρ_{lx} is the reinforcement ratio for steel with x axis direction defined according to Eq. (3.61);

ρ_{ly} is the reinforcement ratio for steel with y axis direction defined according to Eq. (3.62);

$A_{sl,x}$ is the area of the tensile steel cross-section with x axis direction per unit of width;

$A_{sl,y}$ is the area of the tensile steel cross-section with y axis direction per unit of width;

k_1 is a coefficient such that $k_1 = 0.10$.

$$\rho_1 = \sqrt{\rho_{lx}\rho_{ly}} \leq 0.02 \tag{3.60}$$

$$\rho_{lx} = \frac{A_{sl,x}}{db} \tag{3.61}$$

$$\rho_{ly} = \frac{A_{sl,y}}{db} \tag{3.62}$$

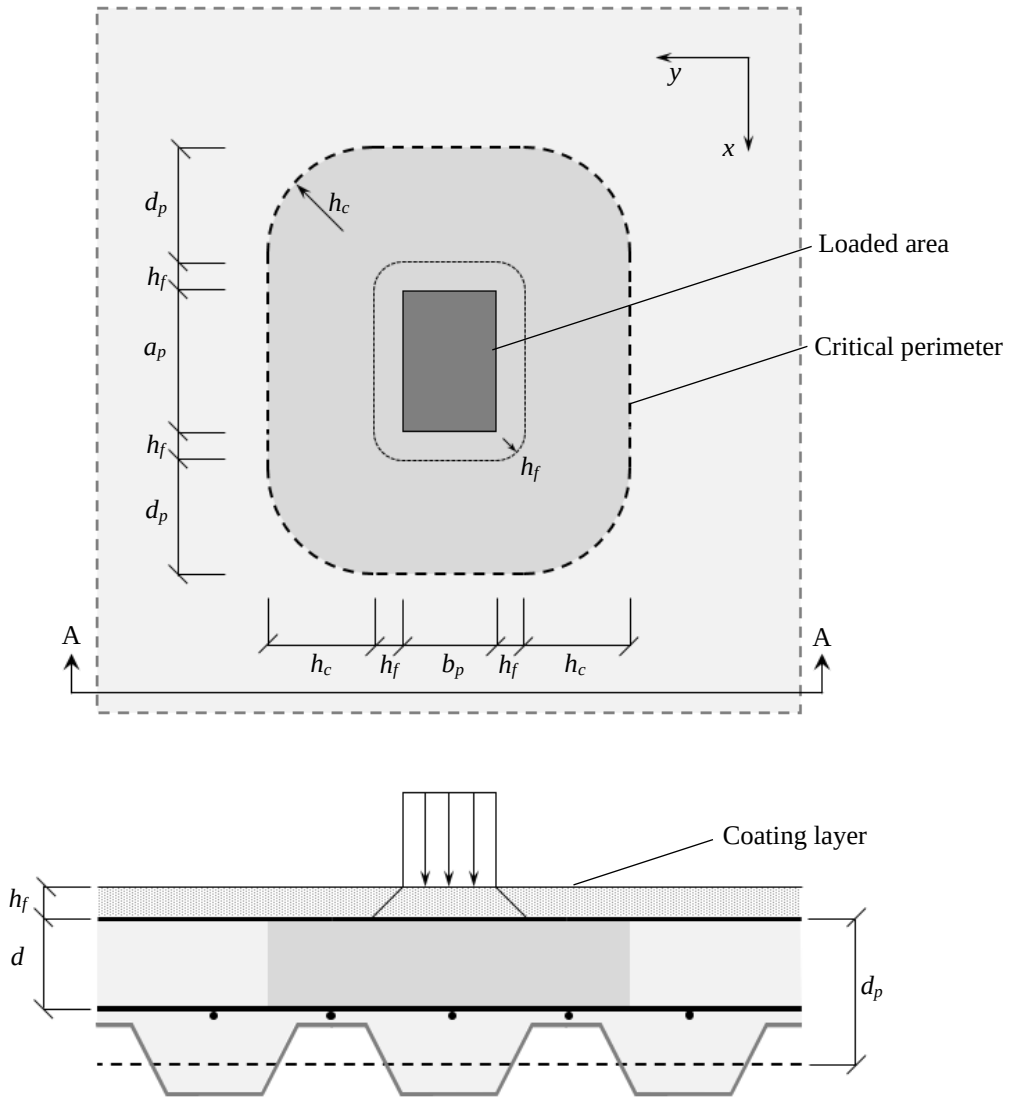

Fig. 3.22 Critical perimeter for punching shear

Other symbols and respective values were already described and defined in the previous section for vertical shear design model. For composite slabs, like was said for the vertical shear resistance, the beneficial effect of the compression in the concrete slab is not accounted, and so $\sigma_{cp} = 0$. Thus, the punching shear stress resistance $v_{p,Rd}$ is defined by Eq. (3.63).

$$v_{p,Rd} = C_{Rd,c} k \left(100 \rho_1 f_{ck}\right)^{1/3} \geq v_{\min} \tag{3.63}$$

So, the design value of the resistance to punching shear $V_{p,Rd}$ is given by Eq. (3.64).

$$V_{p,Rd} = v_{p,Rd} c_p d \tag{3.64}$$

Taking into consideration that punching shear design model for composite slabs from standard EN 1994-1-1 (CEN, 2004b) does not account the contribution of the profiled steel sheeting and the concrete ribs, Eq. (3.64) is likely to give a conservative design resistance (Johnson, 2018).

3.3.4 SLS design

Service limit states of composite slabs is regulated by section 9.8 of standard EN 1994-1-1 (CEN, 2004b). The verification of serviceability limit states of steel-concrete composite slabs must be checked for cracking, deflection and vibrations phenomena.

3.3.4.1 Cracking

The cracks on the concrete slab must be limited to ensure the durability of the slab. The crack control of concrete in composite slabs must be checked according to section 9.8.1 of standard EN 1994-1-1 (CEN, 2004b) which forwards this verification to section 7.3 of standard EN 1992-1-1 (CEN, 2004a). For composite slabs, the crack control just need to be verified in the hogging moment regions, in the top layer of the slab, since the profiled steel sheeting under the concrete protects the bottom part. Cracking is more likely when continuous composite slabs are designed as simply supported slabs and for propped construction.

Taking this influence in consideration, longitudinal reinforcement must be placed in the supports regions. In these situations, the cross-sectional area of the reinforcement above the ribs should not be less than 0.2% of the area of concrete above the sheeting for un-propped construction and 0.4% for propped construction, in accordance with clause 9.8.1(2) of standard EN 1994-1-1 (CEN, 2004b). The reinforcement should be applied in the supports regions and extended at least $0.25L$ to both sides of adjacent spans, where L is the length of the span. However, these conditions do not ensure crack width values lower than 0.3 mm. In order to control the maximum width of cracks in hogging bending moment regions of continuous composite slabs, the minimum reinforcement shall be determined according to clauses 7.4.2 and 7.4.3 of standard EN 1994-1-1 (CEN, 2004b).

3.3.4.2 Deflection

3.3.4.2.1 Initial assumptions

Profiled steel sheeting deflection is irreversible. According to clause 3.4(3) of standard EN 1990 (CEN, 2002a) the verification of serviceability deflection shall be checked concerning the appearance, the comfort of users and the functioning of the structure

(including machines or services) there included. Deflections on composite slabs shall be calculated using elastic analysis, neglecting the effects of shrinkage.

According to clause 9.8.2(3) of standard EN 1994-1-1 (CEN, 2004b), deflection limit states may be omitted if the span to effective depth ratio does not exceed the limits given in EN 1992-1-1 (CEN, 2004a), 7.4, for lightly stressed concrete, and the connection degree η is such that end slip will not occur under service loading (based on experimental results). The first condition is applicable to simply supported slabs with a L/d_p ratio between 14 and 20, where L is the span length and d_p the effective depth, except if other limits are specified in national annexes (Johnson, 2018).

The deflection of composite slabs may be determined using the following approximations: (i) the second moment of area of the composite section I_{eq} may be taken as the average of the values for the cracked $I_{eq,2}$ and un-cracked $I_{eq,1}$ section; (ii) for concrete, an average value of the modular ratio for both long and short-term effects may be used. The modular ratio n is then defined by $n = 2 \cdot E_s/E_{cm}$ for long-term effect and by $n = E_s/E_{cm}$ for short-term effect, where E_s is the Modulus of elasticity of the steel and E_{cm} is the secant modulus of elasticity of concrete.

The equations presented in this sections show the procedure to determine the second moment of area of composite slabs: first it is necessary to find the position of the neutral axis based on the analysis of one slab module section; then the equation to obtain the second moment of area is defined considering a general width b.

3.3.4.2.2 Deflection due to sagging bending moment

In accordance with clause 9.8.2(5) of standard EN 1994-1-1 (CEN, 2004b) the equivalent moment of inertia in sagging bending moment regions I_{eq} should be defined according to Eq. (3.65).

$$I_{eq} = \frac{I_{eq,1} + I_{eq,2}}{2} \tag{3.65}$$

where:

$I_{eq,1}$ is the second moment of area of the effective equivalent steel section assuming that the concrete in tension is un-cracked (un-cracked section);

$I_{eq,2}$ is the second moment of area of the effective equivalent steel section neglecting concrete in tension but including reinforcement (cracked section).

(i) Cracked section

Usually, when a section is analysed as a cracked cross-section the neural axis is above the profiled steel sheeting. The moment of inertia should be determined considering the concrete section above the neutral axis (under compression), the profiled steel sheeting and the longitudinal reinforcing bars area (under tension). The positive contribution of the longitudinal reinforcement on the ribs, if any exist, shall be considered in the evaluation of the bending stiffness of the composite slab.

Fig. 3.23 shows the cracked analysis of a slab module cross-section, where the concrete is transformed in an equivalent steel section by the n ratio. The distance between the neutral axis and the top surface of the composite slab z_{cr} can be given by Eq. (3.66), such that the solution for z_{cr} is given by Eq. (3.67), if $A_{s,m} > 0$, and by Eq. (3.68), if $A_{s,m} = 0$.

$$z_{cr} = \frac{\frac{b_m}{n} z_{cr} \frac{z_{cr}}{2} + A_{pe,m} d_p + A_{s,m} d_s}{\frac{b_m}{n} z_{cr} + A_{pe,m} + A_{s,m}} \tag{3.66}$$

$$z_{cr} = \frac{\sqrt{n\left(A_{pe,m}^2 n + 2A_{pe,m} b_m d_p + 2A_{pe,m} n A_{s,m} + 2b_m A_{s,m} d_s + n A_{s,m}^2\right)} - A_{pe,m} n + A_{s,m} n}{b_m} \tag{3.67}$$

$$z_{cr} = \frac{nA_{pe,m}}{b_m}\left(\sqrt{1 + \frac{2b_m d_p}{nA_{pe,m}}} - 1\right) \tag{3.68}$$

where:

- n is the modular ratio;
- $A_{pe,m}$ is the effective profiled steel sheeting area in a slab module;
- $A_{s,m}$ is the longitudinal reinforcing bar area in a slab module;
- b_m is the width of a slab module;
- d_p is the effective height of the slab;
- d_s is the depth of the reinforcement geometric centre.

So, the moment of inertia of a cracked section $I_{eq,2}$ can be determined in a width equal to b according to Eq. (3.69).

$$I_{eq,2} = \frac{bz_{cr}^3}{3n} + I_p + A_{pe}\left(d_p - z_{cr}\right)^2 + A_s\left(d_s - z_{cr}\right)^2 \tag{3.69}$$

where:

- I_p is the moment of inertia of the profiled steel sheeting in its centroidal axis;
- A_{pe} is the effective profiled steel sheeting cross-section area;
- A_s is the longitudinal reinforcing bar area in a width b.

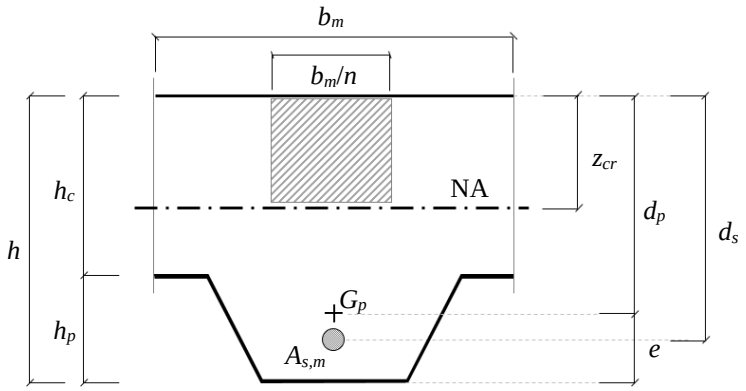

Fig. 3.23 Moment of inertia determination for a cracked cross-section, when subjected to sagging bending moment

(ii) Uncracked section

To analyse the un-cracked section, the all concrete cross-section and the profiled steel sheeting cross-section must be taken into account. In this case the contribution of the longitudinal reinforcing bars can be neglected. It is considered that the concrete in the ribs has a constant width equal to the mean width of a concrete rib b_0.

Fig. 3.24 shows the analysis of the un-cracked slab module cross-section, where the concrete is transformed in an equivalent steel section to steel by the n ratio. The distance between the neutral axis and the top fibre of the composite slab z_{uncr} is given by Eq. (3.70)

$$z_{uncr} = \frac{\frac{b_m h_c^2}{2n} + \frac{b_0 h_p h_c}{n} + \frac{b_0 h_p^2}{2n} + A_{pe,m} d_p}{\frac{b_m h_c}{n} + \frac{b_0 h_p}{n} + A_{pe,m}} \tag{3.70}$$

The result of this equation could lead to two different cases: (i) $z_{uncr} \geq h_c$, so the neutral axis intersects the profiled steel sheeting; (ii) $z_{uncr} < h_c$, so the neutral axis is above the profiled steel sheeting. However, the determination of the second moment of area of an uncracked section does not depend on the netutral axis position. The moment of inertia $I_{eq,1}$ is then given by Eq. (3.71).

$$\begin{aligned} I_{eq,1} = {} & \frac{b h_c^3}{12n} + \frac{b h_c}{n}\left(z_{uncr} - \frac{h_c}{2} \right)^2 + \frac{b b_0 h_p^3}{12 n b_m} + \\ & + \frac{b b_0 h_p}{n b_m}\left(h - z_{uncr} - \frac{h_p}{2} \right)^2 + A_{pe}\left(d_p - z_{uncr} \right)^2 + I_p \end{aligned} \tag{3.71}$$

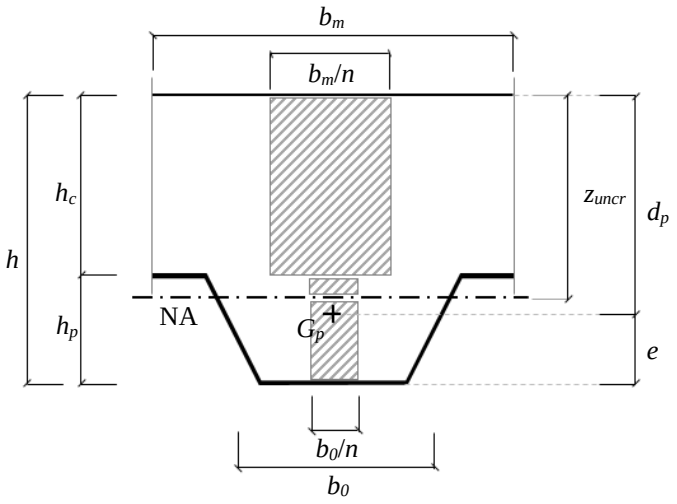

Fig. 3.24 Moment of inertia determination for a uncracked cross-section, when subjected to sagging bending moment (NA intersecting the profiled steel sheeting)

3.3.4.2.3 Deflection due to hogging bending moment

In hogging bending moment regions, the moment of inertia of a composite slab $I_{eq,-}$ should be defined using a cracked analysis of the cross-section, so not considering the concrete area under tension. To determine the moment of inertia in these conditions should be considered (i) the concrete cross-section in the rib under the neutral axis and under compression and (ii) the longitudinal reinforcing bars cross-section placed at the top of the slab to resist the hogging bending moments, as shown in Fig. 3.25.

Fig. 3.25 represents the analysis of a cracked cross-section of a composite slab in a hogging bending moment region. Since the profiled steel sheeting is almost all under compression its contribution is not taken into account. Once again it is considered that the concrete in the ribs has a constant width equal to the mean width of a concrete rib b_0. So, the position of the neutral axis would be given by Eq. (3.72).

$$z_{cr,-} = -\frac{A_{s,-,m}n}{b_0} + \frac{n}{b_0}\sqrt{A_{s,-,m}^2 + 2\frac{b_0}{n}A_{s,-,m}\left(h - d_{s,-}\right)} \tag{3.72}$$

where:

$A_{s,-,m}$ is the longitudinal reinforcing bar area in a slab module;

$d_{s,-}$ is the height of the reinforcement geometric centre.

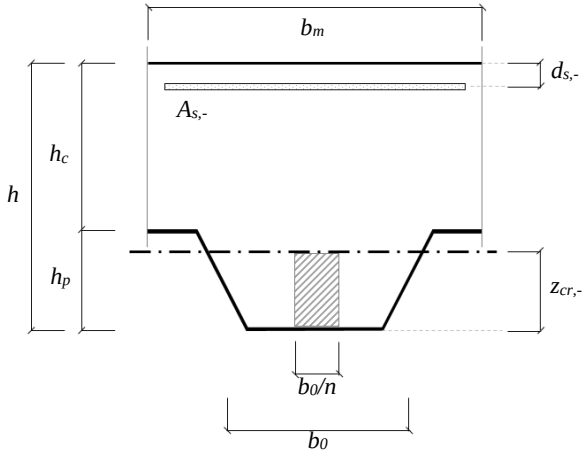

Fig. 3.25 Moment of inertia determination for a cracked cross-section, when subjected to hogging bending moment

Usually, $z_{cr,-} < h_p$ and so the neutral axis intersects the profiled steel sheeting. Then the moment of inertia of a composite slab in a hogging bending moment region $I_{eq,-}$ would be given by Eq. (3.73).

$$I_{eq,-} = \frac{\frac{b_0}{b_m} z_{cr,-}^3}{3n} + A_{s,-}\left(h - z_{cr,-} - d_{s,-}\right)^2 \tag{3.73}$$

where $A_{s,-}$ is the area of the upper longitudinal reinforcement over a width equal to b.

3.3.4.3 Vibrations

Clause 7.3.2(1) of standard EN 1994-1-1 (CEN, 2004b) regulates the vibration limit states of steel-concrete composite members. According to Hechler *et al.* (2008a) the vibration comfort of slabs is not clearly defined in the relevant standards. However, several researchers have been studying the dynamic response of steel-concrete composite slabs (Campista and Silva, 2018; Chen *et al.* , 2018; Hechler *et al.*, 2008; Hicks and Peltonen, 2013) and some design guides have been developed (Feldmann *et al.*, 2009; Hechler *et al.*, 2008b; HIVOSS, 2008) to help designers to take into account the effect of vibrations in their structural design.

According to Feldmann *et al.* (2009) the design procedure of composite floors for vibration limit states comprises three main steps: (i) to determine the dynamic floor characteristics, such as the natural frequency f, the modal mass M_{Mod} and the damping D; (ii) to define the OS-RMS$_{90}$ value and; (iii) to determine the acceptance class.

The natural frequency f, the modal mass M_{Mod} and the damping D of a composite slab are given by Eqs. (3.76), (3.77) and (3.78), respectively.

$$f = \frac{\alpha}{L^2}\sqrt{\frac{Eh^3}{12m(1-\nu^2)}} \tag{3.74}$$

$$M_{Mod} = \beta M \tag{3.75}$$

$$D = D_1 + D_2 + D_3 \tag{3.76}$$

where:

- α; β are coefficients defined according to the boundary conditions;
- L is the span length;
- E is the Young modulus given by $E = 1.1E_{cm}$;
- h is the height of the slab;
- m is the mass of floor including finishing and a representative amount of imposed load by square meter;
- ν is the Poisson coefficient;
- M is the total mass of floor including finishing and a representative amount of imposed load;
- D_1 is the structural damping (see Table 3.3);
- D_2 is the damping due to furniture (see Table 3.3);
- D_3 is the damping due to finishes (see Table 3.3).

Feldmann *et al.* (2009) presented the formulas to determine the coefficient α and the values of β, according to the boundary conditions. Fig. 3.26(a) shows the example of the value of α for simply-supported composite slabs, where β is equal to 0.20. Then, the OS-RMS$_{90}$ value and the acceptance class are defined using diagrams like the one presented on Fig. 3.26(b), also provided by Feldmann *et al.* (2009).

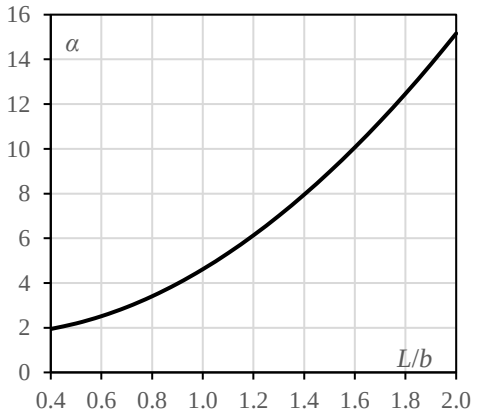

(a) Coefficient α (β = 0.20)

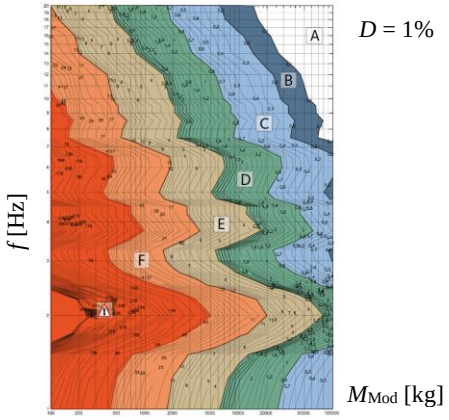

(b) OS-RAMS value and acceptance class

Fig. 3.26 Vibration design of steel-concrete composite slabs

Table 3.3 Determination of the damping

Type	**Damping *D* [%]**
Structural Damping D_1	
Wood	**6%**
Concrete	**2%**
Steel	**1%**
Composite Steel-Concrete	**1%**
Damping due to furniture D_2	
Traditional office for 1 to 3 persons	**2%**
Paperless office	**0%**
Open plan office	**1%**
Library	**1%**
Houses	**1%**
Schools	**0%**
Gymnastic	**0%**
Damping due to finishes D_3	
Ceiling under the floor	**1%**
Free floating floor	**0%**
Swimming screed	**1%**

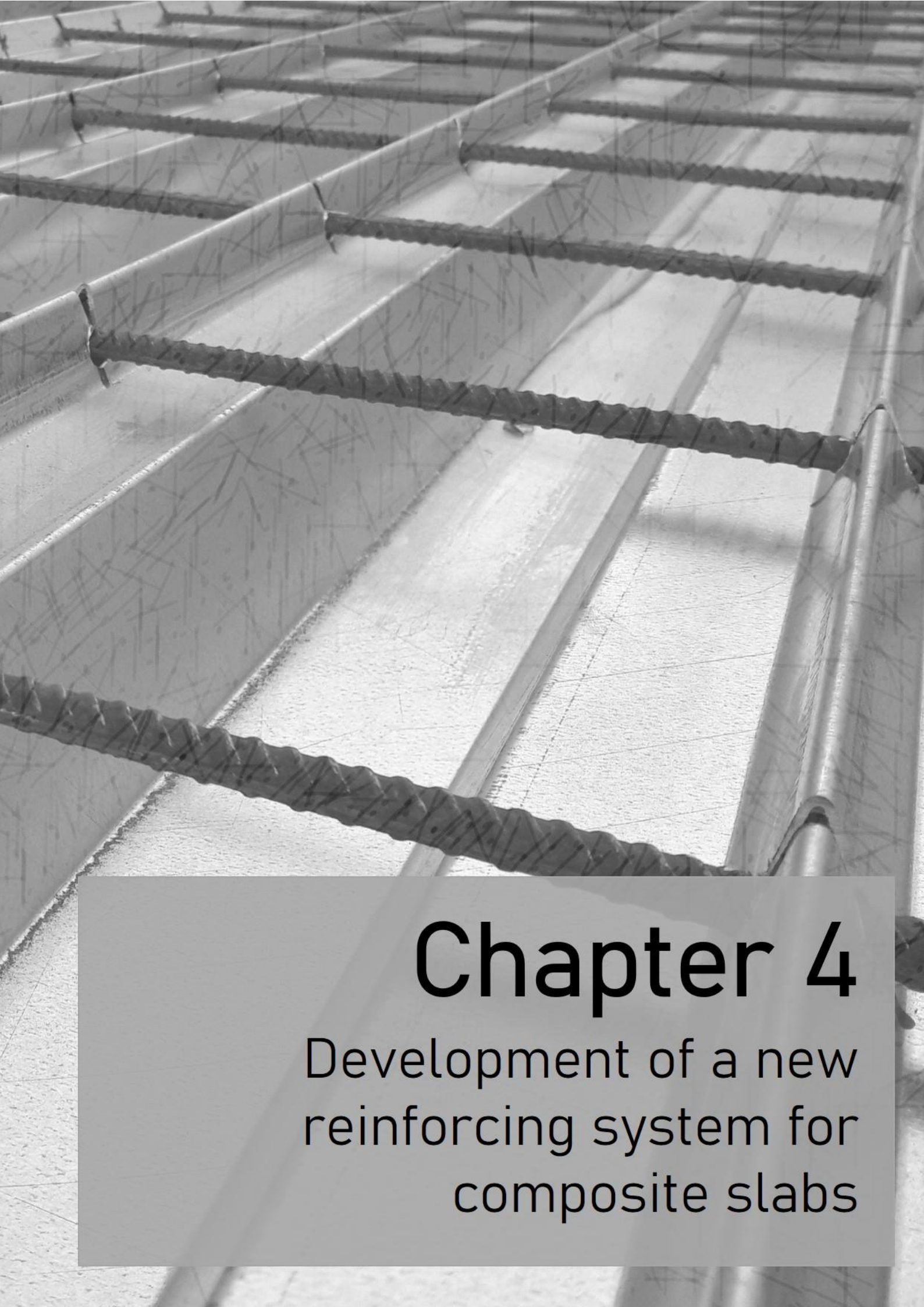

Chapter 4

Development of a new reinforcing system for composite slabs

4.1 Introduction

As it was mentioned before, the resistance of steel-concrete composite slabs is usually governed by longitudinal shear failure due to the low degree of connection between the profiled steel sheeting and the concrete. Usually, this connection is ensured by the embossments of the profile and, in some cases, combined with end anchorage systems constituted by headed studs welded to the top flange of the supporting steel beams through the profiled steel sheeting. However, for the effectiveness of the end anchorage system, headed studs need to be welded on the site and the supporting beam must be a steel beam. As it was presented in the second chapter, several reinforcing systems have been developed by multiple researchers, however these do not allow to achieve the bending capacity of the slab or no design methods were provided to take them into account.

Taking these issues in consideration, and in order to increase the longitudinal shear resistance of steel-concrete composite slabs, a new reinforcing system was developed in the scope of the present thesis. The proposed reinforcing system comprises a transversal reinforcement system that intersects the profiled steel sheeting in pre-drilled holes distributed over longitudinal stiffeners placed on the upper flanges of the profiled steel sheeting. Transversal bars provide a mechanical interlock system to increase the shear transfer over the contact surface and reduce the slip between the profiled steel sheeting and the concrete.

Apart from the development of the reinforcing system, a design methodology to predict its resistance must be provided. So, along this chapter it is presented the proposed reinforcing system, the experimental campaign carried out to prove its efficiency and the development of a design model to predict its resistance.

To prove the efficiency of the developed reinforcing system an extensive experimental programme was carried out. The experimental programme was divided into three distinct parts, with three different objectives:

i. Preliminary experimental programme (preliminary campaign) – a set of full-scale bending tests were performed in order to understand the main basic concepts concerning the behaviour of steel-concrete composite slabs with longitudinal shear behaviour improved by the proposed reinforcing systems;
ii. Small-scale experimental programme – several specimens with reduced dimensions were submitted to push-out experimental tests to evaluate the shear resistance acquired by the proposed system. The experimental results were then compared with theoretical values of the resistance using a statistical method provided by standard EN 1990 (CEN, 2002a). The statistical procedure allowed

to calibrate an equation to obtain the design value of the resistance acquired by the reinforcing system. The obtained design value is then used in the partial connection method provided by standard EN 1994-1-1 (CEN, 2004b);

iii. Full-scale experimental programme (second campaign) – tests on simply-supported and continuous steel-concrete composite slabs with transversal bars were performed to prove the efficiency of the reinforcing system, to validate the design approach developed in the previous step and to study the influence of the proposed reinforcing system on continuous composite slabs.

In the preliminary experimental programme, a second reinforcing system was also studied. This second reinforcing system was defined by folded triangular cuts made in the longitudinal stiffeners of the profiled steel sheeting top flange. Obtained results showed that this reinforcing system also allowed to increase the longitudinal shear resistance of steel-concrete composite slabs. However, this reinforcing system was not as efficient as transversal bars, and so its study was not continued. Actually, the cuts would have to be made on site and promoted some water loss during the concrete cure. Other disadvantages regarding its practical application were also found and will be presented further on.

4.2 Developed reinforcing system

Having the main objectives of (i) increasing the longitudinal shear resistance of steel-concrete composite slabs and, consequently, (ii) increasing the bearing capacity of steel-concrete composite slabs, a new reinforcing system was developed and is described throughout this chapter. The proposed reinforcing system comprises a set of transversal reinforcing steel bars, distributed over the span, and placed in vertical cuts executed in the longitudinal stiffeners, for example in the inverted V-shape, located in the upper flanges of the profiled steel sheeting, as it is illustrated in Fig. 4.1.

The new reinforcing system was based on the end anchorage device developed by Fonseca *et al.* (2015), which was presented in the literature review of this document; that system comprised transversal bars intersecting the webs of the profiled steel sheeting on the supports which allowed to improve the longitudinal shear capacity of steel-concrete composite slabs. Despite of being an effective solution, transversal bars intersecting the profiled steel sheeting require that holes must be drilled and bars must be introduced on site which makes this solution unattractive from the practical applicability point of view. The proposed reinforcing system may be considered as a positive evolution of Fonseca *et al.* (2015) end anchorage system, since transversal bars are placed in slotted holes previously executed in factory.

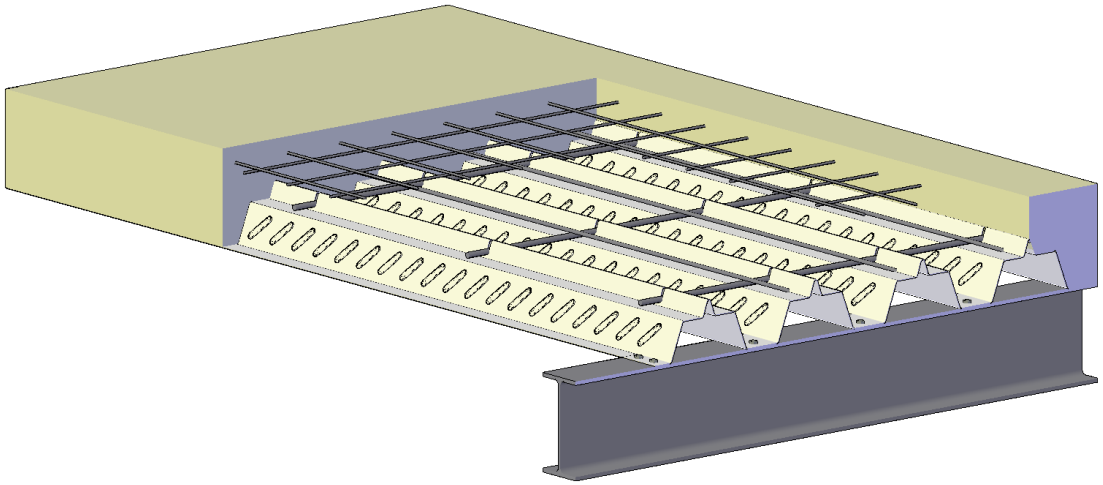

Fig. 4.1 Steel-concrete composite slabs with transversal reinforcement

The main role of these reinforcing bars is to prevent the relative displacement between the profiled steel sheeting and the concrete in the longitudinal direction, allowing the slab to exercise its entire bending resistance. When demands are made on the system, the shear strength of the bars and the bearing strength of the steel sheeting are mobilized. The transference of the longitudinal shear forces is all the more effective, the greater the thickness of the steel sheeting is. To prevent the bars from loosening during concreting, these are fitted into a hole-shaped cut-out located at the base of the vertical cut, whose diameter, approximately equal to the diameter of the bar, may be slightly larger than the width of the cut, thus obtaining a snap fit between the bar and the profiled sheet.

Fig. 4.2 details the proposed reinforcing system, which could be applied in two different ways: (i) simple reinforcing system (Fig. 4.2(a)) which comprises just the transversal bars placed in the pre-drilled holes (Fig. 4.2(c)) or (ii) reinforcement mesh (Fig. 4.2(b)) combining transversal and longitudinal bars. The latter could be prepared in such a way that the transversal bars, which only have a significant role in the region of the intersection with the longitudinal stiffeners, could be folded down to support the longitudinal bars and, consequently, replace the application of bar spacers, as shown in Fig. 4.2(d). Apart from these two ways of application, other variants can be established.

The proposed reinforcing system has the following advantages, some of them obvious, others to be proved by results presented in the next sections: i) an increased load bearing capacity due to the increased longitudinal shear resistance; ii) for a given design loading scenario, the span of the slabs may be increased thereby decreasing the number of supporting beams required; iii) the system may be combined with the most common longitudinal shear resistant system constituted by embossments along the profiled steel sheeting; iv) easy to incorporate in the partial connection method, a less conservative

design method when compared with the *m-k* method; v) the longitudinal shear capacity is no longer dependent on other possible reinforcing systems, such as the end anchorage device provided by headed studs welded to the supporting beams through the steel sheeting, which requires in-situ welding techniques; vi) the efficacy of the system does not depend on the material and shape of the supporting beams (e.g. timber or concrete beams may also be used as supporting beams); vii) increased ductility of the slabs because the most likely failure modes (bending or even longitudinal shear) are ductile; viii) increased transversal stiffness in the plane of the slab, which makes the diaphragm effect more effective (beneficial for resistance to horizontal actions, such as the action of the wind or the action of an earthquake); ix) support for the placement of other wire meshes (longitudinal and/or distribution) required for other functions; x) ease of on-site execution (cuts may be executed previously in the factory).

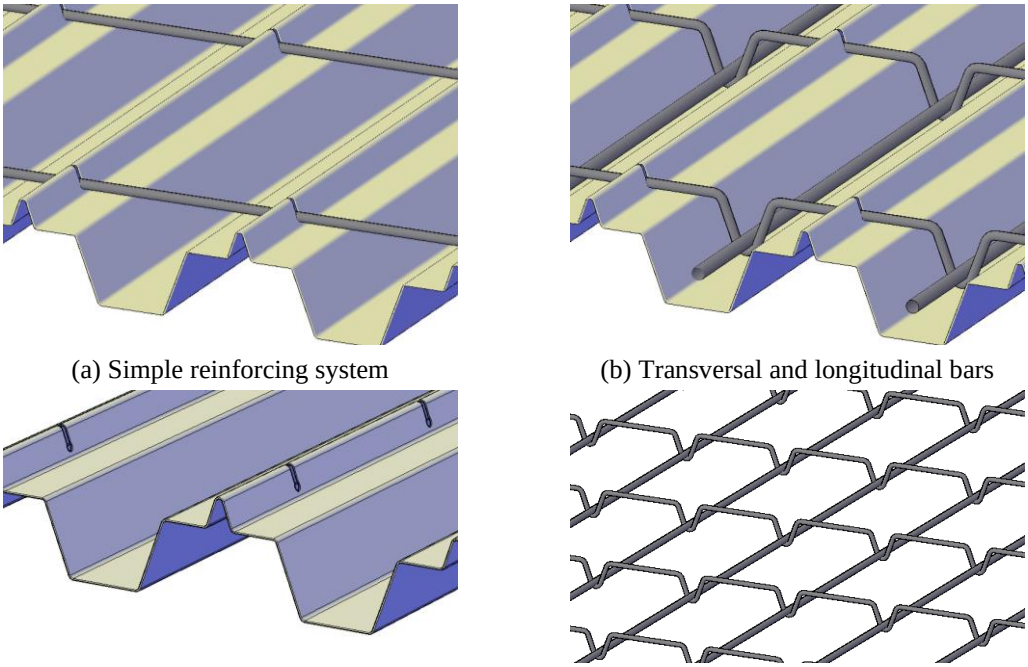

(a) Simple reinforcing system (b) Transversal and longitudinal bars

(c) Vertical cuts in the steel sheet (d) Welded reinforcing mesh

Fig. 4.2 Variations applicable to the reinforcing system

In order to study the behaviour of the proposed reinforcing system in the scope of this research, two new profile configurations were developed: (i) LAMI 60+ and (ii) LAMI 120+. For the purpose of the present study, the steel sheet profile LAMI 60+ was adapted from the profile H60, which is commercialised by the steel company involved in the research project INOV_LAMI, *O Feliz Metalomecânica SA* (see Fig. 4.3). Fig. 4.4 shows the geometry of those two developed profiles that were produced by folding and press braking processes; the geometric quantities specified are the height of the web h_p, the width of a module b_m, the mean width of a rib b_0, the height of the centre

of gravity of the steel sheet *e* and the angle φ between the web and the flange. Two new geometries were developed in order to validate obtained results and conclusions for composite slabs with profiled steel sheeting with current (LAMI 60+) and higher (LAMI 120+) heights.

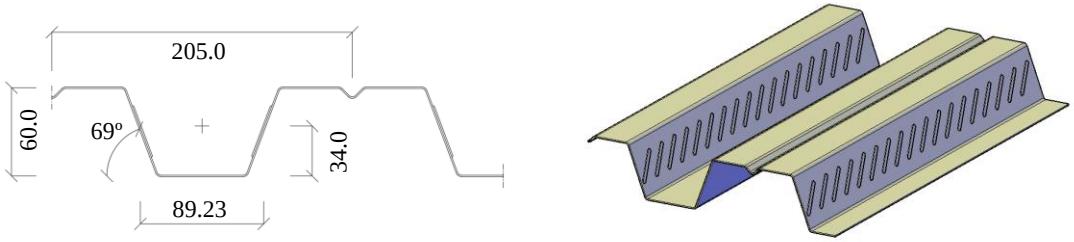

(a) H60 geometry (b) H60 3D perspective

Fig. 4.3 H60 Profile

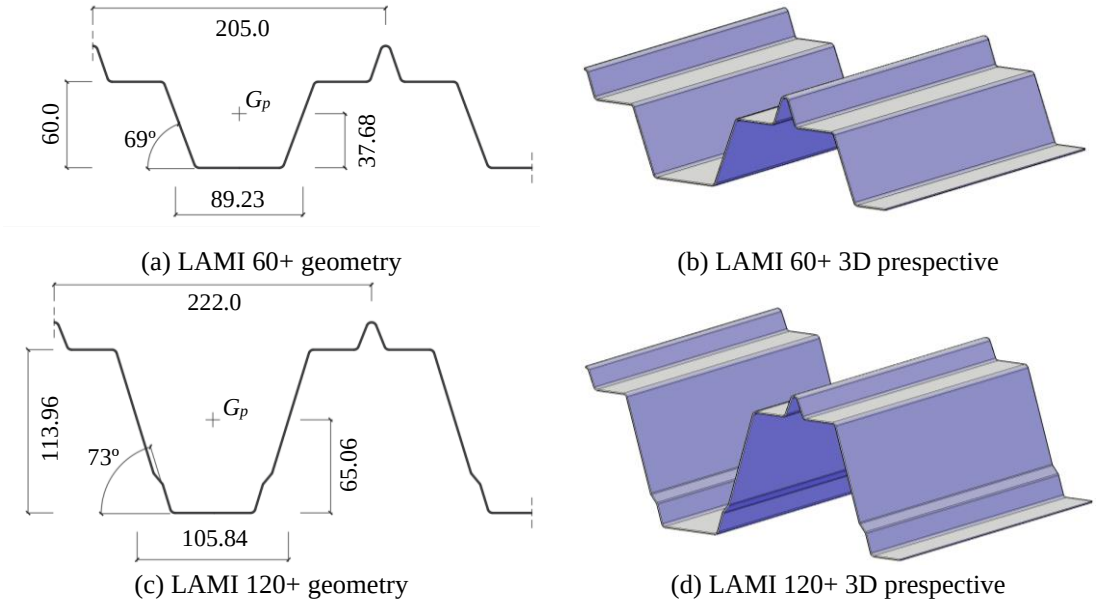

(a) LAMI 60+ geometry (b) LAMI 60+ 3D prespective

(c) LAMI 120+ geometry (d) LAMI 120+ 3D prespective

Fig. 4.4 LAMI 60+ and LAMI 120+ profiles (dimensions in mm)

Geometrical and mechanical properties of profiles H60, LAMI 60+ and LAMI 120 + are presented on Table 4.1, Table 4.2 and Table 4.3, respectively, for a thickness range between 0.70 and 1.50 mm. The steel grade S320 GD+Z, currently used in the H60 profiles, was adopted. As it can be observed from provided tables, the effective cross-sectional area of the profiled steel sheeting A_{pe} is equal to the nominal cross-sectional area A_{nom} on profiles LAMI 60+ and 120+, since these profiles were produced without embossments to perform the present study; as it was mentioned before, LAMI 60+ profile was adapted from H60 profile, and consequently the vertical shear resistance of both profiles is equal; small differences in the geometrical and mechanical

properties between profiles LAMI 60+ and H60 are due to the differences in the longitudinal stiffener geometry. The effective cross-sectional properties of these profiles were determined according to the rules prescribed in standards EN 1993-1-3 (CEN, 2006a) and EN 1993-1-5 (CEN, 2006c).

Table 4.1 Geometrical and mechanical properties of H60 profile

Nominal section					Under Sagging Bending Moment					Shear
t_{nom} [mm]	load [kN/m^2]	A_{nom} [cm^2/m]	A_{pe} [cm^2/m]	I_p [cm^4/m]	A_{eff} [cm^2/m]	$y_{G,eff}$ [mm]	I_{eff} [cm^4/m]	$W_{el,eff}$ [cm^3/m]	$M_{Rd,eff}$ [kN.m/m]	V_{Rd} [kN/m]
0.70	0.079	10.07	9.13	59.86	8.54	31.44	51.34	16.33	5.27	48.47
0.80	0.090	11.51	10.52	68.41	10.06	32.09	61.05	19.02	6.11	64.27
1.00	0.113	14.39	13.28	85.52	13.22	33.16	81.23	24.50	7.84	102.55
1.20	0.136	17.27	16.05	102.62	16.47	33.97	102.05	30.04	9.61	149.73
1.50	0.169	21.58	20.20	128.29	21.01	34.31	130.57	38.05	12.18	237.20

Table 4.2 Geometrical and mechanical properties of LAMI 60+ profile

Nominal section					Under Sagging Bending Moment					Shear
t_{nom} [mm]	load [kN/m^2]	A_{nom} [cm^2/m]	A_{pe} [cm^2/m]	I_p [cm^4/m]	A_{eff} [cm^2/m]	$y_{G,eff}$ [mm]	I_{eff} [cm^4/m]	$W_{el,eff}$ [cm^3/m]	$M_{Rd,eff}$ [kN.m/m]	V_{Rd} [kN/m]
0.70	0.086	11.01	11.01	80.36	10.71	34.97	79.11	22.62	7.24	48.47
0.80	0.099	12.58	12.58	91.84	12.00	36.20	90.35	24.96	7.99	64.27
1.00	0.123	15.73	15.73	114.80	14.66	38.16	112.66	29.52	9.45	102.55
1.20	0.148	18.88	18.88	137.76	17.37	39.62	134.67	33.99	10.88	149.73
1.50	0.185	23.60	23.60	172.21	20.94	40.67	164.62	40.48	12.95	237.20

Table 4.3 Geometrical and mechanical properties of LAMI 120+ profile

Nominal section					Under Sagging Bending Moment					Shear
t_{nom} [mm]	load [kN/m^2]	A_{nom} [cm^2/m]	A_{pe} [cm^2/m]	I_p [cm^4/m]	A_{eff} [cm^2/m]	$y_{G,eff}$ [mm]	I_{eff} [cm^4/m]	$W_{el,eff}$ [cm^3/m]	$M_{Rd,eff}$ [kN.m/m]	V_{Rd} [kN/m]
0.70	0.104	13.25	13.25	253.73	12.03	62.62	243.93	38.96	12.53	58.91
0.80	0.119	15.14	15.14	289.97	14.03	64.41	290.94	45.17	14.60	77.05
1.00	0.149	18.92	18.92	362.47	18.09	66.51	381.08	57.29	18.58	120.37
1.20	0.178	22.71	22.71	434.97	21.95	66.71	462.55	69.34	22.36	173.03
1.50	0.223	28.38	28.38	543.73	27.63	66.71	582.19	87.28	27.97	269.39

4.3 Preliminary experimental analysis on composite slabs

4.3.1 Introduction

A preliminary experimental campaign was carried out in order to: (i) to get a first assessment of the efficiency of the proposed reinforcing system; (ii) study the influence of the combination with longitudinal reinforcement placed on concrete ribs on the

behaviour of steel-concrete composite slabs; (iii) evaluate the efficiency of a second and also innovative reinforcing system.

As it was mentioned before, a second reinforcing system was proposed in the first stage of the study. The second reinforcing system comprised the cut and deformation of longitudinal stiffeners located on the upper flanges of the profiled steel sheeting. For this reinforcing system it was proposed triangular cuts making a 45º angle with the horizontal plane that are perpendicularly folded to outside. The folded parts ensure a contact area working as interlock to avoid the slip between the concrete and the profiled steel sheeting. This reinforcing system is illustrated on Fig. 4.5.

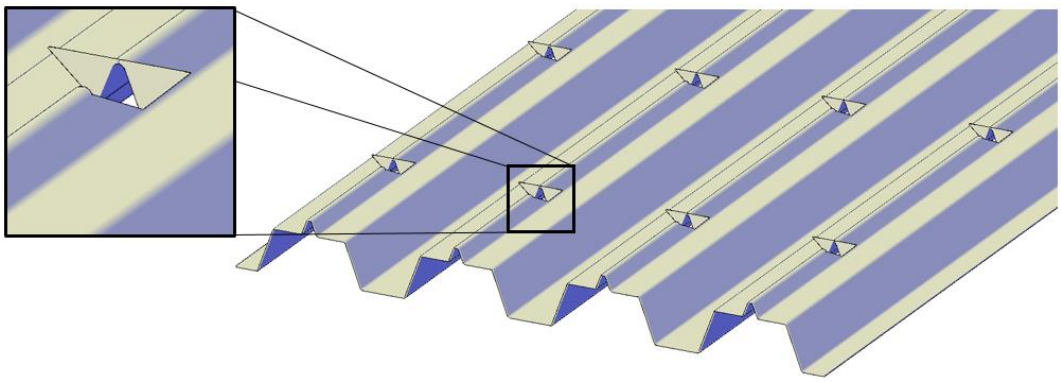

Fig. 4.5 Second reinforcing system

4.3.2 Preliminary experimental programme

The preliminary experimental programme comprised 10 bending tests on simply-supported steel-concrete composite slabs with longitudinal shear behaviour improved by reinforcing systems, divided in three groups: (i) PA group to get a first assessment concerning the effect of transversal bars on the longitudinal behaviour of composite slabs; (ii) PB group to assess the longitudinal reinforcement effect and; (iii) PC group, composed just by one test, to assess the effect of the second reinforcing system referred in the previous section.

Table 4.4 describes the preliminary experimental programme carried out; the symbols used have the following meanings: L is the total span length; L_s is the shear span length (horizontal distance between support and load point); L_b is the span length under constant bending moment (between two load points); h is the total height of the slab and; b is the width of the specimen. On the present study, all the steel sheets used in the tests had a nominal thickness (t_{nom}) of 1.00 mm and a core thickness t_{cor} of 0.96 mm after excluding the corrosion protection by hot-dip galvanizing composed by two 0.02 mm thick layers on each face.

Table 4.4 General description of the preliminary experimental tests

Group	Test	L [m]	L_s [m]	L_b [m]	h [mm]	b [mm]	Profile	Transversal reinforcement	Longitudinal reinforcement
PA	PA_0	2.80	0.70	1.40	150	820	LAMI 60+	-	-
	PA_1	2.80	0.70	1.40	150	820	LAMI 60+	Ø 8 // 200 mm	-
	PA_2	2.80	0.70	1.40	150	820	LAMI 60+	Ø 8 // 200 mm	-
	PA_3	2.80	0.70	1.40	150	820	LAMI 60+	Ø 10 // 200 mm	-
	PA_4	2.80	0.70	1.40	150	820	LAMI 60+	Ø 10 // 200 mm	-
	PA_5	2.80	1.20	0.40	150	820	LAMI 60+	Ø 8 // 400 mm	-
	PA_6	2.80	1.20	0.40	150	820	LAMI 60+	Ø 8 // 400 mm	-
PB	PB_1	2.80	0.70	1.40	150	820	H60	-	Ø 12 // 205 mm
	PB_2	2.80	0.70	1.40	150	820	LAMI 60+	Ø 10 // 200 mm	Ø 12 // 205 mm
PC	PC_1	2.80	0.70	1.40	150	820	LAMI 60+	Triangular Cuts	-

All specimens were produced with a total span L, between supports, of 2.80 m and a total height of 150 mm. All specimens comprised 4 slab modules of width b_m equal to 205 mm making up a total width b of 820 mm. At this stage only slabs with profiled steel sheeting with current height were used (H60 and LAMI 60+).

According to Annex B of standard EN 1994-1-1 (CEN, 2004b), the composite slabs are tested with shear spans of $L/4$ in order to obtain the parameters to characterize their longitudinal shear behaviour (like m and k or $\tau_{u,Rd}$). Two different layouts were used on the tests of the PA group. These two layouts are shown on Fig. 4.6. From the first to the second experimental layout the shear span L_s was increased and the span length under constant bending moment L_b was reduced, in order to increase the bending forces acting on the slab. Shear spans were increased from 0.70 m ($L/4$) to 1.20 m ($3L/7$) on tests PA_5 and PA_6 (see Fig. 4.6(b)). The first layout (see Fig. 4.6(a)) was also used on tests from PB and PC groups.

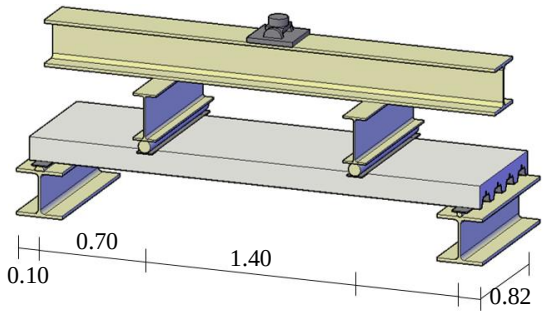

(a) PA_0; PA_1; PA_2; PA_3; PA_4; PB_1; PB_2; PC_1

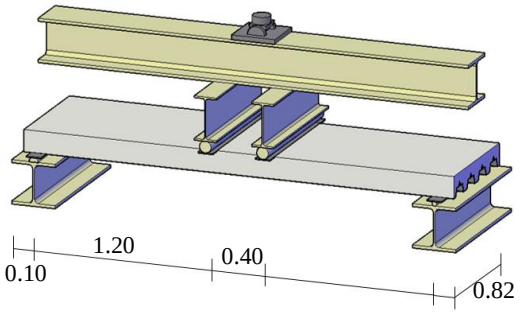

(b) PA_5; PA_6

Fig. 4.6 Preliminary experimental layouts

Transversal reinforcement was distributed just over the shear spans L_s, as it is illustrated by Fig. 4.7. Since the vertical shear acting on the length under constant bending moment L_b is small (almost zero), slip forces on these regions are not significant and so transversal

bars would not contribute significantly to the capacity of the slab. Usually, crack inducers are placed in the loaded sections to delimit the shear span length and to eliminate the tensile resistance of the concrete. However, since a reinforcing system that provides a strong increase of the longitudinal shear resistance was used just along the shear span and the sheets used in the tests were completely smooth (without embossments), the use of crack inducers was avoided.

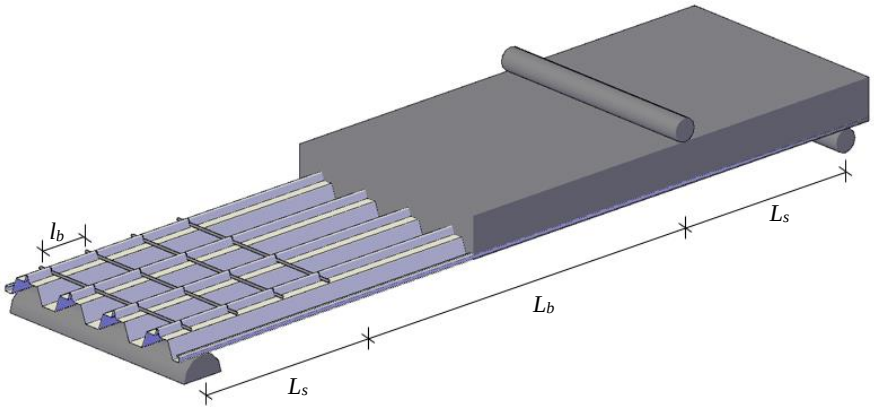

Fig. 4.7 Reinforcement distributed along the shear span

All slabs contained a welded wire mesh placed 25 mm below the top surface of the slab. A welded wire mesh FAQ 38Ø3.8//100 was adopted for the constructive reinforcement which correspond to 113.41 mm^2/m on each direction, higher than the minimum of 80 mm^2/m required on standard EN 1994-1-1 (CEN, 2004b).

Fig. 4.8 shows the preparation of the specimens for the preliminary experimental campaign. First of all, the steel parts were assembled inside the formwork structures prepared for each specimen. After 20 days of concrete cure the formwork structures were removed.

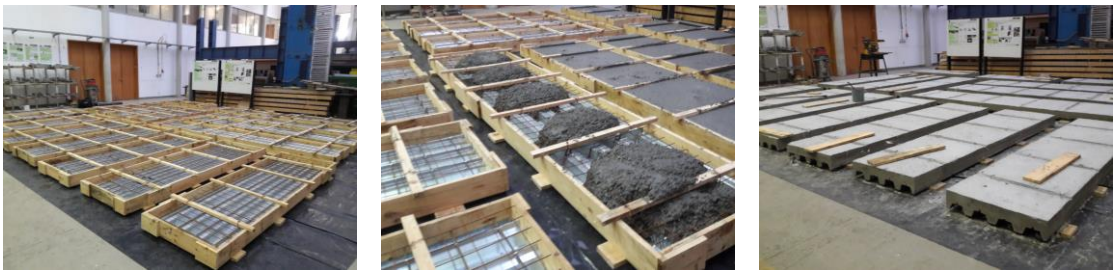

(a) Specimens assembly (b) Concreting (c) Formwork removal

Fig. 4.8 Preliminary experimental programme preparation

The description of each type of specimen and their main differences regarding the objectives of the experimental tests are presented on the following paragraphs.

(i) Group PA (Preliminary, A)

The first group of preliminary tests, PA group, was carried out to get a first assessment regarding the behaviour of steel-concrete composite slabs with transversal reinforcement intersecting the profiled steel sheeting. This group includes the majority of tests of the preliminary programme because it concerns the main objective of the present research. The efficacy of the proposed reinforcing system was evaluated varying the parameters: (i) transversal bars diameter d, (ii) space between transversal bars l_b and (iii) shear span L_s.

In order to quantify the longitudinal shear resistance provided just by the chemical adherence on the contact surface between the concrete and the profile LAMI 60+, the specimen for test PA_0 was produced without transversal and longitudinal reinforcement. Fig. 4.9(a) shows the specimen PA_0 (without concrete). Specimens PA_1 and PA_2 had a transversal reinforcement comprised by 8 mm diameter bars spaced by 200 mm intersecting the profiled steel sheeting over the shear spans – Fig. 4.9(b). Specimens PA_3 and PA_4 were similar to specimens PA_1 and PA_2, but with reinforcing bars with a 10 mm diameter.

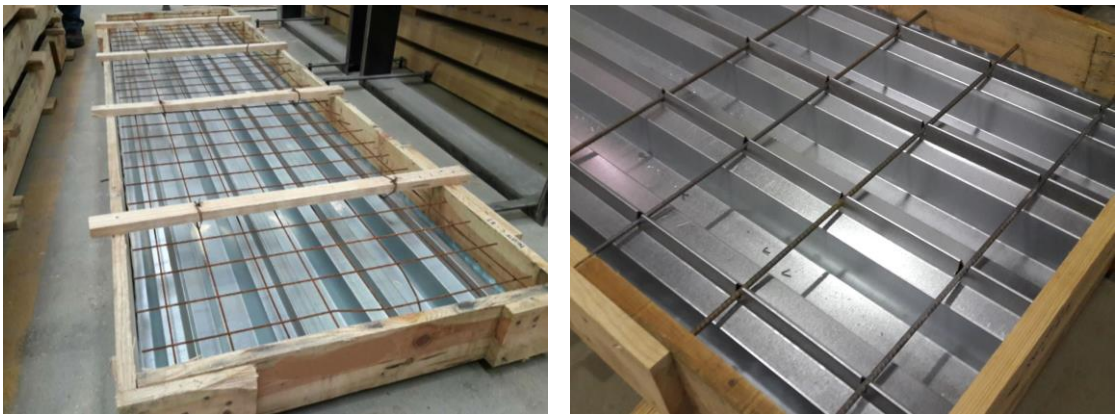

(a) Specimen PA_0 (b) Specimens PA_1-PA_4

Fig. 4.9 PA group specimens PA_0 – PA_4

On the specimens PA_5 and PA_6 the transversal reinforcement, composed by transversal bars of 8 mm diameter spaced by 400 mm, was distributed over the entire span. The only difference between these specimens was the shape of bars. Transversal bars of specimen PA_5 were completely horizontal – Fig. 4.10(a) – and transversal bars of specimen PA_6 were folded up between the intersections with the profiled steel sheeting to support the constructional reinforcement mesh – Fig. 4.10(b). This latter represents a scenario where no additional spacers are needed to place additional reinforcing.

(a) Specimen PA_5

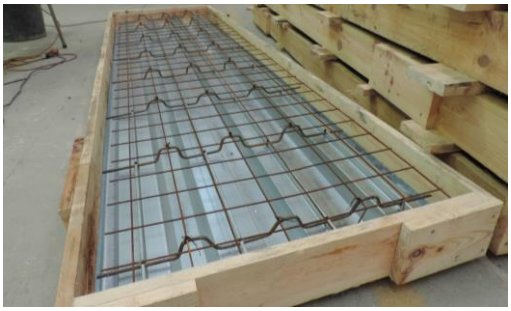

(b) Specimen PA_6

Fig. 4.10 PA group specimens PA_5 – PA_6

(ii) Group PB (Preliminary, B)

The objective of group PB was the assessment of the combined effect of the longitudinal bars on the ribs with the proposed reinforcing system. This group comprised 2 experimental tests: (i) PB_1 specimen was composed by a steel profile H60 and so being the longitudinal shear capacity of the slab provided just by the embossments of the profile, with one 12 mm diameter longitudinal reinforcing bar was placed on each rib – Fig. 4.11(a); (ii) PB_2 specimen was similar to the previous one but using the steel profile LAMI 60+ with transversal bars intersecting the profiled steel sheeting (instead of embossments) – Fig. 4.11(b). Specimen PB_2 represents the reinforcing system where transversal bars are folded down to support the longitudinal reinforcement and dismiss the application of spacers. Longitudinal reinforcement was placed 30 mm above the bottom flanges of the profiled steel sheeting at the ribs centre in both specimens.

(a) Specimen PB_1

(b) Specimen PB_2

Fig. 4.11 PB group specimens

(iii) Group PC (Preliminary, C)

PC group was composed by just one experimental test. PC_1 test allowed get a first assessment concerning the behaviour of steel-concrete composite slabs reinforced by the second proposed system, which consisted of triangular cuts on the profiled steel sheeting. Fig. 4.12 shows those triangular cuts, which were made on the longitudinal stiffeners of

steel profile LAMI 60+ and then bended 90º to the outside. These cuts were just produced along the shear span (between the support sections and the loaded sections) and spaced by 200 mm.

Fig. 4.12 Specimen PC_1

4.3.3 Properties of materials

4.3.3.1 Concrete

The properties of the concrete used on the preliminary experimental programme were obtained from the results of uniaxial compression tests on 150 mm edge cubic specimens, cured in the same conditions as the concrete of the tested composite slabs. Fig. 4.13 shows (a) the used equipment and (b) the appearance of a non-tested specimen and a tested specimen (on the left and on the right, respectively).

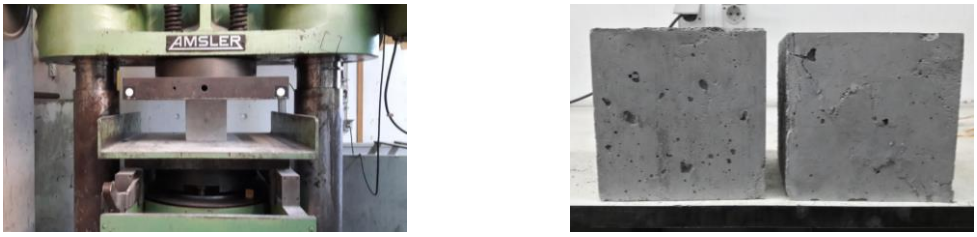

(a) Compression test (b) Concrete cubes before and after test

Fig. 4.13 Uniaxial compression test to concrete cubes

A total of 6 specimens were prepared to characterize the concrete compression resistance: 3 to obtain the concrete strength after 28 days of cure – PAC28 plus 3 specimens to obtain the concrete strength during the full-scale tests – PAC134. Since the experimental campaign started only 134 days after the concreting of the specimens, the variation of the concrete properties during the experimental campaign was considered negligible. The uniaxial compression tests results are presented on Fig. 4.14, where σ is the compression stress given by the applied load divided by the area of the cube (225 cm^2) and ε is the compression strain given by the displacement of the loader divided by the length of the cube (15 cm), so representing indicative values. The strain used in the numerical models were forward defined in accordance with standard EN 1992-1-1 (CEN, 2004a).

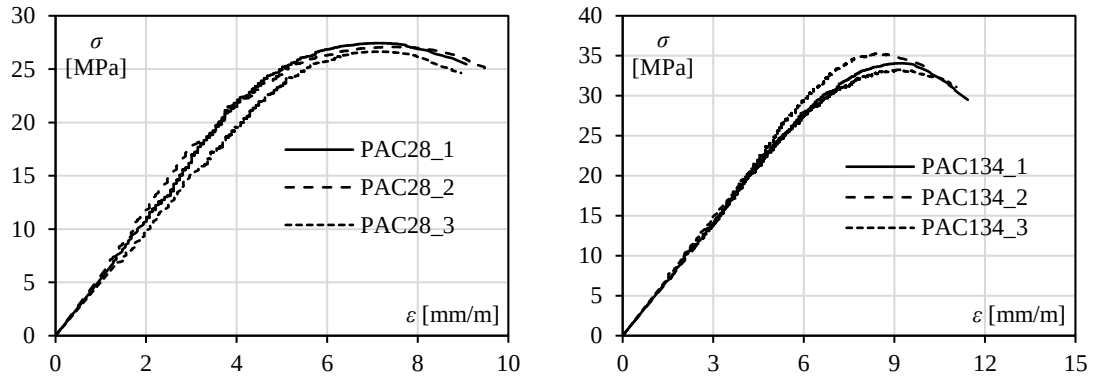

(a) 28 days (b) 134 days

Fig. 4.14 Stress-strain curves for concrete strength definition

The mean value of concrete cube compressive strength $f_{cm,cube}$ should be obtained as the average value between the n peak stress values obtained from each compression test f_{ci}, as it is expressed by Eq. (4.1). The characteristic compressive cube strength of concrete $f_{ck,cube}$ should be then obtained from Eq. (4.3), taking into account the error coefficient δ. The characteristic compressive cylinder strength of concrete f_{ck} is then determined according to Eq. (4.4) and the mean value of concrete cylinder compressive strength f_{cm} by Eq. (4.5). Standard EN 1992-1-1 (CEN, 2004a) provides formulas to define the modulus of elasticity of the concrete, the tensile strength and the compressive strain under maximum stress. The secant modulus of elasticity of concrete E_{cm} is defined by Eq. (4.6), the mean value of axial tensile strength of concrete f_{ctm} by Eq. (4.7) and the compressive strain in the concrete at the peak stress ε_{c1} by Eq. (4.8).

$$f_{cm,cube} = \frac{1}{n}\sum_{i=1}^{n} f_{ci} \tag{4.1}$$

$$\delta = \sqrt{\frac{1}{n}\sum_{i=1}^{n}\left(\frac{f_{ci} - f_{cm}}{f_{cm}}\right)^2} \tag{4.2}$$

$$f_{ck,cube} = (1 - 1.64\delta)\, f_{cm,cube} \tag{4.3}$$

$$f_{ck} = 0.8\, f_{ck,cube} \tag{4.4}$$

$$f_{cm} = f_{ck} + 8 \tag{4.5}$$

$$E_{cm} = 22000\left(\frac{f_{cm}}{10}\right)^{0.3} \tag{4.6}$$

$$f_{ctm} = 0.3\, f_{ck}^{2/3} \tag{4.7}$$

$$\varepsilon_{c1} = 0.7\, f_{cm}^{0.31} \tag{4.8}$$

Table 4.5 presents the mechanical properties of the concrete used in the preliminary experimental programme, defined according to the experimental results and the formulation presented before. The ultimate compressive strain in the concrete ε_{cu1} was defined as 0.0035 mm/mm. According to the characterization results, an average compressive strength f_{cm} of 34.26 MPa for the concrete during the experimental preliminary campaign and a corresponding characteristic value f_{ck} of 26.26 MPa were obtained.

Table 4.5 Properties of concrete

t_c [days]	f_{ci} [MPa]	$(f_{ci}-f_{cm})/f_{cm}$	δ	$f_{cm,cube}$ [MPa]	$f_{ck,cube}$ [MPa]	f_{cm} [MPa]	f_{ck} [MPa]	E_{cm} [MPa]	f_{ctm} [MPa]	ε_{c1} [mm/mm]	ε_{cu1} [mm/mm]
28	27.44	0.014	0.012	27.05	26.51	29.21	21.21	30345	2.30	0.0020	0.0035
	27.08	0.001									
	26.64	-0.015									
134	34.06	-0.005	0.025	34.22	32.82	34.26	26.26	31832	2.65	0.0021	0.0035
	35.33	0.032									
	33.27	-0.028									

4.3.3.2 Profiled steel sheeting

The mechanical properties of the steel used on each type of profile were obtained from uniaxial tensile tests in accordance with standard ISO 6892-1 (ISO, 2009). The steel of H60 profiles it was characterized on smooth (H60S) and embossments (H60E) regions. Fig. 4.15 shows the experimental approach carried out to characterize the steel strength.

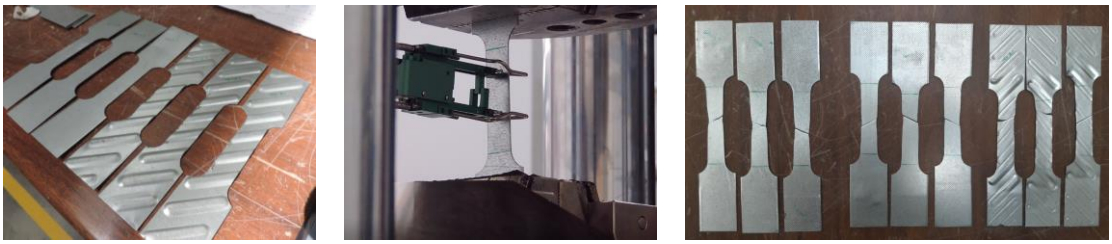

(a) Specimens (b) Tensile test (c) Specimens after failure

Fig. 4.15 Uniaxial tensile tests for the profiled steel sheeting characterization

Fig. 4.16 shows the shape and dimensions of specimens produced. The tensile tests were performed with displacement control; to measure the strains a mechanic strain gauge of 25 mm of base length was used. Fig. 4.17 shows the σ-ε curves experimentally obtained, where ε is the measured strain and σ the tensile stress. Each graphic concerns a specific profile or part of it and comprised always three different curves.

Table 4.6 and Table 4.7 present the measured dimensions and the measured mechanical properties of LAMI 60+ and H60 profiles, respectively. For each specimen the

dimensions presented are: the core thickness t_{cor}, which was obtained by a reduction of 0.04 mm from the measured nominal thickness; the width of the critical section b_0 and; the cross-sectional area of the critical section S_0. The yield strength f_{ypi} and the peak tensile stress f_{upi} obtained in each test are also presented, as well the corresponding average values f_{ypm} and f_{upm}. For the steel of the profiled sheets, average yield stresses f_{yp} of 329.51 MPa (LAMI 60+) and 388.73 MPa (H60) were obtained. Regarding the peak strength, average peak stresses f_{up} of 379.48 MPa (LAMI 60+) and 456.43 MPa (H60) were found.

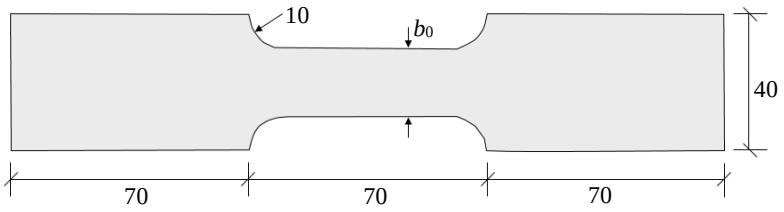

Fig. 4.16 Specimens geometry to characterize the steel sheeting strength

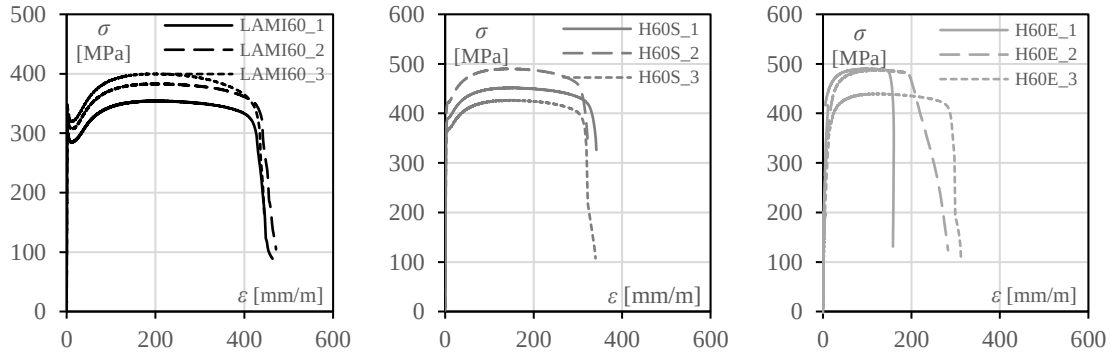

(a) LAMI 60+ (b) H60 smooth region (c) H60 embossments region

Fig. 4.17 Uniaxial tensile tests to steel sheeting specimens

Table 4.6 Mechanical properties of steel used in LAMI 60+ profiles

	t_{cor} [mm]	b_0 [mm]	S_0 [mm^2]	f_{ypi} [MPa]	f_{upi} [MPa]	f_{ypm} [MPa]	f_{upm} [MPa]
LAMI60_1	1.06	20.15	21.359	306.81	354.72		
LAMI60_2	0.98	20.03	19.6294	332.46	383.68	329.51	379.48
LAMI60_3	0.94	20.07	18.8658	349.26	400.02		

Table 4.7 Mechanical properties of steel used in H60 profiles

	t_0 [mm]	b_0 [mm]	S_0 [mm^2]	f_{ypi} [MPa]	f_{upi} [MPa]	f_{ypm} [MPa]	f_{upm} [MPa]
H60S_1	0.96	20.09	19.2864	385.69	451.96		
H60S_2	0.88	20.23	17.8024	417.15	490.48	388.73	456.43
H60S_3	1.01	20.22	20.4222	363.34	426.84		
H60E_1	0.89	20.21	17.9869	241.47	490.14		
H60E_2	0.89	20.26	18.0314	290.04	488.15	254.00	472.73
H60E_3	0.99	20.21	20.0079	230.50	439.92		

4.3.3.3 Reinforcing bars

Over the present research work reinforcing bars with three different diameters were used: 8 mm, 10 mm and 12 mm. The resistance of the reinforcing bars steel was obtained from uniaxial tensile tests, also in accordance with standard ISO 6892-1 (ISO, 2009). Fig. 4.18 shows the experimental approach carried out to obtain the resistance of the steel used in the reinforcing bars. Fig. 4.19 presents curves σ-ε experimentally obtained; each graphic concerns a different diameter.

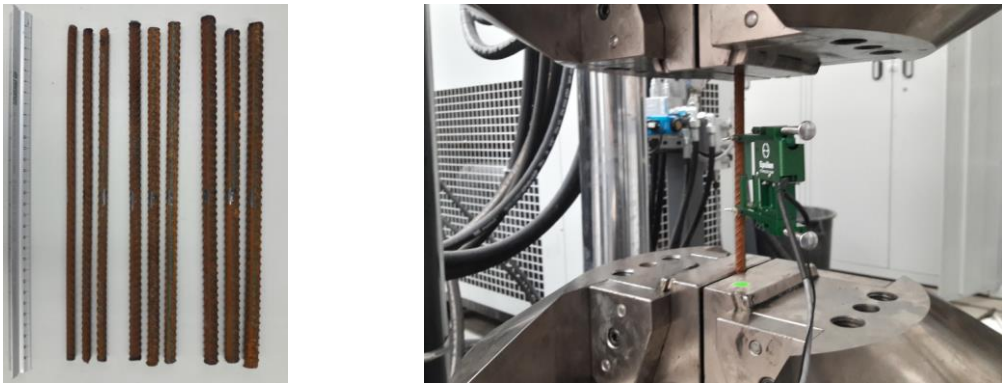

(a) Specimens (b) Tensile test

Fig. 4.18 Uniaxial tensile tests to obtain the reinforcing bars strength

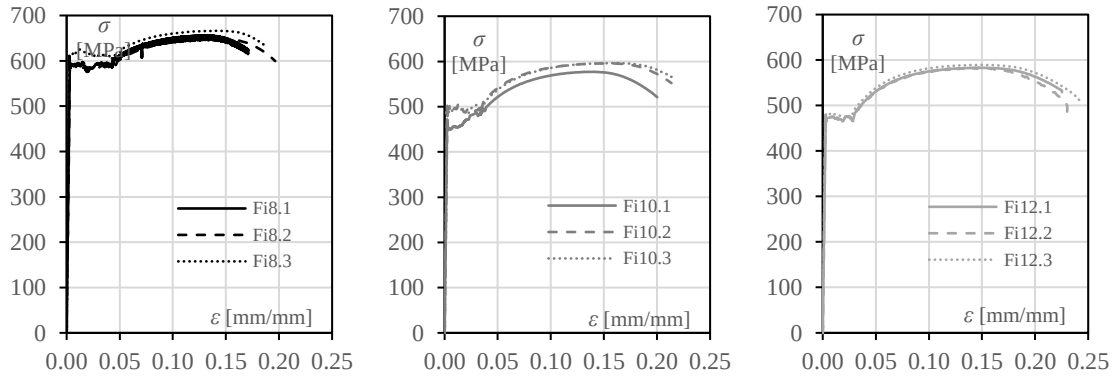

(a) 8 mm (b) 10 mm (c) 12 mm

Fig. 4.19 Uniaxial tensile tests on reinforcing bars specimens

Table 4.8 presents the diameter d_0 and the cross-sectional area S_0 of each specimen tested. The yield strength f_{yi} and the peak value of the tensile stress f_{ui} obtained on each test are also presented, as well as the corresponding average values f_y and f_u. For the steel of the reinforcing bars, average yield stresses f_y of 598.37 MPa (8 mm), 483.89 MPa (10 mm) and 476.89 MPa (12 mm) were obtained. Regarding the peak strength, the values obtained for the average peak stresses f_u were 656.77 MPa (8 mm), 598.44 MPa (10 mm) and 585.13 MPa (12 mm).

Table 4.8 Mechanical properties of the steel of reinforcing bars

	d_0 [mm]	S_0 [mm^2]	f_{yi} [MPa]	f_{ui} [MPa]	f_y [MPa]	f_u [MPa]
Fi8.1	8.0	50.27	590.87	656.28		
Fi8.2	8.0	50.27	591.58	647.80	598.37	656.77
Fi8.3	8.0	50.27	612.67	666.24		
Fi10.1	10.0	78.54	451.15	577.07		
Fi10.2	10.0	78.54	502.11	595.21	483.89	589.44
Fi10.3	10.0	78.54	498.42	596.04		
Fi12.1	12.0	113.10	473.32	582.84		
Fi12.2	12.0	113.10	478.45	583.41	476.89	585.13
Fi12.3	12.0	113.10	478.92	589.15		

4.3.4 Preliminary experimental results

4.3.4.1 Composite slabs with transversal bars

Since two different layouts were used on the first group of tests PA (see Fig. 4.6), the experimental results are also evaluated separately, depending on the layout used. Fig. 4.20 shows *P*-δ curves experimentally obtained from the tests performed in the first group PA. These graphs also present the expected loads (obtained by actual design rules) for similar slabs under the same loading conditions and composed by materials with identical mechanical properties, but with a steel profile H60 ("H60"); in this case the longitudinal shear resistance is ensured by embossments in the webs of the profile instead of transversal bars intersecting the profiled steel sheeting. "H60" values were obtained using the partial connection method and considering the design value of the longitudinal shear strength of the composite slab $\tau_{u,Rd}$ equal to 0.185 MPa (a value obtained by Marques (2011)).

Results from test PA_4 were ignored because the reinforcing system failed prematurely due to an incorrect execution during the specimen production. For this test it was expected a capacity close to the one obtained in test PA_3.

On test PA_0, that was developed just to obtain the resistance of the slab without any longitudinal shear reinforcing system (for comparison reasons), like embossments or transversal bars, the maximum load achieved P_{max} was 37.52 kN. As it was expected, the longitudinal shear behaviour observed during this test was classified as brittle, since the specimen collapsed when the slip between the profiled steel sheeting and the concrete started to increase. Composite slabs from tests PA_1, PA_2 and PA_3 collapsed by longitudinal shear, but exhibiting a ductile longitudinal shear behaviour, as it can be observed by *P*-*s* curves presented on Fig. 4.21(a). The maximum loads P_{max} achieved on these tests were, respectively, 84.62, 80.63 and 87.19 kN. From Table 4.9 it is possible to

observe that the obtained results represent an increase of 55.17, 47.85 and 59.90%, respectively for tests PA_1, PA_2 and PA_3, comparatively to the expected load of a conventional solution in the same conditions where embossments are the only mechanism used to resist to the longitudinal shear forces (P_{H60} = 54.53 kN).

On tests PA_5 and PA_6 the shear span L_s was longer and composite slabs were requested to resist to longitudinal shear over almost all its span L. These specimens were similar to the previous ones; only the shape of transversal bars were different: transversal bars on specimen PA_6 were bended to support the construction reinforcement placed in the top layer of the slab. Fig. 4.20(b) shows that the achieved maximum loads P_{max} were 45.68 and 50.05 kN, which represented an increase of 13.82 and 24.71%, respectively for tests PA_5 and PA_6, comparatively to the expected load of a conventional slab with the same conditions, but where embossments are the only mechanism resisting to the longitudinal shear forces (P_{H60} = 40.13 kN). Also the slabs of this sub-group have collapsed by longitudinal shear and exhibited a ductile behaviour, as it can be observed by the end slip measured and presented on Fig. 4.21(b). The maximum bearing capacity observed on tests PA_5 and PA_6 were similar, so it can be concluded that the effect of bending transversal bars (for instance to support other types of reinforcement) does not affect the efficiency of the reinforcing system.

If the results obtained on tests PA_1, PA_2 and PA_3 are compared with the ones obtained on tests PA_5 and PA_6, it may be observed that the values of the maximum applied load P_{max} were higher in the first sub-group because the shear span L_s was lower. Table 4.9 also present the maximum bending moments M_{max} achieved during these tests and similar values could be found in both sub-groups.

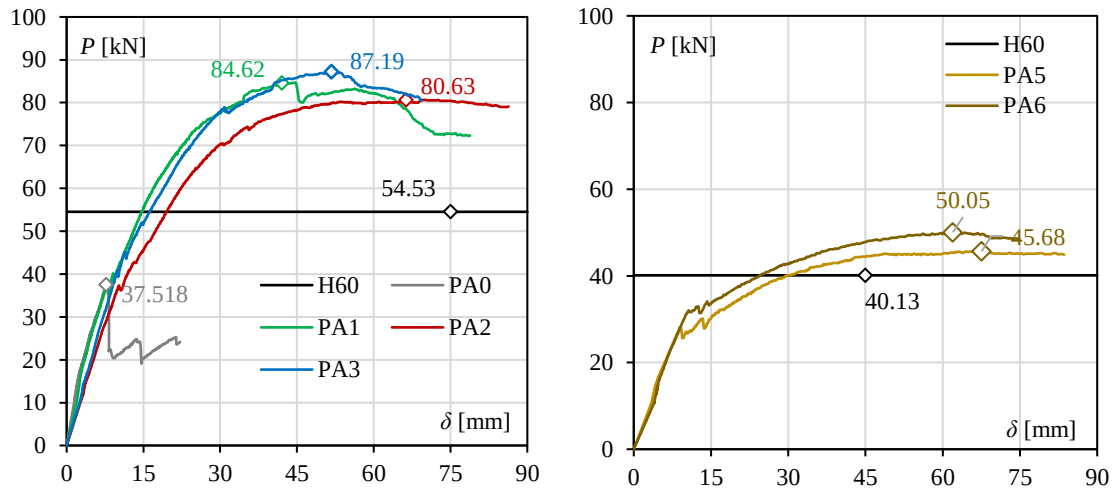

(a) PA_0, PA_1, PA_2 and PA_3 (b) PA_5 and PA_6

Fig. 4.20 P-δ curves obtained from tests of group PA

Table 4.9 Comparison between experimental results and conventional solutions

		PA_0	PA_1	PA_2	PA_3	PA_5	PA_6
P_{max}	[kN]	37.52	84.62	80.63	87.19	45.68	50.05
M_{max}	[kN.m]	13.13	29.62	28.22	30.52	27.41	30.03
P_{H60}	[kN]	54.53	54.53	54.53	54.53	40.13	40.13
M_{H60}	[kN.m]	19.09	19.09	19.09	19.09	24.08	24.08
P_{max}/P_{H60}	[%]	-31.20%	55.17%	47.85%	59.90%	13.82%	24.71%

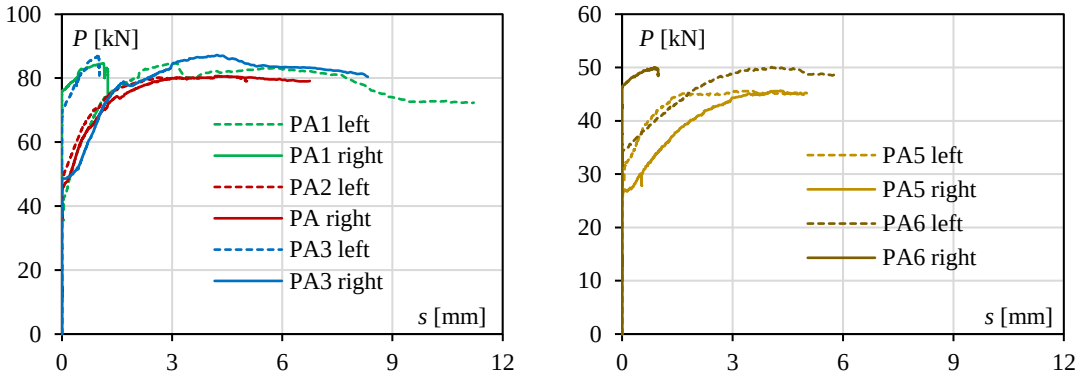

(a) PA_1, PA_2 and PA_3 (b) PA_5 and PA_6

Fig. 4.21 *P-s* curves obtained from tests of group PA

Fig. 4.22 presents the *P-ε* curves obtained on the experiments. Strains were measured on the bottom flange of the profiled steel sheeting at the mid-span cross-section. On these graphs the yield strain of the profiled steel sheeting ε_{yp}, obtained by Eq. (4.9), is also defined. From the obtained results it was observed that in all tests the measured strain attained and exceeded the ε_{yp} value. From these preliminary results it may be stated the proposed reinforcing system, if properly designed, has potential to increase the slab capacity until its bending resistance.

$$\varepsilon_{yp} = \frac{329.51}{210000} = 1.569 \times 10^{-3} \text{ mm/mm} = 1569\ \mu\varepsilon \tag{4.9}$$

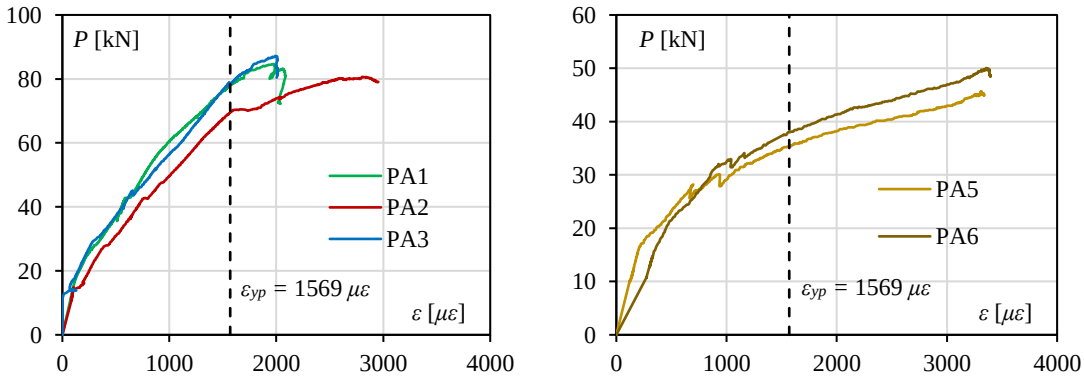

(a) PA_0, PA_1, PA_2 and PA_3 (b) PA_5 and PA_6

Fig. 4.22 *P-ε* curves obtained for tests from group PA

4.3.4.2 Composite slabs with longitudinal bars

The influence of longitudinal reinforcement on the ribs on the capacity of steel-concrete composite slabs is known and usually taken into account. As it was mentioned in the previous chapter, Johnson and Shepherd (2013) showed how longitudinal reinforcing bars should be accounted on the design methods of composite slabs. Nevertheless, two experimental tests were carried out to evaluate the influence of longitudinal reinforcement combined with the proposed longitudinal shear reinforcing system. On test PB_1, an embossed H60 profiled steel sheeting with longitudinal bars placed on the ribs was used. On test PB_2, a LAMI 60+ profiled steel sheeting comprising transversal bars combined with longitudinal reinforcement was used. Fig. 4.23 show the *P*-δ curves obtained on these tests.

On the first test, the specimen collapsed by longitudinal shear, as it can be observed by the slip measured and presented in the graph of Fig. 4.24(a), for a maximum load P_{max} of 109.06 kN. As it was expected, the longitudinal reinforcement contributed significantly to increase the capacity of the slab. Actually, for a slab with the same load and material conditions, but without longitudinal reinforcing bars, the expected collapse load is about 54.53 kN; the specimen PB_1 collapsed for a load 100% higher. The specimen from the second test also failed by longitudinal shear for a load of 120.11 kN, so 120.26% higher than what would be expected for a conventional solution. From the graph of Fig. 4.24(a), it is possible to observe that the end slip measured in the second test was significantly lower, which means that combining transversal reinforcement intersecting the profiled steel sheeting with longitudinal reinforcing bars allow to increase significantly the ductility of the slab.

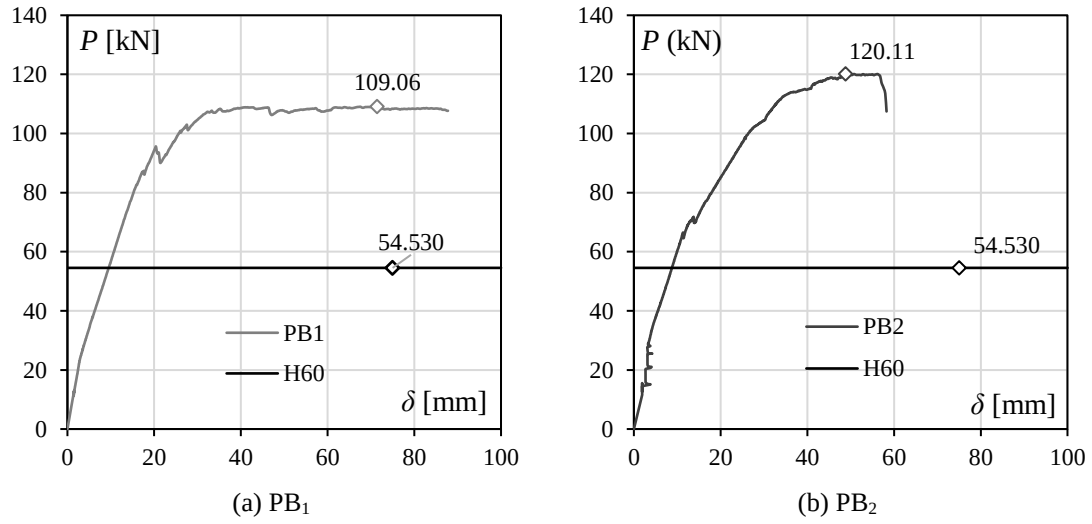

(a) PB_1 (b) PB_2

Fig. 4.23 *P*-δ curves obtained on tests of slabs with longitudinal reinforcement

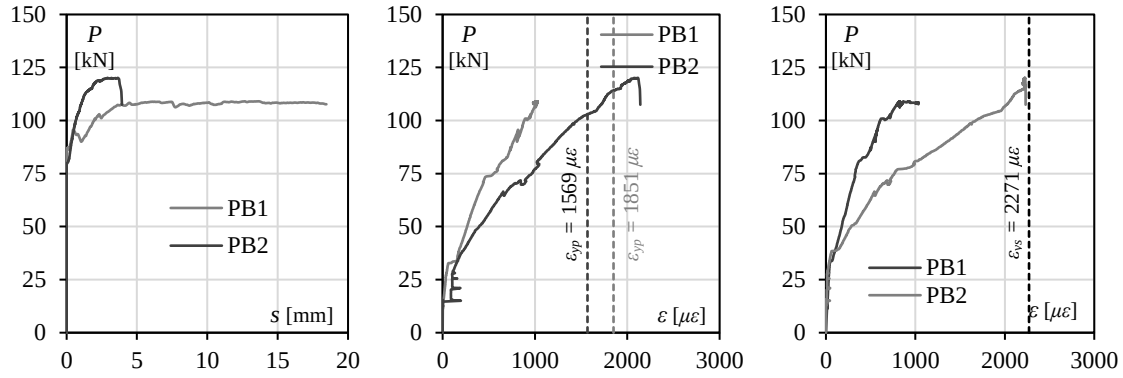

(a) *P-s* curves (b) *P-ε* curves in the steel sheeting (c) *P-ε* curves in the longitudinal reinforcement

Fig. 4.24 *P-s* and *P-ε* curves obtained on tests of slabs with longitudinal reinforcement

Eq. (4.10) defines the yield strain of the steel used in H60 profiles. The yield strain of 12 mm diameter longitudinal reinforcing bars $\varepsilon_{yp,\varnothing 12}$ is defined by Eq. (4.11). Fig. 4.24(b-c) shows *P-ε* curves regarding the steel of the profiled steel sheeting and longitudinal reinforcing bars. Strains were measured on the mid-span cross-sections, at the bottom flange of the profiled steel sheeting and on the most central reinforcing bar. From both graphics it is possible to observe that the longitudinal shear failure in the first test did not allow to reach the yield capacity of profiled steel sheeting and of reinforcing bars. However, on the second test, the developed reinforcing system allowed to attain and even exceed the yield strain on the profiled steel sheeting and longitudinal reinforcing bar. Therefore, these results prove the high efficiency of the proposed reinforcing system; the same conclusion was already established from the results of tests of PA group.

$$\varepsilon_{yp,H60} = \frac{f_{yp,H60}}{E_s} = \frac{388.73}{210000} = 1851.10\ \mu\varepsilon \tag{4.10}$$

$$\varepsilon_{ys,\varnothing 12} = \frac{f_{ys,\varnothing 12}}{E_s}\frac{476.89}{210000} = 2270.91\ \mu\varepsilon \tag{4.11}$$

4.3.4.3 Composite slabs with triangular cuts

The test PC_1 was carried out to evaluate the behaviour of steel-concrete composite slabs with an alternative reinforcing system (see Fig. 4.12) comprising bended triangular cuts executed on the longitudinal stiffeners of the upper flanges of the profiled steel sheeting. These cuts were executed over the shear spans L_s, spaced by 200 mm.

Fig. 4.25(a) shows the *P-δ* curve obtained during the experimental test PC_1. Also the equivalent curves from PA_0 (slab without reinforcing systems) and PA_1 (slab with Ø8 // 200 mm transversal bars) tests are presented for comparison. The collapse of the

specimen from test PC1 was governed by its longitudinal shear resistance for a maximum load of 77.48 kN. The maximum load supported by specimen PC_1 was 8.44% lower than the one supported by specimen from test PA_1, where transversal bars were placed to increase the longitudinal shear resistance of the slab. However, the maximum load supported by specimen PC_1 was 2.07 times higher than the capacity showed by PA_0 specimen, the base case used for comparison. Fig. 4.25(b) shows the slip measured in both ends of the specimen. If compared with the test PA_1, low values of slip were observed and only occurred in the left side of the slab. From these results it was also possible to observe that triangular cuts allowed to achieve a ductile behaviour of the slab, since the maximum load was more than 10% higher than the load corresponding to a slip of 0.1 mm. Fig. 4.25(c) presents the strain measured in the bottom flange of the profiled steel sheeting at the mid-span section. From this graphic it is possible to observe that the collapse occurred just after the yield strain of the profiled steel sheeting was achieved.

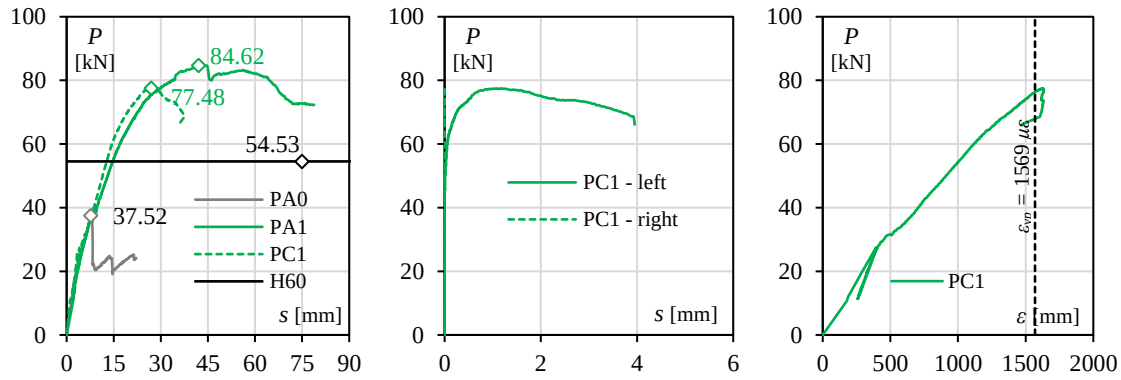

(a) P-δ curves (b) P-s curves (c) P-ε curve

Fig. 4.25 Experimental results obtained for slabs with triangular cuts

The bearing capacity of the slab with bended triangular cuts on the steel sheeting was 42.08% higher than the one that would be expected for a steel-concrete composite slab with an embossed H60 steel profile (P_{H60} = 54.53 kN) under the same loading conditions and material properties. However, this reinforcing system presents some disadvantages if compared with the one composed by transversal bars crossing the steel sheeting:

i. actually, the cuts executed in the profiled steel sheeting promote some water loss during the concrete cure, what could affect its performance. This issue can be solved by closing the holes with some adhesive tape or a polyurethane foam, but this would affect the speed of construction;
ii. these cuts would have to be made on site – what would also affect the speed of construction and promote the geometric irregularity – or in factory – what would increase the production costs and affect the transportation and storage of steel sheets, since they would not be able to fit perfectly on each other;

iii. derivation of an equation to take into account the contribution of this reinforcing system could be very complex, since several parameters could influence its accuracy. The resistance provided by this reinforcing system could be influenced by the height of the cut, the folding angle, among others.

4.3.5 Discussion of the results

Experimental results obtained throughout the preliminary experimental programme allowed to observe the great efficiency of the proposed reinforcing system, consisting of transversal reinforcing bars intersecting the profiled steel sheeting on longitudinal stiffeners placed on their upper flanges. The maximum loads attained on the performed experimental tests were significantly higher than the ones that would be expected for conventional solutions of composite slabs with embossed profiled steel sheeting. Technical limitations did not allow to produce profiled steel sheeting with embossments and prepared to accomplish the transversal reinforcement system; so, it was not possible to combine both reinforcing systems. However, it was possible to observe that transversal bars intersecting the profiled steel sheeting allow to increase the capacity of steel-concrete composite slabs.

The second group (PB group) carried out mainly to study the influence of longitudinal reinforcement in the behaviour of steel-concrete composite slabs when combined with the proposed reinforcing system. The longitudinal reinforcing bars placed on the ribs allow to increase significantly the bearing capacity of composite slabs due to the increase of the bending capacity. The bending capacity of composite slabs can be influenced by (i) the resistance of the concrete in compression or (ii) the resistance of the profiled steel sheeting in tension. Usually, the latter is lower and governs the bending capacity. Consequently, the longitudinal reinforcement placed on the ribs is one of the most effective way to increase the bending capacity of composite slabs.

From test PB_2 it was possible to observe that the combination of transversal with longitudinal reinforcement allow to increase significantly the bearing capacity of steel-concrete composite slabs. Actually, folding transversal bars between the intersection points with the profiled steel sheeting to support longitudinal reinforcement seemed not affect the efficiency of the reinforcing system and dismissed the use of spacers.

A second reinforcing system constituted by folded triangular cuts made on longitudinal stiffeners was also studied. The increase of the acquired resistance seemed not to compensate the disadvantages found on its conception. Disadvantages found would not promote the application of this reinforcing system and so the study of composite slabs with triangular cuts was not continued.

4.4 Evaluation of the reinforcing system resistance

4.4.1 Introduction

A small scale experimental programme and the statistical analysis of the results were carried out to develop the equation to determine the design resistance of a composite slab with transversal bars intersecting the profiled steel sheeting. The statistical analysis of the results was developed according to the standard evaluation procedure - method (a) - described in section D8.2 of Annex D of standard EN 1990 (CEN, 2002a), which requires as first step to develop a design model to obtain the theoretical resistance of the system. Then, to calibrate the design formula, a comparison procedure between the experimental and theoretical results must be done.

The behaviour of the transversal bars crossing the longitudinal stiffeners is similar to the bearing behaviour of a bolted shear connection. So, following the same procedure of Fonseca *et al.* (2015), the equation of the bearing resistance $F_{b,Rd}$ of a bolted shear connection, in accordance with Table 8.4 of standard EN 1993-1-3 (CEN, 2006a), is selected as the basic equation to be calibrated in order to reproduce the equivalent phenomenon, relative to the transversal bars crossing the longitudinal stiffeners (Eq. (4.12)).

$$F_{b,Rd} = \frac{2.5\alpha_b k_t f_u dt}{\gamma_{M2}} \tag{4.12}$$

where:

- α_b is the minimum value between 1.0 and $e_1/(3d)$;
- e_1 is the distance to the end of the steel sheeting;
- d is the bolt diameter;
- k_t follows the equation system (4.13);
- f_u is the ultimate strength of the profiled steel sheeting;
- t is the thickness of the steel sheeting;
- γ_{M2} is the partial safety factor, such that $\gamma_{M2} = 1.25$.

$$k_t = \begin{cases} (0.8t + 1.5)/2.5, \text{ for } 0.75 \text{ mm} \le t \le 1.25 \text{ mm} \\ 1.0, \text{ for } t > 1.25 \text{ mm} \end{cases} \tag{4.13}$$

4.4.2 Small-scale experimental approach

An experimental programme of 15 specimens was carried out to determine the characteristic value of the resistance of each contact point relative to the reinforcing system. Fig. 4.26(a-b) shows the geometry of the tested specimens. These specimens are constituted by a 300 mm long concrete part (in the direction of the load application - axis *x*), and two steel sheets, which are 20 mm longer to allow for the slip movement and consequently the transference of the applied load (by shear through the connecting bars) between the two different materials (steel and concrete). The cross-section of the specimens (*yz* plane sections) were doubly symmetric to avoid eccentricity effects. Two reinforcing bars were placed intersecting each steel sheet at a 50 mm distance from both end sections. Each specimen was loaded in compression along the *x* axis until its failure, using a steel plate with a 15 mm thickness and a cross-section identical to the concrete part - Fig. 4.26(e). Tests were performed with displacement control: a displacement rate of 0.01 mm/s up to a total displacement of 2 mm, followed by a displacement speed of 0.02 mm/s until the collapse. Five groups of three equal specimens each were developed, as it is described in Table 4.10, varying: (i) the steel sheeting thickness *t* - 0.8, 1.0 or 1.2 mm; the bar diameter *d* - 8 or 10 mm; the bar surface - smooth (S) or ribbed (R).

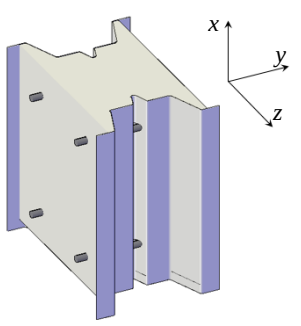

(a) 3D representation

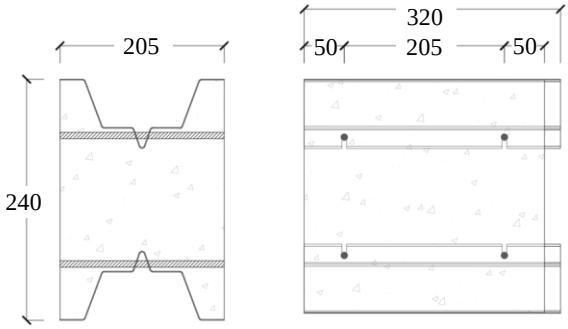

(b) 2D dimensions (*yz* and *xz* sections)

(c) specimen example

(d) specimen compression

(e) steel plate for compression

Fig. 4.26 Experimental approach

A different type of concrete was used on this experimental approach, so, in order to quantify the resistance of the concrete, uniaxial compressive tests on cubic specimens

with edges of 150 mm were performed. The concrete characterization was carried out: (i) after 28 days of cure and; (ii) on the same day as the small-scale tests. The mechanical properties were defined according to the procedure presented on section 4.3.3 and are presented on Table 4.11. When the experimental programme was carried out, an average compressive stress resistance f_{cm} of 40.41 MPa for the concrete and a corresponding characteristic value f_{ck} of 32.41 MPa, in accordance with Eurocode 2 (CEN, 2004a), were obtained. The mechanical properties of the steel used on the steel sheets and reinforcing bars were already defined and presented in the section 4.3.3.

Table 4.10 Experimental specimens tested – small scale test

Specimen Type	t [mm]	d [mm]	Bar Surface	Number of repetitions
SS_0.8_8R	0.8	8	Ribbed (R)	3
SS_1.0_8R	1.0	8	Ribbed (R)	3
SS_1.2_8R	1.2	8	Ribbed (R)	3
SS_1.2_8S	1.2	8	Smooth (S)	3
SS_1.2_10R	1.2	10	Ribbed (R)	3

Table 4.11 Properties of concrete (small-scale experimental programme)

t_c [days]	f_{ci} [MPa]	$(f_{ci}-f_{cm})/f_{cm}$ [-]	δ [-]	$f_{cm,cube}$ [MPa]	$f_{ck,cube}$ [MPa]	f_{cm} [MPa]	f_{ck} [MPa]	E_{cm} [MPa]	f_{ctm} [MPa]	ε_{c1} [mm/mm]	ε_{cu1} [mm/mm]
28	36.436	0.007	0.013	36.19	35.40	36.32	28.32	32395	2.79	0.0021	0.0035
	35.520	-0.019									
	36.627	0.012									
285	45.196	0.024	0.050	44.12	40.52	40.41	32.41	33449	3.05	0.0022	0.0035
	46.111	0.045									
	41.058	-0.069									

4.4.3 Experimental results of the small-scale experimental programme

Fig. 4.27(a) shows the typical shape of *P-s* curves experimentally obtained, where *P* is the applied load and *s* is the measured slip. On a typical *P-s* curve 3 main points are identified: point A represents the moment when the concrete is detached from the steel sheeting; point B represents the yield of the profiled steel sheeting f_{yp} in the contact points with transversal bars and; point C represents the instant when the ultimate resistance of the profiled steel sheeting f_{up} is attained. Between these points, 4 branches can be identified: branch (i) – when the chemical adhesion between the steel sheeting and the concrete is still working and no slip occur; branch (ii) – after the breakdown of the chemical adhesion the mechanical interlock provided by the transversal bars in contact with the profiled steel sheeting starts working with some stiffness until the yield capacity of the profiled steel sheeting is achieved; branch (iii) – the reinforcing system is still

working showing a reduced stiffness and the load increases until the peak strength f_{up} is achieved; branch (iv) – the load decreases after the failure of the reinforcing system.

Fig. 4.27(b-f) represents *P-s* curves for all the specimens of each group. From these graphics it is possible to conclude that the bearing capacity is higher for thicker steel sheets and larger bar diameters. The ductility of the reinforcing system also increases for thicker steel sheets. These observations were already expected and were in accordance with conclusions obtained by Fonseca *et al.* (2015), based on the small scale test campaign carried out by the researchers.

Table 4.12 presents the several peak load values obtained in each group of tests, and also the average values.

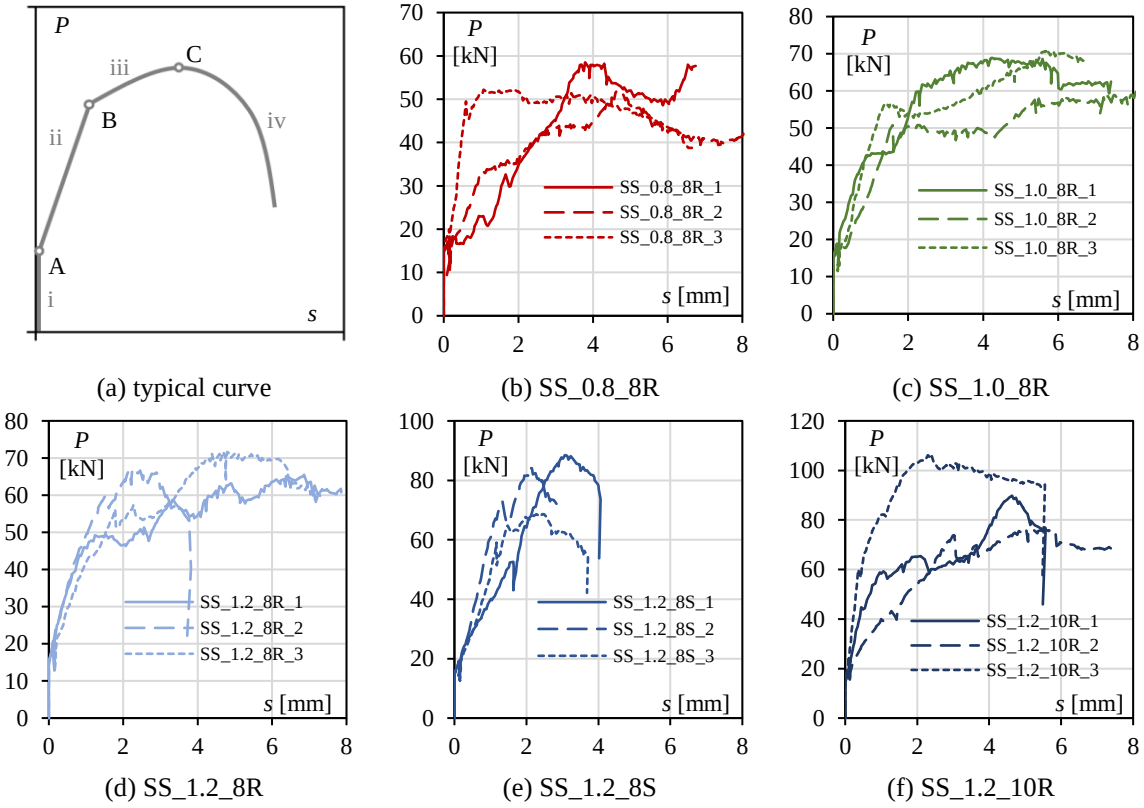

Fig. 4.27 Experimental results – small scale tests

Table 4.12 Experimental results – small scale programme

Specimen Type	t [mm]	d [mm]	Bar surface	P_i [kN]			P_m [kN]
SS_0.8_8R	0.8	8	R	58.50	52.10	52.20	54.27
SS_1.0_8R	1.0	8	R	68.90	69.90	71.20	70.00
SS_1.2_8R	1.2	8	R	65.50	67.40	71.70	68.20
SS_1.2_8S	1.2	8	S	88.50	84.30	68.60	80.47
SS_1.2_10R	1.2	10	R	89.80	76.60	106.30	90.90

4.4.4 Statistical analysis

Annex D from standard EN 1990 (CEN, 2002a) provides guidance to develop design procedures assisted by testing. According to this annex, the design values to be used should wherever practicable be derived from the test results by applying accepted statistical techniques for tests carried out to establish directly the ultimate resistance of structural members. The derivation from tests of the design values for a resistance should be carried out by accessing a characteristic value, which is then divided by a partial factor and possibly multiplied if necessary by an explicit conversation factor.

In order to determine the characteristic and design values of the bearing resistance of the reinforcing system, the results were assessed according to Eq. (4.14). The value of k_n for the 5% characteristic value is obtained from the Table D1 of Annex D of the standard EN 1990 (CEN, 2002a). Considering that V_X is unknown and a number n of 3 experiments for each type of test, then $k_n = 3.37$. In accordance with the referred annex from the standard EN 1990, when V_X is unknown is defined as s_x/m_x, but never smaller than 0.10, like it is established by the Eq. (4.15). Table 4.13 presents the statistical determination of the characteristic and design values of the bearing resistance for each test group. Since η_d and γ_m were considered equal to 1.0, then $X_d = X_k$. In the Table 4.13 are presented design values for the total load resisted by the specimen $X_{d,s}$ and by contact point $X_{d,cp}$, considering 8 contact points by specimen (2 per reinforcing bar; 4 reinforcing bars intersecting the steel sheeting).

$$X_d = \eta_d \frac{X_{k(n)}}{\gamma_m} = \frac{\eta_d}{\gamma_m} m_X \left(1 - k_n V_X\right) \tag{4.14}$$

$$V_X = \max\left\{\frac{s_x}{m_x}; 0.10\right\} \tag{4.15}$$

$$s_x^2 = \frac{1}{n-1}\sum_{i=1}^{n}\left(X_i - m_x\right)^2 \tag{4.16}$$

where:

- X_d is the design value of a property X;
- η_d is the design value of the conversion factor, where $\eta_d = 1.0$;
- X_k is the characteristic value of a property X;
- γ_m is the partial safety factor, where $\gamma_m = 1.0$;
- m_x is the mean value of the n sample results;
- k_n is the characteristic fractile factor;
- V_x is the coefficient of variation of X, defined according to Eq. (4.15);
- s_x is the standard deviation of n sample results, defined according to Eq. (4.16).

Table 4.13 Design values of bearing resistance

Test	X_i [kN]	m_x	s_x^2	s_x	V_x	k_n	$X_{d,s}$	$X_{d,cp}$
SS_0.8_8R	58.50 52.10 52.20	54.267	13.443	3.667	0.100	3.370	35.979	4.497
SS_1.0_8R	68.90 69.90 71.20	70.000	1.330	1.153	0.100	3.370	46.410	5.801
SS_1.2_8R	65.50 67.40 71.70	68.200	10.090	3.176	0.100	3.370	45.217	5.652
SS_1.2_8S	88.50 84.30 68.60	80.467	110.023	10.489	0.130	3.370	45.118	5.640
SS_1.2_10R	89.80 76.60 106.30	90.900	221.430	14.881	0.164	3.370	40.753	5.094

As mentioned before, the main objective of the present analysis was the derivation of an equation to predict the resistance of the proposed reinforcing system. Taking this goal in consideration, a statistical analysis of the experimental results obtained on tests was developed. The statistical analysis of the results was developed according to the method (a) of Annex D of standard EN 1990 (CEN, 2002a). Method (a) standard procedure consists in 7 crucial steps:

Step 1: develop a design model;
Step 2: compare experimental and theoretical values;
Step 3: estimate the mean value correction factor *b*;
Step 4: estimate the coefficient of variation of the errors;
Step 5: analyse compatibility;
Step 6: determine the coefficients of variation V_{Xi} of the basic variables;
Step 7: determine the characteristic value r_k of the resistance.

To proceed the first step, a base design model was chosen to define the theoretical values for the resistance of the reinforcing system. The selected model corresponds to the bearing resistance of a steel sheet in a bolt shear connection, described by Eq. (4.12). Table 4.14 presents the determination of the theoretical resistance for a contact point of each group of specimens, obtained based on the real material properties.

After defining the theoretical values of contact point resistances, these values should be compared with experimental results. Fig. 4.28 presents a plot of all pairs of corresponding

values (r_{ti}, r_{ei}), where r_{ei} corresponds to one eighth of the peak load experimentally obtained (X_i/8). The mean value correction factor b is the "Least Squares" best-fit to the slope represented on the graph and it was defined according to Eq. (4.17). Error term δ_i for each r_{ei} value was defined considering the Eq. (4.18) and the coefficient of variation V_δ was defined by Eq. (4.21).

Table 4.14 Theoretical resistance values r_{ei}

Specimen Type	t [mm]	t_{cor} [mm]	d [mm]	α_b	k_t	f_u [MPa]	γ_{M2}	r_{ti}
SB_0.8_8R	0.8	0.76	8	1.00	0.84	379.48	1.00	**4.86**
SB_1.0_8R	1.0	0.96	8	1.00	0.91	379.48	1.00	**6.61**
SB_1.2_8R	1.2	1.16	8	1.00	0.97	379.48	1.00	**8.55**
SB_1.2_8S	1.2	1.16	8	1.00	0.97	379.48	1.00	**8.55**
SB_1.2_10R	1.2	1.16	10	1.00	0.97	379.48	1.00	**10.69**

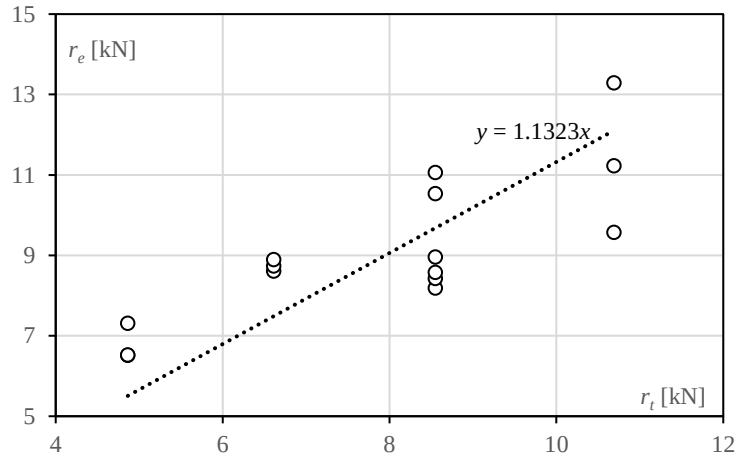

Fig. 4.28 Comparison between theoretical and experimental results

$$b = \frac{\sum_{i=1}^{n} r_{ei} r_{ti}}{\sum_{i=1}^{n} r_{ti}^2} \tag{4.17}$$

$$\delta_i = \frac{r_{ei}}{b \cdot r_{ti}} \tag{4.18}$$

$$\Delta_i = \ln(\delta_i) \tag{4.19}$$

$$\overline{\Delta} = \frac{1}{n}\sum_{i=1}^{n} \Delta_i \tag{4.20}$$

$$V_\delta = \sqrt{\exp(s_\Delta^2) - 1} \tag{4.21}$$

where:

- b is the mean value correction factor;
- r_{ei} is the experimental resistance value for specimen i;
- r_{ti} is the theoretical resistance value for specimen i;
- δ_i is the error term for specimen i;
- Δ_i is the logarithm of the error term δ_i;
- $\bar{\Delta}$ is the estimated value for $E(\Delta)$;
- s_Δ is the standard deviation of Δ_i values;
- V_δ is the coefficient of variation of error terms δ_i.

To determine the characteristic value of the resistance, the coefficients of variation V_{rt} and V_r must be obtained and, for small values of V_δ^2 and V_{Xi}^2, these values could be respectively obtained according to Eq. (4.22) and (4.23). The ultimate tensile strength of the steel sheet f_{up} is the only basic variable included in the initial design model. The coefficient of variation of this variable was founded to be 0.06, as it is shown on Table 4.15. This coefficient of variation was compared with previous studies from the bibliography and similar values for this coefficient were founded (Simões da Silva *et al.*, 2009; Simões da Silva *et al.*, 2018).

$$V_{rt} = \sqrt{\sum_{i=1}^{j} V_{Xi}^2} \tag{4.22}$$

$$V_r = \sqrt{V_\delta^2 + V_{rt}^2} \tag{4.23}$$

where:

- V_{Xi} is the coefficient of variation of the basic variable X.

Table 4.15 Determination of the coefficient of variation of the ultimate strength f_{up}

Basic Variable	$x_{k,i}$	m_x	s_x^2	s_x	V_x
f_{up} [MPa]	354.72 383.68 400.02	379.476	526.228	22.940	0.06

The characteristic resistance value r_k should be obtained from the Eq. (4.24). And so, the calibration factor η to apply to the original base design model is defined according to the equation (4.25).

$$r_k = b \cdot g_{rt}\left(\underline{X}_m\right) \cdot \exp\left(-k_\infty \alpha_{rt} Q_{rt} - k_n \alpha_\delta Q_\delta - 0.5Q^2\right) \tag{4.24}$$

$$\eta = b \cdot \exp\left(-k_\infty \alpha_{rt} Q_{rt} - k_n \alpha_\delta Q_\delta - 0.5Q^2\right) \tag{4.25}$$

where:

$$Q_{rt} = \sqrt{\ln\left(V_{rt}^2 + 1\right)} \tag{4.26}$$

$$Q_{\delta} = \sqrt{\ln\left(V_{\delta}^2 + 1\right)} \tag{4.27}$$

$$Q = \sqrt{\ln\left(V_{r}^2 + 1\right)} \tag{4.28}$$

$$\alpha_{rt} = \frac{Q_{rt}}{Q} \tag{4.29}$$

$$\alpha_{\delta} = \frac{Q_{\delta}}{Q} \tag{4.30}$$

and k_{∞} and k_n are the fractile factors given by 1.64 and 1.84, respectively, for a number of experiments n = 15 and considering V_X unknown, according to Table D.1 of Annex D from standard EN 1990 (CEN, 2002a).

Developing this procedure, a calibration factor of 0.8205 for η was found and the longitudinal shear resistance at each contact point (between the transversal bar and steel sheet) $F_{t,Rd}$ should be defined as expressed in Eq. (4.31) in the design stage, as it is illustrated in Fig. 4.29(a). Considering the transversal bars uniformly distributed along the span and two contact points on each inverted V-shape stiffener, the resistance to longitudinal shear can be defined as a resistant force per unit of area, so a resistant stress $\tau_{t,Rd}$ given by Eq. (4.32). Fig. 4.30 shows the diagram of every pair obtained $F_{b,Rd} - F_{t,Rd}$, with the respective best-fit linear function with a b slope, and the comparison of these with the design equation developed. All pairs r_{ti}-r_{te} are above this line so it could be assumed that the equation developed may adequately represent a design model for the proposed reinforcing system.

$$F_{t,Rd} = 0.8205 \frac{2.5\alpha_b k_t f_u dt}{\gamma_{M2}} \tag{4.31}$$

$$\tau_{t,Rd} = \frac{2 \cdot F_{t,Rd}}{b_m l_b} = 4.103 \frac{\alpha_b k_t f_u dt}{b_m l_b \gamma_{M2}} \tag{4.32}$$

where:

b_m is the width of a composite slab module;

l_b is the length between the transversal bars.

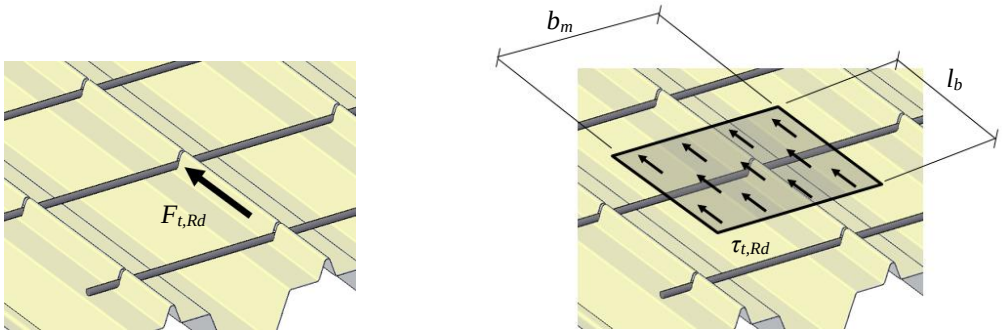

(a) Force resistant on each contact point (b) Tangential resistance stress

Fig. 4.29 Resistance of the reinforcing system

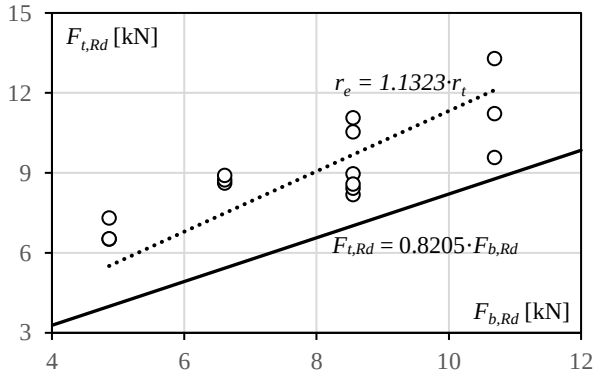

Fig. 4.30 Diagram $F_{t,Rd} - F_{b,Rd}$

4.4.5 Design of composite slabs with transversal reinforcing bars

Based on the experimental results presented in previous sections, a composite slab reinforced with transversal bars intersecting the profiled steel sheeting (the proposed reinforcing system) has a ductile behaviour. So, the partial connection method can be used to predict its bending and longitudinal shear resistance. The application of such methodology, already incorporating the contribution of the proposed reinforcing system, is described hereafter.

On section 3.3.3.2.3 of this document it was presented the longitudinal shear design of steel-concrete composite slabs according to standard EN 1994-1-1 (CEN, 2004b) using the partial connection method. If the partial connection method is used it should be shown that at any cross-section the design bending moment M_{Ed} must be lower than the design resistance M_{Rd}. In composite slabs with transversal bars crossing the profiled steel sheeting, the design shear strength $\tau_{u,Rd}$ should be replaced by $\tau_{t,Rd}$ evaluated according to Eq. (4.32). The design procedure by the partial connection method incorporating the

proposed reinforcing system is validated through the experimental programme comprising full-scale bending tests on steel-concrete composite slabs carried out and described in the next section (section 4.5).

4.5 Experimental evaluation of the new reinforcing system

4.5.1 Introduction

In a second phase of the research, an experimental campaign was carried out to evaluate the efficacy of the proposed reinforcing system on the global behaviour of simply supported and continuous composite slabs. Fig. 4.31 shows the production and composite phases of the specimens. The experimental results obtained in this experimental campaign were also used to verify the accuracy of the design methodology presented in the previous section, the partial connection method of standard EN 1994-1-1 (CEN, 2004b) accounting for the longitudinal shear strength through Eq. (4.32).

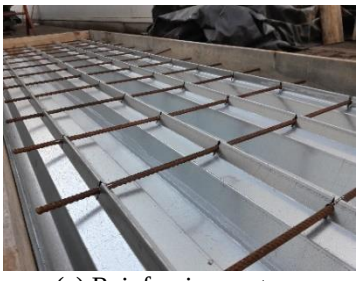

(a) Reinforcing system

(b) Specimens for simply supported slabs

(c) Specimens for continuous slabs

Fig. 4.31 Specimen preparation

On this experimental campaign three different profiles were used: LAMI 60+, LAMI 120+ and H60 (previously described in section 4.2). All the steel sheets used in the tests had a nominal thickness t_{nom} of 1.00 mm, and a core thickness of 0.96 mm after excluding the corrosion protection by hot-dip galvanizing, composed of two 0.02 mm thick layers on each face. In accordance with the production process, the surface of the profiled steel sheeting used in the present research is smooth, without any type of embossments; as a consequence, it must be highlighted that once the adhesion connection is broken, the longitudinal shear resistance is entirely dependent on the bearing resistance of the transversal bars crossing the longitudinal stiffeners, which are the main components of the proposed reinforcing system.

In order to characterize the concrete, uniaxial compressive tests were performed on cubic specimens with edges of 150 mm. The mechanical properties of the concrete, obtained according to the procedure presented on section 4.3.3, are described in Table 4.16. The characterization of the material was carried out in the same week as the full-scale tests. An average compressive stress resistance f_{cm} of 36.32 MPa for the concrete and a corresponding characteristic value f_{ck} of 28.32 MPa, in accordance with Eurocode 2 (CEN 2004a), were obtained.

Table 4.16 Properties of concrete (full-scale experimental programme)

f_{ci} [MPa]	$(f_{ci}-f_{cm})/f_{cm}$ [-]	δ [-]	$f_{cm,cube}$ [MPa]	$f_{ck,cube}$ [MPa]	f_{cm} [MPa]	f_{ck} [MPa]	E_{cm} [MPa]	f_{ctm} [MPa]	ε_{c1} [mm/mm]	ε_{cu1} [mm/mm]
36.436	0.007									
35.520	-0.019	0.013	36.194	35.402	36.322	28.322	32395	2.79	0.0021	0.0035
36.627	0.012									

To obtain the tensile resistance of the steel, uniaxial tensile tests were performed on steel sheet specimens with a geometry according to standard ISO 6892-1 (ISO 2009); material properties of profiles LAMI 60+ and H60 (already used in the preliminary experimental campaign) were already presented on Table 4.6 and Table 4.7, respectively. For profiles LAMI 120+ (used only in this second experimental campaign), three uniaxial tensile tests were performed to define the resistance of steel used on it. These results are graphically presented in Fig. 4.32. The dimensions of the specimens and the experimental results are presented on Table 4.17. An average yield stresses f_{yp} of 363.57 MPa and an average peak stresses f_{up} of 476.59 MPa were obtained.

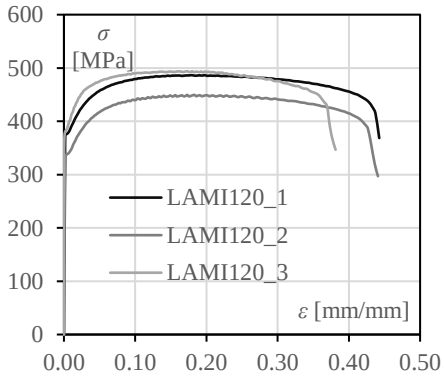

Fig. 4.32 Uniaxial tensile tests to steel from LAMI 120+ profiles

Table 4.17 Mechanical properties of steel used in LAMI 120+ profiles

	t_0 [mm]	b_0 [mm]	S_0 [mm^2]	f_{yp} [MPa]	f_{up} [MPa]	f_{ypm} [MPa]	f_{upm} [MPa]
LAMI120_1	0.97	20.06	19.458	376.23	486.46		
LAMI120_2	0.98	19.99	19.590	338.28	449.49	363.57	476.59
LAMI120_3i	0.94	20.05	18.847	376.18	493.83		

4.5.2 Second full-scale experimental programme

The second experimental programme carried out for the present research work consisted of 6 experimental full-scale tests, divided into two groups: one group of simply supported slabs – group A – and another group constituted by 2 span continuous slabs – group B. Group A comprised four bending tests of simply supported composite slabs with 2.8 m span lengths L. These slabs were loaded with four transversal linear loads applied symmetrically in relation to the half span cross-section and spaced by $L/4$, as shown in Fig. 4.33. This loading system was established in order to approximate as much as possible the conditions to a real loading scenario, which, in general, is constituted by a uniformly distributed load. Fig. 4.34 shows the cross-section of each specimen from test group A, specifying the reinforcing bars applied. Group B comprised two bending tests on continuous slabs with 2 equal spans of 2.8 m in length. These slabs were also loaded with four linear transversal loads applied symmetrically to the intermediate support section, as shown in Fig. 4.35. Fig. 4.36 shows the cross-section of each specimen from test group B, specifying the reinforcing bars applied.

The effect of the transversal bars crossing the profiled steel sheeting was studied for slabs with LAMI 60+ (A_1 and A_2) or LAMI 120+ (A_3 and A_4) profiles in group A. In all specimens of this group, 8 mm diameter transversal bars were uniformly distributed over the span, with a space l_b of 200 mm between them. Specimens A_1 and A_2 were identical, although the surface roughness of the bars used was different: bars with a smooth (S) surface in specimen A_1 and bars with a ribbed (R) surface in specimen A_2. Specimens A_3 and A_4 were also identical, but the specimen A_4 had 2 additional longitudinal bars, one in each concrete rib.

The specimens from group B were identical, except for the longitudinal shear reinforcing system: specimen B_1 was constituted by an H60 profiled steel sheeting without any type of longitudinal shear reinforcement, therefore the longitudinal shear resistance was acquired only from the embossments on the profile (a base case) and; specimen B_2 was constituted by a LAMI 60+ profiled steel sheeting, reinforced with 10 mm diameter transversal bars uniformly distributed over the slabs, crossing the longitudinal stiffeners with a space of 400 mm between them (a specimen with the proposed reinforcing system). In the region of the intermediate support, 12 mm diameter longitudinal bars were placed with a space of 150 mm between them in both specimens; the coverings, measured between the centroids of the longitudinal bars and the top concrete surface, were 30 mm.

The tests were carried out applying an increasing load, controlled by a displacement increase of 0.02 mm/s until the plastic behaviour was reached and 0.04 mm/s in a

subsequent phase until failure. In all the specimens, strain gauges were applied on the steel sheeting. Load cells were used on the supports and on the loading system to measure the reaction forces and the load applied. Several displacement transducers (LVDTs) were also used to measure the deflections along the span and the slip between the steel and the concrete at both ends.

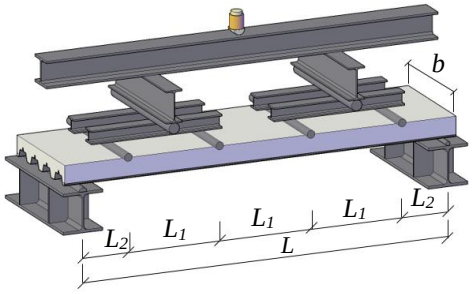

	A_1	A_2	A_3	A_4
b	820	820	666	666
h	150	150	200	200
h_p	60.0	60.0	113.96	113.96
h_c	90	90	86.04	86.04
L	2800	2800	2800	2800
L_1	700	700	700	700
L_2	350	350	350	350

Fig. 4.33 Experimental layout – Group A (dimensions in mm)

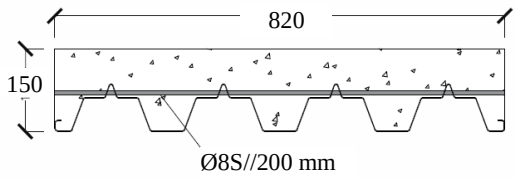

(a) A_1

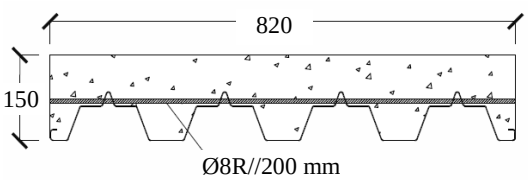

(a) A_2

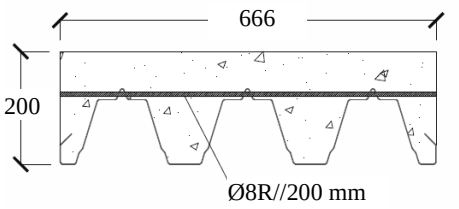

(a) A_3

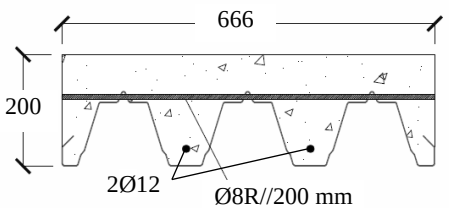

(a) A_4

Fig. 4.34 Cross-section of the specimens – Group A (dimensions in mm)

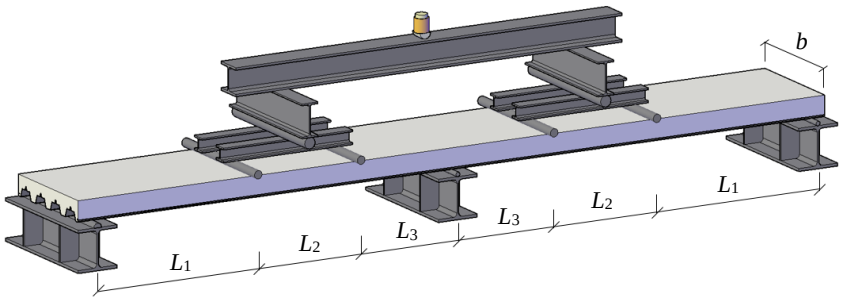

b = 820 mm
h = 150 mm
h_p = 60 mm
h_c = 90 mm
L = 2800 mm
L_1 = 1250 mm
L_2 = 800 mm
L_3 = 750 mm

Fig. 4.35 Experimental layout – Group B

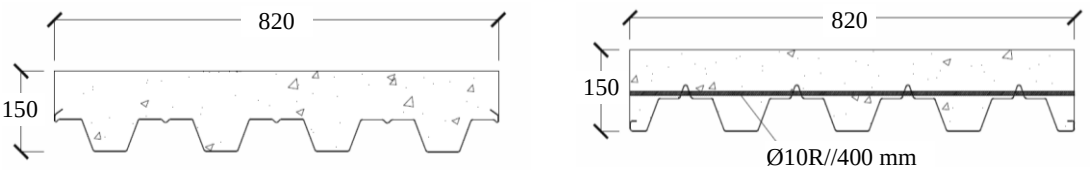

(a) B_1 (b) B_2

Fig. 4.36 Cross-section of the specimens – Group B (dimensions in mm)

Fig. 4.37 shows the instrumentation prepared for tests from groups A (Fig. 4.37(a)) and B (Fig. 4.37(b)). In all the specimens, strain gauges (SG) were applied on the steel sheeting. These strain gauges were placed at the bottom flange of the middle rib on cross-sections A and B, respectively for specimens from groups A and B, according to Fig. 4.37.

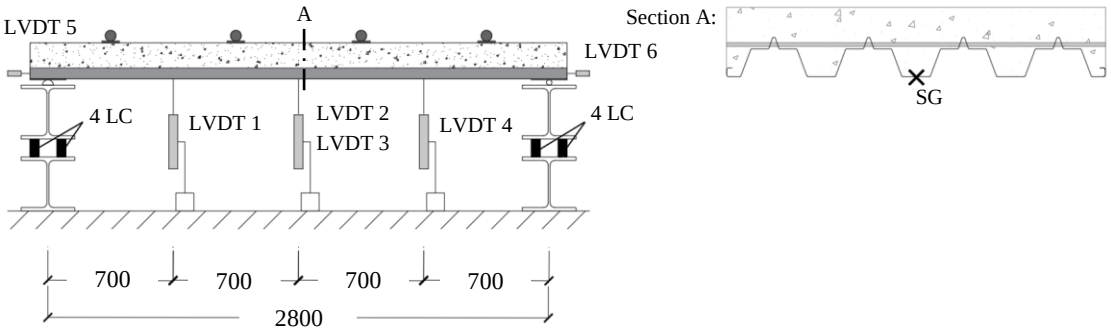

(a) Group A

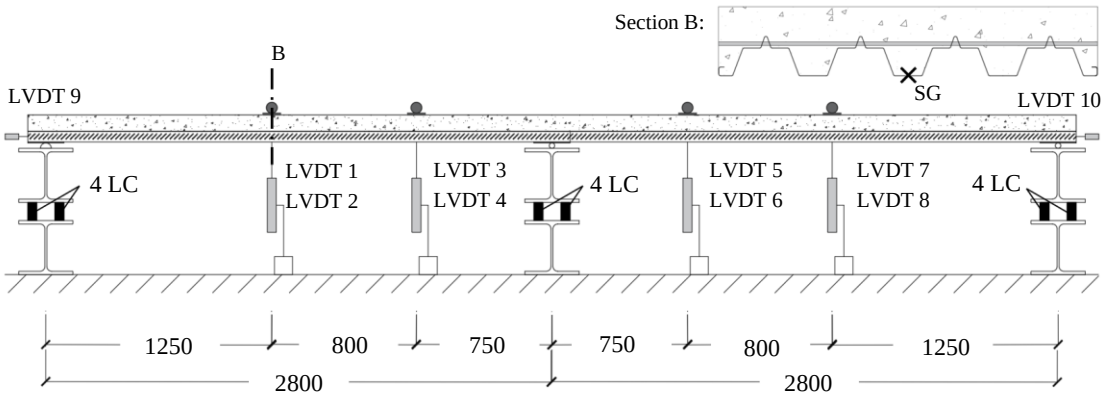

(b) Group B

Fig. 4.37 Instrumentation of experimental tests

4.5.3 Experimental results of the second campaign

4.5.3.1 Group A – simply supported slabs

All the slabs of the present group reached failure by longitudinal shear, but for a loading level close to the bending moment capacity. In all the specimens tensile cracks developed in the concrete, in the tension zone of the the slab, along the span length with uniform bending moment (close to the mid-span) (see Fig. 4.38(a)). The longitudinal shear failure was governed by the bearing of the steel sheeting, as shown in Fig. 4.38(b).

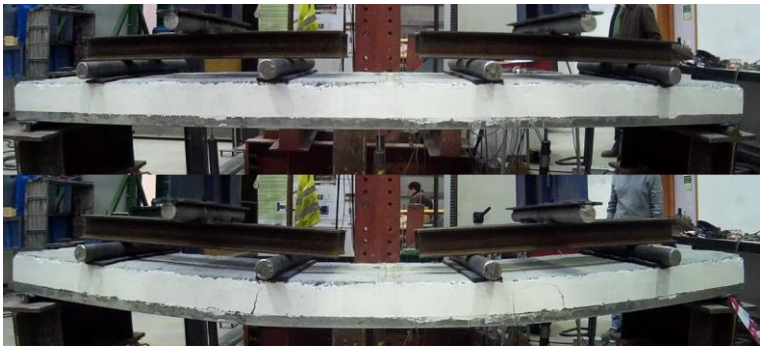

(a) Experimental test set-up

(b) Bearing of the steel sheet

Fig. 4.38 Experimental approach

If the results from tests A_1 and A_2 are compared, a similar maximum applied load and general behaviour are observed, as it can be observed on Fig. 4.39. No significant effects were observed due to the difference in the surface roughness of the transversal bars used. However, the use of longitudinal reinforcing bars significantly increased the resistance of the composite slab, which can be verified from the comparison of the test results of specimens A_3 and A_4 on Fig. 4.40; the maximum load achieved increased 34.56% from specimen A_3 to specimen A_4 just with 2 additional longitudinal bars. The greater thickness of the slabs of specimens A_3 and A_4 results in a larger bending stiffness as expected. Generally, all the specimens showed a high resistance and high ductility; the low values of the end slips measured at both ends (see Fig. 4.39(b) and Fig. 4.40(b)) allow us to conclude that the incorporation of the transversal bars crossing the profiled steel sheeting makes it possible to reach high degrees of longitudinal shear connection.

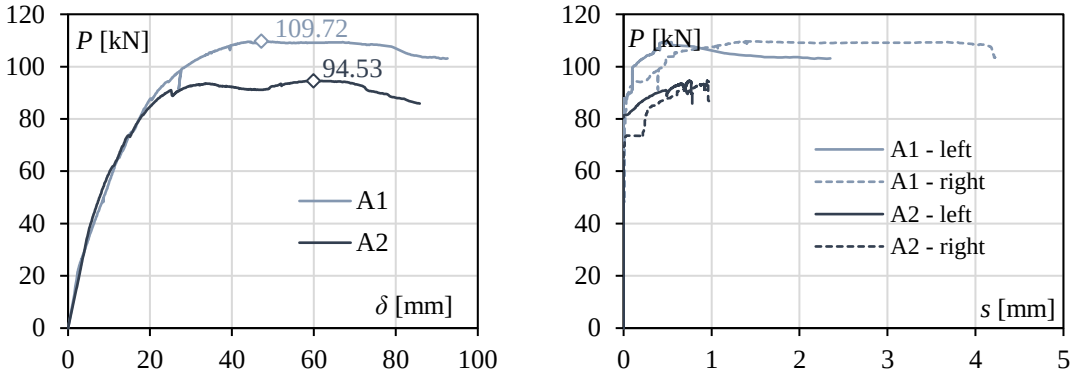

(a) *P*-δ curves (b) *P*-*s* curves

Fig. 4.39 Experimental results – *P*-δ and *P*-*s* curves from tests A_1 and A_2

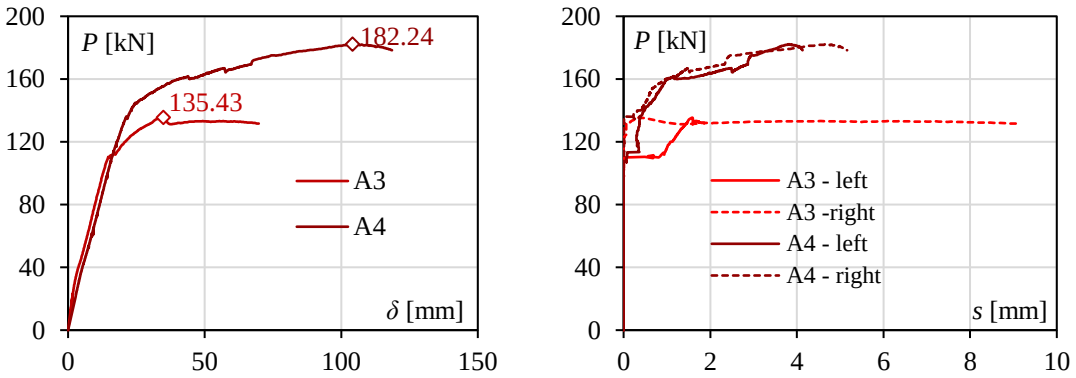

(a) *P*-δ curves (b) *P*-*s* curves

Fig. 4.40 Experimental results – *P*-δ and *P*-*s* curves from tests A_3 and A_4

Fig. 4.41(a) shows the strains measured during tests A_1 and A_2 at the bottom (A1,b and A2,b, respectively) and upper flanges (A1,u and A2,u, respectively) of the steel sheet at the mid-span cross-section. Fig. 4.41(b) shows the equivalent results for tests A_3 and A_4 but just at the bottom flange (A3,b and A4,b, respectively). The maximum strain values measured at the bottom flange of the steel sheet at the mid-span cross-sections of all the specimens were also much higher than the yield strain of the steel used ε_{yp} (see Fig. 4.41), which means that the plastic bending capacity of the slabs tested was almost attained.

For each test, Fig. 4.42 and Fig. 4.43 show: (i) the sagging bending moment measured along the span – M_{test}; (ii) the cross-sectional sagging bending moment resistance of the slab under full shear connection – $M_{pl,Rd}$; (iii) the sagging bending moment resistance according to the partial connection method predicted in standard EN 1994-1-1 (CEN, 2004b), already incorporating the proposed reinforcing system, depending on the connection degree η – M_{Rd}; (iv) the design values of the sagging bending moment along the span, for the type of loading used in the tests, if governed by the longitudinal shear resistance – M_{Ed}. The analytical values were evaluated using the average mechanical

properties (real properties) of the materials instead of the design values. In tests A_1, A_2, A_3 and A_4 the maximum sagging bending moments measured M_{test} were 36.99 %, 17.94 %, 27.90 % and 11.51 % respectively higher than the maximum bending moments that were expected M_{Ed}. Furthermore, the maximum sagging bending moment measured M_{test} in test A_1 was 8.23 % higher than the plastic moment resistance $M_{pl,Rd}$; in the remaining tests, lower values were reached although they were always very close to the cross-sectional plastic bending resistance of the slab.

The results obtained in this group of tests allow us to conclude that: (i) the proposed reinforcing system constituted by transversal bars crossing the profiled steel sheeting, if adequately designed, allows the full bending capacity of a composite slab to be reached and; (ii) the design methodology based on the partial connection method, incorporating the longitudinal shear strength acquired by the proposed reinforcing system, can be used to predict the resistance of a composite slab.

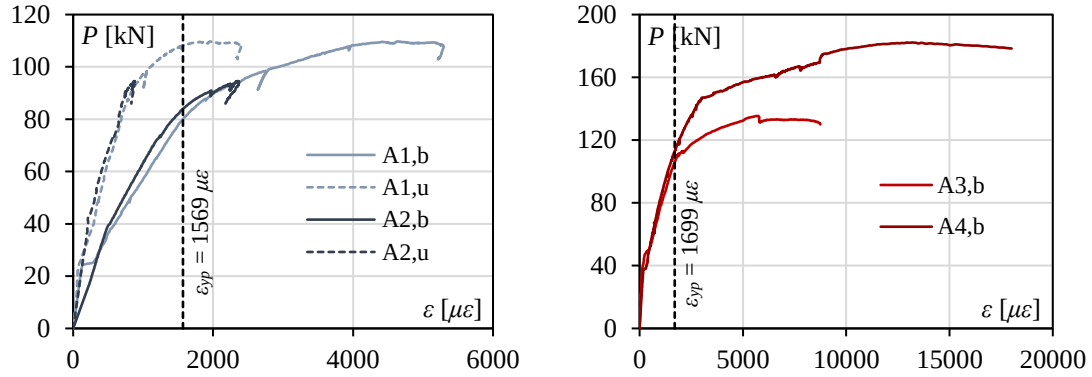

(a) A1 and A_2 (b) A_3 and A_4

Fig. 4.41 *P*-ε curves – Group A

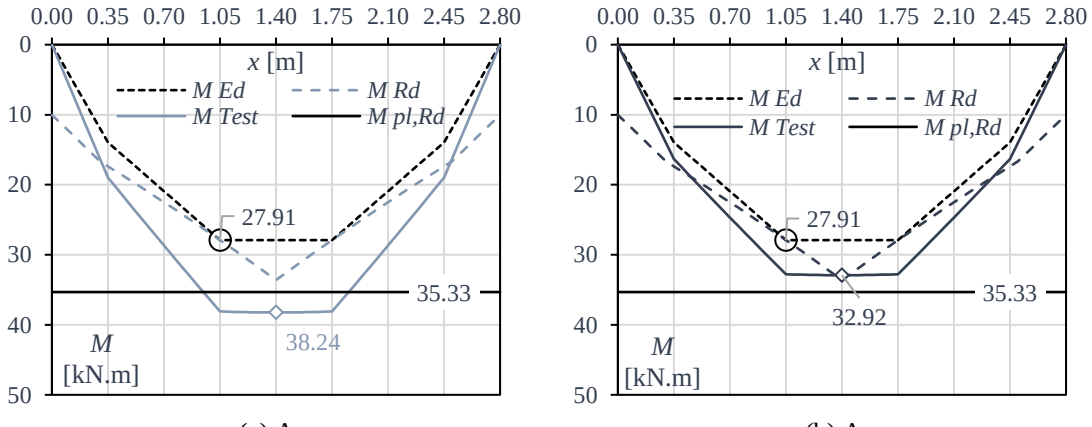

(a) A_1 (b) A_2

Fig. 4.42 Bending moment diagrams – Tests A_1 and A_2

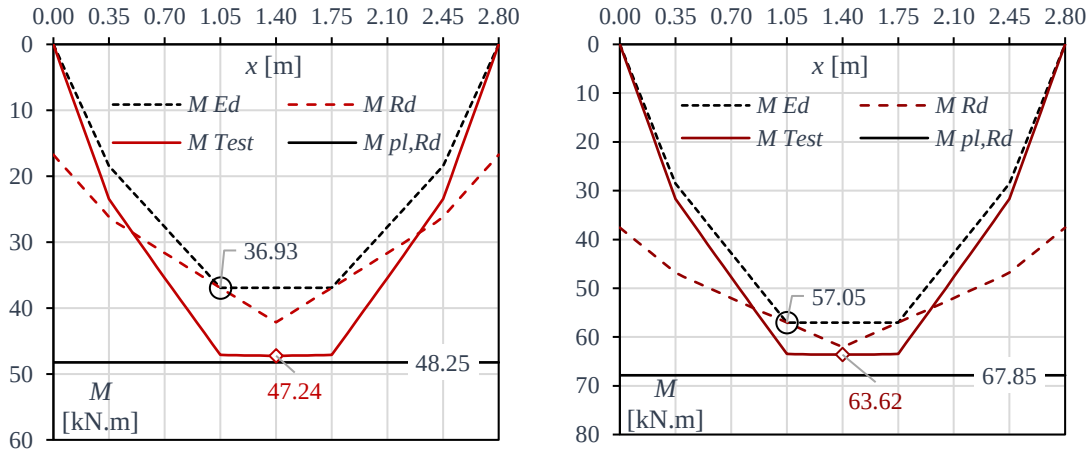

(a) A_3 (b) A_4

Fig. 4.43 Bending moment diagrams – Tests A_3 and A_4

4.5.3.2 Group B – continuous slabs

Test group B was developed to verify the efficacy of the proposed reinforcing system when applied in continuous composite slabs. Fig. 4.44 shows the similar results obtained for the tests on group B. *P-δ* and *P-s* curves are represented in Fig. 4.44(a)-(b), respectively. *P-ε* curves are represented in Fig. 4.45. The strains were measured in the bottom flanges of the profiled steel sheeting at cross-sections A and D. Sections A and D, as it is illustrated in Fig. 4.45, represent the cross-sections where the outer linear loads are applied – section A on the left span and section D on the right span.

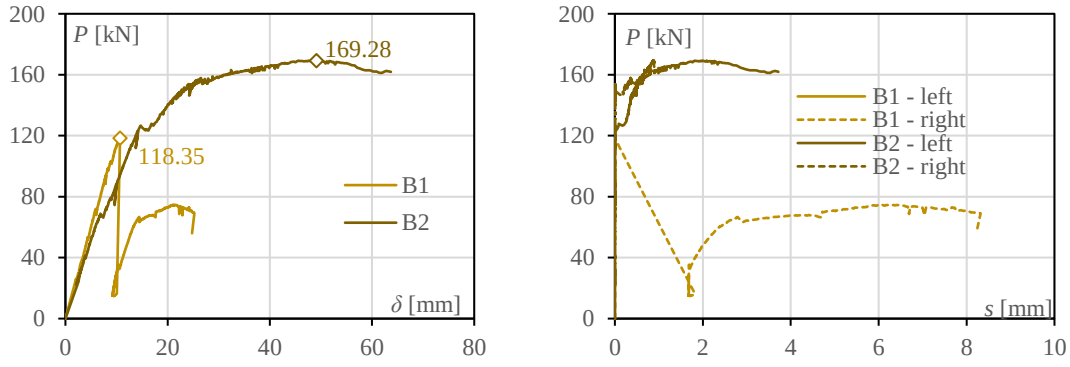

(a) *P-δ* curves (b) *P-s* curves

Fig. 4.44 Experimental results – Group B

Based on the results obtained, an increase of 43.03 % was observed in the maximum load achieved caused by replacing the embossments in the steel sheet profile (test B_1) with the transversal bars crossing the longitudinal stiffener (test B_2). Furthermore, the increase of ductility acquired was significant. In test B_1 a brittle behaviour was obtained, since the slip started immediately after the maximum load level was reached, while in test B_2, the

load significantly increased even after the first slip. The slip developed in test B_1 was also significantly higher, when compared with the one in test B_2.

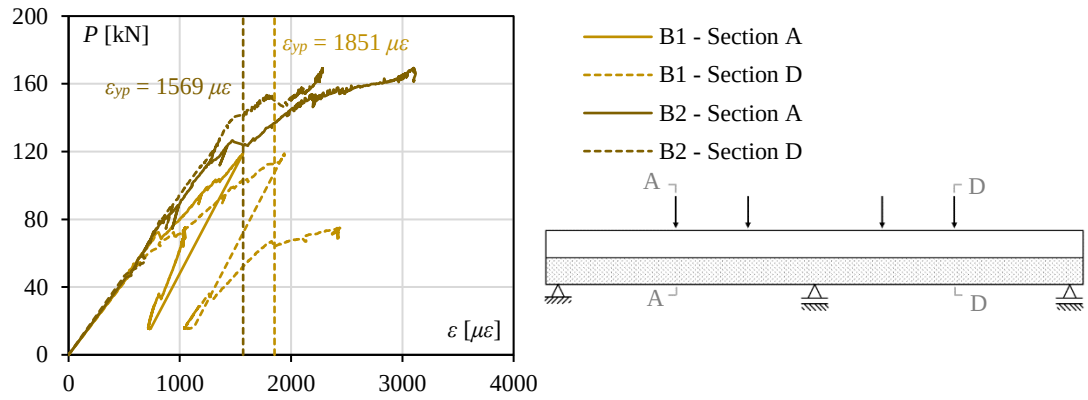

Fig. 4.45 P-ε curves – Group B

Fig. 4.46 shows the vertical shear and bending moment diagrams in the collapse of both tests. Following the same procedure used for group A, Fig. 4.47 presents the bending moment diagrams M_{test}, $M_{pl,Rd}$ along the span and M_{Rd} and M_{Ed} for test B_2. Since specimen B_1 presented a brittle behaviour according to standard EN 1994-1-1 classification, the partial connection method must not be applied to evaluate its resistance to longitudinal shear.

The results of group B show that the proposed reinforcing system makes it possible to significantly increase the ductility of steel-concrete composite slabs. The bending moment diagram M_{test} obtained in test B_2, compared with the predicted diagram M_{Ed} according to the methodology proposed in the previous chapter, was very accurate.

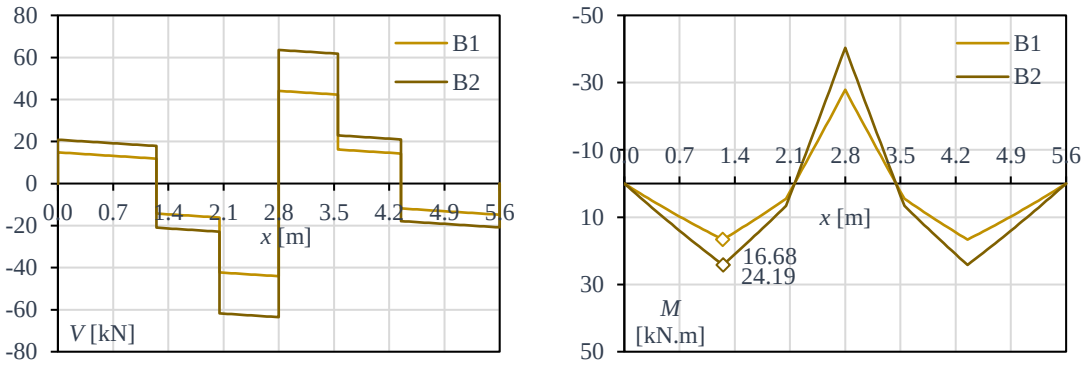

(a) Vertical shear (b) Bending

Fig. 4.46 Vertical shear and bending moment diagrams – Tests B_1 and B_2

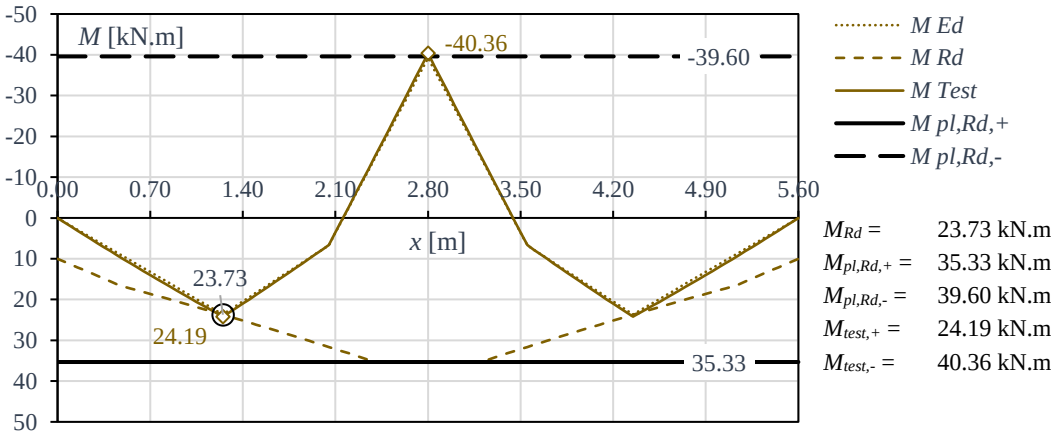

Fig. 4.47 Bending moment diagram – Test B_2

4.5.4 Discussion of the results

Over this chapter several experimental campaigns were presented. A first experimental campaign was carried out to get a first assessment concerning the behaviour of steel-concrete composite slabs with transversal bars intersecting the profiled steel sheeting. The first results showed that the proposed reinforcing system was very effective and so, a small-scale experimental programme was carried out to derive an equation to take into account the contribution of the mechanical interlock provided. Then another full-scale experimental programme was carried out to prove the efficiency of the reinforcing system and also to validate the design approach developed to take it into account.

Small-scale and full-scale experimental results allowed to verify that proposed reinforcing system allows to (i) increase the longitudinal shear capacity, (ii) increase the ductility, (iii) reduce the longitudinal slip and (iv) use the full bending capacity of composite slabs.

On the second full-scale experimental programme, 4 simply-supported composite slabs with transversal bars intersecting the profiled steel sheeting were tested (group A). The obtained results allowed to conclude that the incorporation of transversal bars intersecting the steel sheeting makes it possible to reach high degrees of longitudinal shear connection. The proposed reinforcing system, developed to increase the longitudinal shear capacity, has allowed to achieve the full bending capacity on test A_1.

From the results obtained on the continuous composite slabs group of tests (group B) it was concluded that transversal bars intersecting the profiled steel sheeting allow to increase the ductility of the longitudinal shear behaviour of continuous composite slabs.

If compared with slabs with embossed profiled steel sheeting (test B_1), slip measured on the slab with the proposed reinforcing system (test B_2) was significantly lower and the bearing capacity increased.

Experimental campaigns on steel-concrete composite members are expensive and time consuming. It is the best way to reproduce the reality but the amount of results is always scarce. Experimental results have allowed to prove the efficiency of the proposed system; but to study the influence of several mechanic or geometric parameters a parametric analysis is usually required. Taking this into consideration, in the scope of the present research work, a numerical study was carried out and described in the next chapter. Experimental results from the second full-scale experimental campaign were used to calibrate numerical models in *Abaqus* software and then a parametrical study was performed.

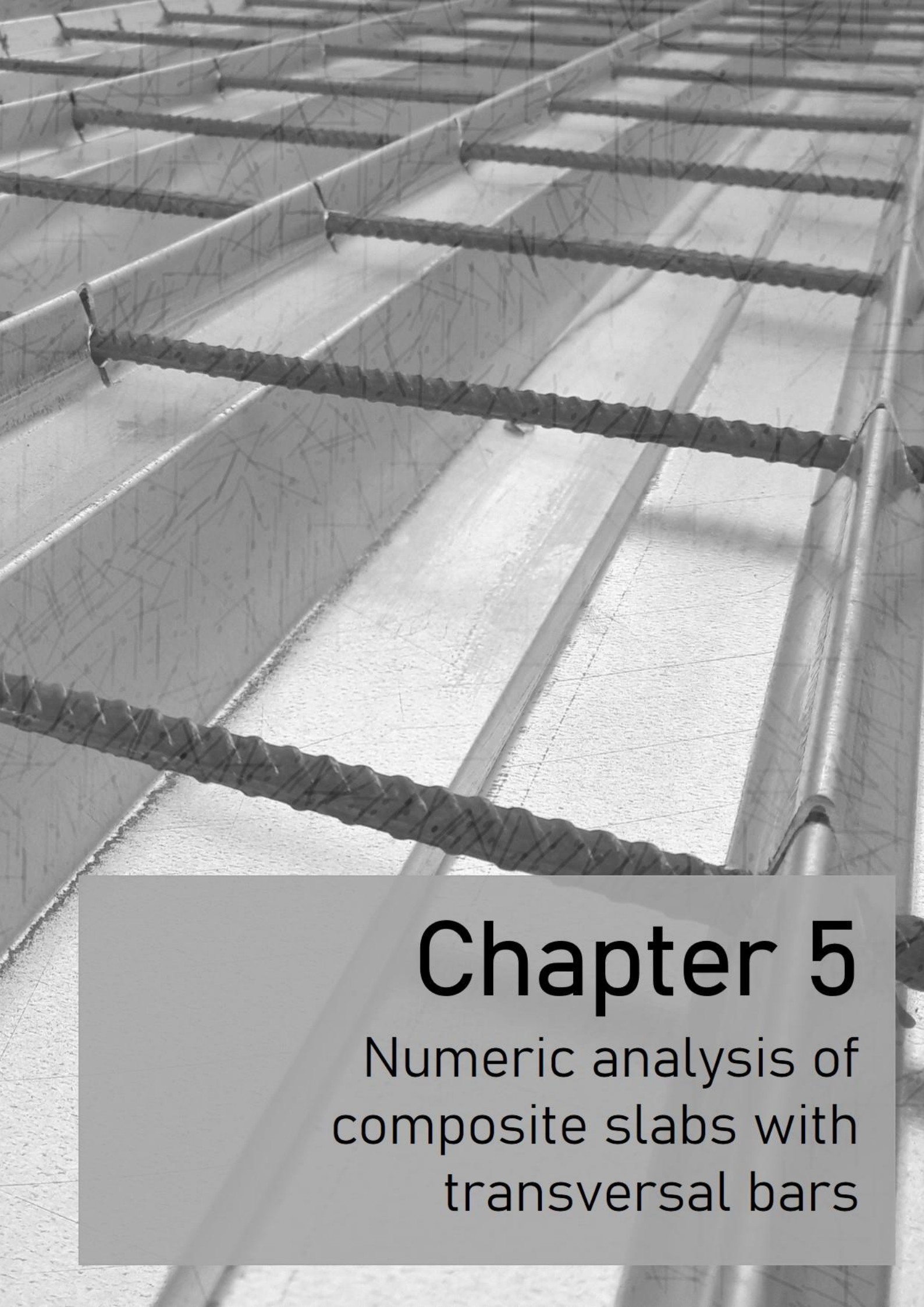

Chapter 5

Numeric analysis of composite slabs with transversal bars

5.1 Introduction

Abaqus is a Finite Element Analysis (FEA) software widely used to simulate complex engineering problems in several types of industries. This software uses a graphical user interface named CAE (Computer-Aided Engineering). It provides several types of material models, analysis and techniques promoting its use by the industry and the academic community. *Abaqus* product offers four main types of products to cover a vast spectrum of applications: *Abaqus/CAE*, to quickly and efficiently create, edit, monitor, diagnose, and visualize advanced *Abaqus* analyses; *Abaqus/standard*, to employ solution technology specially for static and low-speed dynamic problems where highly accurate stress solutions are critically important; *Abaqus/Explicit*, to simulate brief transient dynamic events such as consumer electronics drop testing, automotive crashworthiness, and ballistic impact and; *Abaqus Multiphysics*, to simulate electrical, thermal, acoustic, structural, fluid or pore pressure environments problems. The multipurpose of this software makes it a mighty FEA software capable of simulating the behaviour of structures, parts of structures or structural elements considering material and geometric nonlinear behaviour.

The use of finite element analysis among researchers has been growing constantly. Numerical simulations using computer technologies have been implementing an efficient alternative to experimental tests due to the reduction of time and of resource needs. Numerical simulations are especially useful to carry out extensive parametrical studies. However, finite element analyses are not able of completely replacing experimental campaigns, because the finite element models should be calibrated and validated using experimental results. Nevertheless, numerical studies allow to reduce significantly the amount of experimental tests needed.

Experimental results obtained and presented in the previous chapter were used to calibrate numerical models using the software *Abaqus*. In order to obtain accurate results, all parts should be properly modelled, specially the connection between the profiled steel sheeting and the concrete. These models were validated, mainly based on the ultimate load attained in experimental tests. A comparison between the end slip, the crack pattern and the failure mode experimentally and numerically obtained were also provided. Then, after validating the numerical models, a parametrical study was carried out in order to study the effect of several mechanical or geometric parameters on the behaviour of the proposed reinforcing system and the capacity of composite slabs. Numerical results allowed to conclude that the steel sheeting thickness influences significantly the structural performance of the reinforcing system.

5.2 Base concepts for the numerical modelling

5.2.1 Introduction

In order to calibrate and validate the results from the numerical modelling using the software *Abaqus* (SIMULIA, 2015), two of the experimental tests performed and described in the previous chapter (tests A_2 and A_3) were considered (see Fig. 5.1(a)). To simplify the complexity of the models, and regarding the geometrical symmetry of the specimens and the concept of the one directional behaviour of those elements, the numerical models were developed considering only half a span and half a module of a slab – see Fig. 5.1(b)-(c). Abdullah *et al.* (2007) also made this simplification to carry out a numerical study about the behaviour of steel-concrete composite slabs.

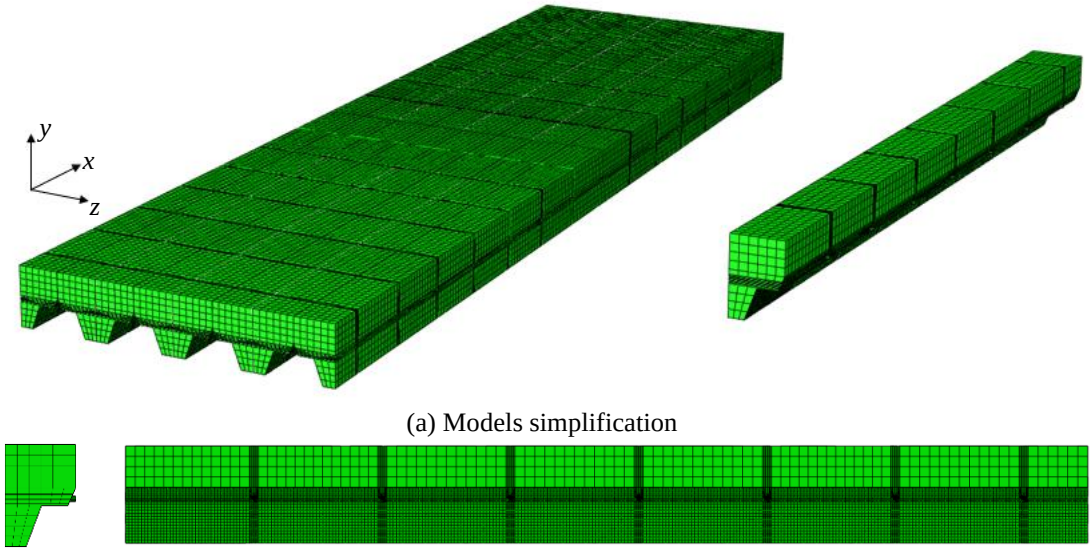

(a) Models simplification

(b) *yz*

(c) *xy* section view

Fig. 5.1 Finite element models

The validation of numerical results, presented later in section 5.3, was carried out based on the experimental tests A_2 and A_3, presented in the previous chapter (results presented in Fig. 4.39). These tests were adopted in order to develop a parametrical study concerning the behaviour of composite slabs with the proposed reinforcing system, using steel sheeting with current and higher heights.

It was intended to simulate the behaviour of composite slabs after failure; so, to avoid problems of convergence, a quasi-static simulation using dynamic implicit procedure was developed.

Regarding the type of elements, cold-formed elements are usually modelled using shell elements. *Abaqus* provides several types of shell elements, depending on the number of nodes, the integration process (reduced integration or other) and the number of degrees of freedom at each node. On the present study, S4R elements (four-node doubly curved thin or thick shell elements and reduced integration) were used to model the cold-formed profiled steel sheeting members. The other components, concrete and reinforcement parts, were modelled using solid C3D8R elements (three-dimensional eight-node linear brick and reduced integration solid elements).

The accuracy of the numerical results is also influenced by the mesh size. Different mesh sizes were used for different parts: concrete parts were meshed with 15 mm elements, reinforcing bars with 10 mm elements and steel sheeting with 5 mm elements.

5.2.2 Material models

5.2.2.1 Concrete

5.2.2.1.1 Basic concepts

Several researchers have been studying the behaviour of concrete in order to characterize their behaviour under tension or compression (Ali *et al.*, 1990; Chaudhari and Chakrabarti, 2012; Hsu and Hsu, 1994; J. Lee and Fenves, 1998).

The density of concrete γ_c assumed in the numerical models developed in the aim of the research studies above referred, was considered to be 24.0 kN/m^3 in accordance with Annex A of standard EN 1991-1-1 (CEN, 2002b). The concrete behaviour is then defined in two distinct types: (i) elastic behaviour and; (ii) plastic behaviour using the Concrete Damage Plasticity (CDP) model.

5.2.2.1.2 Elastic behaviour of concrete

The elastic behaviour of concrete is defined by two main parameters: the initial modulus of elasticity E_{cm} and the Poisson coefficient v. The initial modulus of elasticity E_{cm} was defined in accordance with the recommendations of standard EN 1992-1-1 (CEN, 2004a) expressed on Eq. (5.1). The Poisson ratio v was established as 0.20.

$$E_{cm} = 2200\left(\frac{f_{cm}}{10}\right)^{0.3} \tag{5.1}$$

Taking into account an average compressive resistance f_{cm} of 36.32 MPa obtained in the full-scale experimental programme, from the Eq. (5.1) a value of 32.395 GPa was adopted for the initial modulus of elasticity E_{cm} to be used in the calibration models.

5.2.2.1.3 Concrete Damage Plasticity (CDP)

(i) General

The nonlinear behaviour of the concrete was simulated using the Concrete Damaged Plasticity (CDP) model, which provides a general capability for modelling concrete and other quasi-brittle materials in all types of structures. CDP model, which was developed by Lubliner *et al.* (1989) and later by Lee and Fenves (1998), allows the simulation of the inelastic behaviour of concrete under monotonic, cyclic and dynamic types of loading. The input data to reproduce this type of model comprises the uniaxial response of concrete in compression and tension, compressive and tension damage evolution and the stiffness recovery parameters.

Several researchers have been modelling concrete or composite members using CDP models for different circumstances (Attarde, 2014; Chaudhari and Chakrabarti, 2012; Dere and Koroglu, 2017; Hossain *et al.*, 2019; Jankowiak and Lodygowski, 2005; Ríos *et al.*, 2017; Szczecina and Winnicki, 2015; Tao and Chen, 2014; Wahalathantri *et al.*, 2011). The CDP model approach which allowed to reach the most accurate results was therefore adopted in this study.

CDP model is initially defined by five plasticity coefficients. Under the scope of present study these coefficients were defined according to the default values of the software, wich were validated by the calibrated models from the relevant bibliography. Therefore: (i) a dilation angle ψ of 31º, (ii) a flow potential eccentricity ε_{CDP} of 0.1, (iii) a ratio between the biaxial compressive strength and the uniaxial compressive strength f_{b0}/f_{c0} of 1.16, (iv) a ratio of the second stress invariant on the tensile meridian to the one on the compressive meridian K_c of 0.667 and (v) a viscosity parameter μ of 0.005, were assumed. Biaxial resistance of the concrete is defined according to the uniaxial resistance values, taking into account the ratio f_{b0}/f_{c0}, as it is illustrated in Fig. 5.2.

1. Uniaxial tension
2. Uniaxial compression
3. Biaxial tension
4. Biaxial compression

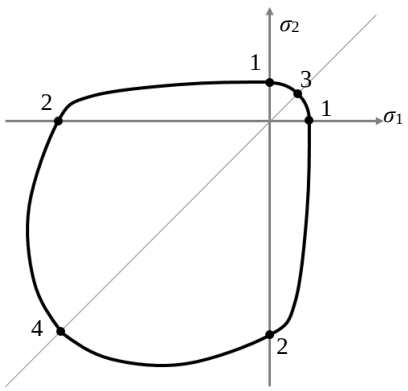

Fig. 5.2 Biaxial yield surface in CDP Model

(ii) Compressive behaviour

The uniaxial stress-strain curve for the compressive behaviour of the concrete is defined according to the compressive strength f_{cm}. Fig. 5.3(a) shows the typical σ_c-ε curve adopted to define the compressive response of concrete. This curve was adopted based on some examples provided in the bibliography (Balan *et al.*, 2001; Birtel and Mark, 2006; Nguyen and Whittaker, 2017) and is defined by three different parts: (i) one elastic branch up to an initial compressive yield stress equal to 50% the concrete strength f_{cm} following Eq. (5.2); (ii) the second ascending part that follows the formula developed by Popovics (1973) – Eq. (5.3) – and (iii) one softening part that follows the equation developed by Saenz (1964) – Eq. (5.4). The introduction of the softening branch is relevant to characterize the behaviour of concrete after the peak load.

$$\sigma_c = \varepsilon E_{cm} \tag{5.2}$$

$$\sigma_c = f_{cm} \frac{K\left(\frac{\varepsilon}{\varepsilon_{c,1}}\right)}{1+(K-1)\left(\frac{\varepsilon}{\varepsilon_{c,1}}\right)^r} \tag{5.3}$$

$$\sigma_c = f_{cm} \frac{K\left(\frac{\varepsilon}{\varepsilon_{c,1}}\right)}{1+A\left(\frac{\varepsilon}{\varepsilon_{c,1}}\right)+B\left(\frac{\varepsilon}{\varepsilon_{c,1}}\right)^2+C\left(\frac{\varepsilon}{\varepsilon_{c,1}}\right)^3} \tag{5.4}$$

where:

σ_c is the compression stress;
ε is the total strain;
f_{cm} is the average maximum compressive strength;
$\varepsilon_{c,1}$ is the strain at peak strength;
$K = E_{cm}\,\varepsilon_{c,1}/f_{cm}$;
$A = C + K - 2$;
$B = 1 - 2C$;
$C = K\,(K_\sigma - 1)/(K_\varepsilon - 1)^2$;
$K_\sigma = f_{cm}/f_{cu}$;
$K_\varepsilon = \varepsilon_{c,1}/\varepsilon_{cu,1}$;
$r = K/(K - 1)$.

The strength and the stiffness decrease when the concrete is subjected to higher loading levels. The damage parameter in compression d_c represents the loss of stiffness over the

compression stress σ_c. Making use of a CDP model, *Abaqus* allows to define the mathematical relationship to provide the linear unloading and reloading path in tension and compression. Based on the methodology adopted by Nguyen and Whittaker (2017), a linear relationship was considered based on the unloading and reloading behaviour of the concrete in tension and compression. It was considered that unloading branches intersect all in a constant focal point FP (see Fig. 5.3(b)). FP coordinates can be determined using Eqs. (5.6) and (5.7). Sinha *et al.* (1964) proposed a stiffness degradation for test data where the damage parameter at peak strength $d_{c,1}$ is 0.3. This value can be obtained from cyclic loading tests to cylindrical concrete specimens. Since these tests were not carried out in the aim of the present study, the value of 0.3 was adopted in this study. Fig. 5.3(c) shows the evolution of the damage parameter under compression d_c when the strain ε is increased.

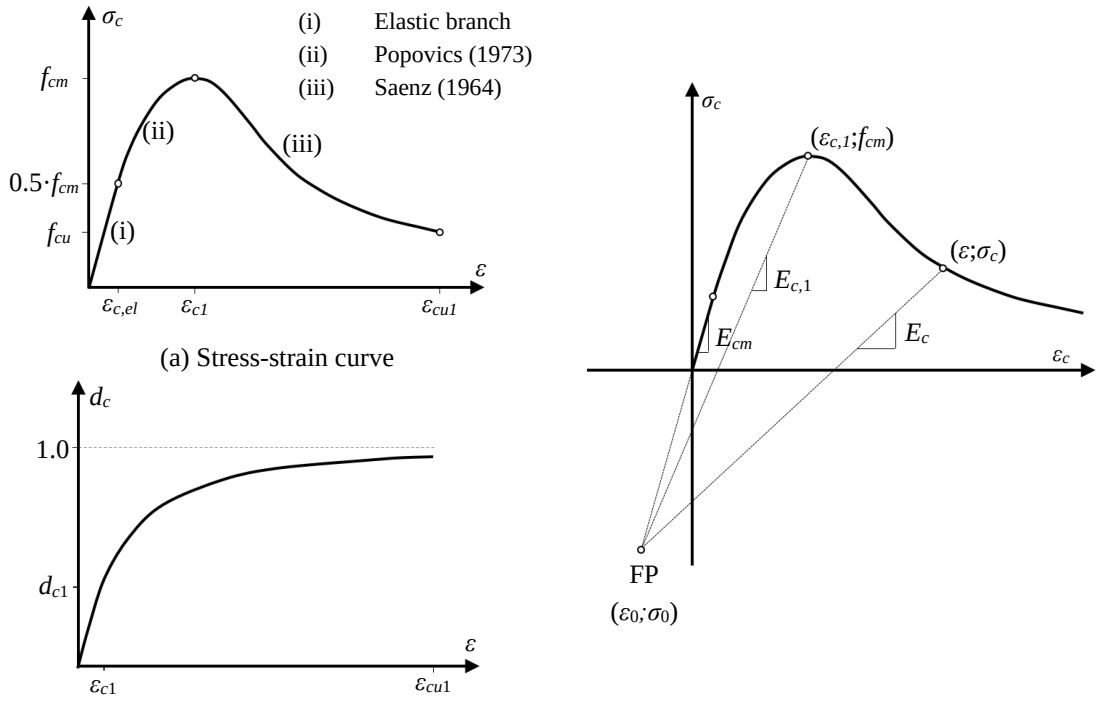

(a) Stress-strain curve

(b) Damage-strain curve

(c) Focal Point (FP)

Fig. 5.3 Compressive strength of concrete

$$d_c = 1 - \frac{1}{E_{cm}} \frac{\sigma_c - \sigma_0}{\varepsilon - \varepsilon_0} \tag{5.5}$$

$$\varepsilon_0 = \frac{f_{cm} - E_{c,1}\varepsilon_{c,1}}{E_{cm} - E_{c,1}} \tag{5.6}$$

$$\sigma_0 = E_{cm} \frac{f_{cm} - E_{c,1}\varepsilon_{c,1}}{E_{cm} - E_{c,1}} \tag{5.7}$$

where:

- ε_0 is the strain coordinate of the focal point (FP);
- σ_0 is the stress coordinate of the focal point (FP);
- $E_{c,1}$ is the unloading stiffness at peak strength related to $d_{c,1}$;
- $d_{c,1}$ is the damage parameter when the peak strength is achieved, such that $d_{c,1} = 0.3$.

(iii) Tensile behaviour

Several researchers have been modelling the tensile stiffening behaviour of concrete and defining the best models to simulate this phenomena (Bažant, 2002; Cornellissen *et al.*, 1986; Genikomsou and Polak, 2015; Hordijk, 1991; Nayal and Rasheed, 2006; Sümer and Aktaş, 2015; Tao and Chen, 2014). *Abaqus* software allows to define the tensile behaviour of the concrete in three different ways: (i) stress-strain σ_t-ε curve, (ii) stress-displacement σ_t-w curve and (iii) fracture energy G_F. For unreinforced concrete problems, like composite slabs without longitudinal bars, it is appropriate to define the behaviour of concrete in terms of fracture energy instead of specifying a stress-strain relation in tension, to avoid unreasonable mesh sensitivity in the results.

According to Hillerborg *et al.* (1976), the fracture energy G_F can be defined as the energy required to develop a unit area of crack, in order to obtain a stress free crack. In concrete, when cracks start developing, the energy stored in the material converts to fracture energy. Hillerborg *et al.* (1976) developed an approach to define the brittle behaviour of concrete by a stress-displacement relation, instead of a stress-strain one, considering the fracture energy value.

The concrete tensile response considered is defined by two different parts, as represented in Fig. 5.4(a). Initially it comprises a linear stress-strain σ_t-ε curve up to the peak tensile strength f_{ctm}. After reaching the tensile strength, the concrete response was defined by a stress-displacement σ_t-w curve, where w is the crack opening displacement. The area under this curve represent the fracture energy G_F. Stress-displacement σ_t-w curve was defined according to the bilinear model proposed by Peterson (1981) and is illustrated on Fig. 5.4(b).

According to standard EN 1992-1-1 (CEN, 2004a), the tensile strength of the concrete f_{ctm} can be defined according to the characteristic value of the compressive strength f_{ck}, as it is shown in Eq. (5.8). The reference value for the fracture energy G_{F0} can be defined according to Eq. (5.9). The aggregates of concrete used in specimens tested were not measured. However, the concrete classification regarding the maximum dimension of the aggregates was D22, so it was always assumed that $d_{\max} = 22$ mm. Therefore, the reference value for the fracture energy G_{F0} was defined as 37.70 J/m^2. The fracture energy

G_F can be defined by Eq. (5.10). w_{ch} is the reference crack opening displacement defined according to Eq. (5.11).

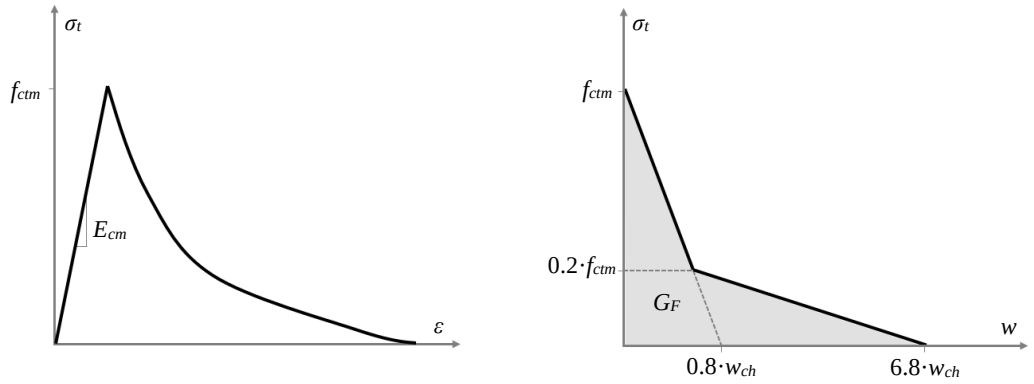

(a) Stress-strain tensile curve (b) Bilinear tensile behaviour

Fig. 5.4 Behaviour of concrete under uniaxial tension

$$f_{ctm} = 0.3 f_{ck}^{2/3} \tag{5.8}$$

$$G_{F0} = 0.0469 d_{\max}^2 - 0.5 d_{\max} + 26 \tag{5.9}$$

$$G_F = G_{F0} \left(\frac{f_{cm}}{10} \right)^{0.7} \tag{5.10}$$

$$w_{ch} = \frac{G_F}{f_{ctm}} \tag{5.11}$$

Under tension, the damage parameter d_t was defined according to Eq. (5.12), as proposed by Gopalaratnam and Shah (1985), where the stiffness loss is directly proportional to the reduction of strength. In theory, the damage variable reaches a value of 1.0 only asymptotically at infinite equivalent plastic displacement. In practice, *Abaqus* will set damage parameter equal to one when the dissipated energy reaches a value of $0.99 \cdot G_F$.

$$d_t = 1 - \frac{\sigma_t}{f_{ctm}} \tag{5.12}$$

5.2.2.2 Steel

The steel from the profiled steel sheeting and from the reinforcing bars in this numerical study was modelled by three different parts: (i) density; (ii) elasticity; (iii) plasticity.

The density of steel γ_s was assumed to be 78.5 kN/m^3 (8.01x10-9 tonne/mm^3 for *Abaqus* input), in accordance with Annex A of standard EN 1991-1-1 (CEN, 2002b), in all numerical models developed in the scope of present research.

The elastic behaviour of the steel is characterized by the modulus of elasticity E_s and the Poisson ratio v. The modulus of elasticity E_s was considered to be 210 GPa. The Poisson ratio v was established as 0.30.

Regarding the plasticity behaviour, *Abaqus* requires the true strain and true stress values to interpret the data correctly. Usually material test results comprise values of nominal stress and strain. For this situations it is mandatory to convert the plastic material data from nominal stress-strain values to true stress-strain values. Fig. 5.5(a) shows an example of a steel bar with initial length and area l_0 and A_0, respectively, under a tensile force F. In these conditions, the area of the critical cross-section tends to decrease and the total length tends to increase, especially after the yield of the material. In uniaxial tensile tests, the stress-strain σ-ε curves are defined considering the initial area A_0 and initial length l_0, so some procedure must be adopted to consider the real behaviour of the steel components when modelling it.

The true stress σ_{true} can be defined according to Eq. (5.13). Eq. (5.14) shows the relationship between true strain ε_{true} and nominal strain ε. Since *Abaqus* software requires the definition of the plastic behaviour separately from the elastic behaviour, the plastic true strain is defined according to Eq. (5.15).

$$\sigma_{true} = \sigma(1+\varepsilon) \tag{5.13}$$

$$\varepsilon_{true} = \ln(1+\varepsilon) \tag{5.14}$$

$$\varepsilon_{pl,true} = \varepsilon_{true} - \varepsilon_{el,true} = \varepsilon_{true} - \frac{\sigma_{true}}{E_s} \tag{5.15}$$

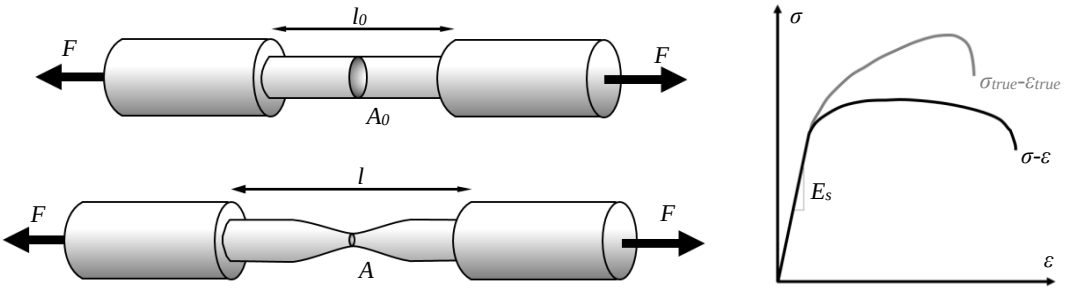

(a) Area reduction in tension (b) Stress-strain curve

Fig. 5.5 True behaviour in plasticity stage

Two different types of steel were used in this study: the steel of profiled steel sheeting and the steel of reinforcing bars.

In the scope of the present study the steel from the profiled steel sheeting is requested until its last strain. So, the steel used in the profiled steel sheeting was modelled by a trilinear curve in order to simulate: (i) the elastic behaviour; (ii) the elastic-plastic behaviour after yielding until its maximum strength f_{up} and; (iii) a descending branch after the peak load until its final strain ε_{fp}. This curve is represented on Fig. 5.6(a). For the present study it was considered that the nominal final stress f_{fp} was equivalent to 25% of the yield stress f_{yp} and the values of the nominal ultimate and final strains ε_{up} and ε_{fp} were assumed to be 0.45 and 0.7 mm/mm, respectively.

The stress-strain σ-ε curve of the steel used in the transversal bars was assumed to exhibit an elastic-perfectly plastic behaviour, as it shown on Fig. 5.6(b).

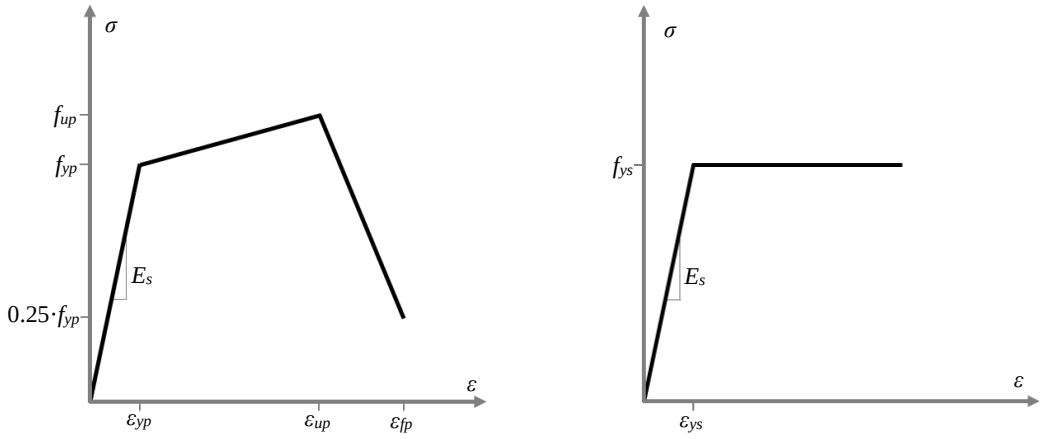

(a) Profiled steel sheeting (b) Reinforcing bars

Fig. 5.6 Stress-strain curves of steel

5.2.3 Interaction properties

Abaqus provides several approaches to define the contact interactions: general contact; contact pair; contact elements. A contact pair algorithm surface-to-surface was used to define the interaction between the different parts in the model. In *Abaqus* software, every contact interaction between two different regions requires the definition of the master and the slave surface. This definition needs to be done taking into consideration the stiffness of the structure and the materials used.

(i) Profiled steel sheeting – Concrete

Considering that the steel sheeting is less stiff than the concrete slab, thanks to its thinness, the top surface of the steel sheeting was considered the slave surface and the bottom surface of the concrete was considered the master (see Fig. 5.7). The interaction between

these two surfaces was defined by two different behaviours: normal and tangential. Normal behaviour was defined as a hard contact, with a default constraint enforcement method. Based on different studies available on the bibliography (Kim *et al.*, 2019; Nguyen and Whittaker, 2017) the tangential behaviour was considered as "Penalty", with a friction coefficient μ of 0.4.

The sliding formulation was considered as finite sliding which is the most used and because it allows any arbitrary motion of the surfaces. Finite-sliding allows to calculate contact area and pressures according to the deformed shape of the model.

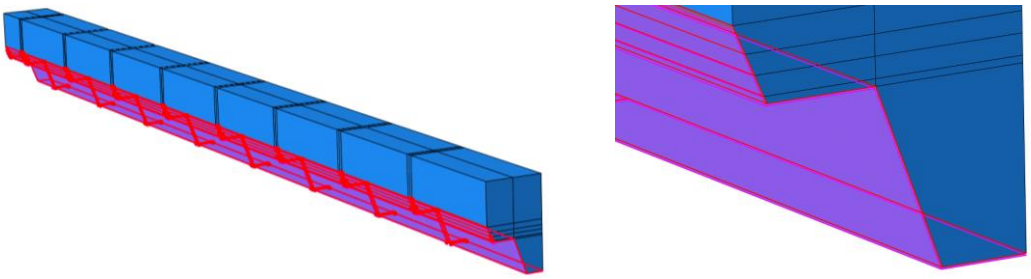

(a) Simplified model (b) Detail

Fig. 5.7 Surface-to-surface contact between the concrete and the profiled steel sheeting

(ii) Reinforcing bars – Profiled steel sheeting

Interaction between the profiled steel sheeting and reinforcing bars were simulated making use of a surface-to-surface contact algorithm. For this interaction the master surface (red colour) was defined by the bar surface and the slave surface (pink colour) comprised a node region composed by the partitions surrounding the steel bar but just in the direction of the slip (see Fig. 5.8). Once again, this interaction was defined by two different behaviours: normal and tangential. Normal behaviour was also defined as a hard contact, with a default constraint enforcement method. The tangential behaviour was considered as "Penalty", with a friction coefficient μ of 0.20.

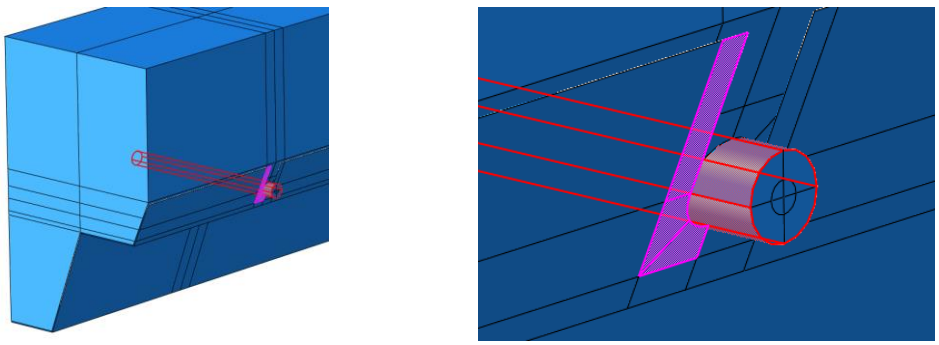

(a) General (b) Detail

Fig. 5.8 Surface-to-surface contact between reinforcing bars and profiled steel sheeting

(iii) Transversal reinforcing bars - Concrete

Usually, reinforcing bars in reinforced concrete members are modelled as embedded regions, in order to consider that the concrete host the bars completely inside of it. In the aim of the present study, reinforcing bars, between the contact points with the profiled steel sheeting, are partially outside the concrete part and so this constraint technique cannot be applied. So, the interaction between the reinforcement and the concrete was also modelled making use of a surface-to-surface contact algorithm. For this interaction the reinforcing bars surfaces were classified as "slave surface" (pink colour) and the concrete contact surfaces as "master surface" (red colour), as it is presented on Fig. 5.9. The interaction properties considered were the same as the ones considered for the interaction between the profiled steel sheeting and the concrete.

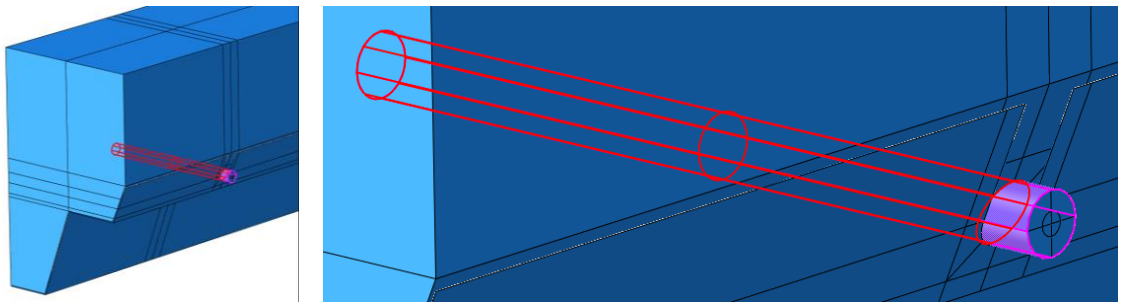

(a) General (b) Detail

Fig. 5.9 Surface-to-surface contact between reinforcing bars and concrete

5.2.4 Boundary and loading conditions

5.2.4.1 Boundary Conditions

As it was mentioned before, numerical models developed were a simplification of the real problem. Just half of a module and half of a span was modelled due to the symmetry and continuity conditions of steel-concrete composite slabs. So, proper boundary conditions should be provided to avoid unreal effects due to a wrong loading distribution.

Taking into account the transversal continuity of steel-concrete composite slabs, the movements of the nodes on the external *xy* concrete surfaces were restricted only in the *z* direction. On the lateral edges of the profiled steel sheeting the movements in the *z* direction and the rotation around axis *x* and *y* were restricted (see Fig. 5.10(a)).

The movements of the nodes on the concrete at the mid-span cross-section were restricted only in the *x* direction due to symmetry on the span. Regarding the symmetry of the

profiled steel sheeting, the movements in the *x* direction and rotations around *y* and *z* axis at the mid-span cross-section were also restricted (see Fig. 5.10(b)).

The supports of the slab were simulated by the restriction of the movements in the *y* direction (vertical displacements) in an edge of the profiled steel sheeting 100 mm away from the steel sheeting end (see Fig. 5.10(c)).

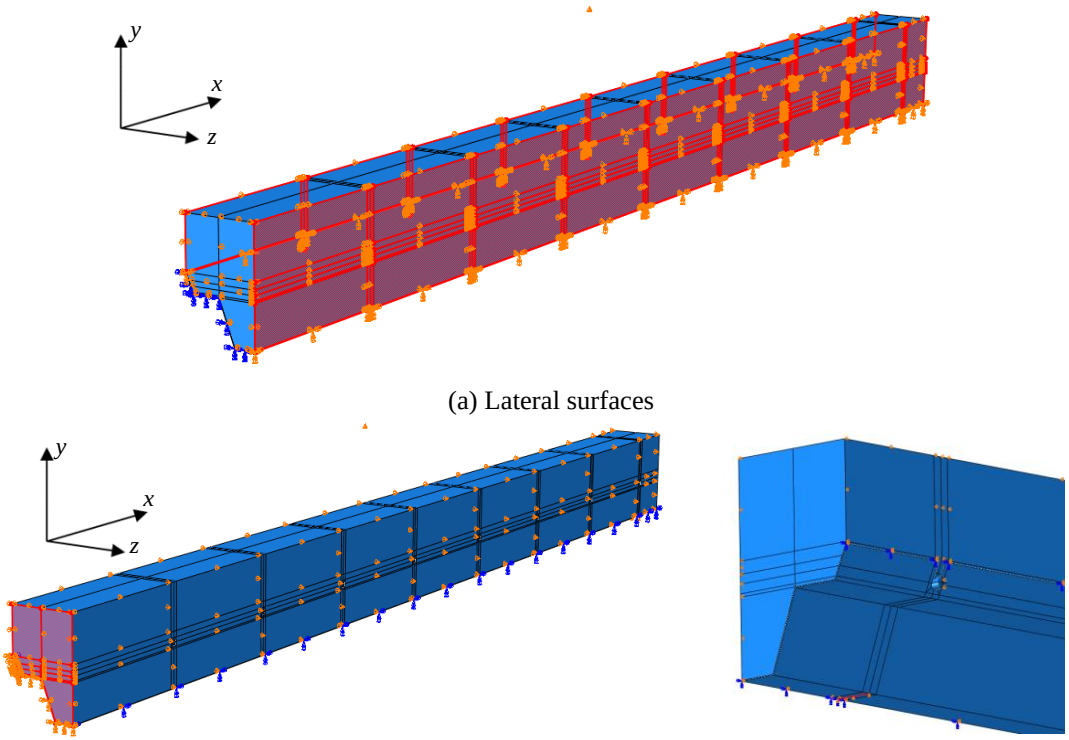

(a) Lateral surfaces

(b) Mid-span surface

(c) Support

Fig. 5.10 Boundary conditions

5.2.4.2 Loading Conditions

The loading scheme on numerical models should simulate the same conditions of experimental tests. Simply-supported composite slabs, on the experimental tests, were subjected to linear loads applied at a distance of $L/8$ and $3L/8$ from the supports. In order to simulate these conditions, a reference point (RP) was submitted to a vertical displacement, as it is illustrated on Fig. 5.11. The RP was coupled to the edges in the top surface of the concrete where the load should be applied. The coupling constraint allowed the rotation around the *z* axis, in order to make it possible the bending of the slab. Displacements of the coupling and rotations around *x* and *y* axis were restricted. Displacement controlled simulations are more appropriate to check the behaviour of the slab after achieving the peak load, otherwise if a force controlled simulation was used it would stop when the peak load was achieved.

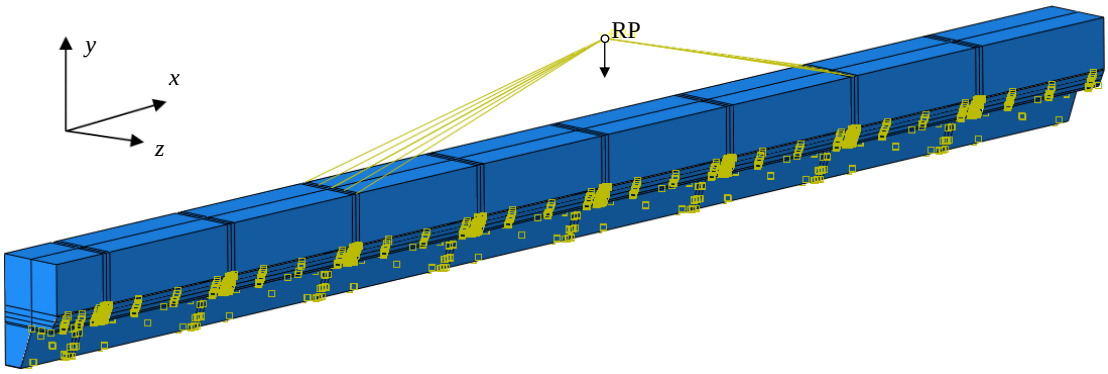

Fig. 5.11 Loading conditions

5.3 Finite Element Model Validation

The numerical models developed to simulate the behaviour of steel-concrete composite slabs with transversal bars intersecting the profiled steel sheeting was validated based on the comparison of the numerical results with the ones obtained in the experimental campaign. The main results used in the comparison analysis were those based on the load-deflection curves, namely the maximum load achieved.

As it was mentioned before, the comparison was established for tests A_2 and A_3. Fig. 5.12(a) and Fig. 5.13(a) show the comparison between the load-displacement P-δ curves obtained experimentally (Test) and numerically (FEM) for tests A_2 and A_3, respectively. Fig. 5.12(b) and Fig. 5.13(b) present the load-end slip P-s curves observed in both experimental tests and numerical simulations. Table 5.1 presents the maximum load achieved on experimental tests P_{test}, the maximum load attain on numerical simulations P_{FEM} and the ratio between both values P_{FEM}/P_{test}.

As it can be seen on Fig. 5.12(a), Fig. 5.13(a) and Table 5.1, numerical simulations have provided accurate results in terms of maximum attained load when compared to the experimental ones. Actually, the value P_{FEM} obtained on test A_2 simulation was just 1.8% higher than the respective experimental result. Regarding experimental test A_3, the maximum load achieved in the numerical simulation was 2.4% lower than the one obtained in the experimental test. Therefore, it was found that numerical models showed accurate results in terms of the load capacity of composite slabs with their longitudinal behaviour improved by the proposed reinforcing system. Nevertheless, the numerical models showed a stiffer behaviour than the one showed by experimental ones. However, in terms of global behaviour, numerical results showed a good approximation to the experimental results, namely based on the shape of the load-displacement curve, the maximum load and the measured end slip.

Concerning the slip between the profiled steel sheeting and the concrete, the load respective to the initiation of the slip between the two components and the slip measured for the peak load obtained in numerical simulations showed a good approximation to experimental results (see Fig. 5.12(b) and Fig. 5.13(b)).

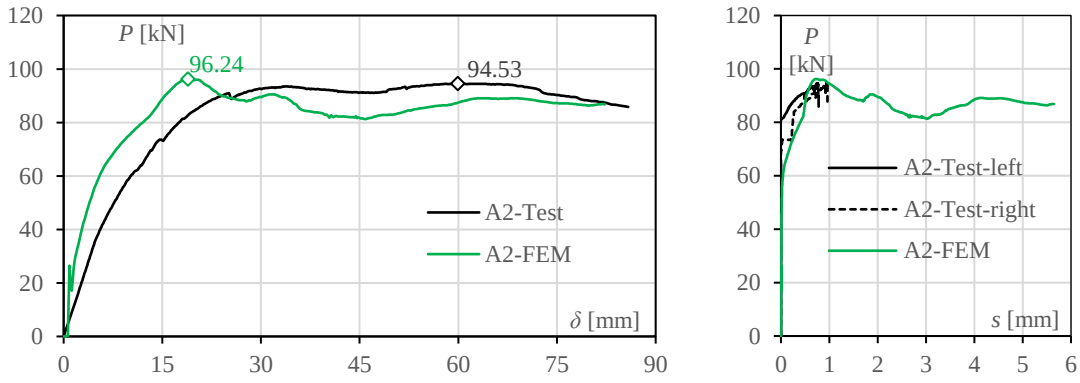

(a) *P*-δ curve (b) *P*-*s* curve

Fig. 5.12 Numerical models validation – Test A_2

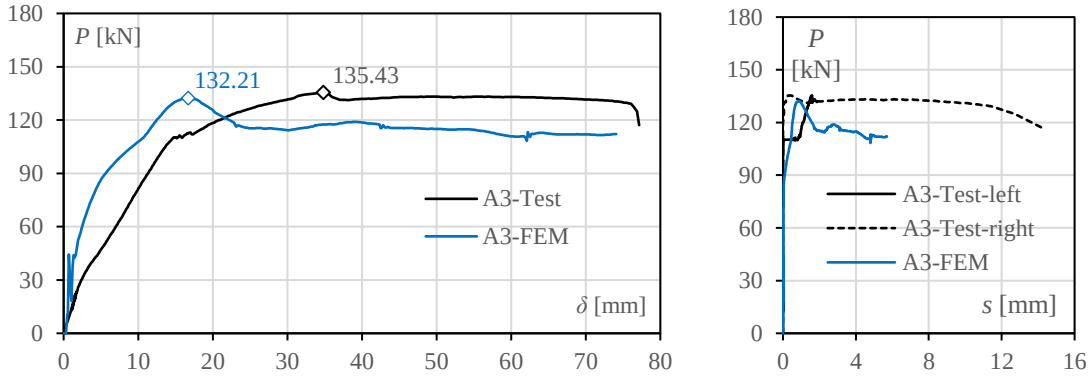

(a) *P*-δ curve (b) *P*-*s* curve

Fig. 5.13 Numerical models validation – Test A_3

Table 5.1 Numerical models validation

Test/Simulation	P_{test} [kN]	P_{FEM} [kN]	P_{FEM}/P_{test}
A_2	94.53	96.24	1.018
A_3	135.43	132.21	0.976

As it can be seen on the Fig. 5.14, a good agreement in the crack pattern (Fig. 5.14(a)) and end slip (Fig. 5.14(b)) was also obtained between the experimental tests and numerical models. Having in mind the complexity of the models, the general approximation was considered satisfactory enough to validate the numerical models developed.

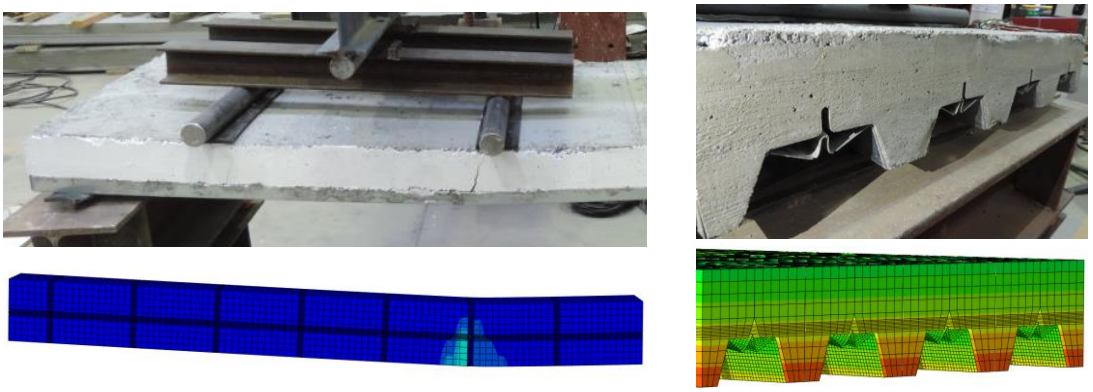

(a) Crack pattern (b) End slip

Fig. 5.14 Comparison between numerical and experimental observations (test A_2)

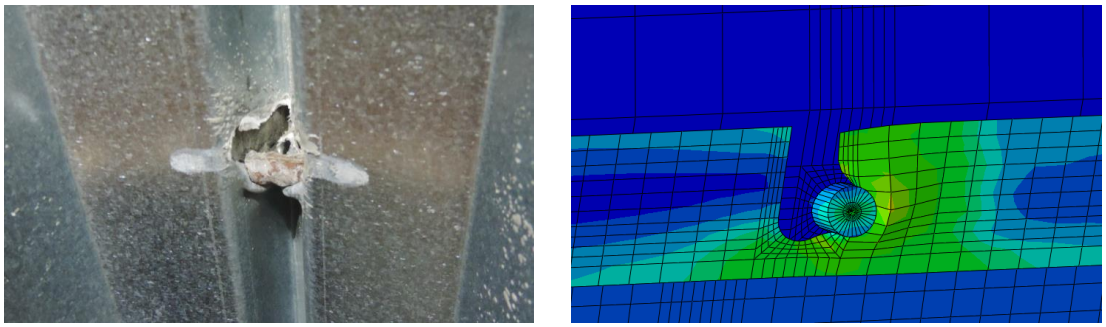

(a) Experimental (b) Numerical

Fig. 5.15 Collapse mode by bearing capacity of the steel sheeting (test A_2)

5.4 Parametric study

5.4.1 Introduction

After the numerical model validation, a parametric study was carried out in order to evaluate the accuracy of the design methodologies and to evaluate the influence of variation parameters on the structural performance of composite slabs. A group of 25 new numerical models were developed to understand the influence of several parameters on the capacity of steel-concrete composite slabs comprising the proposed reinforcing system constituted by transversal bars intersecting the profiled steel sheeting.

Two reference (REF) models were developed in order to have base models for comparison with the others: one reference (REF) model was developed for each type of steel sheeting profile used – LAMI 60+ and LAMI 120+ (see Fig. 5.16). Reference models were defined as simply-supported composite slabs with a total span L of 4.0 m. The longitudinal shear behaviour of these slabs was improved by 8 mm diameter transversal bars intersecting the profiled steel sheeting spaced by 250 mm [Ø8//250mm;

d = 8 mm; l_b = 250 mm]. The loading scheme was equivalent to the one used in experimental campaign and calibration models: 4 linear loads symmetrically applied relative to the mid-span cross-section, at a distance of $L/8$ and $3L/8$ from the nearest supports (see Fig. 5.16).

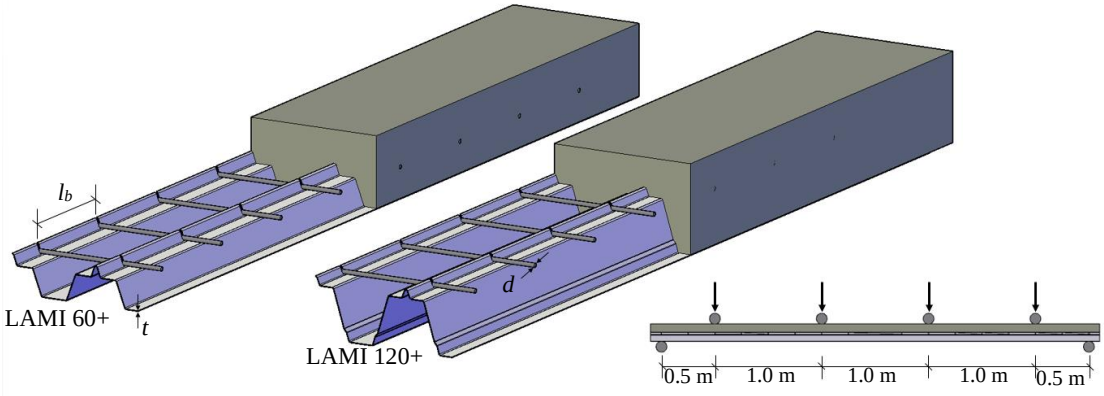

Fig. 5.16 Reference numerical models

The height defined for reference models with a LAMI 60+ and a LAMI 120+ steel profiles were respectively 160 and 200 mm. The materials used were the steel grade S320GD+Z on the steel sheeting and the concrete grade C25/30 on the concrete. The steel from transversal bars was considered with a yield stress f_{ys} of 500 MPa. The mechanical properties used to model the different materials are presented in the next section.

In order to evaluate the influence on the behaviour of composite slabs with the proposed reinforcing system, the variation of the following mechanic and geometric parameters was considered:

i. the profile of the steel sheeting – LAMI 60+ or LAMI 120+;
ii. the loading scheme – composite slabs subjected to 4 linear loads (4-point) or a uniformly distributed load (UDL);
iii. the total slab thickness h;
iv. steel grade of the steel sheet – S280GD+Z, S320GD+Z or S350GD+Z;
v. concrete strength grade – C20/25, C25/30 or C35/45;
vi. steel sheet thickness t – 0.8, 1.2 or 1.5 mm;
vii. transversal bars diameter d – 8 or 10 mm;
viii. distance between transversal bars l_b – 250, 200, 150 or 125 mm.

Table 5.2 presents the description of each numerical model developed in the aim of the present parametric study. The numerical models (FEM) are designated according to the steel sheet profile considered and the parameter/condition changed in relation to the respective reference model.

Table 5.2 General description of models developed for the parametric study

Model	Steel profile	Loading scheme	h [mm]	Steel grade	Concrete grade	t [mm]	d [mm]	l_b [mm]
FEM-60-Ref	**LAMI 60+**	4-point	160	S320GD+Z	C25/30	1.2	8	250
FEM-120-Ref	**LAMI 120+**	4-point	200	S320GD+Z	C25/30	1.2	8	250
FEM-60-UDL	LAMI 60+	**UDL**	160	S320GD+Z	C25/30	1.2	8	250
FEM-120-UDL	LAMI 120+	**UDL**	200	S320GD+Z	C25/30	1.2	8	250
FEM-60-h190	LAMI 60+	4-point	**200**	S320GD+Z	C25/30	1.2	8	250
FEM-60-h230	LAMI 60+	4-point	**240**	S320GD+Z	C25/30	1.2	8	250
FEM-120-h240	LAMI 120+	4-point	**240**	S320GD+Z	C25/30	1.2	8	250
FEM-120-h280	LAMI 120+	4-point	**280**	S320GD+Z	C25/30	1.2	8	250
FEM-60-S280	LAMI 60+	4-point	160	**S280GD+Z**	C25/30	1.2	8	250
FEM-60-S350	LAMI 60+	4-point	160	**S350GD+Z**	C25/30	1.2	8	250
FEM-120-S280	LAMI 120+	4-point	200	**S280GD+Z**	C25/30	1.2	8	250
FEM-120-S350	LAMI 120+	4-point	200	**S350GD+Z**	C25/30	1.2	8	250
FEM-60-C20	LAMI 60+	4-point	160	S320GD+Z	**C20/25**	1.2	8	250
FEM-60-C30	LAMI 60+	4-point	160	S320GD+Z	**C30/37**	1.2	8	250
FEM-120-C20	LAMI 120+	4-point	200	S320GD+Z	**C20/25**	1.2	8	250
FEM-120-C30	LAMI 120+	4-point	200	S320GD+Z	**C30/37**	1.2	8	250
FEM-60-t0.8	LAMI 60+	4-point	160	S320GD+Z	C25/30	**0.8**	8	250
FEM-60-t1.5	LAMI 60+	4-point	160	S320GD+Z	C25/30	**1.5**	8	250
FEM-120-t0.8	LAMI 120+	4-point	200	S320GD+Z	C25/30	**0.8**	8	250
FEM-120-t1.5	LAMI 120+	4-point	200	S320GD+Z	C25/30	**1.5**	8	250
FEM-60-d10	LAMI 60+	4-point	160	S320GD+Z	C25/30	1.2	**10**	250
FEM-120-d10	LAMI 120+	4-point	200	S320GD+Z	C25/30	1.2	**10**	250
FEM-60-l200	LAMI 60+	4-point	160	S320GD+Z	C25/30	1.2	8	**200**
FEM-60-l150	LAMI 60+	4-point	160	S320GD+Z	C25/30	1.2	8	**150**
FEM-60-l125	LAMI 60+	4-point	160	S320GD+Z	C25/30	1.2	8	**125**

Over the next sections, the numerical results and the conclusions from them obtained are presented. As before, taking into account the symmetry and continuity conditions of composite slabs, the numerical models have been drawn up considering just half span and half module; however, the results are presented for one meter of width (b = 1.0 m). In the following sections, the numerical results and the main conclusions concerning the influence of each studied parameter on the behaviour of steel-concrete composite slabs with transversal bars intersecting the profiled steel sheeting are presented.

All the composite slabs simulated collapsed by longitudinal shear or bending. Therefore, the maximum bending moment achieved in each simulation M_{FEM} is compared with the design value of the plastic bending moment resistance of the slab $M_{pl,Rd}$ and the design value of the bending moment resistance for the collapse of the reinforcing system M_{Rd}, obtained by the partial connection method as described in section 4.4. The influence of each parameter on the ductility coefficient ρ_d is analysed over next sections.

5.4.2 Materials used in the parametric study

The mechanical properties of the steel sheets were defined according to standard EN 1993-1-3 (CEN, 2006a) as presented in Table 5.3. Mechanical properties adopted on different models for concrete, which were defined according to standard EN 1992-1-1 (CEN, 2004a) and the approach presented in section 5.2.2.1, are presented in Table 5.4.

Table 5.3 Material properties of the steel sheet

			S280 GD+Z	S320 GD+Z	S350 GD+Z
Yield strength of the steel of the steel sheet	f_{yp}	[MPa]	280	320	350
Ultimate strength of the steel of the steel sheet	f_{up}	[MPa]	350	390	420
Modulus of elasticity	E_s	[GPa]	210	210	210

Table 5.4 Material properties of the concrete

			C 20/25	C 25/30	C 30/37
Characteristic value of the compressive strength of the concrete	f_{ck}	[MPa]	20.00	25.00	30.00
Mean value of the compressive strength of the concrete	f_{cm}	[MPa]	28.00	33.00	38.00
Secant modulus of elasticity of concrete	E_{cm}	[MPa]	29962	31476	32837
Strain of concrete for the peak compressive strength	$\varepsilon_{c,1}$	[mm/mm]	0.00197	0.00207	0.00216
Ultimate strain of concrete	$\varepsilon_{cu,1}$	[mm/mm]	0.03000	0.03000	0.03000
Relation between the ultimate and the peak strength	f_{cu}/f_{cm}	[%]	20	20	20
Ultimate strength of concrete	f_{cu}	[MPa]	1.40	1.65	1.90
Compression damage for peak compressive strength	$d_{c,1}$		0.30	0.30	0.30
Mean value of the tensile strength of the concrete	f_{ctm}	[MPa]	2.21	2.56	2.90
Maximum dimension of concrete aggregates	$d_{\max}$	[mm]	22	22	22
Reference value for the fracture energy	$G_{F,0}$	[J/m^2]	37.700	37.700	37.700
Fracture energy	G_F	[J/m^2]	77.509	86.956	95.982
Fracture energy	G_F	[N/mm]	0.078	0.087	0.096
Reference crack width	w_{ch}	[mm]	0.035	0.034	0.033

5.4.3 Numerical results of the parametric study

5.4.3.1 Reference results

The two reference models developed were two simply-supported composite slabs with a total span L of 4.0 m; one slab with a LAMI 60+ profile and height 160 mm and another with a LAMI 120+ profile and height 200 mm. Both the slabs were constituted by the same structural scheme and the same reinforcing system – simple reinforcing system defined by 8 mm diameter transversal bars spaced by 250 mm. The load-displacement P-δ curves obtained from the reference models are shown in the Fig. 5.17(a). Maximum loads P_{FEM} of 111.80 and 147.74 kN were obtained for models FEM-60-REF and FEM-120-REF respectively. The load-slip P-s curves from both models are shown in the Fig. 5.17(b). Like it was observed on experimental results, a slight loss of load can be

observed when the chemical bond between the concrete and the steel sheeting is broken and the slip starts to increase significantly.

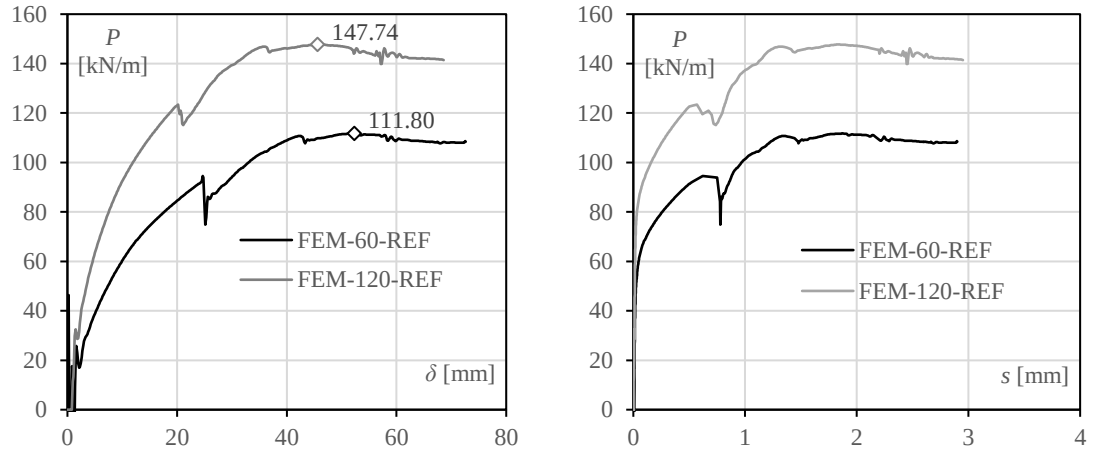

(a) *P-δ* curves (b) *P-s* curves

Fig. 5.17 Numerical results – reference models

Table 5.5 presents the maximum load P_{FEM} achieved on the numerical simulations, the respective bending moment M_{FEM}, the design value of the plastic bending moment resistance of the slab with full connection $M_{pl,Rd}$, the design value of the resistance moment using the partial connection method M_{Rd} and the ductility coefficient ρ_d, defined by the ratio between the maximum load attained P_{FEM} and the load corresponding to an end slip of 0.1 mm $P_{0.1mm}$ ($\rho_d = P_{FEM}/P_{0.1mm}$). In order to provide a fair comparison, the design values were defined according to Eurocode standards using partial safety factors equal to 1.0 and the mean values of the mechanical properties. The numerical results from models FEM-60-REF and FEM-120-REF showed that the full bending capacity was not achieved since M_{FEM} was lower than $M_{pl,Rd}$ in both cases. The collapse of the slabs was governed by the capacity of the reinforcing system. On models FEM-60-REF and FEM-120-REF the values of the maximum bending moment achieved M_{FEM} were, respectively, only 5 and 11% higher than the design values M_{Rd} obtained by the design approach proposed in the previous chapter.

Table 5.5 Numerical results – reference models

Model	P_{FEM} [kN/m]	M_{FEM} [kN.m/m]	$M_{pl,Rd}$ [kN.m/m]	M_{Rd} [kN.m/m]	$M_{FEM}/M_{pl,Rd}$	M_{FEM}/M_{Rd}	$P_{0.1mm}$ [kN/m]	ρ_d $P_{FEM}/P_{0.1mm}$
FEM-60-Ref	111.80	55.90	67.32	53.16	0.83	1.05	68.07	1.64
FEM-120-Ref	147.74	73.87	88.64	66.67	0.83	1.11	93.54	1.58

5.4.3.2 Influence of the loading system

Usually, steel-concrete composite slabs are designed to resist to the load imposed by the current use of the buildings. These loads are typically uniformly distributed loads (UDL) defined according to standard EN 1991-1-1 (CEN, 2002b). So, in order to verify the influence of the loading system on the behaviour of composite slabs with the proposed reinforcing system, two new numerical models were developed. Numerical models FEM-60-UDL and FEM-120-UDL are, respectively, equivalent to models FEM-60-REF and FEM-120-REF, but with the loading scheme constituted by a uniformly distributed load. These models with a uniformly distributed load applied on the slab were run with load control, so no results were obtained after achieving the maximum capacity of these models. Fig. 5.18(a-b) shows the *P*-δ and *P*-*s* curves obtained and their comparison with the ones previously obtained from the reference models. The maximum load applied P_{FEM} and the respective maximum bending moment, defined according to Eq. (5.16), are presented in Table 5.6.

$$M_{FEM} = \frac{p_{FEM} L^2}{8} = \frac{\frac{P_{FEM}}{L} L^2}{8} = \frac{P_{FEM} L}{8} \tag{5.16}$$

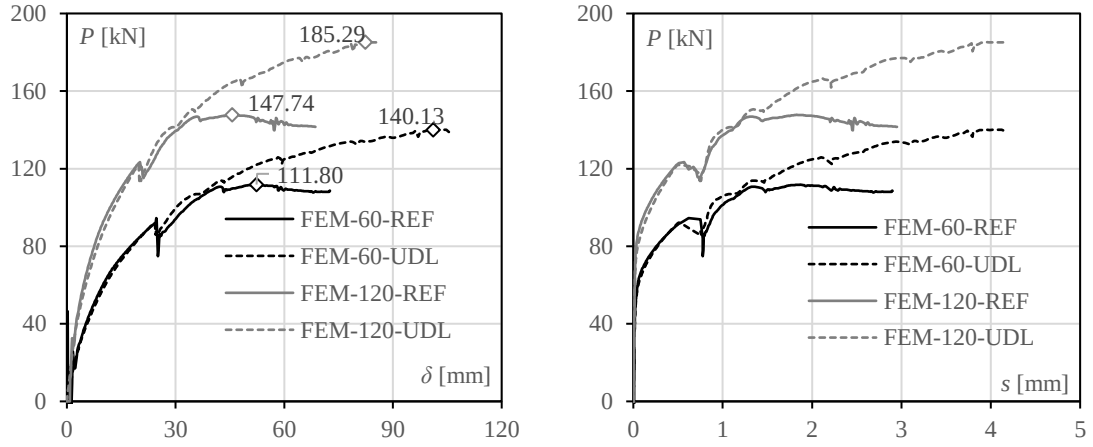

(a) *P*-δ curves (b) *P*-*s* curves

Fig. 5.18 Numerical results – influence of the loading system

The obtained results allowed to conclude that the changing of the loading scheme from 4 linear loads to a uniformly distributed loads led to an increase the bearing capacity of models FEM-60 and FEM-120 on 28.34 and 37.55 kN, respectively, 25.35 and 25.42 %. The increase is due to the better distribution of the load which make it possible to achieve the full bending capacity of the slab.

Fig. 5.19 shows the yielding condition on the profiled steel sheeting (close to the mid-span cross-section) on models FEM-60-REF and FEM-60-UDL at the collapse stage. The red

colour means that the yielding of the material was attained and the blue colour represents parts even in the elastic range. During the collapse of the reference model, the elements from the bottom flange achieved the yielding point but the upper flange was still exhibiting an elastic behaviour, which means that the collapse was due to the reinforcing system resistance and the bending capacity of the slab was not attained (see Fig. 5.19(b)). However, the numerical results of model FEM-60-UDL showed that the yielding stress was attained in all cross-section (see Fig. 5.19(c)), which means that the full bending capacity was achieved. Some results from Table 5.6 reiterate these observations. On UDL models the maximum bending moments achieved M_{FEM} were not just higher than the resistance moment M_{Rd} but also higher than the plastic resistance moment of the slab $M_{pl,Rd}$. Results presented on Table 5.6 also allowed to conclude that the ductility induced by the reinforcing system, given by the ductility coefficient ρ_d defined according to Eq. (5.17), increases when the load is distributed.

Table 5.6 Numerical results – influence of the loading system

Model	P_{FEM} [kN/m]	M_{FEM} [kN.m/m]	$M_{pl,Rd}$ [kN.m/m]	M_{Rd} [kN.m/m]	$M_{FEM}/M_{pl,Rd}$	M_{FEM}/M_{Rd}	$P_{0.1mm}$ [kN/m]	ρ_d $P_{FEM}/P_{0.1mm}$
FEM-60-Ref	111.80	55.90	67.32	53.16	0.83	1.05	68.07	1.64
FEM-60-UDL	140.13	70.07	67.32	54.12	1.04	1.29	65.74	2.13
FEM-120-Ref	147.74	73.87	88.64	66.67	0.83	1.11	93.54	1.58
FEM-120-UDL	185.29	92.64	88.64	71.12	1.05	1.30	87.81	2.11

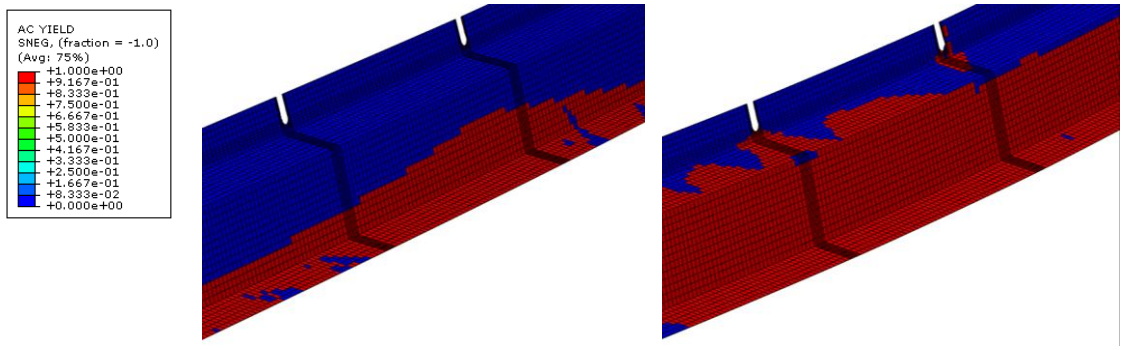

(a) Colour code (b) FEM-60-REF (c) FEM-60-UDL

Fig. 5.19 Yield in the profiled steel sheeting

$$\rho_d = \frac{P_{FEM}}{P_{0.1mm}} \tag{5.17}$$

5.4.3.3 Influence of the height of the slab *h*

The influence of the height of the slab on the longitudinal behaviour of composite slabs with transversal bars was studied in the second parametric study performed. 4 new numerical models were carried out based on the reference models but increasing the

thickness of the slab *h* by 40 and 80 mm. Fig. 5.20(a) shows the *P*-δ curves obtained from models FEM-60-REF, FEM-60-h200 and FEM-60-h240 with slabs with heights 160, 200 and 240 mm, respectively. Fig. 5.20(b) presents equivalent results from models FEM-120-REF, FEM-120-h240 and FEM-120-h280 with slabs with heights 200, 240 and 280 mm, respectively.

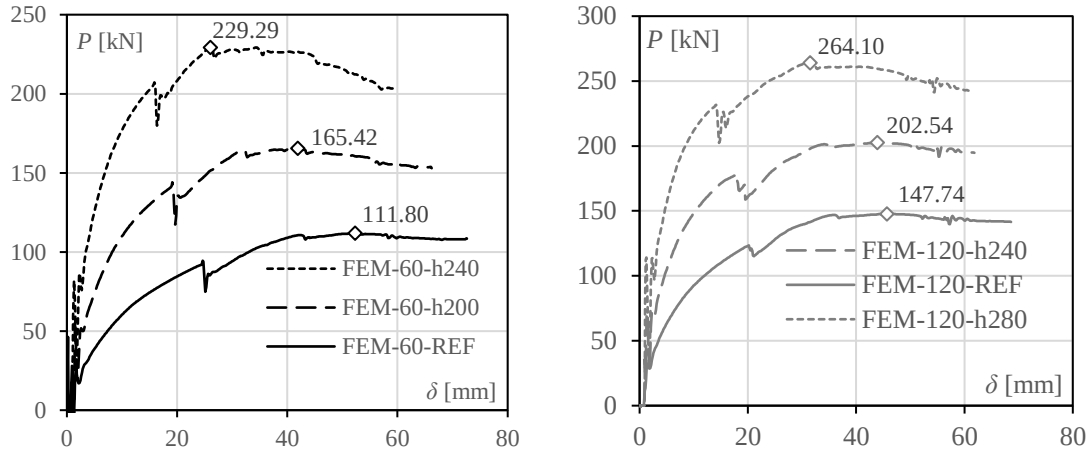

(a) *P*-δ curves for slabs with LAMI 60+ (b) *P*-δ curves for slabs with LAMI 120+

Fig. 5.20 Numerical results – influence of the height of the slab

As it was expected, the bearing capacity of composite slabs increases when the height of the slab is increased. However, the height of the slab *h* does not influence the resistance of the reinforcing system because the longitudinal shear resistance $F_{t,Rd}$ and the consequent longitudinal shear stress resistance due to the transversal bars $\tau_{t,Rd}$ does not depend of the slab height *h*. The increase on the bearing capacity and of the design value of the bending moment resistance M_{Rd} (see Eq. (3.37)) is due to the increase of the vertical distance (lever arm *z*) between forces N_c and N_p.

Table 5.7 presents: (i) the maximum load achieved P_{FEM} on each model; (ii) the respective bending moment M_{FEM}; (iii) the design value of the plastic resistance moment of the composite slab $M_{pl,Rd}$; (iv) the design value of the bending moment resistant M_{Rd}; (v) the ratio between the bending moment M_{FEM} and design value M_{Rd} and; (vi) the ductility coefficient ρ_d. In all models the longitudinal shear collapse was the governing mode. As it can be observed from these results, when the height of the slab increases the bending resistance $M_{pl,Rd}$ and the longitudinal shear bending resistance M_{Rd} increase. The design methodology proposed in the previous chapter allows once again to obtain safe estimation because the values of the maximum bending moment achieved M_{FEM} were always higher than the respective design value of the bending moment resistant M_{Rd}. Actually, it was observed that the proposed design method tends to be more conservative for higher slabs.

It was also observed that higher slabs have a longitudinal shear behaviour less ductile, but for general situations this should remain ductile ($\rho_d > 1.10$).

Table 5.7 Numerical results – influence of the height of the slab

Model	P_{FEM} [kN/m]	M_{FEM} [kN.m/m]	$M_{pl,Rd}$ [kN.m/m]	M_{Rd} [kN.m/m]	$M_{FEM}/M_{pl,Rd}$	M_{FEM}/M_{Rd}	$P_{0.1mm}$ [kN/m]	ρ_d $P_{FEM}/P_{0.1mm}$
FEM-60-Ref	111.80	55.90	67.32	53.16	0.83	1.05	68.07	1.64
FEM-60-h200	165.42	82.71	91.48	70.85	0.90	1.17	111.26	1.49
FEM-60-h240	229.29	114.65	115.65	88.55	0.99	1.29	171.31	1.34
FEM-120-Ref	147.74	73.87	88.64	66.67	0.83	1.11	93.54	1.58
FEM-120-h240	202.54	101.27	117.71	83.01	0.86	1.22	139.99	1.45
FEM-120-h280	264.10	132.05	146.77	99.35	0.90	1.33	197.36	1.34

5.4.3.4 Influence of the steel strength f_{yp}

The influence of the steel strength was studied in this section. Once again, 4 new numerical models were carried out based on the reference models and changing the steel sheeting grade. Fig. 5.21(a) shows the *P-δ* curves obtained from simulations FEM-60-REF, FEM-60-S280 and FEM-60-S350 which refer to slabs with steel sheets of steel grades S320GD+Z, S280GD+Z and S350GD+Z, respectively, according to standard EN 1993-1-3 (CEN, 2006a). The equivalent results from simulations FEM-120-REF, FEM-120-S280 and FEM-120-S350 are presented in Fig. 5.21(b).

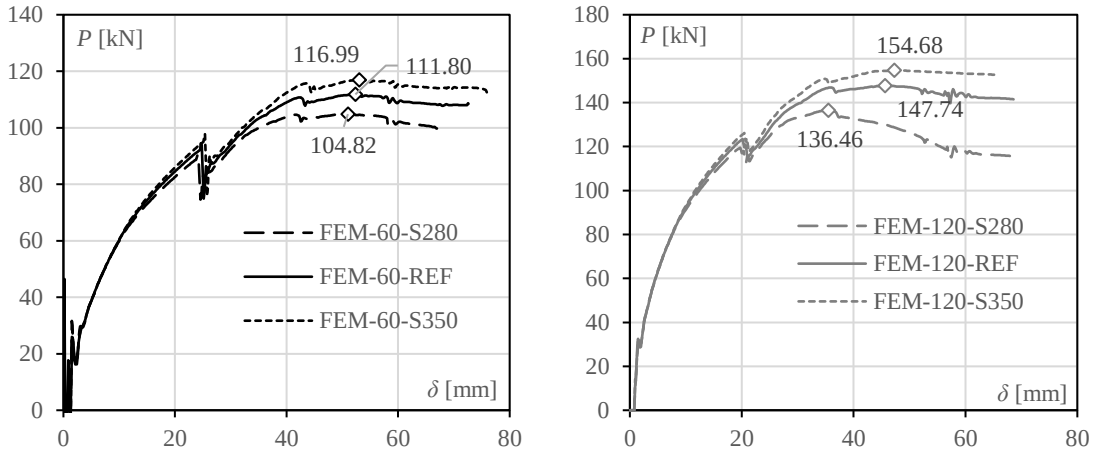

(a) *P-δ* for slabs with LAMI 60+ (b) *P-δ* for slabs with LAMI 120+

Fig. 5.21 Numerical results – influence of the steel grade

On these numerical models, all slabs collapsed by longitudinal shear. In slabs with profiled steel sheets with current and higher heights it was found that the steel strength does not influence significantly the bearing capacity of the slab. Changing the steel grade from S320GD+Z to S280GD+Z allowed to decrease the bearing capacity by 6.24% and 7.64% on slabs with LAMI 60+ and LAMI 120+ profiles, respectively. When the steel

grade was increased to S350GD+Z the bearing capacity increased respectively 4.64 and 4.70% comparatively to the reference models FEM-60-REF and FEM-120-REF.

The results concerning the influence of the steel strength in the longitudinal shear resistance of composite slabs are presented in Table 5.8. As it can be observed from these results, when the steel strength increases, the bending resistance $M_{pl,Rd}$ and the longitudinal shear bending resistance M_{Rd} increase also. The design methodology proposed in the previous chapter allowed to obtain safe and accurate predictions, being the higher difference between the numerical result M_{FEM} and he analytical prediction M_{Rd} of 13%. The ratio M_{FEM}/M_{Rd} seemed to slightly decrease when the steel strength increase. Concerning the influence of the steel grade in the ductility, numerical results showed that increasing the steel strength allow to increase the ductility of the slab.

Table 5.8 Numerical results – influence of the steel grade

Model	P_{FEM} [kN/m]	M_{FEM} [kN.m/m]	$M_{pl,Rd}$ [kN.m/m]	M_{Rd} [kN.m/m]	$M_{FEM}/M_{pl,Rd}$	M_{FEM}/M_{Rd}	$P_{0.1mm}$ [kN/m]	ρ_d $P_{FEM}/P_{0.1mm}$
FEM-60-S280	104.82	52.41	59.62	48.88	0.88	1.07	65.55	1.60
FEM-60-Ref	111.80	55.90	67.32	53.16	0.83	1.05	68.07	1.64
FEM-60-S350	116.99	58.49	72.97	57.03	0.80	1.03	70.34	1.66
FEM-120-S280	136.46	68.23	78.59	60.32	0.87	1.13	90.01	1.52
FEM-120-Ref	147.74	73.87	88.64	66.67	0.83	1.11	93.54	1.58
FEM-120-S350	154.68	77.34	95.99	71.91	0.81	1.08	95.42	1.62

5.4.3.5 Influence of the concrete strength f_{ck}

Regarding the influence of the concrete strength in the longitudinal shear resistance of steel-concrete composite slabs with the proposed reinforcing system, 4 new numerical models were performed. Numerical models FEM-60-C20 and FEM-60-C30 were developed based on the reference model FEM-60-REF but changing the concrete grade from C25/30 to C20/30 and C30/37, respectively. On FEM-120-C20 and FEM-120-C30 the same changes were performed, but with reference to FEM-120-REF model. The mechanical properties of the materials, defined according to standard EN 1992-1-1 (CEN, 2004a), were already presented in the previous section.

Fig. 5.22 shows the load-deflection P-δ curves obtained in the models performed to study the influence of the concrete strength. Such as the influence of the steel strength, it was observed that when the concrete strength is increased, the bearing capacity of the slab increases but not significantly. The stiffness of the slab seems to slightly increase when higher concrete grades are adopted. All slabs collapsed by longitudinal shear.

Table 5.9 presents the obtained results and their comparison with the predicted values of the slab resistance. As it was expected, higher concrete resistance values allow to increase

the bending resistance $M_{pl,Rd}$ and the longitudinal shear bending resistance M_{Rd}. The design methodology proposed has provided again accurate prediction values. The ratio M_{FEM}/M_{Rd} seemed to not change with the concrete resistance. Concerning the influence of the concrete grade in the ductility, numerical results showed that the ductility of the slab reduces for higher concrete grades.

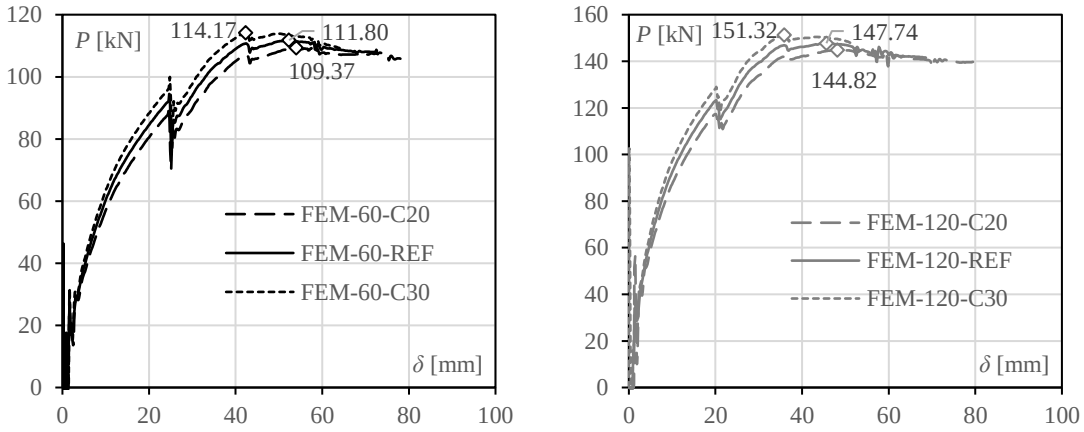

(a) *P-δ* for slabs with LAMI 60+ (b) *P-δ* for slabs with LAMI 120+

Fig. 5.22 Numerical results – influence of the concrete strength

Table 5.9 Numerical results – influence of the concrete grade

Model	P_{FEM} [kN/m]	M_{FEM} [kN.m/m]	$M_{pl,Rd}$ [kN.m/m]	M_{Rd} [kN.m/m]	$M_{FEM}/M_{pl,Rd}$	M_{FEM}/M_{Rd}	$P_{0.1mm}$	ρ_d $P_{FEM}/P_{0.1mm}$
FEM-60-C20	109.37	54.69	66.16	52.31	0.83	1.05	63.98	1.71
FEM-60-Ref	111.80	55.90	67.32	53.16	0.83	1.05	68.07	1.64
FEM-60-C30	114.17	57.08	68.18	53.78	0.84	1.06	71.99	1.59
FEM-120-C20	144.82	72.41	86.96	65.73	0.83	1.10	87.21	1.66
FEM-120-Ref	147.74	73.87	88.64	66.67	0.83	1.11	93.54	1.58
FEM-120-C30	151.32	75.66	89.88	67.37	0.84	1.12	98.92	1.53

5.4.3.6 Influence of the steel sheeting thickness *t*

The influence of the profiled steel sheeting in the longitudinal shear resistance of composite slabs with transversal bars intersecting the profiled steel sheeting was studied on this section. Taking into consideration the reference models, 4 new numerical models were performed considering the profile steel sheeting thickness in a range between 0.8 mm (FEM-60-t0.8 and FEM-120-t0.8) and 1.5 mm (FEM-60-t1.5 and FEM-120-t1.5). Fig. 5.23 presents the numerical results obtained on these simulations. Once again, all slabs collapsed by longitudinal shear.

As it was observed on the experimental results from the small-scale experimental campaign presented in the previous chapter, numerical results showed that the thickness of the profiled steel sheeting influences significantly the resistance of the reinforcing

system. Increasing the thickness of the profiled steel sheeting allow to increase the longitudinal shear resistance of composite slabs and so their bearing capacity. This effect is due to the increase of the contact area and force between transversal bars and the steel sheeting (see Eq. (4.31)). Actually, on slabs with a total height of 160 mm and a LAMI 60+ steel profile, when the steel sheeting thickness was increased from 0.8 mm to 1.2 mm and 1.5 mm the bearing capacity increased from 76.67 kN to 111.80 and 133.46 kN, respectively (representing an increase of 43.94 and 71.83% respectively). For slabs with a total height of 200 mm composed by LAMI 120+ steel profile, the bearing capacity increased from 102.35 kN to 147.74 and 176.88 kN, respectively (representing an increase of 44.35 and 72.82% respectively).

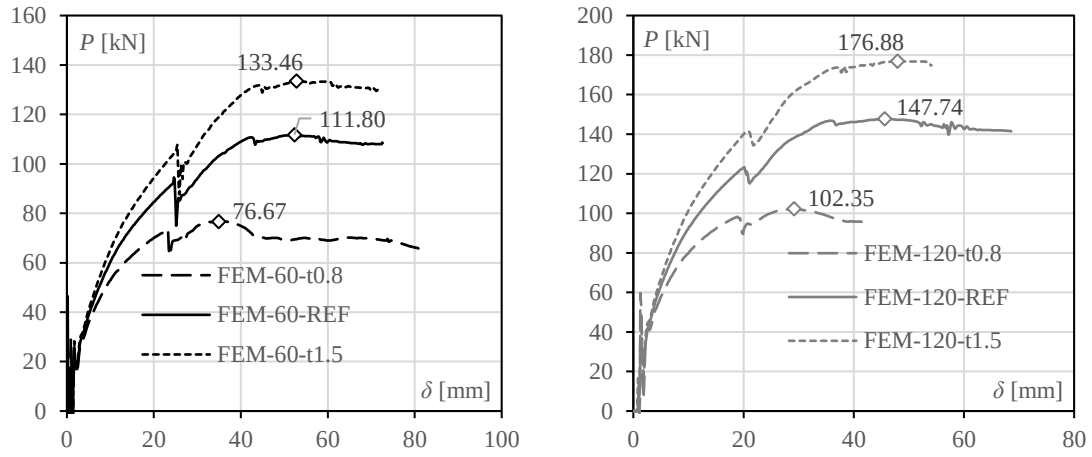

(a) P-δ for slabs with LAMI 60+ (b) P-δ for slabs with LAMI 120+

Fig. 5.23 Numerical results – influence of the steel sheet thickness

Table 5.10 presents the obtained results and its comparison with the resistance values concerning the influence of the steel sheet thickness t in the longitudinal shear resistance of composite slabs. From the obtained results it was possible to observe that the longitudinal shear behaviour tends to be more ductile for thicker steel profiles. The design approach proposed in the previous chapter has provided again accurate predictions values for the slab resistance. The resistance values obtained from the proposed design approach tends to be more accurate for slabs with thicker profiles.

Table 5.10 Numerical results – influence of the steel sheet thickness

Model	P_{FEM} [kN/m]	M_{FEM} [kN.m/m]	$M_{pl,Rd}$ [kN/m]	M_{Rd} [kN/m]	$M_{FEM}/M_{pl,Rd}$	M_{FEM}/M_{Rd}	$P_{0.1mm}$	ρ_d $P_{FEM}/P_{0.1mm}$
FEM-60-t0.8	76.67	38.33	46.33	33.12	0.83	1.16	57.15	1.34
FEM-60-Ref	111.80	55.90	67.32	53.16	0.83	1.05	68.07	1.64
FEM-60-t1.5	133.46	66.73	82.12	65.70	0.81	1.02	73.23	1.82
FEM-120-t0.8	102.35	51.18	61.19	42.99	0.84	1.19	81.04	1.26
FEM-120-Ref	147.74	73.87	88.64	66.67	0.83	1.11	93.54	1.58
FEM-120-t1.5	176.88	88.44	107.86	82.24	0.82	1.08	102.62	1.72

5.4.3.7 Influence of the bars diameter *d*

The influence of the diameter of the transversal bars on the longitudinal shear behaviour of composite slabs improved by the proposed reinforcing system is presented in this section. 2 new numerical models were developed and carried out based on the reference models but with 10 mm diameter transversal reinforcing bars intersecting the profiled steel sheeting. Fig. 5.24 shows the numerical results obtained from these simulations. Increasing the diameter from 8 to 10 mm of the transversal bars allowed to increase the maximum load achieved P_{FEM} from 111.80 to 131.43 kN on FEM-60 models and from 147.74 to 170.38 kN on FEM-120 models, which represented an increase of 17.56 and 15.32%, respectively. Like in the previous analysis, this effect is due to the increase of the contact area and force between transversal bars and the steel sheeting (see Eq. (4.31)).

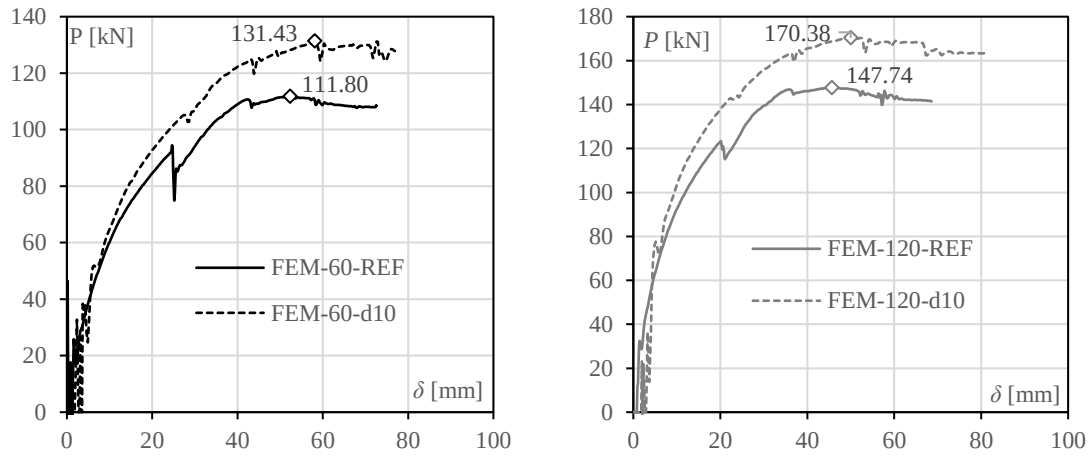

(a) *P-δ* for slabs with LAMI 60+ (b) *P-δ* for slabs with LAMI 120+

Fig. 5.24 Numerical results – influence of the bars diameter

On Table 5.11 the obtained results and their comparison with the resistance values concerning the influence of the diameter of the transversal bars *d* are presented. From these results it was possible to observe that the efficiency of the reinforcing system increases, and consequently the longitudinal shear bending moment resistance M_{Rd} and the plastic bending moment capacity $M_{pl,Rd}$, with the increase of the diameter of transversal bars. This effect allows to take more advantage of the bending moment capacity of composite slabs as it is observed by the increase of the ratio $M_{FEM}/M_{pl,Rd}$. Regarding the ductility of the longitudinal shear behaviour it seems that the value of *d* does not influence it.

Table 5.11 Numerical results – influence of the bars diameter

Model	P_{FEM} [kN/m]	M_{FEM} [kN.m/m]	$M_{pl,Rd}$ [kN/m]	M_{Rd} [kN/m]	$M_{FEM}/M_{pl,Rd}$	M_{FEM}/M_{Rd}	$P_{0.1mm}$	$P_{FEM}/P_{0.1mm}$
FEM-60-Ref	111.80	55.90	67.32	53.16	0.83	1.05	68.07	1.64
FEM-60-d10	131.43	65.72	67.32	62.76	0.98	1.05	78.27	1.68
FEM-120-Ref	147.74	73.87	88.64	66.67	0.83	1.11	93.54	1.58
FEM-120-d10	170.38	85.19	88.64	73.78	0.96	1.15	109.98	1.55

5.4.3.8 Influence of the spacing between the bars l_b

The influence of the spacing between transversal reinforcing bars was still addressed. 3 new numerical models were performed based on the reference model FEM-60-REF but decreasing the spacing between transversal bars l_b to 200, 150 or 125 mm. Fig. 5.25(a) presents the load-displacement curves P-δ obtained on these models and Fig. 5.25(b) the respective load-slip curves P-s. Composite slabs with transversal bars spaced by 250 or 200 mm collapsed by longitudinal shear. Slabs from models FEM-60-l150 and FEM-60-l125 achieved their bending capacity.

Maximum loads P_{FEM} of 111.80, 128.89, 135.74 and 140.79 kN were obtained on simulations FEM-60-REF, FEM-60-l200, FEM-60-l150 and FEM-60-l125. These results showed that when transversal bars are closer to each other the resistance of the slab tends to increase. However, this increase only exists (or only it is significant) while the behaviour of the composite slab is governed by longitudinal shear. For lower values of l_b is more likely to achieve the full connection and so decrease the spacing of bars in these situations does not bring advantages in the design. For that reason, the bearing capacity of the slab did not increase significantly from model FEM-60-l150 to FEM-60-l125 as it did from model FEM-60-REF to FEM-60-l200.

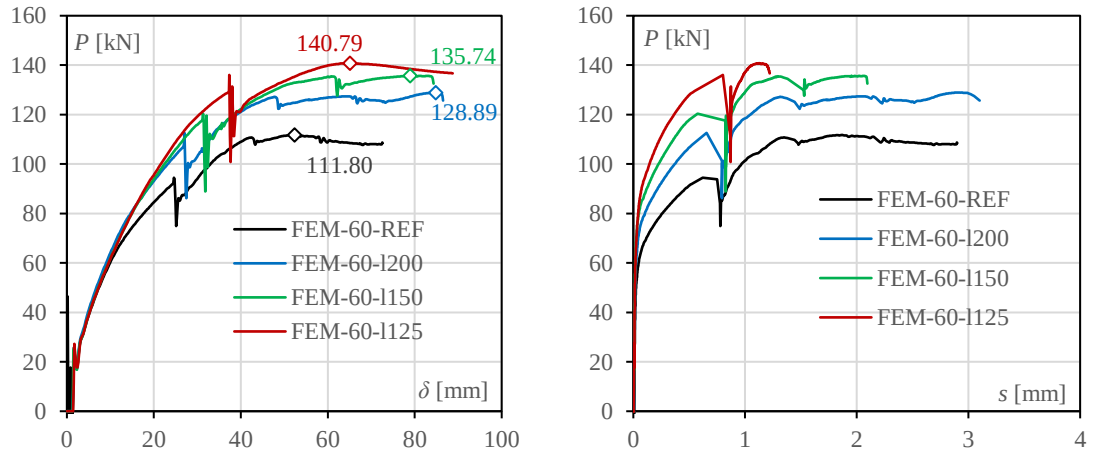

(a) P-δ curves (b) P-s curves

Fig. 5.25 Numerical results – influence of the space between transversal bars

Table 5.12 presents the obtained results and a comparison between these values and the resistance values concerning the influence of the spacing between transversal bars l_b. From this table it was possible to observe that reducing the spacing between transversal bars allows to increase the longitudinal shear capacity and, consequently, the bearing capacity of composite slabs. According to obtained results, slabs with transversal bars with lower spacing between transversal bars have a less ductile longitudinal shear behaviour.

Table 5.12 Numerical results – influence of the space between transversal bars

Model	P_{FEM} [kN/m]	M_{FEM} [kN.m/m]	$M_{pl,Rd}$ [kN.m/m]	M_{Rd} [kN.m/m]	$M_{FEM}/M_{pl,Rd}$	M_{FEM}/M_{Rd}	$P_{0.1mm}$	$P_{FEM}/P_{0.1mm}$
FEM-60-Ref	111.80	55.90	67.32	53.16	0.83	1.05	68.07	1.64
FEM-60-l200	128.89	64.44	67.32	62.76	0.96	1.03	79.00	1.63
FEM-60-l150	135.74	67.87	67.32	67.32	1.01	1.01	87.30	1.55
FEM-60-l125	140.79	70.39	67.32	67.32	1.05	1.05	93.81	1.50

5.5 Final remarks

The main objective of the performed parametric study was accomplished: the design methodology proposed in the previous chapter, defined by the replacement of the value $\tau_{t,Rd}$ by the $\tau_{u,Rd}$ value in the partial connection method, was validated. Fig. 5.26 shows the relation between the bending moment M_{FEM} achieved on each simulation performed. As it was mentioned before, all design values were defined taking in consideration the average properties of the materials and partial safety factors equal to 1.0. As it is observed, all pairs of values satisfy the condition $M_{FEM} > M_{Rd}$ and allow to validate the design approach to take into account the effect of transversal bars in the design of steel concrete composite slabs.

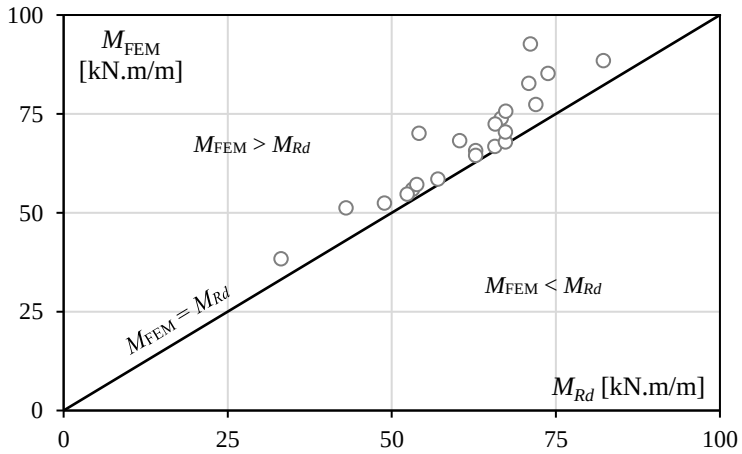

Fig. 5.26 Design approach validation

According to numerical results obtained and presented along this chapter it was also possible to establish some conclusions and to validate some previous assumptions:

i. developed reinforcing system allows to increase significantly the longitudinal shear resistance of steel-concrete composite slabs;
ii. proposed reinforcing system allows to achieve higher levels of ductility, which means that the maximum load achieved is significantly higher than the load observed when the slip starts to occur;
iii. as it was expected, because of the parameters taken into account in the design of composite slabs with transversal bars (see Eq. (4.32)), the efficiency of the proposed reinforcing system increases when the total height of the slab h, the steel sheeting thickness t, the diameter of transversal bars d and the steel grade increase or when the spacing between transversal bars l_b is reduced.

Fig. 5.27 presents a graphical summary of the obtained results. Fig. 5.27(a-c) shows, respectively, the influence of the height of the slab h, the steel grade (represented by f_{yp}) and the concrete grade (represented by f_{ck}) in the maximum bending moment M_{FEM}. Fig. 5.27(d-f) presents the influence of these parameters on the ductility coefficient ρ_d. Then, Fig. 5.27(g-i) shows, respectively, the influence of the steel sheet thickness t, the diameter d and the spacing l_b in the maximum bending moment M_{FEM}, as well as Fig. 5.27(j-l) shows the influence of these values in the value of the ductility coefficient ρ_d.

The main objective of the present study is to develop a new reinforcing system for steel-concrete composite slabs to increase their longitudinal shear capacity and take more advantage of their bending resistance. Nevertheless, short span slabs or slabs with current spans and reinforcing systems to improve their behaviour to longitudinal shear have their design governed by vertical shear. So, to take real advantage of the proposed reinforcing system the vertical shear design model should be reviewed. Therefore, next chapter presents a brief study carried out about the vertical shear resistance of steel-concrete composite slabs focused in the respective design model.

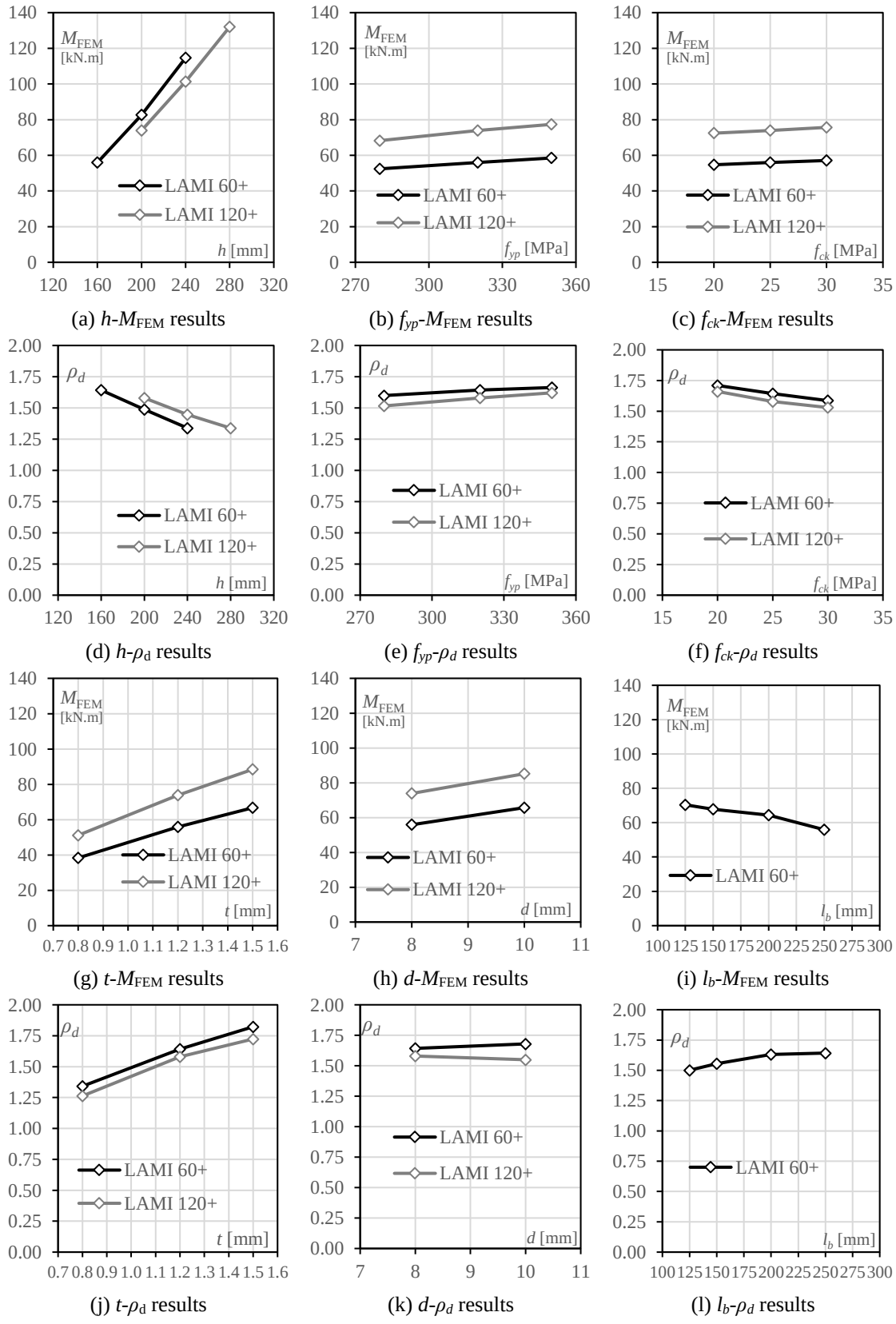

(a) h-M_{FEM} results (b) f_{yp}-M_{FEM} results (c) f_{ck}-M_{FEM} results

(d) h-ρ_d results (e) f_{yp}-ρ_d results (f) f_{ck}-ρ_d results

(g) t-M_{FEM} results (h) d-M_{FEM} results (i) l_b-M_{FEM} results

(j) t-ρ_d results (k) d-ρ_d results (l) l_b-ρ_d results

Fig. 5.27 Resistance and ductility of the reinforcing system

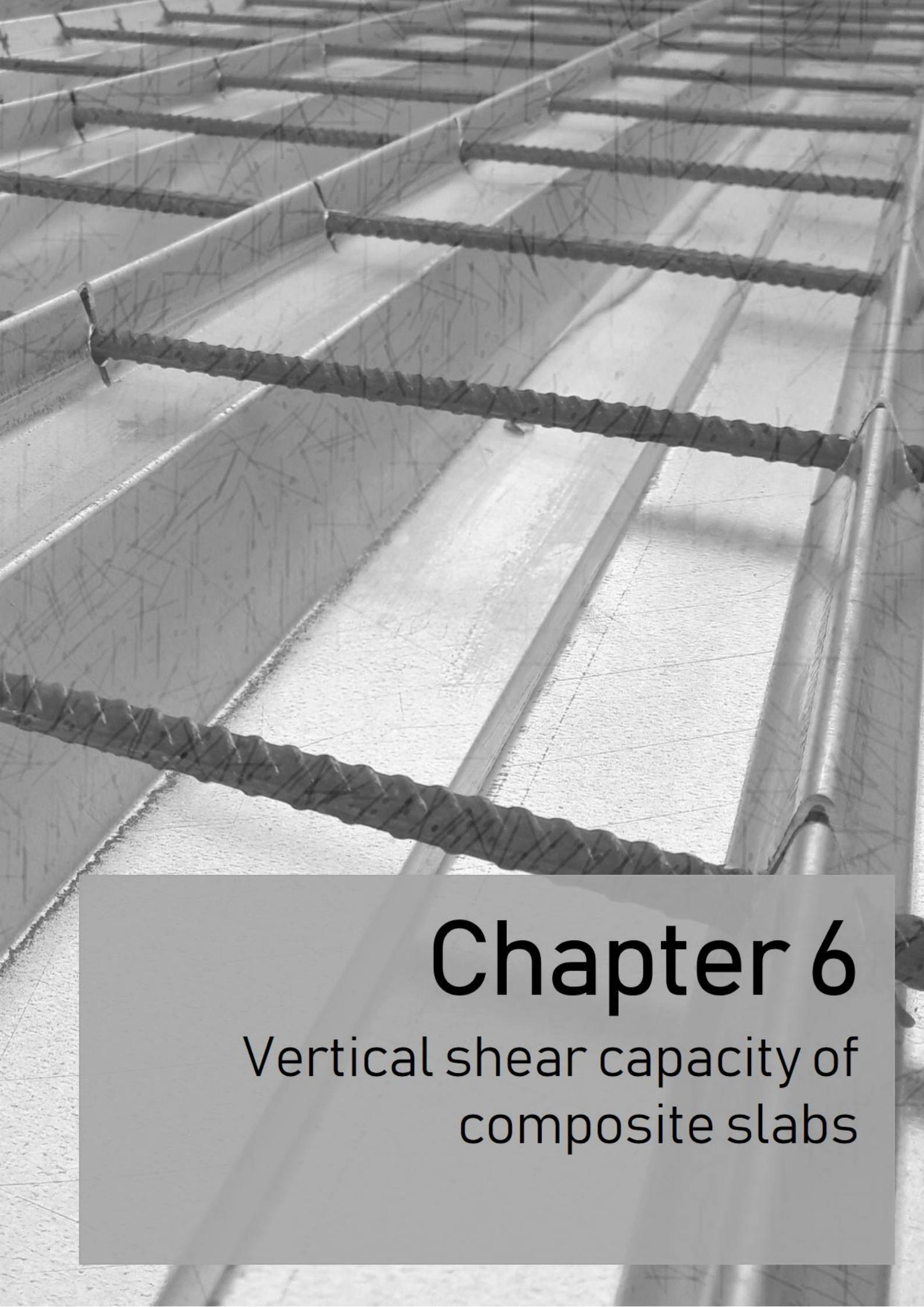

Chapter 6

Vertical shear capacity of composite slabs

6.1 Introduction

Eurocode 4 (CEN, 2004b) establishes that the design of composite slabs for vertical shear resistance shall be done according to the design methodology prescribed in Eurocode 2 (CEN, 2004a) applicable to reinforced concrete slabs. However, this design model leads to an underestimation of the slab capacity, since the high shear capacity provided by the profiled steel sheeting is not taken into account properly. This underestimation of the slab capacity is especially relevant in composite slabs with short spans, or even with the spans currently used in building construction when the longitudinal shear behaviour is improved by some type of reinforcement system, such as end anchorage devices.

A tendency to converge and standardize structural design models is a current trend within the scientific community, as can be observed by the development and future revision of the Eurocodes (Crisinel and Marimon, 2004). Nevertheless, it is still possible to find some inconsistencies in the design rules for identical structural members. For example, composite slabs have a similar behaviour to that of composite beams, especially because both are members that bend mainly in one direction, but some differences in the evaluation of the resistance of each one's cross-section still remain. A comparison of the principles for the design of composite slabs and composite beams for ultimate limit states is described in Table 6.1. Although the design principles for the bending resistance are identical, those concerning the evaluation of the vertical shear resistance are almost the opposite: in composite slabs, only the concrete cross-section is accounted for when determining the shear resistance. On the contrary, for composite beams the shear resistance essentially takes into account the resistance of the steel cross-section. The longitudinal shear design model is also based on different procedures: in composite slabs full scale tests are required while in composite beams the shear resistance of the connectors is obtained by push-out tests (small-scale specimens).

However, neither for composite slabs the contribution of the profiled steel sheeting should be neglected, neither for composite beams the concrete part should be neglected in the vertical shear design value. Actually, some researchers noticed that the reinforced concrete slab has an important contribution in the vertical shear resistance of steel-concrete composite slabs (Ansourian, 1981; Liang *et al.*, 2004). The experimental results obtained by Ansourian (1981) showed that the concrete part could carry 20% of the total vertical shear on continuous composite beams subjected to bending and shear.

The vertical shear resistance formula available on standard EN 1992-1-1 (CEN, 2004a) was defined based on an experimental campaign carried out on reinforced concrete

specimens, which have a behaviour significantly different from steel-concrete composite elements.

Table 6.1 Comparison between the design principles for composite slabs and composite beams

	Calculation of the bending resistance	Calculation of the vertical shear resistance	Calculation of the longitudinal shear resistance
Composite beams	uses the stress distribution given by the curvature of the composite cross-section	at least the web of the steel section contributes to the shear resistance	the number of shear connectors depends on the longitudinal shear forces at the steel-concrete interface and the design shear resistance of the connectors is given by push-out tests on small-scale specimens
Composite slabs	uses the stress distribution given by the curvature of the composite cross-section	only the concrete part of composite cross-section contributes to the shear resistance (a composite slab is treated as a reinforced concrete slab)	requires full-scale testing of composite slabs

In the section 2.4 of the Chapter 2 (Literature review), some vertical shear design approaches were presented. Brazilian and American standards were presented as examples of codes in which the contribution of the profiled steel sheeting is accounted on the determination of the design value of the vertical shear resistance. On the other hand, standard EN 1994-1-1 (CEN, 2004b) does not account the contribution of the webs of the cold-formed steel profiles in the vertical shear resistance of composite slabs.

In order to optimize the design methodologies of composite slabs, especially those with high-performance longitudinal behaviour, a complementary study to evaluate the vertical shear resistance and the accuracy of the design model prescribed in standard EN 1994-1-1 (CEN, 2004b) is presented on this chapter.

First, two preliminary tests were carried out to get a first assessment regarding the real behaviour of composite slabs with short spans and higher resistance to longitudinal shear. From these results it was found that the real vertical shear resistance of a steel-concrete composite slab can reach a value 5 times higher than its design value when evaluated according to Eurocode 4 (CEN, 2004b). This fact allowed to conclude that the design model is too conservative and consequently can lead to the conception of non-economical structural solutions. A comparison between the results obtained in the preliminary experimental tests, presented previously on section 4.3 of the Chapter 4 (Development of a new reinforcing system for composite slabs), and the respective design values for the vertical shear resistance according to standard EN 1994-1-1 (CEN, 2004b), is also being

presented. Even exhibiting a longitudinal shear failure, these tests (PA, PB and PC experimental tests) allowed to reach a maximum load significantly higher than the vertical shear resistance obtained according to standard EN 1994-1-1 (CEN, 2004b).

With the main objectives of expanding these results and broadening the present knowledge concerning the real behaviour of steel-concrete composite slabs, four additional experimental tests were carried out for the purpose of the present study and are then presented. Making use of the numerical simulations calibrated and validated in the previous chapter a new numerical study was carried out in order to perform a parametric study regarding the vertical shear resistance of steel-concrete composite slabs. In this parametric study, the influence of the following mechanic and geometric parameters in the vertical shear resistance of composite slabs was studied: the height of the slab *h*, the steel sheet profile, the concrete grade and the profiled steel sheeting thickness *t*.

6.2 Preliminary study of the vertical shear behaviour of composite slabs

6.2.1 Introduction

In a first stage, aiming to study the vertical shear behaviour of steel-concrete composite slabs, two tests were performed on simply supported composite slabs. Both tests were performed in specimens using a profiled steel sheeting with a height h_p of 60 mm (LAMI 60+), a free span between supports L of 2.0 m and a width b of 820 mm, corresponding to 4 slab modules.

The higher the shear span L_s, the higher would be the bending moments and also the longitudinal shear forces acting on the slab. Taking this issue into account, the slabs were tested with short shear spans to force the occurrence of a vertical shear failure, instead of a longitudinal shear failure. The slab of the first test (Test PV_1) had a height h of 150 mm and was subjected to two linear loads symmetrically applied at a distance of 250 mm from the supports (shear span L_s), corresponding to 1/8 of the total span. The slab of the second test (Test PV_2) had a height h of 200 mm and was subjected to two linear loads symmetrically applied at a distance of 333 mm from the supports, corresponding to 1/6 of the total span.

The longitudinal shear capacity of the tested slabs was increased by transversal bars in order to avoid a failure by this mode. The reinforcing system of the slab from test PV_1 was constituted by 10 mm diameter transversal bars spaced by 50 mm and distributed

over the shear span, Ø10//50mm (see Fig. 6.1(a)). On the test PV_2, the reinforcing system was constituted by 8 mm diameter transversal bars spaced by 50 mm and distributed over the shear span, Ø8//50 mm (see Fig. 6.1(b)).

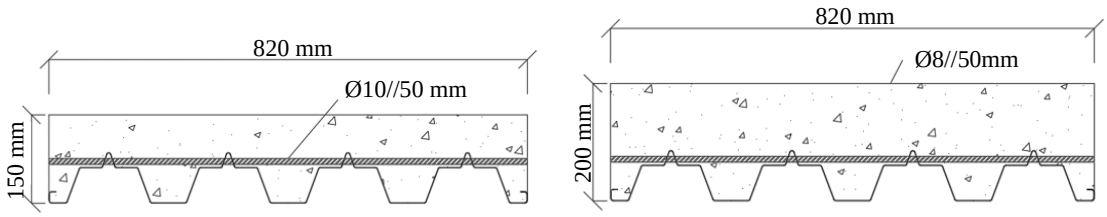

(a) Test PV_1 (b) Test PV_2

Fig. 6.1 Cross-section geometry of PV specimens

Fig. 6.2 shows the structural scheme of both tests, where L_s represents the shear span, L_b the constant bending moment span, s_{left} and s_{right} the measured slip on left and right ends, respectively, P is the total applied load and δ is the measured vertical displacement at the mid-span cross-section.

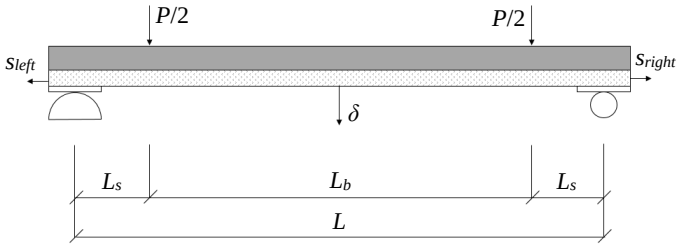

Test PV_1:	Test PV_2:
L = 2.0 m;	L = 2.0 m;
L_s = 0.25 m;	L_s = 0.33 m;
L_b = 1.50 m.	L_b = 1.34 m.

(b) Test PV_1

(a) Structural system (c) Test PV_2

Fig. 6.2 Preliminary experimental tests to study the vertical shear behaviour

Table 6.2 contains the description of the geometry of one module of a composite slab, the amount of reinforcement and the shear span, where: h is the slab total height, e is the distance from the centroidal axis of profiled steel sheeting to the extreme fibre of the composite slab in tension, d_p is the distance between the centroidal axis of the profiled steel sheeting and the extreme fibre of the composite slab in compression, b_m is the width of a composite slab module, b_0 is the mean width of a concrete rib and L_s is the shear span.

Table 6.2 Specimens description

Test	h [mm]	h_p [mm]	e [mm]	d_p [mm]	b_m [mm]	b_0 [mm]	Transversal reinforcement	L_s [mm]
PV_1	150	60	37.68	112.32	205	89.23	Ø 10 // 50 mm	250
PV_2	200	60	37.68	162.32	205	29.23	Ø 8 // 50 mm	333

In order to quantify the concrete strength, uniaxial compressive tests on cubic specimens with edges of 150 mm were performed. To obtain the steel tensile resistance uniaxial tensile tests were performed on steel sheets with a geometry according to the standard ISO 6892-1 (ISO, 2009). Mechanical properties of materials used in this experimental programme were already presented in section 4.3.3. An average compressive stress resistance f_{cm} of 34.26 MPa for concrete and an average yield stress f_{yp} of 329.51 MPa for steel were obtained.

6.2.2 Design values of the vertical shear resistance

According to EN 1994-1-1 (CEN, 2004b) with reference to EN 1992-1-1 (CEN, 2004a), the vertical shear resistance of a composite slab, attending that the steel sheet only has an extension of 100 mm beyond the supports section and $100 < d_p + l_{b,min}$, is obtained according to Eq. (6.1).

$$V_{Rd,c} = v_{\min} b_0 d_p \tag{6.1}$$

So, the values of the maximum vertical shear force expected in tests PV_1 and PV_2 were 23.23 kN and 33.57 kN, respectively, as it is presented on Table 6.3. In order to make a direct comparison with the experimental results, the resistance values (design values) were determined taking into consideration the average mechanical properties of materials and partial safety coefficients equal to 1.0.

Table 6.3 Vertical shear resistance evaluated in accordance with standard EN 1994-1-1 (CEN, 2004b)

			PV_1	PV_2
Total thickness of the slab	h	[mm]	150.00	200.00
Position of the centroidal axis of the profiled steel sheeting	e	[mm]	37.68	37.68
Effective height of the slab	d_p	[mm]	112.32	162.32
Constant	k	[-]	2.00	2.00
Characteristic value of the compressive strength of the concrete	f_{ck}	[MPa]	26.26	26.26
Mean value of the compressive strength of the concrete	f_{cm}	[MPa]	34.26	34.26
Minimum value of the shear stress resistance	$v_{\min}$	[MPa]	0.58	0.58
Mean width of a concrete rib	b_0	[mm]	89.23	89.23
Vertical shear resistance of a module of the composite slab	$V_{v,Rd,m}$	[kN/mod.]	5.81	8.39
Number of modules in the slab	n_m		4	4
Vertical shear resistance of the slab	$V_{v,c,Rd}$	**[kN]**	**23.23**	**33.57**

To evaluate the contribution of the profiled steel sheeting in the vertical shear resistance of composite slabs, the vertical shear resistance of the profiled steel sheeting was determined (see Table 6.4). Using the design approach prescribed in standard EN 1993-1-3 (CEN, 2006a), presented in the section 3.2.3.3 of this document, the vertical shear resistance of the profiled steel sheeting $V_{v,p,Rd}$ is given by 82.60 kN.

Table 6.4 Vertical shear capacity of the profiled steel sheeting in accordance with standard EN 1993-1-3 (CEN, 2006a)

			LAMI 60+
Web height measured between the midlines of the flanges	h_w	[mm]	60.00
Slope of the web relative to the flanges	φ	[º]	69.00
Slant height of the web between the midpoints of the corners	s_w	[mm]	64.08
Total developed slant height of the web	s_d	[mm]	64.08
Thickness of the profiled steel sheeting	t	[mm]	1.00
Steel core thickness	t_{cor}	[mm]	0.96
Mean value of the yield strength of the steel sheet	f_{yp}	[MPa]	329.51
Modulus of Young	E_s	[GPa]	196.78
Relative web slenderness	λ_w	[-]	0.945
Shear buckling strength	f_{bv}	[MPa]	167.35
Partial safety factor	γ_{M0}	[-]	1.00
Vertical shear resistance of one web	$V_{v,w,Rd}$	[kN]	10.33
Number of webs	n_w		8
Vertical shear resistance of the profiled steel sheeting	$\boldsymbol{V_{v,p,Rd}}$	**[kN]**	**82.60**

6.2.3 Analysis of the experimental results of preliminary tests

(i) Test PV_1

Fig. 6.3 shows the appearance of the specimen of test PV_1 after the failure. Fig. 6.3(a-b) allows to conclude that the failure of the specimen was due to vertical shear resistance, by the vertical cracks that appeared in the loading zone, instead of a cracking pattern along the span between the loads (constant bending span). In the other image, Fig. 6.3(c), it is shown the slip observed at the end of the test, in one of the ends. Fig. 6.3(c) allows to observe the low deformation of the steel and also the low level of slip between steel and concrete.

Fig. 6.4(a) presents the load-displacement P-δ curve of the first test – test PV_1 – where P is the total applied load and δ is the midspan vertical displacement. Fig. 6.4(b) shows the measured slip on both ends. The ultimate load achieved on the present test was 220.15 kN. The failure on the test was governed by the slab vertical shear resistance, as it is proved by the vertical cracks on the loading zone – Fig. 6.3(a-b) – and by the low values of measured end slip – Fig. 6.4(b) and Fig. 6.3(c). In the same graph (Fig. 6.4(a)), the

levels relative to (i) the vertical shear resistance of the slab according to EN 1994-1-1 (CEN, 2004b) and (ii) the sum of the previous value with the vertical shear resistance of the steel sheet according to standard EN 1993-1-3 (CEN, 2006a), are shown.

(a) Failure (b) Cracking (c) End slip

Fig. 6.3 Failure of the specimen PV_1

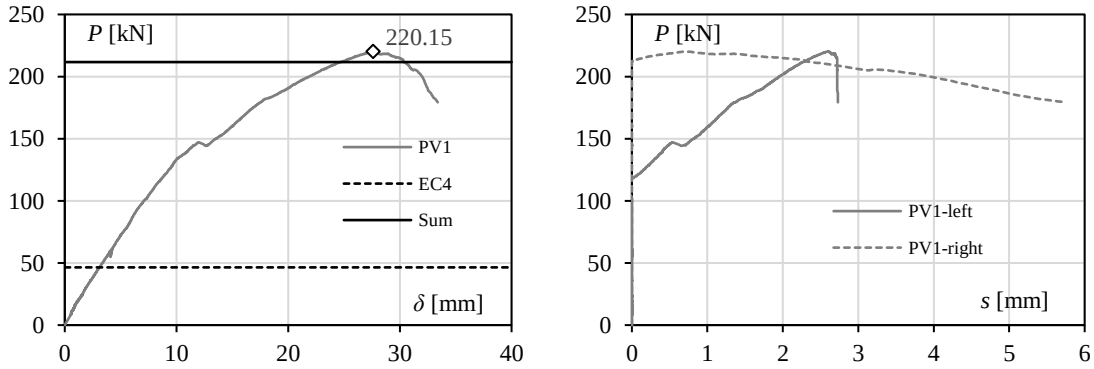

(a) *P*-δ curve (b) *P*-*s* curve

Fig. 6.4 Experimental results for Test PV_1

Table 6.5 presents the maximum load P_{test} reached in test PV_1 and the respective vertical shear value V_{test}; this result is even compared with vertical shear resistance values calculated in the previous section of (i) the composite slab $V_{v,c,Rd}$, evaluated according to EN 1994-1-1 (CEN, 2004b), (ii) the profiled steel sheeting $V_{v,p,Rd}$, evaluated according to EN 1993-1-3 (CEN, 2006a) and (iii) the sum of both quantities $V_{v,sum,Rd}$. According to standard EN 1994-1-1 (CEN, 2004b), with reference to standard EN 1992-1-1 (CEN, 2004a), the vertical shear resistance of test PV_1 is 23.23 kN, that corresponds to only 21.10% of the total achieved load. The ultimate vertical shear of the profiled steel sheet used according to standard EN 1993-1-3 (CEN, 2006a) is 82.60 kN, which represents 75.04% of the maximum load achieved. Even the sum of the two contributions for the resistance values (concrete and steel parts) is equal to 105.83 kN, which represents only 96.15% of the maximum vertical shear achieved. This latter estimative, which take into account the vertical shear resistance of the webs, seems to be a closer to the vertical shear resistance obtained in the tested slab.

Table 6.5 Comparison between the test result (PV_1) and the resistance values according to Eurocodes

				PV_1
Experimental test	**Maximum load achieved**	$\boldsymbol{P_{test}}$	**[kN]**	**220.15**
	Vertical shear value	$\boldsymbol{V_{test}}$	**[kN]**	**110.08**
EN 1994-1-1	Vertical shear resistance	$V_{v,c,Rd}$	[kN]	23.23
		$V_{v,c,Rd}/V_{test}$	[%]	21.10%
EN 1993-1-3	Vertical shear resistance	$V_{v,p,Rd}$	[kN]	82.60
		$V_{v,p,Rd}/V_{test}$	[%]	75.04%
Sum	Sum of the values	$\boldsymbol{V_{v,sum,Rd}}$	[kN]	105.83
		$V_{v,sum,Rd}/V_{test}$	[%]	96.15%

The graph of Fig. 6.5 represents, along the span: (i) the vertical shear diagram when the peak load was achieved; (ii) the vertical shear resistance of the slab $V_{v,c,Rd}$ according to standard EN 1994-1-1 and (iii) the sum of the previous value with the vertical shear resistance of the profiled steel sheeting (Sum). These results allow to observe that the vertical shear resistance of the slab is significantly higher than the value obtained from the standard EN 1994-1-1, according to the EN 1992-1-1 methodologies.

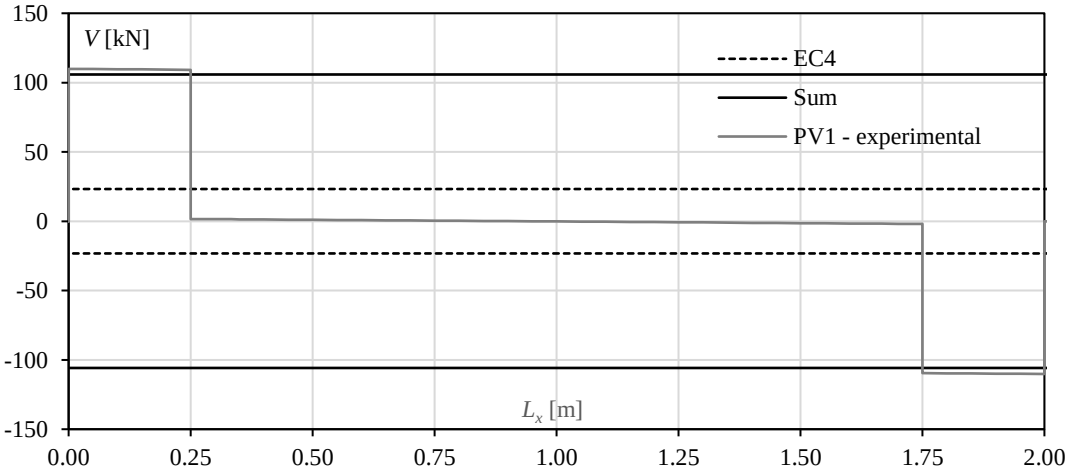

Fig. 6.5 Vertical shear diagram acting on the collapse moment

(ii) Test PV_2

Fig. 6.6 shows the appearance of the composite slab of test PV_2 after failure. These images can show the cracking pattern that appeared on the constant bending moment span (between the load sections) and the high measured slip between concrete and the steel sheet.

Fig. 6.7 shows the evolution of the behaviour of the slab in the test PV_2 and the measured slip in both ends of the specimen. Again, the P-δ curve is presented in the same graph of the levels corresponding to (i) the vertical shear resistance of the slab according to

standard EN 1994-1-1 (EC4) and (ii) the sum of the previous value with the steel sheeting resistance (Sum), to allow an easy comparison between them. For a load level of 173.18 kN, the slab of test PV_2 reached the failure by longitudinal shear, as it is possible to conclude from the high slip measured on the left end of the slab.

(a) Failure (b) Cracking (c) Slip

Fig. 6.6 Failure of the specimen PV_2

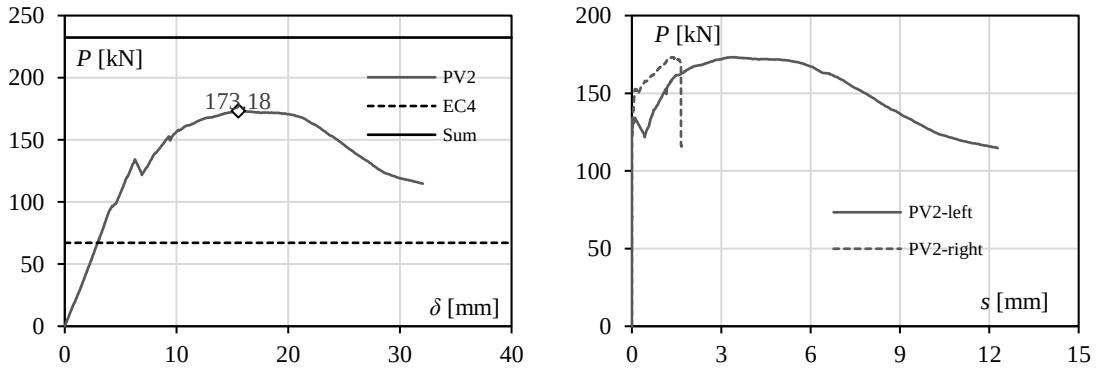

(a) P-δ curve (b) P-s curve

Fig. 6.7 Experimental results for Test PV_2

Although the fact of the slab of test PV_2 had a height 50 mm higher than the slab of test PV_1, the maximum load achieved was lower because (i) the shear span was higher, (ii) the bending forces were higher and mainly because (iii) the reinforcing system for longitudinal shear did not work properly, due to some imperfections in the execution of the slab.

Although it was not possible to achieve a failure by vertical shear and consequently to quantify experimentally the vertical shear resistance of the slab of test PV_2, it is even possible to verify that the design model of standard EN 1994-1-1 (CEN, 2004b) is quite conservative. Actually, the vertical shear resistance of the composite slab according to EN 1994-1-1 (CEN, 2004b) would be 33.57 kN, which only corresponds to 38.77% of the maximum vertical shear achieved on the test, as it is described on Table 6.6. Attending to the previous issues, the value obtained from standard EN 1994-1-1 (CEN, 2004b) would represent an even lower percentage of the real vertical shear resistance of the slab.

Table 6.6 Comparison between the test result (PV_2) and the resistance values according to Eurocodes

				PV_2
Experimental tests	**Maximum load achieved**	$\boldsymbol{P_{test}}$	**[kN]**	**173.18**
	Vertical shear value	$\boldsymbol{V_{test}}$	**[kN]**	**86.59**
EN 1994-1-1	Vertical shear resistance	$\boldsymbol{V_{v,c,Rd}}$	**[kN]**	33.57
		$V_{v,c,Rd}/V_{test}$	[%]	38.77
EN 1993-1-3	Vertical shear resistance	$\boldsymbol{V_{v,p,Rd}}$	**[kN]**	82.60
		$V_{v,p,Rd}/V_{test}$	[%]	95.40
Sum	Sum of the values	$\boldsymbol{V_{v,sum,Rd}}$	**[kN]**	116.17
		$V_{v,sum,Rd}/V_{test}$	[%]	134.17

(iii) Final discussion

Although the number of tests carried out at this stage was low, some preliminary conclusions can be established:

i. the design model for vertical shear resistance for steel-concrete composite slabs as prescribed in standard EN 1994-1-1 (CEN, 2004b) is quite conservative; this model could lead to the overdesign of composite slabs with short spans, or even slabs with current spans but where some reinforcing systems to improve the longitudinal shear behaviour are implemented;
ii. the experimental results obtained, even that in a low quantity, show that the vertical shear resistance of composite slabs can be approximately 5 times higher than the value obtained according to the design model prescribed in Eurocode 4;
iii. the overdesign leaded from the design model of standard EN 1994-1-1 (CEN, 2004b) is due the fact that the contribution of the steel sheet is not taken into account adequately in the vertical shear resistance of the slab;
iv. to avoid the overdesign of composite slabs, a revision of the vertical shear resistance model for composite slabs prescribed on Eurocode 4 is suggested.

To enhance the above conclusions, Table 6.7 is provided to present the comparison between the maximum vertical shear achieved V_{test} on preliminary tests presented on section 4.3 of this document and the corresponding design values of vertical shear resistance $V_{v,c,Rd}$. The V_{test} is defined as $0.5P_{test}$, where P_{test} is the maximum load achieved on the test. Due to the identical cross-section, the design value of the vertical shear resistance $V_{v,c,Rd}$ of these specimens is the same as the one obtained for test PV_1 (23.23 kN). As it can be seen from Table 6.7, the design value of the vertical shear resistance of these slabs represented only 39 to 60% of the maximum vertical shear achieved on all experiments, except for tests from PB group. That means that their vertical shear failure load would be even higher and the ratio to the respective design value even lower. Slabs from PB group were submitted to higher shear spans, and that is why they achieved lower values of maximum load.

Table 6.7 Vertical shear resistance of tests presented on section 4.3

Test	P_{test} [kN]	V_{test} [kN]	$V_{v,c,Rd}$ [kN]	$V_{v,c,Rd}/V_{test}$ [%]
PA_1	84.62	42.31	23.23	55%
PA_2	80.63	40.31	23.23	58%
PA_3	87.19	43.60	23.23	53%
PA_5	45.68	22.84	23.23	102%
PA_6	50.05	25.02	23.23	93%
PB_1	109.06	54.53	23.23	43%
PB_2	120.11	60.05	23.23	39%
PC_1	77.48	38.74	23.23	60%

These conclusions motivated a further investigation to get more and more accurate results to assess the real vertical shear behaviour of steel-concrete composite slabs and their design model. A new experimental campaign was carried out after the improvement of the reinforcing system, which is described in the next section.

6.3 Experimental evaluation of the vertical shear capacity of composite slabs

6.3.1 Introduction

After the preliminary analysis, a second experimental programme was performed in order to evaluate the vertical shear behaviour of composite slabs and its relation to the design models. The present study was carried out to evaluate the vertical shear behaviour and the accuracy of the corresponding design models prescribed in european standards. It was based on the experimental results of the four tests described in Fig. 6.8. Each name of the specimen comes from the height of the profiled sheet h_p, after the letter V (Vertical shear), followed by the total thickness of the slab h (e.g. V-h_p-h). Two different steel sheet profiles, LAMI 60+ and LAMI 120+, were designed and studied in the scope of this research work. These profiles had different heights in order to understand the contribution of the steel sheet in the vertical shear resistance of the slab. All tests were performed on simply supported composite slabs with a 2.0 m span, with different steel sheet heights h_p or different slab thicknesses h. Fig. 6.8 illustrates the geometry of the four specimens tested, where: h is the thickness of the slab, h_p is the height of the profiled steel sheeting, b_m is the width of a module of the composite slab, b is the width of the specimen and b_0 is the mean width of a concrete rib. The specimens with a steel sheet height of 60 mm were composed of 4 modules with a 205 mm width each and the specimens with a steel sheet height of 120 mm had only 3 slab modules with a 222 mm width each (see Fig. 6.9).

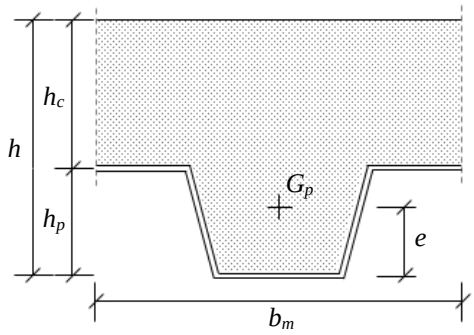

Test	h_p [mm]	h [mm]	b_m [mm]	b [mm]	b_0 [mm]
V-60-150	60	150	205	820	89.23
V-60-200	60	200	205	820	89.23
V-120-200	120	200	222	666	90.49
V-120-240	120	240	222	666	90.49

Fig. 6.8 Geometrical characterization of the specimens

For the experimental evaluation of the longitudinal shear or bending resistance of composite slabs, shear spans of $L/4$ are commonly adopted. The greater the shear span L_s is, the higher the possibility of reaching slab failure by bending or longitudinal slip is too. Taking this into account, the slabs were tested with short shear spans to force a vertical shear failure instead of a longitudinal shear failure. Fig. 6.10 shows the structural scheme of these tests, where L_s represents the shear span, L_b the constant bending moment span, s_{left} and s_{right} the measured slip on the left and right ends respectively, P is the total applied load and δ the vertical displacement in the middle span. All slabs were subjected to two linear loads symmetrically applied at a distance L_s equal to 250 mm from the supports, corresponding to 1/8 of the total span and a constant bending moment span L_b equal to 1500 mm (same experimental layout of test PV_1 from preliminary analysis). The distance between the supports and the ends of the specimens was 100 mm on both sides.

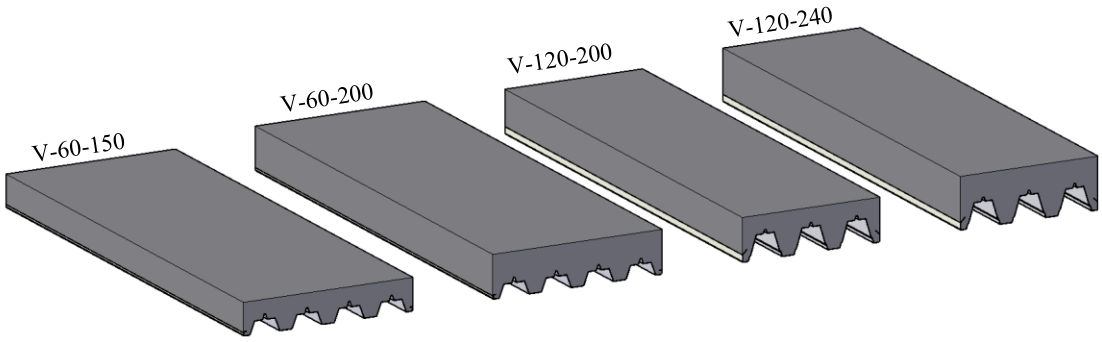

Fig. 6.9 Test specimens

In order to quantify the resistance of the concrete, uniaxial compressive tests on cubic specimens with edges of 150 mm were performed. To obtain the tensile resistance of the steel, uniaxial tensile tests were performed on steel sheet specimens with a geometry according to standard ISO 6892-1 (ISO 2009). The characterization of the materials was carried out in the same week as the full-scale tests. An average compressive stress

resistance f_{cm} of 36.32 Mpa for the concrete (more details were presented before on Table 4.16) and a corresponding characteristic value f_{ck} of 28.32 MPa, in accordance with Eurocode 2 (CEN 2004a) was obtained; for the steel of the profiled sheets, average yield stresses, f_{yp} of 329.51 MPa (*LAMI 60+*) and 363.57 MPa (*LAMI 120+*) were obtained.

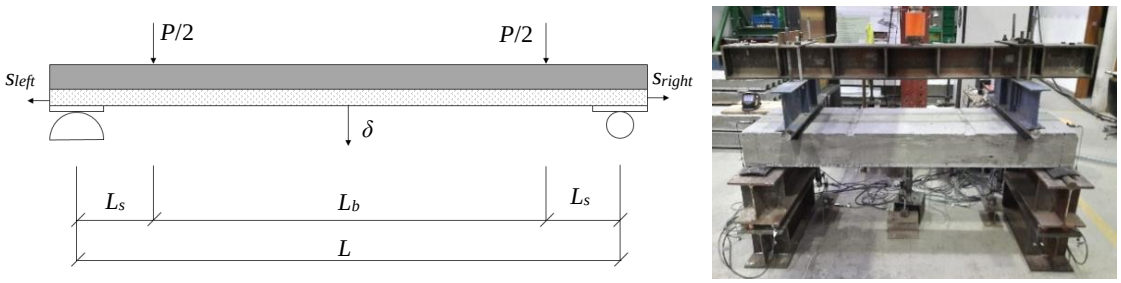

(a) Structural system (b) Experimental layout

Fig. 6.10 Experimental tests

6.3.2 Vertical shear resistance values

6.3.2.1 Vertical shear resistance of the slabs according to Eurocode 4

As it was mentioned in the previous section, according to EN 1994-1-1 (CEN, 2004b) with reference to EN 1992-1-1 (CEN, 2004a), the vertical shear resistance of a module of a composite slab, taking in consideration the same anchorage conditions, is given by Eq. (6.1).

The vertical shear resistance of the four specimens tested and evaluated in accordance with Eurocodes 2 (CEN, 2004a) and 4 (CEN, 2004b) using the mean values of the real geometric and mechanical properties, is presented in Table 6.8. The symbols in this table have the following meanings: h is the total thickness of the slab; e is the distance from the centroidal axis of the profiled steel sheeting to the top fibre of the composite slab in tension; d_p is the distance from the centroidal axis of profiled steel sheeting to the top fibre of the composite slab in compression; k and v_{min} are constants given in standard EN 1992-1-1 (CEN, 2004a); f_{ck} is the characteristic value of the compressive resistance of the concrete; f_{cm} is the mean value of the compressive resistance of the concrete; b_0 is the mean width of a concrete rib; $V_{v,Rd,m}$ is the design value of the vertical shear resistance of a module of the composite slab; n_m is the number of modules in the slab; $V_{v,c,Rd}$ is the design value for the vertical shear resistance.

Table 6.8 Vertical shear resistance of all specimens according to the Eurocode design model

	h [mm]	e [mm]	d_p [mm]	k [-]	f_{ck} [MPa]	f_{cm} [MPa]	v_{min} [MPa]	b_0 [mm]	$V_{v,Rd,m}$ [kN/mod.]	n_m [-]	$V_{v,c,Rd}$ [kN]
V-60-150	150	37.68	112.32	2.0	28.32	36.32	0.60	89.23	5.98	4	**23.92**
V-60-200	200	37.68	162.32	2.0	28.32	36.32	0.60	89.23	8.64	4	**34.56**
V-120-200	200	65.06	134.94	2.0	28.32	36.32	0.60	105.84	8.52	3	**25.56**
V-120-240	240	65.06	174.94	2.0	28.32	36.32	0.60	105.84	11.05	3	**33.14**

6.3.2.2 Vertical shear resistance of the steel sheeting according to Eurocode 3

The vertical shear design of a profiled steel sheeting was already presented on the section 3.2.3.3 (see page 50). Table 6.9 presents (i) the geometric properties of both profiles and (ii) the vertical shear resistance for both profiles $V_{v,p,Rd}$. According to standard EN 1993-1-3 (CEN 2006) the vertical shear resistance of the steel sheets LAMI 60+ and LAMI 120+ is 82.60 kN and 77.66 kN, respectively, for 820 and 666 mm of width. So, the maximum load supported by the steel sheet in both types of specimens, corresponding to the design values for a vertical shear failure, would be 165.21 kN and 155.33 kN for type tests V-60 and V-120, respectively.

Table 6.9 Vertical shear resistance of the steel sheets according to standard EN 1993-1-3

			LAMI 60+	LAMI 120+
Web height between the midlines of the flanges	h_w	[mm]	60.00	113.96
Slope of the web relative to the flanges	φ	[º]	69.00	73.00
Slant height of the web between the midpoints of the corners	s_w	[mm]	64.08	120.47
Total developed slant height of the web	s_d	[mm]	64.08	121.17
Slant height of the largest plane element in the web	s_p	[mm]	-	90.25
Steel core thickness	t_{cor}	[mm]	0.96	0.96
Mean value of steel yield strength	f_{yp}	[MPa]	329.51	363.57
Modulus of Young	E_s	[GPa]	196.78	214.04
Relative web slenderness	λ_w	[-]	0.945	1.467
Coefficient to account for longitudinal stiffener	k_τ	[-]	-	8.035
Shear buckling strength	f_{bv}	[MPa]	172.89	113.14
Partial safety factor	γ_{M0}	[-]	1.00	1.00
Vertical shear resistance of one web of the profile	$V_{Rd,w}$	[kN]	10.33	12.94
Number of webs	n_w	[-]	8	6
Vertical shear resistance of the steel sheet	$V_{v,p,Rd}$	**[kN]**	**82.60**	**77.66**

6.3.3 Experimental results

Fig. 6.11 shows the failure modes that occurred during the four tests performed, detailing the crack patterns developed on the concrete part. In all the specimens, the cracks occurred in the shear span almost perfectly aligned in the direction between the loading

points and the supports, which means that all the specimens collapsed in a vertical shear failure mode, however the results for slabs with higher thicknesses shall be used with caution as the shear span was too short. Fig. 6.12 shows the load-deformation P-δ curves and Fig. 6.13(a) the load-slip P-s curves obtained from the tests; in this figure: P is the total applied load, δ is the mid-span deformation and s is the longitudinal slip between the steel sheet and the concrete measured at each end of the specimens. Fig. 6.13(b) presents the load-strain curve, where the measured ε is the strain in the steel sheet measured at the bottom flange of the mid-span section. The curves obtained show that high levels of applied load were achieved with low levels of strain and longitudinal slip between the steel and concrete. Fig. 6.13(b) shows the strain growth in the bottom flange of the steel sheet at mid-span cross-section. It can be observed in this figure that the maximum strain attained in the steel ε_{up} was only slightly higher than the yield strain ε_{yp} at the collapse stage (bending capacity not reached); this observation proves that the vertical shear failure was the main failure mode.

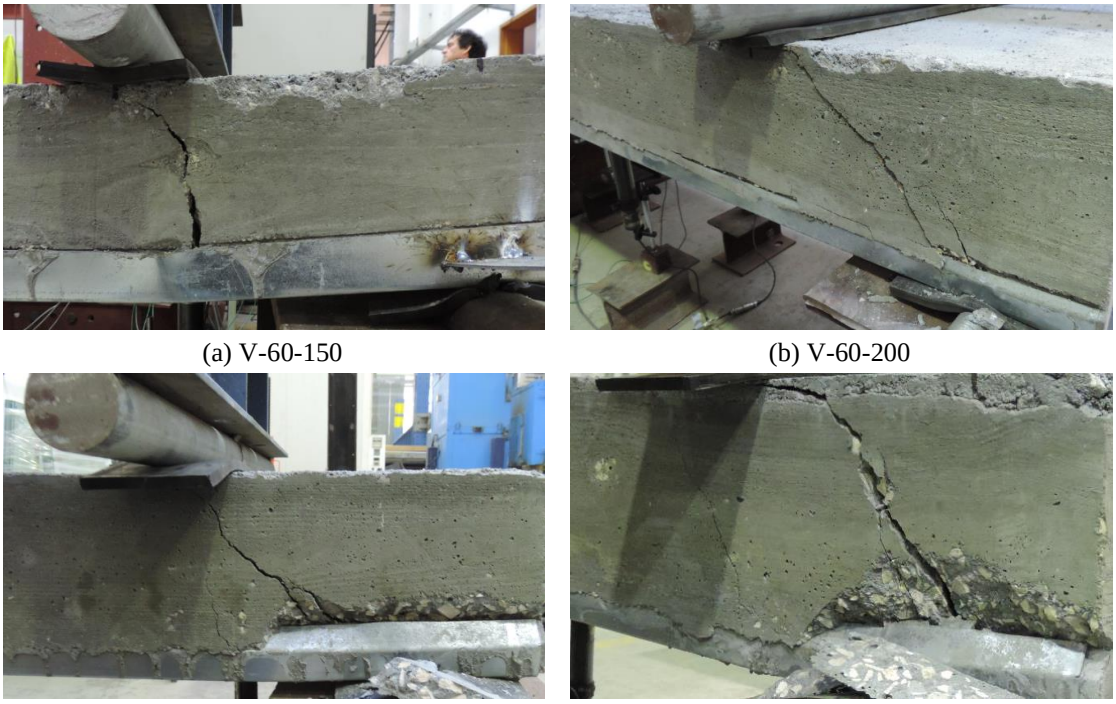

(a) V-60-150 (b) V-60-200

(c) V-120-200 (d) V-120-240

Fig. 6.11 Vertical shear cracks in all four specimens

Table 6.10 presents the maximum loads, P_{test} reached in the experimental tests and the respective vertical shear value V_{test}; these results are even compared with the vertical shear resistance values of (i) the composite slab $V_{v,c,\mathrm{Rd}}$, evaluated according to standard EN 1994-1-1, (ii) the steel sheet $V_{v,p,Rd}$, evaluated according to standard EN 1993-1-3, and (iii) the sum of these two quantities $V_{v,sum,Rd}$. Thus, it is possible to compare the real

vertical shear behaviour of a composite slab and the corresponding design values according to European standards.

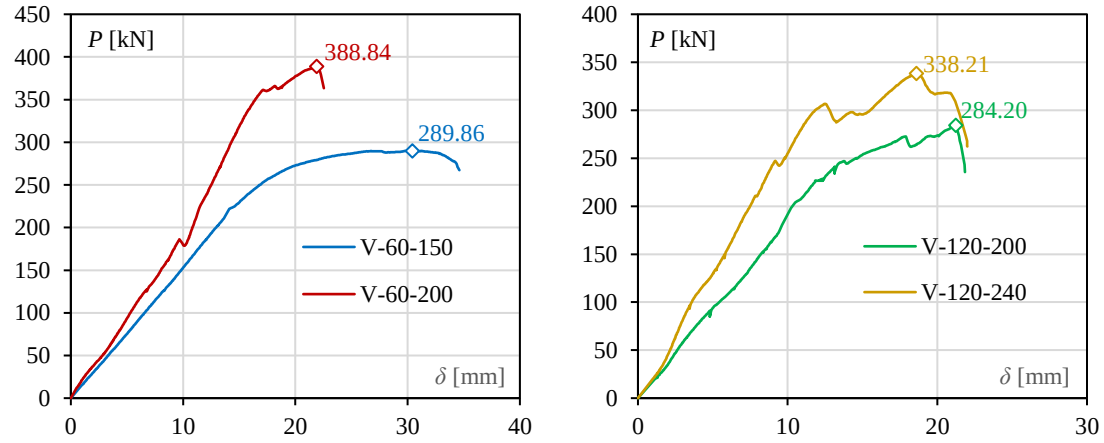

(a) V-60 tests (b) V-120 tests

Fig. 6.12 Experimental results: *P*-δ curves

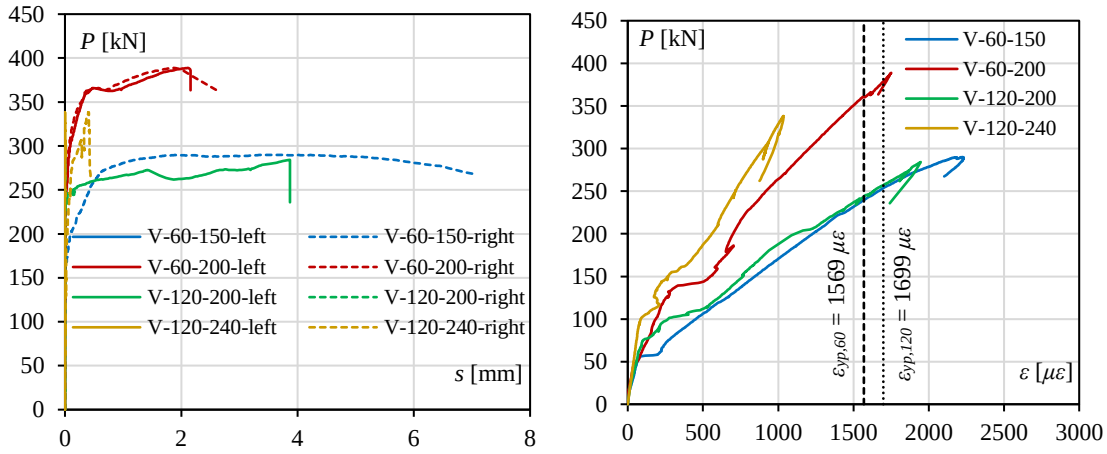

(a) *P*-*s* curves (b) *P*-ε curves

Fig. 6.13 Experimental results

In the group of specimens tested in the present study, the vertical shear resistance of the composite slab, according to Eurocode 4, did not represent more than 19.60% of the real vertical shear force reached in the respective specimen. This maximum relative value was obtained for the thickest specimen (V-120-240). Furthermore, the vertical shear resistance of the steel sheet is very high due to the contribution of the web. The ultimate vertical shear resistance of the steel sheet, according to standard EN 1993-1-3, in test V-60-150 corresponds to 57.00% of the maximum load achieved (a maximum of the four tests performed). Also the sum of the resistance of the two components (concrete slab and steel sheet) was never higher than 73.50% of the corresponding maximum load reached. The

values of the vertical shear resistance, which take into account the vertical shear resistance of the webs, seems to be closer to the high vertical shear resistance of composite slabs.

Table 6.10 Comparison between the experimental results and the resistance values according to Eurocode rules

				V-60-150	V-60-200	V-120-200	V-120-240
Experimental test	**Maximum load achieved**	P_{test}	**[kN]**	**289.86**	**388.84**	**284.20**	**338.21**
	Vertical shear value	V_{test}	**[kN]**	**144.93**	**194.42**	**142.10**	**169.10**
EN 1994-1-1	Vertical shear resistance	$V_{v,c,Rd}$	[kN]	23.92	34.56	25.56	33.14
		$V_{test}/V_{v,c,Rd}$	[%]	16.50	17.78	17.99	19.60
EN 1993-1-3	Vertical shear resistance	$V_{v,p,Rd}$	[kN]	82.60	82.60	77.66	77.66
		$V_{test}/V_{v,p,Rd}$	[%]	57.00	42.49	54.65	45.93
Sum	Sum of the values	$\boldsymbol{V_{v,sum,Rd}}$	[kN]	106.52	117.17	103.23	110.80
		$V_{test}/V_{v,sum,Rd}$	[%]	73.50	60.27	72.64	65.52

The widths of the test specimens with steel sheets with a height of 60 mm or 120 mm were different (see Fig. 6.8); therefore, for a direct comparison between the test results, Table 6.11 shows the maximum load achieved during the experimental tests per metre of width.

Table 6.11 Maximum loads per unit of width reached in the tests

Test	P_{test} [kN]	δ [mm]	b [mm]	P/b [kN/m]
V-60-150	289.86	30.4	820	353.49
V-60-200	388.84	21.9	820	474.20
V-120-200	284.20	21.2	666	426.73
V-120-240	338.21	18.6	666	507.82

Fig. 6.14 shows the vertical shear diagrams, for tests V-60-150, V-60-200, V-120-200 and V-120-240. The vertical shear resistance of the slab according to standard EN 1994-1-1 and the sum of the previous value with the vertical shear resistance of the steel sheet according to standard EN 1993-1-3 is also represented in each diagram. These diagrams also show that the vertical shear resistance of the slab is actually significantly higher than the value obtained from standard EN 1994-1-1, according to the EN 1992-1-1 design model.

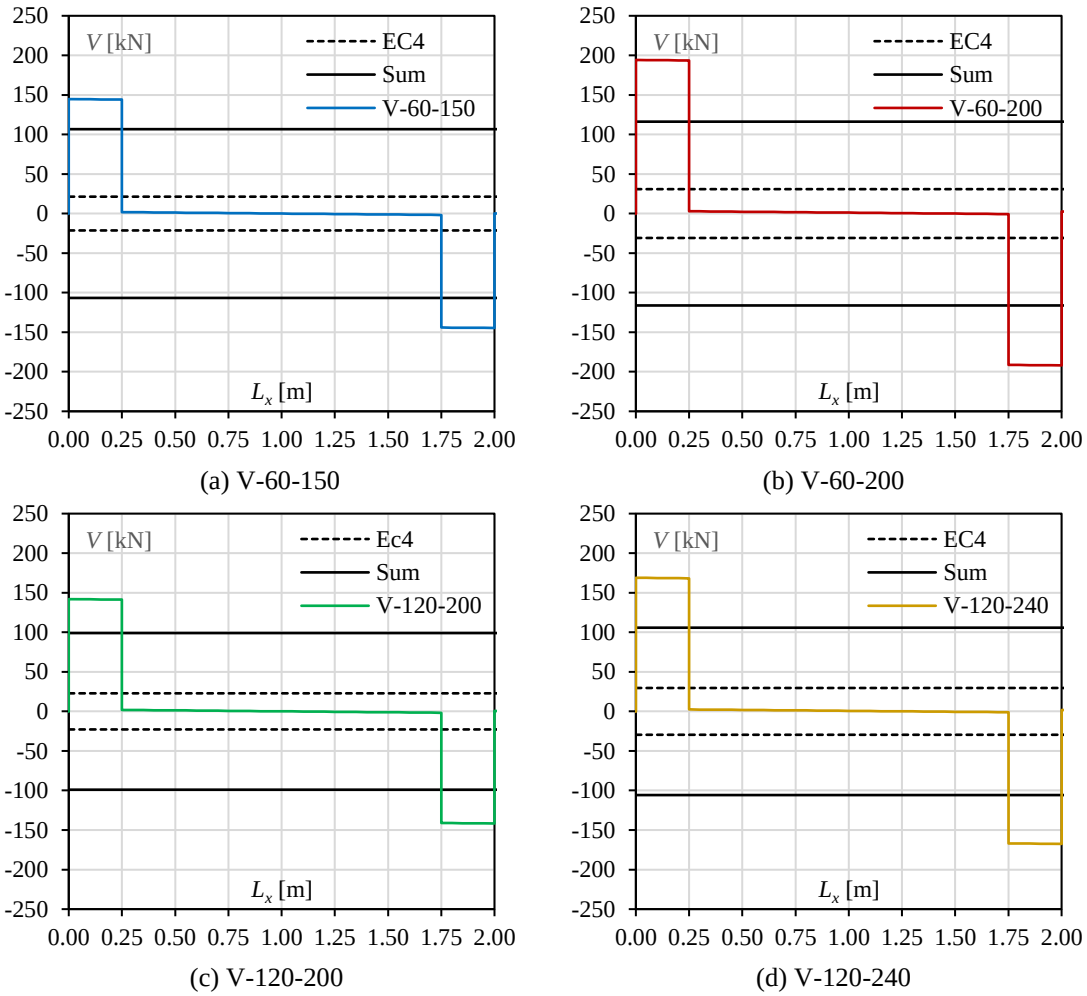

Fig. 6.14 Shear force diagrams at the collapse stage in the tests

6.4 Numerical study

6.4.1 General description

As it was mentioned before, experimental research is expensive and time consuming. Because of that, several studies have been developed to improve existing knowledge about the numerical modelling of composite slabs using finite element analysis (FEA). Numerical modelling can be a cheap and accurate tool to predict the behaviour of composite slabs.

In order to add to the data related to the vertical shear behaviour of composite slabs, the four experimental tests performed and presented in the previous section, were modelled using the software *Abaqus* – see Fig. 6.15(a). Once again, to simplify the complexity of the models, and regarding the geometrical symmetry of the specimens and the concept of

the one directional behaviour of those elements, the numerical models were developed considering only half a span and half a module of a slab – see Fig. 6.15(b-c).

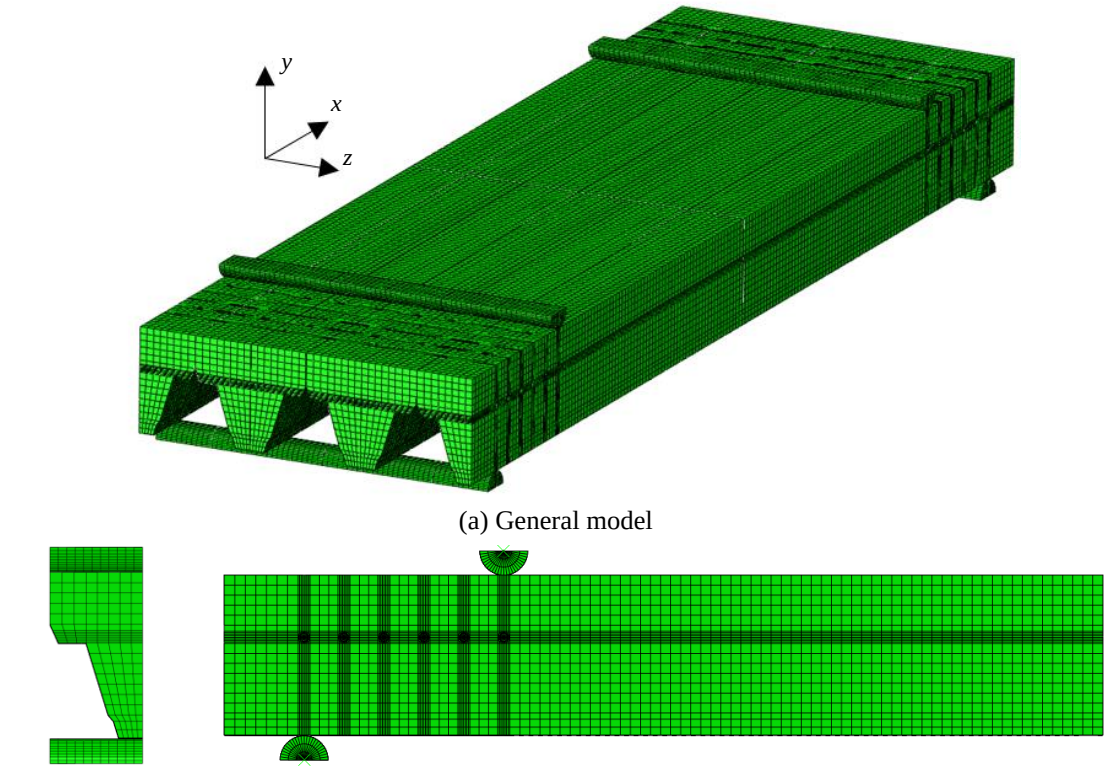

(a) General model

(b) Cross-section

(c) Span

Fig. 6.15 Numerical simulation of short-span composite slabs

The mesh sizes, the materials properties and the interaction properties were defined in the same way as presented in the previous chapter.

Since that for high levels of load, such the ones reached on vertical shear study tests, neoprene band has an almost complete compression influencing the total deflection of the composite slab. The 10 mm thick neoprene band, applied between the slab and the steel supports, was also modelled for a better approximation between the experimental and numerical results, especially concerning the deformation of the specimens. This material was modelled as a hyperelastic material, using the Neo-Hookean model, which is the most indicated for hyperelastic materials with insufficient data, where $C_{10} = 1.786$ and $D_1 = 0.12$.

Numerical results were compared with the experimental results obtained in order to validate numerical models developed. After validating the numerical simulations, a new parametrical study was carried out to complement the results and conclusions obtained in the experimental programme.

6.4.2 Validation of the numerical models

The four specimens tested experimentally were used to calibrate the numerical models for the future parametric studies. For example, a comparison between the load-displacement *P*-δ and load-slip *P*-*s* curves concerning to the V-120-200 and V-120-200 tests is presented on Fig. 6.16(a-b), respectively. As it can be seen on the Fig. 6.17, a good agreement in the end slip and crack pattern was obtained between the experimental tests and numerical models. Although the numerical models are stiffer than the experimental ones, numerical results showed a good approximation to the experimental results, in terms of curve load-displacement shape, maximum load and measured slip.

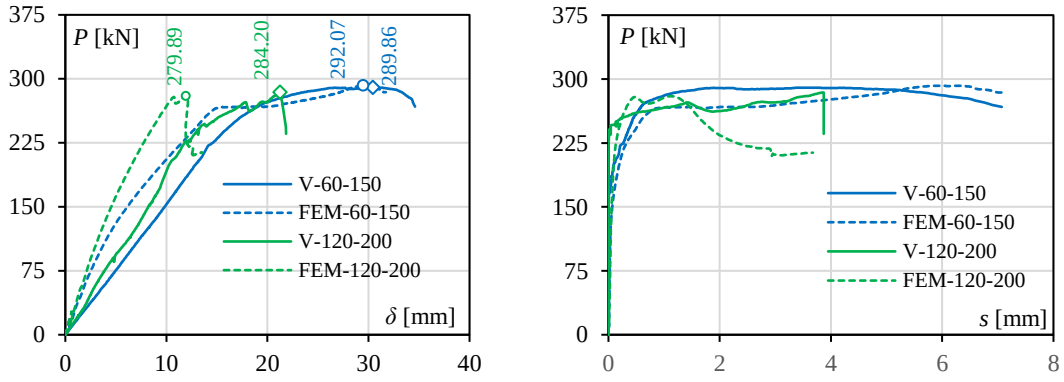

(a) *P*-δ curves (b) *P*-*s* curves

Fig. 6.16 Validation of numerical models

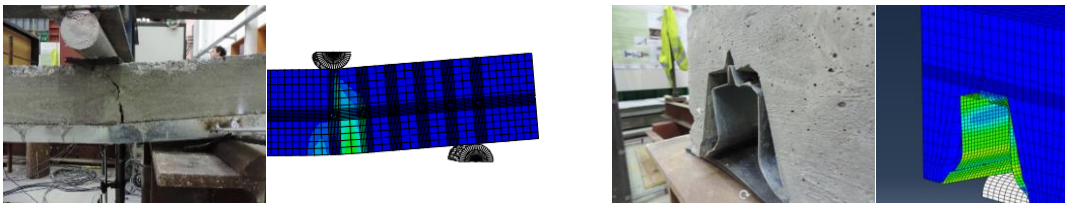

(a) Crack pattern (V-60-150) (b) End slip (V-120-200)

Fig. 6.17 Comparison between numerical and experimental results

Table 6.12 presents the values for the maximum load achieved in the finite element analysis (FEA) models and compares these values with the respective experimental ones (test). As may be seen, a maximum of 9.6% difference was observed between the numerical and experimental results. This approximation was satisfactory enough to validate the numerical models developed.

Table 6.12 Validation of numerical models

Specimen/ Model	P_{test} [kN]	P_{FEA} [kN]	P_{FEA}/P_{test}
V-60-150	289.86	292.07	1.008
V-60-200	388.84	422.71	1.087
V-120-200	284.20	279.89	0.985
V-120-240	338.21	370.58	1.096

6.4.3 Parametric analysis

The numerical models were validated for a vertical shear failure, so it was observed that *Abaqus* was capable to simulate a vertical shear failure on composite slabs. Then, a parametric study was carried out to get more results showing the actual vertical shear resistance of steel-concrete composite slabs. A group of 8 new numerical models were developed under the same modelling conditions as the previous ones, including the span length, the loading scheme and the longitudinal shear reinforcement. These new models are described on Table 6.13 and were defined under some different geometric/strength conditions: steel sheet profile – *LAMI 60+* or *LAMI 120+;* total slab thickness – 160, 200 or 240 mm; concrete strength grade – C20/25, C25/30 or C35/45; steel sheet thickness – 0.8, 1.0 or 1.2. The deck steel material was modelled according to standard EN 1993-1-3 (CEN, 2006a) for a S320GD+Z steel grade, being: f_{yp} = 320 MPa, f_{up} = 390 MPa and E_s = 210 GPa.

Table 6.13 Description of numerical models developed on the parametric study

Model	Steel Profile	h [mm]	t [mm]	f_{ck} [MPa]
FEM-60-Ref	**LAMI 60+**	200	1.0	25
FEM-120	**LAMI 120+**	200	1.0	25
FEM-60-h160	LAMI 60+	**160**	1.0	25
FEM-60-h240	LAMI 60+	**240**	1.0	25
FEM-60-t0.8	LAMI 60+	200	**0.8**	25
FEM-60-t1.2	LAMI 60+	200	**1.2**	25
FEM-60-C20	LAMI 60+	200	1.0	**20**
FEM-60-C30	LAMI 60+	200	1.0	**30**

Table 6.14 shows (i) the maximum load and vertical shear resistance achieved in the respective numerical model and (ii) the different vertical shear resistance values. All models collapsed by vertical shear failure. Considering the results of the models, the vertical shear resistance design value never represented more than 22% of the maximum achieved load. Even the sum of both vertical shear resistance values (concrete and steel sheet parts) did not represent more than 89% of the failure load. These results allowed to conclude again that the vertical shear design model recommended in standard EN 1994-1-1 is very conservative for not taking in consideration the strength of the steel sheet on it. Load-deflection P-δ curves obtained are presented then on Fig. 6.18.

Table 6.14 Numerical results and resistance values

Model	P_{FEA} [kN/m]	V_{FEA} [kN/m]	$V_{v,c,Rd}$ [kN/m]	$V_{v,c,Rd}/V_{FEA}$ [-]	$V_{v,p,Rd}$ [kN/m]	$V_{v,p,Rd}/V_{FEA}$ [-]	$V_{v,sum,Rd}$ [kN/m]	$V_{v,sum,Rd}/V_{FEA}$ [-]
FEM-60-Ref	505.97	252.98	40.18	0.16	102.55	0.41	142.73	0.56
FEM-120	337.01	168.50	36.59	0.22	113.91	0.68	150.50	0.89
FEM-60-h160	324.72	162.36	30.28	0.19	102.55	0.63	132.83	0.82
FEM-60-h240	729.06	364.53	49.86	0.14	102.80	0.28	152.66	0.42
FEM-60-t0.8	442.34	221.17	40.18	0.18	64.58	0.29	104.76	0.47
FEM-60-t1.2	576.94	288.47	40.18	0.14	150.80	0.52	190.98	0.66
FEM-60-C20	495.27	247.63	37.01	0.15	103.52	0.42	140.53	0.57
FEM-60-C30	547.32	273.66	43.12	0.16	103.77	0.38	146.88	0.54
		Average		**0.17**		**0.45**		**0.62**

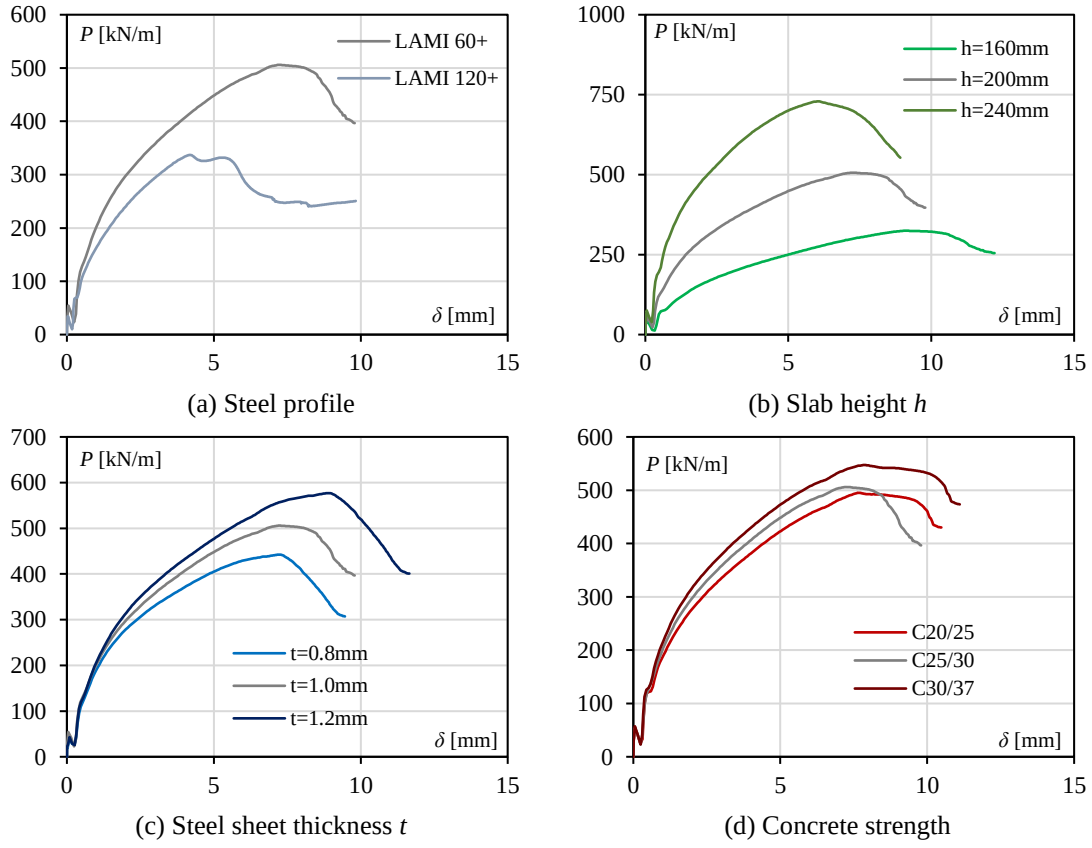

(a) Steel profile (b) Slab height h

(c) Steel sheet thickness t (d) Concrete strength

Fig. 6.18 Parametric study on the vertical shear resistance

Fig. 6.19 shows the maximum vertical shear V_{FEM} obtained on numerical simulations influenced by the height of the slab h, the steel sheet thickness t or the concrete grade (represented by f_{ck}). From these results it is possible to observe that both steel and concrete influence the vertical shear resistance of composite slabs and so both shall be taken into account.

The obtained results allowed also to observe that vertical shear resistance of composite slabs increased significantly for higher values of the height of the slab h or concrete h_c and for higher steel sheet thickness t. These results showed that the steel deck has an important contribution for the vertical shear resistance of composite slabs.

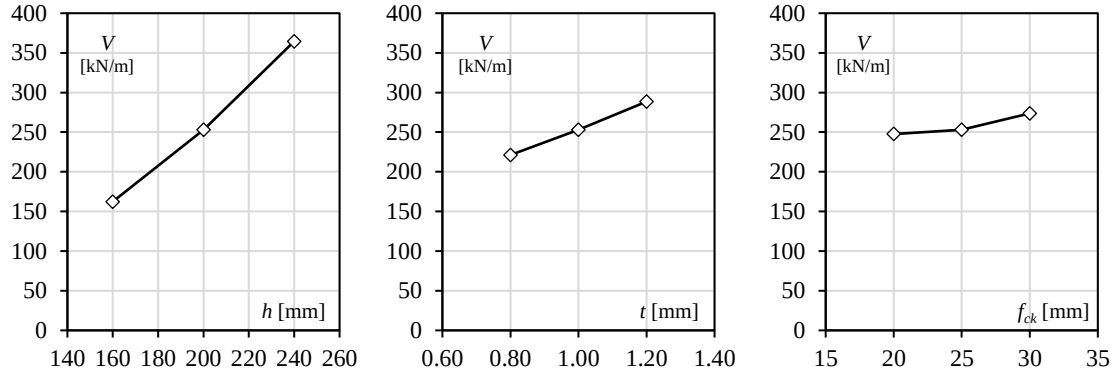

(a) h-V_{FEM} results (b) t-V_{FEM} results (c) f_{ck}-V_{FEM} results

Fig. 6.19 Influence of geometric and mechanical parameters in the vertical shear resistance

6.5 Final remarks

The obtained results allowed to get the following conclusions:

i. the vertical shear resistance of those composite slabs were more than 5 times higher than vertical shear design value in accordance with standards EN 1992-1-1 (CEN, 2004a) and EN 1994-1-1 (CEN, 2004b);
ii. the vertical shear resistance value of the steel sheet, according to standard EN 1993-1-3 (CEN, 2006a), represented, in average, only 45% of the actual vertical shear resistance of those composite slabs;
iii. the sum of the resistance values from the concrete slab, from Eurocodes 2 (CEN, 2004a) and 4 (CEN, 2004b), and the steel sheet, from standard EN 1993-1-3 (CEN, 2006a), represented, in average, only 62% of the vertical shear resistance of those composite slabs, which represent a better approximation and still in the safety side;
iv. the sum of the contribution of the concrete ribs with the contribution of the steel webs of profiled steel sheeting can be used for prediction of the vertical shear resistance of composite slabs with high degree of longitudinal shear connection, such as the ones considered and tested in the scope of the present research work; for composite slabs with low degree of longitudinal degree of shear connection (in general with a non-ductile behaviour) further studies should be carried out.

Therefore, a revision of the vertical shear design model is advised in order to avoid the overdesign of these elements. If the contribution of the profiled steel sheeting is taken in consideration in the vertical shear design of composite slabs these elements could be even more efficient and competitive.

The real efficiency of the proposed reinforcing system for steel-concrete composite slabs is not used if the design is governed by the conservative model for vertical shear design.

The aim of the next chapter is to emphasis the efficiency of the proposed reinforcing system on the structural performance of composite slabs with high connection degree. So, instead of the design model for vertical shear resistance prescribed in the actual version of standard EN 1994-1-1 (CEN, 2004b), the Eq. (6.2) is used.

$$V_{v,Rd} = V_{v,c,Rd} + V_{v,p,Rd} \tag{6.2}$$

where:

$V_{v,c,Rd}$ is the design value of the vertical shear resistance of the concrete part according to standard EN 1994-1-1 (CEN, 2004b);

$V_{v,p,Rd}$ is the design value of the vertical shear resistance of the profiled steel sheeting according to standard EN 1993-1-3 (CEN, 2006a).

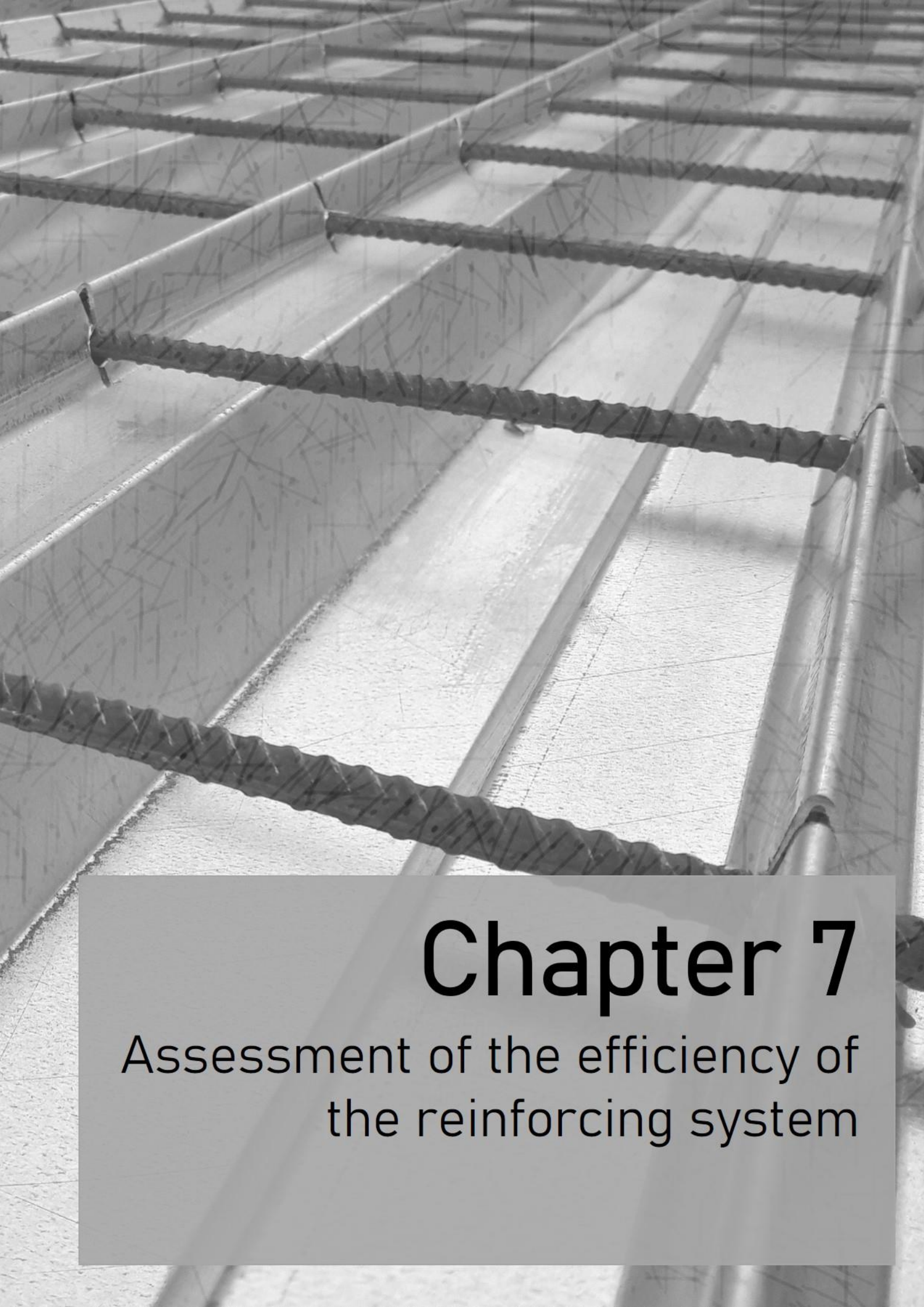

Chapter 7

Assessment of the efficiency of the reinforcing system

7.1 Introduction

In current applications, the resistance of composite slabs tends to be governed by the longitudinal shear behaviour and consequently the bending capacity is not completely taken in advantage. Over the previous chapters an innovative reinforcing system constituted by transversal reinforcing bars intersecting the profiled steel sheeting, developed to increase the longitudinal shear resistance of composite slabs, was presented. It was demonstrated that it allows to increase the connection degree between the concrete and the steel sheeting and so the longitudinal shear resistance of composite slabs.

The efficiency of the proposed reinforcing system depends on its structural performance, allowing the conception of high-performance composite slabs, and also on its ease of execution. Using the concepts developed over the previous chapters, the main advantages and the efficiency of the proposed reinforcing system are addressed and highlighted on this chapter. In order to present the main advantages of this reinforcing system different analyses were carried out.

A quantitative and economic analysis was performed comparing three different cases of simply-supported composite slabs subjected to uniformly distributed loads, where the longitudinal shear behaviour is improved by different reinforcing systems (embossments or transversal bars). The first case concerns in a conventional solution of a steel-concrete composite slab with a steel sheeting H60 with embossments. The other two cases refer to composite slabs with LAMI 60+ profile and transversal bars with different diameters and spacing. For several load levels and span lengths, these slabs are designed to support the same specified load. Then the total height of the slab h needed to check the longitudinal shear resistance is compared. Regarding the amount of concrete needed the cost of the slab by square meter is compared.

Usually, steel producers of profiled steel sheets provide catalogues containing design tables to help the structural engineers on the design of composite slabs and hence promote the application of this construction product on steel and composite buildings. Typically, these design tables provide the characteristic or design value of the maximum load that a composite slab can support in function of geometric and mechanical parameters such as the span length L, the height of the slab h, the steel sheet thickness t, etc... In the scope of the present research work, a design tool was performed to provide the design tables of composite slabs including the innovative aspects developed. This design tool is presented in the Annex A (Developed design tool for composite slabs). Two different cases were then considered in order to show the improvement of the structural performance on composite slabs with transversal bars. Several design tables are presented to show the

influence of the reinforcing system with transversal bars in several practical applications. The output presented showed that: the *m-k* method is conservative when compared with the partial connection method; for current applications transversal bars allow to take advantage of the bending capacity of composite slabs and; the vertical shear resistance just govern the design of steel-concrete composite slabs for short spans and thicker slabs.

7.2 Efficiency of the reinforcing system

7.2.1 Quantitative and economic analysis

The developed reinforcing system, beyond the improvement of the structural performance, also need to be profitable from the economic point of view. Taking this in consideration, a simplified economic analysis was carried out and presented over this section. The economic study comprised the analysis of three case studies comprising three types of simply-supported composite slabs submitted to the same level of uniformly distributed load. For each one, the height of concrete h_c necessary to verify the safety to the longitudinal shear failure was determined. Taking into account the standard unit costs of each material in Portugal, the global cost of each solution was determined.

Fig. 7.1 shows the three different cases considered for this analysis: case i) represents a composite slab with a total height *h* and embossments on the webs of the H60 profiled steel sheeting; case ii) represents a composite slab with a total height *h* and a steel profile LAMI 60+ with 8 mm diameter transversal bars intersecting the profiled steel sheeting spaced by 250 mm; case iii) represents a composite slab with a total height *h* and a steel profile LAMI 60+ with 10 mm diameter transversal bars intersecting the profiled steel sheeting spaced by 200 mm. The same following characteristics were considered in all cases: steel sheet thickness *t* of 1.20 mm; S320GD+Z steel grade and; C25/30 concrete grade.

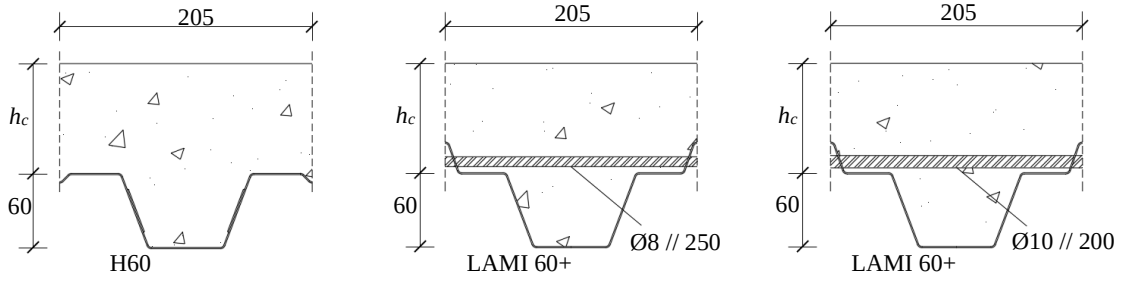

(a) Case i) (b) Case ii) (c) Case iii)

Fig. 7.1 Case studies (dimensions in mm)

The height of the concrete h_c needed to verify the longitudinal shear safety was defined for several values of load p and length spans L. Only results concerning slabs with the neutral axis above the profiled steel sheeting were considered.

Fig. 7.2(a-f) shows the concrete height h_c needed so the slab could be designed to support a uniformly distributed load p for a length span of 2.0, 3.0, 4.0, 5.0, 6.0 and 7.0 m.

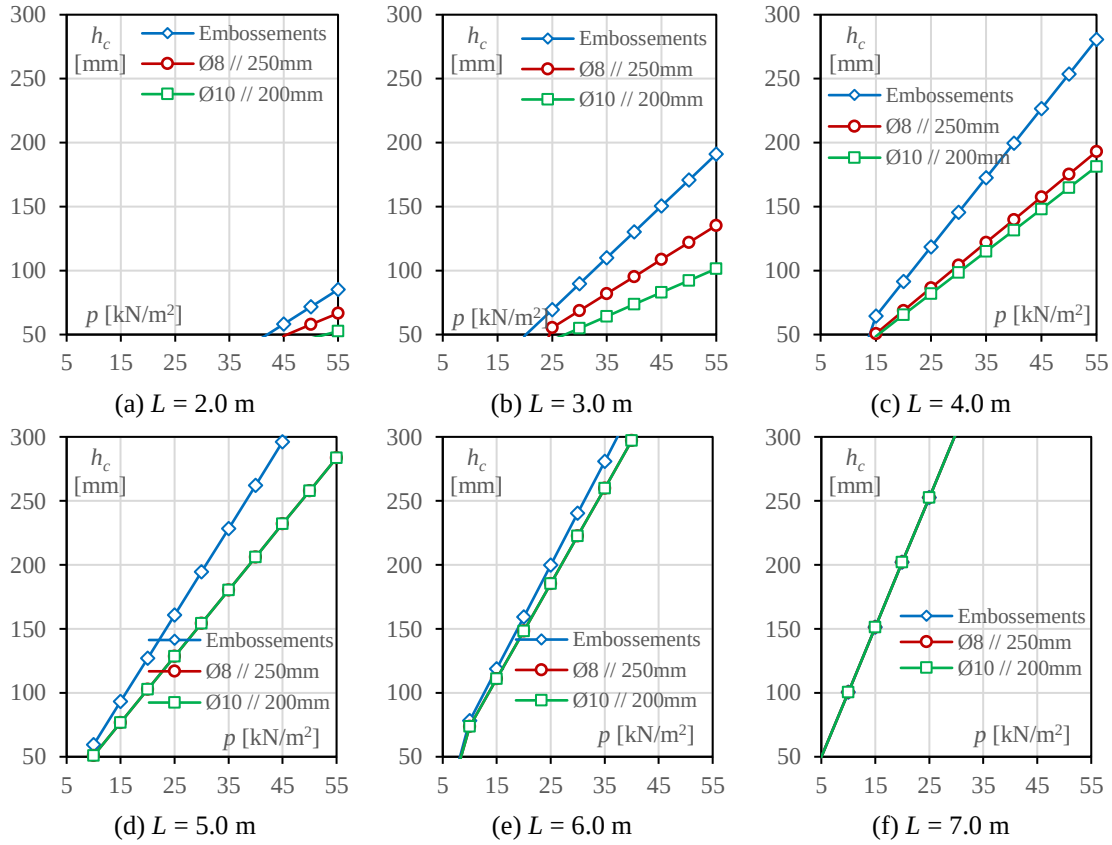

Fig. 7.2 Concrete height of the slab above the profiled steel sheeting for the three case studies

As it was expected, higher spans require higher slabs to verify enough resistance to the same load p. From the obtained results it was possible to verify that for current spans, between 3.0 and 5.0 m, composite slabs with transversal bars need to have a total height significantly lower than composite slabs with an embossed steel sheeting to resist the same load. Actually, for this range of spans, whenever the design was governed by the longitudinal shear resistance, transversal bars allow to reduce the height of the slab between 10 and 100 mm for lower and higher loads, respectively (see Fig. 7.2(c)). This reduction also causes a decrease of the load on the structure up to 2.61 kN/m^2 (see Table 7.1(b)). For longer spans, the connection degree at the critical section tends to be higher and so the difference in the h_c value is lower. This statement is due the fact that from case i) to case iii) the considered design value of the longitudinal shear strength τ_{Rd} tends to

increase and so the distance from the support to attain the full shear connection L_{sf} tends to decrease. For longer spans (L = 7.0 m), it was observed that the design was governed by the bending capacity on all cases. Therefore, to support the same level of load p, all cases shall have the same value of h_c, as it can be overserved by graphic from Fig. 7.2(f).

Table 7.1 Weight variation from case i) to cases ii) and iii)

$p \setminus L$	2.00	3.00	4.00	5.00	6.00	7.00
5	-	-	-	-	-	0.02
10	-	-	-	-0.19	-0.10	0.02
15	-	-	-0.31	-0.38	-0.17	0.02
20	-	-	-0.53	-0.57	-0.25	0.02
25	-	-0.32	-0.76	-0.76	-0.33	0.02
30	-	-0.49	-0.98	-0.95	-0.41	0.02
35	-	-0.66	-1.20	-1.14	-0.49	0.02
40	-	-0.82	-1.42	-1.33	-0.57	0.02
45	-0.20	-0.99	-1.64	-1.52	-0.65	0.02
50	-0.31	-1.16	-1.87	-1.71	-0.73	0.02
55	-0.42	-1.32	-2.09	-1.90	-0.81	0.02
60	-0.54	-1.49	-2.31	-2.09	-0.89	0.02

(a) Weight variation to case ii) [kN/m^2]

$p \setminus L$	2.00	3.00	4.00	5.00	6.00	7.00
5	-	-	-	-	-	0.03
10	-	-	-	-0.18	-0.08	0.03
15	-	-	-0.34	-0.37	-0.16	0.03
20	-	-	-0.60	-0.56	-0.24	0.03
25	-	-0.54	-0.85	-0.75	-0.32	0.03
30	-	-0.80	-1.10	-0.94	-0.40	0.03
35	-	-1.07	-1.35	-1.13	-0.48	0.03
40	-	-1.33	-1.60	-1.32	-0.55	0.03
45	-	-1.59	-1.85	-1.51	-0.63	0.03
50	-0.56	-1.86	-2.10	-1.70	-0.71	0.03
55	-0.75	-2.12	-2.36	-1.89	-0.79	0.03
60	-0.93	-2.38	-2.61	-2.08	-0.87	0.03

(b) Weight variation to case iii) [kN/m^2]

After determining the amount of each material, a simplified cost comparison was carried out. As referred before, the performed economic analysis was based just on materials quantity. The following simplifications were considered for this comparison: the investment costs, such as the profiler equipment and the embossments production, were neglected and it was assumed to be the same for both types of profiles and; the costs from the construction phase, such as the manual labour or construction equipment, were considered to be the same for all the three case studies. Therefore, the differences considered in the total cost of these slabs reflect just the amount of concrete and reinforcement.

The total costs were considered to be composed by: (i) the profiled steel sheeting cost; (ii) the concrete cost and; (iii) the reinforcing bars cost. Unit costs considered over this analysis are presented on Table 7.2, where: c_p is the cost of 1 kg, 1kN or 1 m^2 of profiled steel sheeting; c_c is the cost considered for one cubic meter of concrete and; c_s is the cost considered for 1 kg or 1 kN of reinforcing bars.

Table 7.2 Unit costs considered

c_p			c_c	c_s	
[€/kg]	[€/kN]	[€/m^2]	[€/m^3]	[€/kg]	[€/kN]
1.00	101.94	15.10	65.00	1.20	122.32

For all three case studies, Fig. 7.3 shows the cost C of 1 m^2 of a simply-supported composite slabs designed to support a uniformly distributed load p. Once again, the

graphics on Fig. 7.3(a-f) refer to slabs with 2.0, 3.0, 4.0, 5.0, 6.0 and 7.0 m, respectively. Table 7.3(a-b) presents the cost variation of 1 m^2 of composite slab, in percentage, when the solution is changed from slab with embossed profile to slab with transversal bars.

The obtained results showed that for current spans, whenever the longitudinal shear resistance governs the design, the slab with the proposed system is less expensive. For the analysed situations, it was possible to observe that the proposed reinforcing system allows to save more money for slabs with span lengths between 3.0 and 5.0 m and when these are designed to support higher loads ($p \geq 30$ kN/m^2). As it was expected, for longer spans, where the bending resistance is considered to be achieved, all slabs would need the same amount of concrete and so the reinforcement cost is an additional cost that would not be necessary. Overall, for the considered cases, the proposed system makes it possible to save up to 11.9% of the total cost of the slab. If the composite slab of case i) was designed using the *m-k* method, which is mandatory for composite slabs showing a brittle behaviour (typical situation for these type of slabs), the cost differences would be even higher. The reduction of the thickness of the slab also allow to reduce the total costs of the whole structure, including the foundations, depending on the whole height of the building.

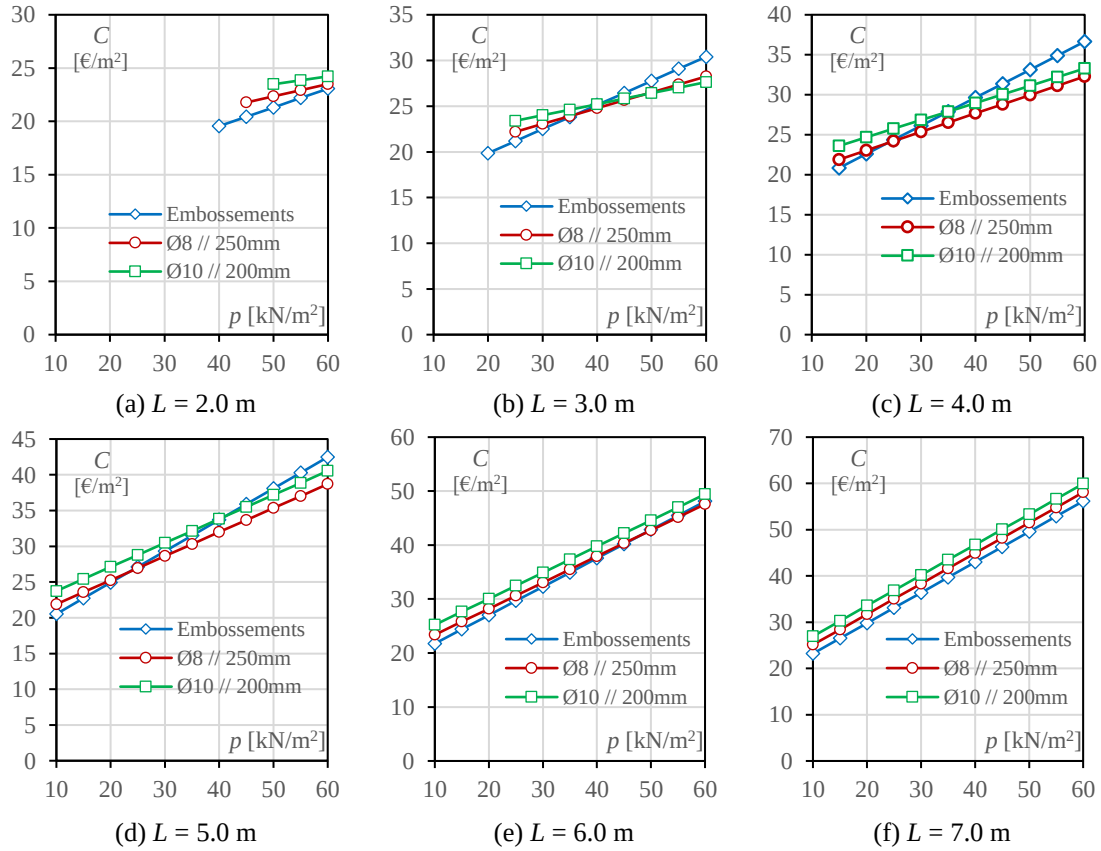

(a) L = 2.0 m (b) L = 3.0 m (c) L = 4.0 m

(d) L = 5.0 m (e) L = 6.0 m (f) L = 7.0 m

Fig. 7.3 Cost of the slab per square meter C [€/m^2]

Table 7.3 Cost variation from case i) to cases ii) and iii)

$p \setminus L$	2.0	3.0	4.0	5.0	6.0	7.0
5	-	-	-	-	-	9.7
10	-	-	-	6.7	7.5	8.3
15	-	-	5.0	3.8	5.8	7.3
20	-	-	2.0	1.4	4.5	6.5
25	-	4.8	-0.7	-0.6	3.3	5.8
30	-	2.5	-2.9	-2.3	2.4	5.3
35	-	0.4	-4.9	-3.8	1.6	4.9
40	-	-1.4	-6.6	-5.1	0.9	4.5
45	6.6	-3.0	-8.2	-6.2	0.3	4.2
50	4.9	-4.5	-9.6	-7.2	-0.2	3.9
55	3.3	-5.8	-10.8	-8.1	-0.6	3.7
60	1.9	-7.1	-11.9	-8.9	-1.1	3.4

(a) Cost variation from case i to case ii [%]

$p \setminus L$	2.0	3.0	4.0	5.0	6.0	7.0
5	-	-	-	-	-	19.0
10	-	-	-	15.6	16.0	16.3
15	-	-	13.2	11.9	13.4	14.2
20	-	-	9.2	8.8	11.3	12.7
25	-	10.5	5.7	6.1	9.5	11.4
30	-	6.7	2.7	3.9	8.1	10.4
35	-	3.3	0.1	2.0	6.9	9.5
40	-	0.3	-2.2	0.4	5.8	8.8
45	-	-2.4	-4.2	-1.1	4.9	8.2
50	10.2	-4.8	-6.1	-2.4	4.1	7.6
55	7.5	-7.1	-7.7	-3.5	3.4	7.1
60	5.0	-9.1	-9.2	-4.6	2.8	6.7

(b) Cost variation from case i to case iii [%]

7.2.2 The efficiency influenced by different parameters

The experimental campaign of small-scale tests and the parametric numerical study have allowed to conclude that the reinforcing system tends to be more effective for: higher slabs; higher steel sheeting thicknesses and higher steel grades. Those observations are consistent with the design methodology of steel-concrete composite slabs with the proposed reinforcing system.

Fig. 7.4 shows the influence of the profiled steel sheeting thickness t in the characteristic value of the maximum load p_k, supported by the slab, in function of the span length L. Fig. 7.4(a) presents the results for slabs with embossed profiles (H60) and Fig. 7.4(b) for slabs with transversal bars (LAMI 60+ with Ø8//250). Fig. 7.5 and Fig. 7.6 present the equivalent results but to showing the influence of the height of the slab h and the steel grade, respectively. All slabs were composed by concrete of the strength grade C25/30. As it was mentioned before, the design value of the longitudinal shear strength $\tau_{u,Rd}$ of composite slabs with a H60 steel profile was considered to be 0.185 MPa (obtained by Marques (2011)).

While in a conventional slab the increase of the steel sheeting thickness or the steel strength does not increase significantly the longitudinal shear resistance of composite slabs (see Fig. 7.4(a) and Fig. 7.6(a)), when transversal bars are intersecting the profiled steel sheeting the bearing capacity increases significantly with the steel sheet thickness (see Fig. 7.4(b) and Fig. 7.6(b)). For example, when the thickness of a conventional composite slab with 4.0 mm of span is increased from 0.7 to 1.5 mm, the maximum load supported by the slab increases from 10.57 to 14.70 kN (increases 39.07 %; see Fig. 7.4(a)). On the other hand, when the thickness of a composite slab with the proposed reinforcing system and 4.0 mm of span is increased from 0.7 to 1.5 mm, the maximum

load supported by the slab increases from 8.33 to 24.67 kN (increases 196.15 %; see Fig. 7.4(b)). Differently, the increase of the slab capacity with the slab height is similar for composite slabs with H60 profile or LAMI 60+ profile and transversal bars (see Fig. 7.5(a-b)).

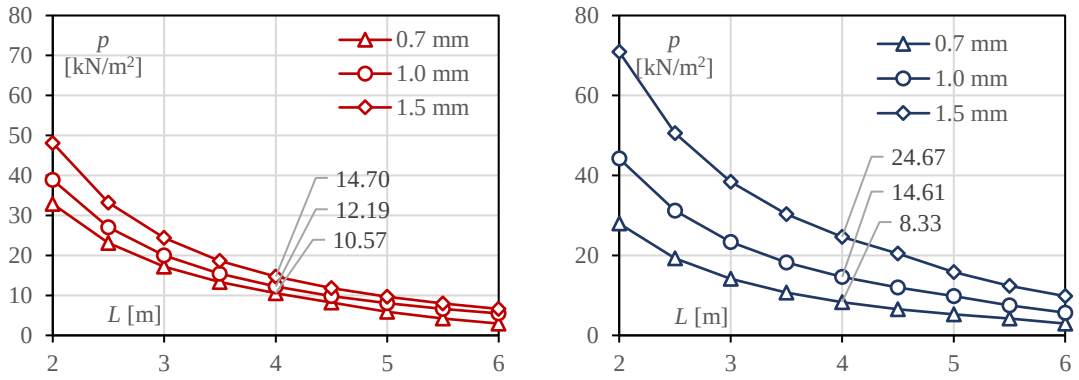

(a) H60 with embossments (b) LAMI 60+ with Ø8//250

Fig. 7.4 Influence of the steel sheet thickness *t* on the maximum load

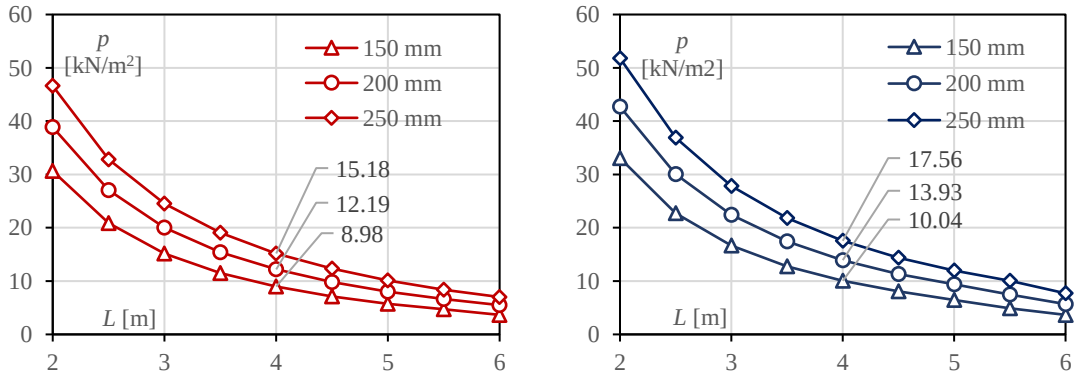

(a) H60 with embossments (b) LAMI 60+ with Ø8//250

Fig. 7.5 Influence of the height of the slab *h* on the maximum load

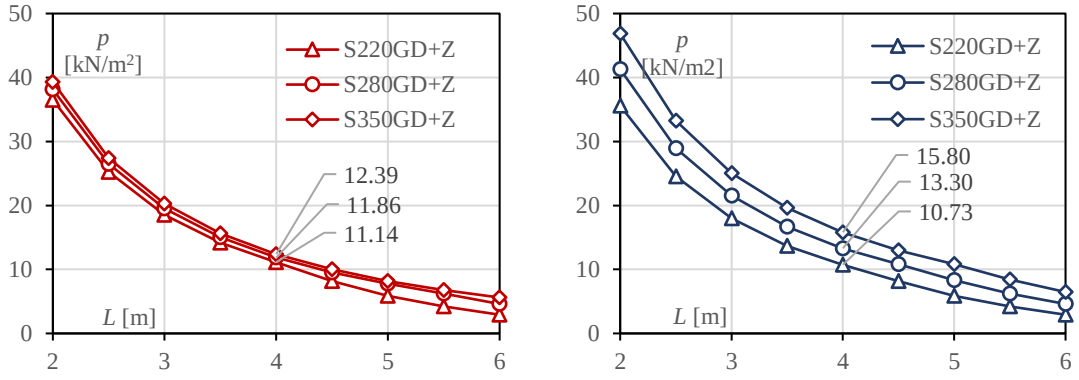

(a) H60 with embossments (b) LAMI 60+ with Ø8//250

Fig. 7.6 Influence of the steel grade on the maximum load

7.3 Design tables of composite slabs with transversal bars

7.3.1 Introduction

In a final stage of the present research work, a design tool to provide the design tables for the composite slabs including the innovative aspects studied over this research was developed; the design tool is presented in detail in the Annex A (Developed design tool for composite slabs) of this thesis. In order to show the efficiency of the reinforcing system and the effect of the design methods, the design tool was used to generate some examples of design tables considering the several possible approaches: (i) using the *m-k* method or the partial connection method (PCM); (ii) considering the vertical shear resistance as prescribed on standard EN 1994-1-1 (CEN, 2004b) or the sum of this value with the vertical shear resistance of the profiled steel sheeting according to standard EN 1993-1-3 (CEN, 2006a); (iii) transversal bars of 8 mm diameter spaced by 200 mm or 10 mm diameter spaced by 200 mm (Ø8 // 200 mm or Ø10 // 200 mm); (iv) with or without longitudinal reinforcement on the ribs.

Two different cases of simply-supported composite slabs with a LAMI 60+ steel profile and a steel grade S320GD+Z were considered: (i) on Case 1 it was considered a profiled steel sheeting with thickness *t* 0.8 mm and a concrete grade C20/25; (ii) on Case 2 it was considered a profiled steel sheeting with thickness *t* 1.5 mm and a concrete grade C30/37 (see Table 7.4). The generated design tables report the characteristic value of the maximum load supported p_k for several *L-h* relations, where *L* and *h* are the length of the span and the height of the slab, respectively. The colour of each value of p_k identifies the governing design mode according to the meanings presented on Table 7.5.

Table 7.4 Case studies

Case	Profile	*t* [mm]	Steel grade	Concrete grade
1	LAMI 60+	0.8	S320GD+Z	C20/25
2	LAMI 60+	1.5	S320GD+Z	C30/37

Table 7.5 Modes governing the design – colour meanings

q	ULS: Vertical Shear
q	ULS: Longitudinal Shear
q	ULS: Bending
q	SLS: Deflection

For both cases it was considered that: (i) reinforcing bars (transversal or longitudinal) had a characteristic yield stress f_{sk} equal to 500 MPa; the geometric centre of the longitudinal reinforcement is placed 30 mm above the bottom flange of the profiled steel sheeting; the design value of the longitudinal shear strength $\tau_{u,Rd}$ of slabs with H60 profile was considered to be 0.185 MPa (obtained by Marques (2011)); the empirical factors for longitudinal shear design using the *m-k* method *m* and *k* were considered to be 98.32 MPa and 0.080 MPa, respectively; no values under 2 kN/m^2 were considered in the design tables.

7.3.2 Case 1

Table 7.6 presents the description of the approach considered on each subcase, concerning the principals defined in the previous section. Table 7.7 presents the design table using the approach defined for subcase 1.1. This table gives the characteristic value of the maximum uniformly distributed load p_k using the *m-k* method for the longitudinal shear design and the vertical shear resistance is determined according to standard EN 1994-1-1 (CEN, 2004b). This is the approach adopted on design tables typically provided by the steel companies to promote the application of their profiles.

Table 7.6 Subcases of Case 1

Subcase	Longitudinal shear	$V_{v,Rd}$	Transversal reinforcement	$\tau_{u,Rd}$	Longitudinal reinforcement
1.1	*m-k*	$V_{c,Rd}$	-	-	-
1.2	PCM	$V_{c,Rd}$	-	$\tau_{u,Rd}$	-
1.3	*m-k*	$V_{c,Rd} + V_{p,Rd}$	-	-	-
1.4	PCM	$V_{c,Rd} + V_{p,Rd}$	-	$\tau_{u,Rd}$	-
1.5	PCM	$V_{c,Rd} + V_{p,Rd}$	Ø8 // 200 mm	$\tau_{t,Rd}$	-
1.6	PCM	$V_{c,Rd} + V_{p,Rd}$	Ø10 // 200 mm	$\tau_{t,Rd}$	-
1.7	PCM	$V_{c,Rd} + V_{p,Rd}$	Ø10 // 200 mm	$\tau_{t,Rd}$	Ø12 // 205 mm

Table 7.7 Conventional design table (Subcase 1.1)

L\ h	100	125	150	175	200	225	250
2.0	6.4	8.9	11.4	13.8	16.3	18.7	20.5
2.5	4.8	6.7	8.6	10.4	12.3	14.1	15.4
3.0	3.8	5.2	6.7	8.1	9.6	11.1	12.0
3.5	2.3	3.6	4.7	5.7	6.7	7.7	8.7
4.0	-	2.5	3.3	4.0	4.7	5.4	6.1
4.5	-	-	2.3	2.8	3.3	3.8	4.3
5.0	-	-	-	-	2.2	2.5	2.9
5.5	-	-	-	-	-	-	-
6.0	-	-	-	-	-	-	-

Table 7.8(i) to Table 7.10(i) present the design tables using the approaches defined for subcases 1.2 to 1.4, respectively, and Table 7.8(ii) to Table 7.10(ii) the load variation, in percentage, of these subcases compared to subcase 1.1 (see Table 7.7). Table 7.8 allowed to confirm that *m-k* method tends to be very conservative when compared to the PCM. Actually, for this case, when the PCM is used instead of the *m-k* method, the longitudinal shear resistance never governs the design, which becomes governed by vertical shear for most cases. It was observed an increase of the load up to 92.5% when the PCM is used instead of the *m-k* method. Table 7.9 showed that when the profiled steel sheeting vertical shear resistance $V_{v,p,Rd}$ is taken into account the vertical shear failure does not govern any analysed situation. Table 7.10 shows how influent the design approaches adopted could be. Actually, as it was observed for this example, when the PCM method is used for the longitudinal shear design and the vertical shear resistance of the steel sheeting is considered in the vertical shear resistance of the slab the maximum load considered in the design could increase up to 224.1%.

Table 7.8 Design table using the PCM instead of the *m-k* method (Subcase 1.2)

L\ h	100	125	150	175	200	225	250
2.0	6.4	8.9	11.4	13.8	16.3	18.7	20.5
2.5	4.8	6.7	8.6	10.4	12.3	14.1	15.4
3.0	3.8	5.2	6.7	8.1	9.6	11.1	12.0
3.5	2.3	4.2	5.3	6.5	7.7	8.9	9.6
4.0	-	3.4	4.3	5.3	6.2	7.2	7.8
4.5	-	-	3.6	4.4	5.1	5.9	6.4
5.0	-	-	2.2	3.6	4.2	4.9	5.3
5.5	-	-	-	2.5	3.5	4.1	4.3
6.0	-	-	-	-	2.8	3.4	3.6

(i) Design table

L\ h	100	125	150	175	200	225	250
2.0	0.0	0.0	0.0	0.0	0.0	0.0	0.0
2.5	0.0	0.0	0.0	0.0	0.0	0.0	0.0
3.0	0.0	0.0	0.0	0.0	0.0	0.0	0.0
3.5	0.0	14.7	14.6	14.6	14.6	14.6	9.8
4.0	-	33.6	33.5	33.4	33.3	33.2	27.3
4.5	-	-	57.9	57.7	57.5	57.4	49.7
5.0	-	-	-	-	92.5	92.2	81.9
5.5	-	-	-	-	-	-	-
6.0	-	-	-	-	-	-	-

(ii) Comparison with Subcase 1.1

Table 7.9 Design table considering the contribution of the steel sheeting $V_{v,Rd}$ (Subcase 1.3)

L\ h	100	125	150	175	200	225	250
2.0	9.1	12.6	16.1	19.6	23.0	26.5	30.0
2.5	5.7	7.9	10.1	12.3	14.5	16.7	18.9
3.0	3.8	5.3	6.8	8.2	9.7	11.2	12.7
3.5	2.3	3.6	4.7	5.7	6.7	7.7	8.7
4.0	-	2.5	3.3	4.0	4.7	5.4	6.1
4.5	-	-	2.3	2.8	3.3	3.8	4.3
5.0	-	-	-	-	2.2	2.5	2.9
5.5	-	-	-	-	-	-	-
6.0	-	-	-	-	-	-	-

(i) Design table

L\ h	100	125	150	175	200	225	250
2.0	41.7	41.6	41.6	41.5	41.5	41.5	46.4
2.5	18.4	18.4	18.3	18.3	18.3	18.3	22.7
3.0	1.2	1.2	1.2	1.2	1.2	1.2	5.2
3.5	0.0	0.0	0.0	0.0	0.0	0.0	0.0
4.0	-	0.0	0.0	0.0	0.0	0.0	0.0
4.5	-	-	0.0	0.0	0.0	0.0	0.0
5.0	-	-	-	-	0.0	0.0	0.0
5.5	-	-	-	-	-	-	-
6.0	-	-	-	-	-	-	-

(ii) Comparison with Subcase 1.1

Table 7.10 Design table using the PCM instead of the *m-k* method and considering the contribution of the steel sheeting $V_{v,Rd}$ (Subcase 1.4)

L \ *h*	100	125	150	175	200	225	250
2.0	17.8	22.4	26.7	30.8	34.7	38.5	42.3
2.5	9.2	15.1	18.3	21.4	24.3	27.1	29.9
3.0	4.6	10.8	13.3	15.7	18.0	20.2	22.4
3.5	2.3	6.6	10.1	12.0	13.9	15.7	17.4
4.0	-	3.6	7.2	9.5	11.0	12.5	13.9
4.5	-	-	4.2	7.6	8.9	10.1	11.3
5.0	-	-	2.2	4.6	7.0	8.2	9.3
5.5	-	-	-	2.5	4.9	6.1	7.0
6.0	-	-	-	-	2.8	4.4	5.1

(i) Design table

L \ *h*	100	125	150	175	200	225	250
2.0	177.3	152.5	135.5	123.0	113.3	105.5	106.2
2.5	91.1	125.1	114.0	105.1	98.0	92.1	94.1
3.0	22.6	106.2	99.4	93.2	87.8	83.2	86.4
3.5	0.0	79.7	116.5	111.7	107.2	103.0	99.3
4.0	-	42.5	120.1	138.2	134.4	130.5	127.0
4.5	-	-	84.0	174.6	171.5	168.0	164.5
5.0	-	-	-	-	219.5	224.1	220.5
5.5	-	-	-	-	-	-	-
6.0	-	-	-	-	-	-	-

(ii) Comparison with Subcase 1.1

Table 7.11 to Table 7.13 present equivalent results but concerning subcases 1.5 to 1.7 and the load variation, in percentage, to the subcase 1.4. These subcases are now compared to subcase 1.4 to take into consideration the same design principles. From Table 7.11 and Table 7.12 it is possible to observe that, for this example, the bearing capacity of composite slabs with transversal bars systems of Ø8 // 200 mm and Ø10 // 200 mm could increase up to 15.0 and 39.0%, respectively, when compared with slabs with an embossed profiled steel sheeting. Once again, it was possible to confirm that transversal bars intersecting the profiled steel sheeting make it possible to achieve the bearing capacity of the slab in some cases, especially for higher slabs and longer spans. Table 7.13 shows that when transversal bars are combined with longitudinal reinforcement, 1Ø12/rib, the longitudinal shear resistance never governed the design for this situation and, for short spans, the design tends to be governed by vertical shear because the longitudinal shear and bending resistances tends to increase significantly with longitudinal reinforcement. Actually, when a transversal reinforcement of Ø10 // 200 mm is combined with a longitudinal one of 1Ø12/rib, the bearing capacity could increase up to 131.1%.

Table 7.11 Design table for slabs with a transversal reinforcement of Ø8 // 200 mm (Subcase 1.5)

L \ *h*	100	125	150	175	200	225	250
2.0	18.5	23.9	28.8	33.5	38.1	42.5	46.8
2.5	9.2	16.1	19.9	23.5	26.9	30.2	33.4
3.0	4.6	11.6	14.6	17.4	20.1	22.7	25.3
3.5	2.3	6.6	11.2	13.5	15.7	17.8	19.8
4.0	-	3.6	7.2	10.7	12.5	14.3	16.0
4.5	-	-	4.2	7.6	9.6	11.2	12.9
5.0	-	-	2.2	4.6	7.0	8.3	9.5
5.5	-	-	-	2.5	4.9	6.1	7.0
6.0	-	-	-	-	2.8	4.4	5.1

(i) Design table

L \ *h*	100	125	150	175	200	225	250
2.0	3.8	6.3	7.9	8.9	9.7	10.3	10.7
2.5	0.0	7.2	8.8	9.9	10.7	11.3	11.8
3.0	0.0	7.9	9.7	10.9	11.7	12.3	12.8
3.5	0.0	0.0	10.6	11.8	12.7	13.3	13.9
4.0	-	0.0	0.0	12.9	13.8	14.4	15.0
4.5	-	-	0.0	0.3	8.3	11.5	14.4
5.0	-	-	0.0	0.0	0.0	0.3	2.8
5.5	-	-	-	0.0	0.0	0.0	0.0
6.0	-	-	-	-	0.0	0.0	0.0

(ii) Comparison with Subcase 1.4

Table 7.12 Design table for slabs with a transversal reinforcement of Ø10 // 200 mm (Subcase 1.6)

L\ h	100	125	150	175	200	225	250
2.0	19.6	26.4	32.6	38.5	44.1	49.6	55.0
2.5	9.2	18.0	22.8	27.3	31.6	35.8	39.8
3.0	4.6	11.8	16.9	20.5	23.9	27.3	30.5
3.5	2.3	6.6	12.1	15.2	18.3	21.4	24.2
4.0	-	3.6	7.2	10.9	13.1	15.4	17.6
4.5	-	-	4.2	7.6	9.6	11.2	12.9
5.0	-	-	2.2	4.6	7.0	8.3	9.5
5.5	-	-	-	2.5	4.9	6.1	7.0
6.0	-	-	-	-	2.8	4.4	5.1

(i) Design table

L\ h	100	125	150	175	200	225	250
2.0	10.2	17.6	21.9	24.9	27.1	28.8	30.2
2.5	0.0	19.8	24.6	27.7	30.0	31.8	33.2
3.0	0.0	9.3	27.1	30.4	32.8	34.6	36.1
3.5	0.0	0.0	19.9	26.4	31.8	36.5	39.0
4.0	-	0.0	0.0	15.1	19.5	23.4	26.8
4.5	-	-	0.0	0.3	8.3	11.5	14.4
5.0	-	-	0.0	0.0	0.0	0.3	2.8
5.5	-	-	-	0.0	0.0	0.0	0.0
6.0	-	-	-	-	0.0	0.0	0.0

(ii) Comparison with Subcase 1.4

Table 7.13 Design table for slabs with a transversal reinforcement of Ø10 // 200 mm and a longitudinal reinforcement of Ø12 // 205 mm (Subcase 1.7)

L\ h	100	125	150	175	200	225	250
2.0	22.0	49.4	53.5	56.0	58.4	60.9	62.6
2.5	10.4	24.7	42.3	44.1	46.0	47.9	49.1
3.0	5.3	13.3	23.8	36.2	37.7	39.2	40.1
3.5	2.7	7.5	13.9	22.9	31.8	32.9	33.7
4.0	-	4.3	8.3	14.2	22.1	27.7	28.9
4.5	-	2.3	5.0	8.9	14.3	21.0	24.2
5.0	-	-	2.8	5.5	9.3	14.2	18.7
5.5	-	-	-	3.3	5.9	9.5	14.0
6.0	-	-	-	-	3.6	6.2	9.5

(i) Design table

L\ h	100	125	150	175	200	225	250
2.0	23.6	120.3	100.1	81.7	68.3	58.0	48.2
2.5	13.0	63.9	131.1	106.7	89.3	76.3	64.2
3.0	15.0	23.4	78.4	130.5	109.2	93.4	79.0
3.5	19.2	14.7	37.4	90.4	128.7	110.0	93.3
4.0	-	17.8	16.1	49.8	101.0	122.7	107.8
4.5	-	-	19.4	17.3	61.2	108.5	115.1
5.0	-	-	26.4	20.5	31.5	72.0	102.2
5.5	-	-	-	27.7	21.3	55.5	99.7
6.0	-	-	-	-	28.7	39.8	86.6

(ii) Comparison with Subcase 1.4

7.3.3 Case 2

For Case 2, an equivalent analysis was performed, as it is presented on Table 7.14. Table 7.15 present the design table using the approach defined for subcase 2.1, when the *m-k* method is used and the vertical shear resistance is defined according to standard EN 1994-1-1 (CEN, 2004b).

Table 7.14 Subcases of Case 2

Subcase	Longitudinal shear	$V_{v,Rd}$	Transversal reinforcement	$\tau_{u,Rd}$	Longitudinal reinforcement
	m-k	$V_{c,Rd}$	-	-	-
2.2	PCM	$V_{c,Rd}$	-	$\tau_{u,Rd}$	-
2.3	*m-k*	$V_{c,Rd} + V_{p,Rd}$	-	-	-
2.4	PCM	$V_{c,Rd} + V_{p,Rd}$	-	$\tau_{u,Rd}$	-
2.5	PCM	$V_{c,Rd} + V_{p,Rd}$	Ø8 // 200 mm	$\tau_{t,Rd}$	-
2.6	PCM	$V_{c,Rd} + V_{p,Rd}$	Ø10 // 200 mm	$\tau_{t,Rd}$	-

2.7	PCM	$V_{c,Rd}$ + $V_{p,Rd}$	Ø10 // 200 mm	$\tau_{t,Rd}$	Ø12 // 205 mm

Table 7.15 Conventional design table (Subcase 2.1)

L \ *h*	100	125	150	175	200	225	250
2.0	8.2	11.4	14.6	17.8	21.0	24.2	26.5
2.5	6.3	8.7	11.2	13.6	16.0	18.5	20.2
3.0	5.0	6.9	8.8	10.8	12.7	14.7	16.0
3.5	3.6	5.6	7.2	8.8	10.3	11.9	13.0
4.0	-	4.6	5.9	7.3	8.6	9.9	10.8
4.5	-	3.4	4.6	5.7	6.7	7.7	8.7
5.0	-	-	3.4	4.2	5.0	5.7	6.5
5.5	-	-	2.3	3.1	3.7	4.2	4.8
6.0	-	-	-	2.2	2.7	3.1	3.5

Table 7.16 to Table 7.18 present the design tables using the approaches defined for subcases 2.2 to 2.4, respectively, and the respective load variation, in percentage, from subcase 2.1. Once again it was observed that the value of p_k can be more than 200% higher when the PCM method is used for the longitudinal shear design and the vertical shear capacity of the slab is taken as the sum of the contribution of both components.

Table 7.16 Design table using the PCM instead of the *m-k* method (Subcase 2.2)

L \ *h*	100	125	150	175	200	225	250
2.0	8.2	11.4	14.6	17.8	21.0	24.2	26.5
2.5	6.3	8.7	11.2	13.6	16.0	18.5	20.2
3.0	5.0	6.9	8.8	10.8	12.7	14.7	16.0
3.5	3.6	5.6	7.2	8.8	10.3	11.9	13.0
4.0	-	4.6	5.9	7.3	8.6	9.9	10.8
4.5	-	3.4	5.0	6.1	7.2	8.3	9.0
5.0	-	-	4.1	5.1	6.1	7.0	7.6
5.5	-	-	2.3	4.4	5.2	6.0	6.5
6.0	-	-	-	2.8	4.4	5.1	5.5

(i) Design table

L \ *h*	100	125	150	175	200	225	250
2.0	0.0	0.0	0.0	0.0	0.0	0.0	0.0
2.5	0.0	0.0	0.0	0.0	0.0	0.0	0.0
3.0	0.0	0.0	0.0	0.0	0.0	0.0	0.0
3.5	0.0	0.0	0.0	0.0	0.0	0.0	0.0
4.0	-	0.0	0.0	0.0	0.0	0.0	0.0
4.5	-	0.0	7.6	7.6	7.5	7.5	3.0
5.0	-	-	19.2	22.7	22.6	22.5	16.9
5.5	-	-	0.0	41.6	41.3	41.1	34.2
6.0	-	-	-	24.3	66.4	66.0	57.1

(ii) Comparison with Subcase 2.1

Table 7.17 Design table considering the contribution of the steel sheeting $V_{v,Rd}$ (Subcase 2.3)

L \ *h*	100	125	150	175	200	225	250
2.0	16.1	22.2	28.4	34.5	40.7	46.9	53.0
2.5	10.1	14.1	18.0	21.9	25.8	29.7	33.6
3.0	6.7	9.5	12.2	14.9	17.5	20.2	22.8
3.5	3.6	6.7	8.6	10.5	12.4	14.3	16.2
4.0	-	4.9	6.3	7.7	9.0	10.4	11.8
4.5	-	3.4	4.6	5.7	6.7	7.7	8.7
5.0	-	-	3.4	4.2	5.0	5.7	6.5
5.5	-	-	2.3	3.1	3.7	4.2	4.8
6.0	-	-	-	2.2	2.7	3.1	3.5

(i) Design table

L \ *h*	100	125	150	175	200	225	250
2.0	94.7	94.3	94.0	93.9	93.8	93.7	100.2
2.5	61.7	61.3	61.1	61.0	60.9	60.8	66.4
3.0	35.5	38.1	37.9	37.8	37.7	37.7	42.8
3.5	0.0	20.2	20.1	20.1	20.0	20.0	24.7
4.0	-	5.6	5.6	5.5	5.5	5.5	9.9
4.5	-	0.0	0.0	0.0	0.0	0.0	0.0
5.0	-	-	0.0	0.0	0.0	0.0	0.0
5.5	-	-	0.0	0.0	0.0	0.0	0.0
6.0	-	-	-	0.0	0.0	0.0	0.0

(ii) Comparison with Subcase 2.1

Table 7.18 Design table using the PCM instead of the *m-k* method and considering the contribution of the steel sheeting $V_{v,Rd}$ (Subcase 2.4)

L\ h	100	125	150	175	200	225	250
2.0	26.9	35.2	39.8	44.2	48.2	52.1	56.0
2.5	12.9	23.3	26.8	30.2	33.4	36.5	39.5
3.0	6.7	16.6	19.4	22.0	24.5	26.9	29.3
3.5	3.6	9.9	14.6	16.7	18.8	20.7	22.6
4.0	-	5.8	10.9	13.1	14.8	16.4	18.0
4.5	-	3.4	6.7	10.5	11.9	13.3	14.6
5.0	-	-	4.1	7.5	9.8	10.9	12.0
5.5	-	-	2.3	4.7	8.0	9.0	10.0
6.0	-	-	-	2.8	5.2	7.6	8.4

(i) Design table

L\ h	100	125	150	175	200	225	250
2.0	226.7	207.3	172.0	148.1	129.6	115.5	111.3
2.5	105.9	167.6	140.5	121.8	108.1	97.4	95.6
3.0	35.5	140.6	119.1	104.0	92.7	83.8	83.2
3.5	0.0	76.4	103.5	91.0	81.4	73.8	74.2
4.0	-	25.8	83.0	81.0	72.8	66.2	67.4
4.5	-	0.0	45.5	86.2	78.5	72.2	66.9
5.0	-	-	19.2	78.2	96.6	90.1	84.6
5.5	-	-	0.0	52.1	119.3	113.2	107.3
6.0	-	-	-	24.3	95.8	145.1	138.5

(ii) Comparison with Subcase 2.1

Table 7.19 to Table 7.21 present the design tables using the approaches defined for subcases 2.5 to 2.7, respectively, and the respective load variation, in percentage, from subcase 2.4. As it was observed in Case 1, it was possible to achieve the bearing capacity and increase the bearing capacity of composite slabs with transversal bars intersecting the profiled steel sheeting. Actually, the capacity of the slabs with transversal bars systems of Ø8 // 200 mm and Ø10 // 200 mm increased up to 107.8 and 135.3%, respectively, when compared with slabs with an embossed profiled steel sheeting. The magnitude of the load increase was more significant for Case 2 because the profiled steel sheeting thickness was higher and, as it was observed on previous analysis, the thickness of the steel sheeting influences significantly the efficiency of the reinforcing system. From the last subcase it was observed that when a transversal reinforcement of Ø10 // 200 mm is combined with a longitudinal amount of 1Ø12/rib, the bearing capacity could increase up to 207.5%, for this type of slab.

Table 7.19 Design table for slabs with a transversal reinforcement of Ø8 // 200 mm (Subcase 2.5)

L\ h	100	125	150	175	200	225	250
2.0	26.9	49.0	60.6	71.4	81.9	92.1	102.1
2.5	12.9	31.3	42.7	51.1	59.2	67.1	74.7
3.0	6.7	17.1	29.9	38.8	45.4	51.7	57.9
3.5	3.6	9.9	17.7	28.8	36.2	41.5	46.7
4.0	-	5.8	10.9	18.1	27.7	32.6	37.4
4.5	-	3.4	6.7	11.6	18.2	24.8	28.5
5.0	-	-	4.1	7.5	12.1	18.2	22.1
5.5	-	-	2.3	4.7	8.0	12.4	17.4
6.0	-	-	-	2.8	5.2	8.4	12.6

(i) Design table

L\ h	100	125	150	175	200	225	250
2.0	0.0	39.5	52.2	61.6	69.9	76.7	82.4
2.5	0.0	34.4	59.1	69.4	77.4	83.8	89.2
3.0	0.0	3.1	54.6	76.7	85.3	92.1	97.7
3.5	0.0	0.0	21.3	72.1	92.9	100.2	106.1
4.0	-	0.0	0.0	37.7	87.3	98.2	107.8
4.5	-	0.0	0.0	10.3	52.7	86.7	95.3
5.0	-	-	0.0	0.0	24.2	66.7	84.4
5.5	-	-	0.0	0.0	0.0	37.5	74.6
6.0	-	-	-	0.0	0.0	11.8	50.5

(ii) Comparison with Subcase 2.4

Table 7.20 Design table for slabs with a transversal reinforcement of Ø10 // 200 mm (Subcase 2.6)

L\ h	100	125	150	175	200	225	250
2.0	26.9	53.9	68.2	81.7	94.7	107.3	119.6
2.5	12.9	31.3	48.4	58.9	69.0	78.8	88.3
3.0	6.7	17.1	29.9	43.3	52.3	61.2	69.0
3.5	3.6	9.9	17.7	28.8	37.4	43.9	50.4
4.0	-	5.8	10.9	18.1	27.7	32.6	37.4
4.5	-	3.4	6.7	11.6	18.2	24.8	28.5
5.0	-	-	4.1	7.5	12.1	18.2	22.1
5.5	-	-	2.3	4.7	8.0	12.4	17.4
6.0	-	-	-	2.8	5.2	8.4	12.6

(i) Design table

L\ h	100	125	150	175	200	225	250
2.0	0.0	53.3	71.5	84.8	96.2	105.7	113.6
2.5	0.0	34.4	80.6	95.4	106.8	115.9	123.5
3.0	0.0	3.1	54.6	97.0	113.5	127.3	135.3
3.5	0.0	0.0	21.3	72.1	99.3	111.7	122.4
4.0	-	0.0	0.0	37.7	87.3	98.2	107.8
4.5	-	0.0	0.0	10.3	52.7	86.7	95.3
5.0	-	-	0.0	0.0	24.2	66.7	84.4
5.5	-	-	0.0	0.0	0.0	37.5	74.6
6.0	-	-	-	0.0	0.0	11.8	50.5

(ii) Comparison with Subcase 2.4

Table 7.21 Design table for slabs with a transversal reinforcement of Ø10 // 200 mm and a longitudinal reinforcement of Ø12 // 205 mm (Subcase 2.7)

L\ h	100	125	150	175	200	225	250
2.0	28.7	67.5	104.5	127.9	131.1	134.3	136.6
2.5	13.8	33.4	57.6	84.3	102.6	106.6	108.3
3.0	7.2	18.3	32.1	51.4	70.1	82.6	89.4
3.5	3.9	10.6	19.1	31.0	46.8	59.5	68.6
4.0	2.0	6.3	11.8	19.5	29.9	43.2	51.4
4.5	-	3.7	7.4	12.6	19.7	28.9	39.5
5.0	-	2.1	4.5	8.2	13.2	19.7	27.9
5.5	-	-	2.7	5.3	8.9	13.6	19.6
6.0	-	-	-	3.2	5.8	9.3	13.8

(i) Design table

L\ h	100	125	150	175	200	225	250
2.0	6.4	91.9	162.8	189.4	171.8	157.6	144.0
2.5	6.8	43.0	114.9	179.4	207.5	192.2	174.1
3.0	7.6	10.2	65.6	133.6	186.0	206.8	205.1
3.5	9.0	7.5	30.4	85.0	149.2	187.2	203.1
4.0	-	8.5	8.2	48.7	102.1	163.1	185.5
4.5	-	10.3	9.3	19.9	65.4	117.5	171.0
5.0	-	-	11.2	9.9	35.5	81.0	132.1
5.5	-	-	14.9	11.8	10.3	50.4	95.9
6.0	-	-	-	15.4	12.3	23.7	65.0

(ii) Comparison with Subcase 2.4

7.4 Summary

Over this chapter three types of analyses were performed, concerning the design values and the bearing capacity of steel-concrete composite slabs with transversal bars intersecting the profiled steel sheeting.

On a first stage, a quantitative and economic analysis was performed taking in consideration three slabs with the same load conditions but composed by three different types of reinforcement to increase the longitudinal shear resistance. From the quantitative and economic analysis, it was observed that composite slabs with transversal bars intersecting the profiled steel sheeting could be less expensive for slabs with current spans and submitted to higher loads. The examples considered allowed to observe a reduction of cost higher than 10% for these cases, just in terms of costs associated to the raw materials used on the slabs. For longer spans, where even composite slabs with embossed profiles could attain their bending capacity, the amount of concrete necessary to resist a

certain level of load does not depend on the reinforcing system and composite slabs with transversal bars would be more expensive. The reduction of the height of the slabs due to the improvement of their longitudinal shear behaviour also allow to reduce their self-weight and the global cost of the whole structure.

On the second stage, the efficiency of the reinforcing system was assessed in function of the profiled steel sheeting thickness, the total height of the slab and the steel grade. As it was observed on experimental and numerical studies that were presented on previous chapters, the thickness and the steel grade of the profiled steel sheeting influence significantly the efficiency of the proposed reinforcing system. It was observed that these values could influence more the capacity of composite slabs with transversal bars intersecting the profiled steel sheeting than of composite slabs just with embossments on the steel profile. The height of the slab was found to have the same influence on the capacity of the slab for both situations.

Finally, the efficiency of the proposed reinforcing system in terms of load capacity was shown, making use of the design tables of steel-concrete composite slabs developed on the scope of the present research work.

The design tables were even used to show the influence of other items, such as the use of the *m-k* method versus the partial connection method and the use of the design model for vertical shear with or without the profiled steel sheeting contribution. From the several comparative analyses performed, some final remarks can be established:

i. the proposed reinforcing system, combined or not with longitudinal reinforcement, increase significantly the bearing capacity of composite slabs with current spans; this effect is higher in composite slabs with thicker steel sheeting (Case 2);
ii. as it was expected, the *m-k* method is too conservative because it assumes that all slabs are characterized by a brittle behaviour; moreover, the method is not prepared to predict the longitudinal shear resistance of composite slabs that incorporates additional reinforcing systems, with additional experimental tests.
iii. the vertical shear resistance only governs the capacity of slabs with very short spans; however, to reproduce it in the design stage, the design model of standard EN 1994-1-1 (CEN, 2004b) needs revision.

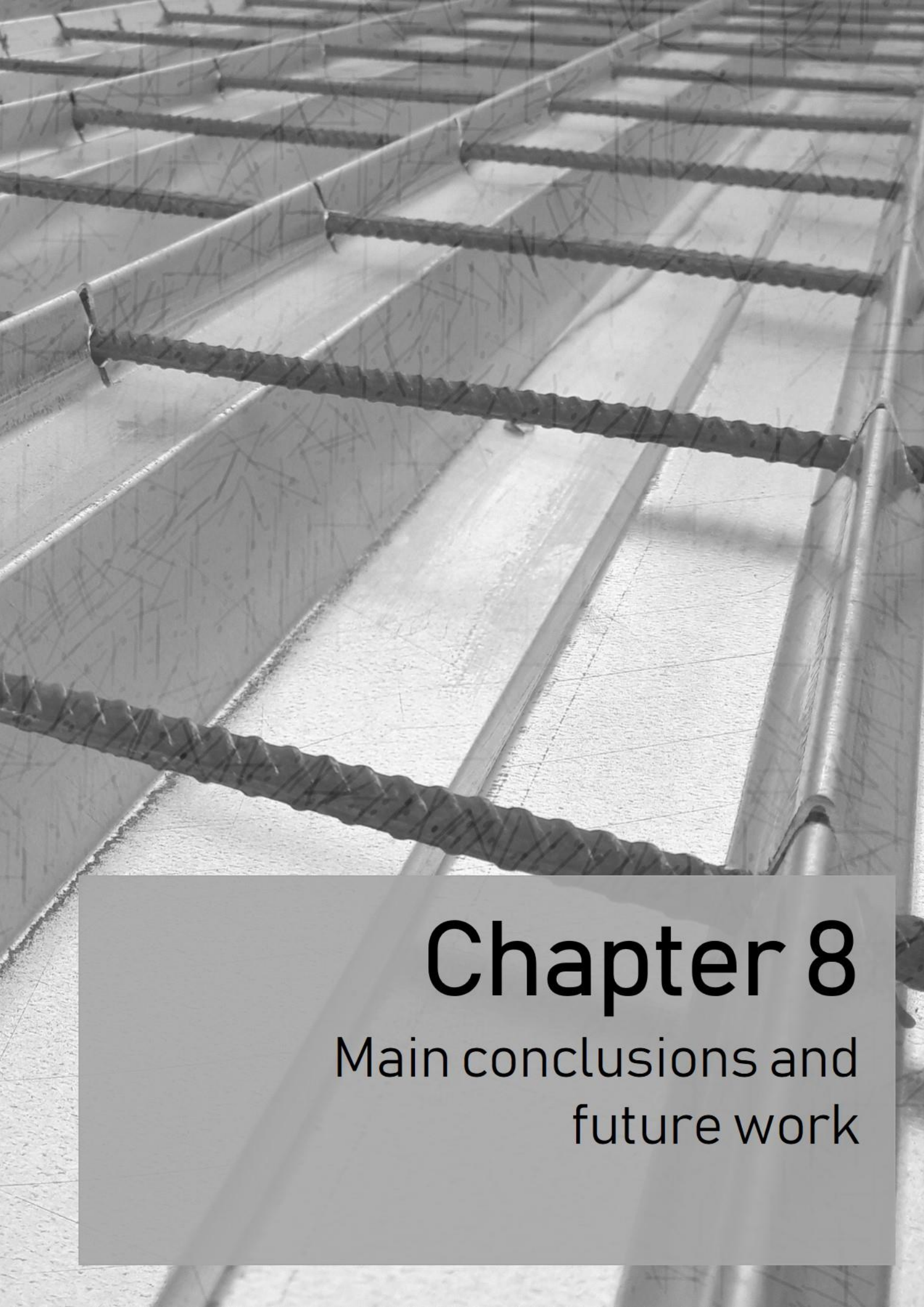

Chapter 8

Main conclusions and future work

8.1 Summary of the developed work

The main objective of the present research work was the development of an innovative reinforcing system in order to optimise the structural performance of composite slabs in the building construction. The reinforcing system proposed is defined by transversal bars intersecting longitudinal stiffeners placed on the upper flanges of the profiled steel sheeting. This intersection provides a mechanical interlock device which allows an increase in the connection degree between the steel sheeting and the concrete. In addition, design models were discussed and some proposals for revision were presented to allow to take advantage of the proposed reinforcing system. Particular emphasis was given to the design model of Eurocode 4 for the vertical shear resistance.

In the first chapter, a brief introduction to the topic was presented. The main objectives were defined at the beginning and after the presentation of all the development work it may be assumed that these objectives were successfully achieved, i.e., a new reinforcing system was developed and the experimental programmes and numerical studies that were carried out proved its high efficiency.

The second chapter presented the state of the art concerning the behaviour of steel-concrete composite slabs and reinforcing systems that have been developed over the last years. First, a brief presentation about different experimental approaches was made to show how the longitudinal shear behaviour is typically characterised. Then, several reinforcing systems developed by several researchers were presented. However, these previous proposals do not allow for the bending resistance of steel-concrete composite slabs to be achieved or no approaches were provided in order to take it into consideration on the design model of steel-concrete composite slabs. These facts also motivated the actual investigation to contribute with new methods to the improvement of the behaviour of composite slabs. A literature review about the vertical shear behaviour and design of steel-concrete composite slabs was also presented. Some different approaches to design steel-concrete composite slabs for vertical shear were found and were presented as a starting point for the discussion of the design model prescribed on standard EN 1994-1-1 (CEN, 2004b).

In Chapter 3 the design of steel-concrete composite slabs according to standard EN 1994-1-1 (CEN, 2004b) was presented. Some basic concepts were described at the beginning which were important to understand the main concepts involved in the design of steel-concrete composite slabs on the two stages: construction phase and definitive (composite) phase. Firstly, the design of the constructive phase was explained, during which the profiled steel sheeting should be designed to support all the construction loads

(self-weight and construction imposed loads); the design at this stage is performed according to standard EN 1993-1-3 (CEN, 2006a). Then, the design for the definitive phase, according to standard EN 1994-1-1 (CEN, 2004b), was presented and explained, where the slab should be designed as a composite member to support all additional loads (self weight of finishing, partition walls, imposed loads, amongst others).

In Chapter 4 the development of the reinforcing system and the experimental study were presented. An extensive experimental campaign was carried out and presented along the chapter. Firstly, several experimental tests were carried out on a first and preliminary experimental campaign in order to establish a first assessment concerning the behaviour of steel-concrete composite slabs with transversal bars. From the preliminary experimental campaign, it was possible to verify the potential of the reinforcing system on the improvement of the behaviour of composite slabs. Based on the results obtained during that experimental programme, a push-out experimental campaign was carried out on small-scale experimental specimens to obtain the resistance on each contact point between the transversal bars and the steel sheeting, the two main components of the reinforcing system. Then, a statistical approach, based on these latter experimental results, such as prescribed by Annex D from standard EN 1990 (CEN, 2002a), was performed. The statistical approach comprised the comparison of the experimental results with theoretical values, which made it possible to calibrate an equation to determine the design value of the resistance of the reinforcing system. This model was then accounted in the partial connection method provided by standard EN 1994-1-1 (CEN, 2004b). Finally, a second experimental programme on simply-supported and continuous composite slabs, incorporating some improvements relative to the ones carried out on the preliminary campaign, was carried out. This second programme allowed the validation of the design approach previously developed and to prove the efficiency and ductility provided by the reinforcing system.

In order to complement the findings from the experimental tests and to validate the accuracy of the design approach proposed for composite slabs with transversal bars intersecting the profiled steel sheeting, a numerical study using the software *Abaqus* was performed and presented in Chapter 5. Based on several approaches available in the bibliography, numerical models were calibrated to simulate the behaviour of composite slabs with the proposed reinforcing system. These models were validated using the experimental results obtained in the second experimental programme and then used to perform an extensive parametric study to show the influence of several geometric and mechanical parameters on the resistance of the reinforcing system and on the ductility of the slabs.

The Chapter 6 presented a study concerning the vertical shear behaviour of steel-concrete composite slabs. As was mentioned before, european standard EN 1994-1-1 (CEN, 2004b) prescribes that composite slabs should be designed for vertical shear in accordance with EN 1992-1-1 (CEN, 2004a), using expressions derived and calibrated for reinforced concrete slabs, which does not take into account profiled steel sheeting. Steel sheets however have a significant vertical shear resistance provided by the webs of the profile, which is used to resist all loads on construction phase, and that is then not taken into account adequately in the design of composite slabs on the definitive (composite) phase. To accomplish his issue, an experimental campaign was carried out on short span composite slabs with transversal bars distributed over the shear span to make them fail by vertical shear. The obtained results were then compared with the sum of the vertical shear design value according to standard EN 1994-1-1 (CEN, 2004b) and the vertical shear design value of the profiled steel sheeting according to standard EN 1993-1-3 (CEN, 2006a). Also a numerical parametric study was performed to study the contribution of profiled steel sheeting in the vertical shear resistance of composite slabs.

Finally, taking into account all the work developed over the previous chapters, the efficiency of the reinforcing system was assessed through several comparative analyses performed and presented in Chapter 7. Firstly, a quantitative and economical study was performed to understand the variation of the quantity of materials and the cost of slabs with transversal bars (the reinforcing system developed) comparatively with traditional composite slabs with embossed profiles. Then, using a design tool developed to provide design tables considering the innovative aspects developed over this research (which is presented in Annex A), the influence of the steel sheet thickness, the steel grade and the height of the slab on the bearing capacity of composite slabs was studied. The final analysis performed was developed to show the efficiency of the proposed reinforcing system by comparison of design tables obtained from the developed tool. The influence of the longitudinal and vertical shear design approaches was also shown in this manner. Finally, some examples were presented to show the load increase when transversal bars are placed intersecting the profiled steel sheeting and also when these are combined with longitudinal reinforcement.

The main conclusions obtained and presented over the thesis are described in the section 8.2; section 8.3 contains some proposals for future research work concerning the behaviour of steel-concrete composite slabs with transversal bars and; the scientific material developed in the scope of the present study is listed in the section 8.4.

8.2 Main conclusions

The work developed on this thesis was mainly conducted in the scope of the national research project INOV_LAMI – *Desenvolvimento de Sistemas de Reforço Inovadores e Aperfeiçoamento dos Modelos de Cálculo para Lajes Mistas de Aço e Betão* (Development of innovative reinforcing systems and improvement of the design models for steel-concrete composite slabs) – financed by FEDER funds through the Competitivity Factors Operational Programme – COMPETE 2020/Portugal 2020/EU and also designated as project POCI-01-0247-FEDER-003483. This research project was carried out in the University of Coimbra, in a partnership between the Department of Civil Engineering and the Portuguese steelwork company *O Feliz Metalomecânica, SA*.

In the scope of this research, an innovative reinforcing system for steel-concrete composite slabs was proposed and studied experimentally, numerically and analytically. The reinforcing system is defined by transversal bars uniformly distributed over the span, crossing longitudinal stiffeners executed on the upper flange of the profiled steel sheeting. The main conclusions obtained from this study are the following:

i. the reinforcing system developed allows for an increase in the connection degree and therefore the longitudinal shear resistance of steel-concrete composite slabs;
ii. the reinforcing system developed allows for utilising the high bending capacity of composite slabs, if properly designed; the efficiency of the proposed reinforcing system increases when the total height of the slab h, the steel sheeting thickness t, the diameter of transversal bars d and the steel grade are increased or when the spacing between transversal bars l_b is reduced;
iii. proposed reinforcing system allows for achieving higher levels of ductility, which means that the maximum load achieved is significantly higher than the load observed when the slip starts to occur;
iv. taking into account the bearing failure mode at the contact points between the transversal bars and the profiled steel sheeting, the proposed reinforcing system is all the more effective the greater the thickness and the higher the steel grade of the steel sheet;
v. if the transversal bars are continuous along the perpendicular direction of the ribs of profiled steel sheeting, the transversal stiffness in the plane of the slab is increased, making the diaphragm effect more effective, which is beneficial to the resistance to horizontal actions, such as the wind and seismic actions;
vi. the proposed reinforcing system could be combined with the most common longitudinal shear resistant system constituted by embossments along the

profiled steel sheeting, although this needs to be confirmed through additional research;

vii. with the proposed reinforcing system, the behaviour of the slab is independent of end anchorage devices, which are normally dependent on the way the slab is supported, and the material and shape of the supporting beams;

viii. the longitudinal shear capacity is no longer dependent on other possible reinforcing systems, such as the end anchorage device provided by headed studs welded to the supporting beams through the steel sheeting, which requires in-situ welding techniques;

ix. the design methodology based on the partial connection method, incorporating the longitudinal shear strength acquired by the proposed reinforcing system, was validated experimentally and numerically and may be used to predict the resistance of a composite slab;

x. analytical predictions allow for the observation that in some cases it is possible to achieve a load around two times higher on slabs with transversal bars intersecting the profiled steel sheeting when compared to traditional solutions; if longitudinal reinforcement is combined with transversal bars the bearing capacity is even higher;

xi. analytical predictions allow for the observation that the reinforcing system tends to be more effective for steel-concrete composite slabs with current spans and subjected to higher levels of load.

Regarding the study on the vertical shear resistance of composite slabs presented in Chapter 6, some conclusions were reached and presented:

i. the experimental results obtained in the scope of this study, even if there are few in quantity, show that the vertical shear capacity of composite slabs can be much higher (up to 5 times higher in the tests performed) than the resistance value obtained according to the design model prescribed in Eurocode 4;

ii. the same conclusions were established from numerical simulations performed;

iii. the design model for the vertical shear resistance of steel-concrete composite slabs, as prescribed in standard EN 1994-1-1 is rather conservative; this model could lead to an over-dimensioning of composite slabs with short spans, or even slabs with spans currently used in construction but where some reinforcing systems to improve the longitudinal shear behaviour are used;

iv. the over-dimensioning originated from the design model of Eurocode 4 is due to the fact that the contribution of the steel sheet to the vertical shear resistance of the slab is not taken into account adequately;

v. based on the results obtained and presented in the present thesis, the sum of the contribution of the concrete ribs with the contribution of the steel web of profiled sheet can be used to predict the vertical shear resistance of composite slabs with high degree of longitudinal shear connection.

8.3 Proposals for future research work

The main objectives of the present research were accomplished: an innovative reinforcing system to increase the longitudinal shear resistance which allow to achieve the full bending capacity of composite slabs was developed; additionally, a design methodology to take into account its contribution on the design of steel-concrete composite slabs was also developed and validated based on experimental and numerical studies. However, in order to optimise the use of composite slabs with the reinforcing system developed in construction industry, further additional investigation is still needed. In order to complement the outcome of the current research, the following topics are proposed to be object of future research:

i. the first topic refers to the combined effect of the transversal bars intersecting the profiled steel sheeting and the embossments in the profile. Actually, if end anchorages devices, such as headed studs welded to the supporting beams through the profiled steel sheeting are used, clause 9.7.4(2) of standard EN 1994-1-1 (CEN, 2004b) allows to sum the resistance of head studs to the value of the design value of the compressive normal force in the concrete N_c for application of the partial connection method. Therefore, additional studies would be necessary to verify if the longitudinal shear resistance acquired by the transversal bars can be summed to the longitudinal shear resistance acquired by the embossments of the profiled steel sheeting in composite slabs where both solutions are adopted; this combined effect of the two systems could lead to a reduction of the number and/or diameter of the transversal bars necessary to ensure a required load capacity;
ii. over this research, it was shown that the vertical shear design model of steel-concrete composite slabs in accordance with standard EN 1994-1-1 (CEN, 2004b) is conservative. Based on the experimental tests carried out a proposal based on the sum of the contribution of the concrete rib plus the webs of the steel sheeting was presented. However, this may be valid only for composite slabs with high degree of longitudinal shear connection. For current slabs, typically working in partial shear connection, additional studies (experimental and numerical approaches) should be carried out, to allow for a revision of the design model, of the referred standard, in order to increase the competitiveness of the solution;

iii. the knowledge concerning the longitudinal shear behaviour of steel-concrete continuous composite slabs could also be deepened. Standard EN 1994-1-1 (CEN, 2004b) prescribes that continuous composite slabs may be designed as a series of simply supported spans. However, for slabs with higher connection degree, this approach tends to be too conservative. The longitudinal shear behaviour on the hogging bending moment regions should be further investigated and the existing design methodologies improved accoredingly;
iv. the numerical simulations carried out were validated according to the load capacity of the slab, the crack pattern and the end slip. However, the initial stiffness of the slabs obtained through numerical results was around two times higher than the one observed through experimental results. This fact could be justified by the perfect full contact between the profiled steel sheeting and the transversal bars considered on the numerical simulations, whereas in the real experiments, the contact between the profiled steel sheeting and the profiled steel sheeting on the produced specimens has presented some gaps, which may result in a reduction of the stiffness of the slab. Taking this issue into consideration, some additional numerical studies may be carried out in order to reach a better approximation to the experimental results and to allow for additional findings regarding the structural behaviour of composite slabs.

8.4 Dissemination of the present work

(i) Patent

i. "*Sistema de reforço para lajes mistas com chapa perfilada*" (Reinforcing system for composite slabs with profiled steel sheeting) – Patent registered

(ii) Journal papers

i. Simões, R. and Pereira, M. (2020). An innovative system to increase the longitudinal shear capacity of composite slabs. *Steel and Composite Structures* (submitted, under review);
ii. Pereira, M. and Simões, R. (2019). Contribution of the steel sheeting to the vertical shear capacity of composite slabs. *Journal of Constructional Steel Research, 161*, 275–284. (Pereira and Simões, 2019).

(iii) Other papers

i. Simões, R. and Pereira, M. (2019). Vertical shear behaviour of steel-concrete composite slabs. Ce/papers – the online collection for conference papers in civil engineering. Vol. 3, issue 3&4, 289-294. (Simões and Pereira, 2019);
ii. Pereira, M., Simões, R. and Duarte, J. (2017). Analysis of the vertical shear design model for steel-concrete composite slabs. Ce/papers – the online collection for conference papers in civil engineering. Vol. 1, issue 4, 405-414. (Pereira *et al.*, 2017b).

(iv) Proceeding papers

i. Pereira, M., Simões R. and Craveiro, H. (2020). Conception and design of high-performance steel-composite slabs. The 9th European Conference on Steel and Composite Structures – EUROSTEEL 2020. Ernst & Sohn. Sheffield, United Kingdom 9th – 11th September 2020 (accepted);
ii. Pereira, M. and Simões R. (2019). Avaliação numérica da eficácia de um Sistema de reforço ao corte longitudinal em lajes mistas de aço e betão. XII Congresso de Construção Metálica e Mista. CMM – Associação Portuguesa de Construção Metálica e Mista. Coimbra, Portugal 21st - 22nd November 2019, 575-583;
iii. Simões, R. and Pereira, M. (2019). Sistema inovador para reforço de lajes mistas ao corte longitudinal. XII Congresso de Construção Metálica e Mista. CMM – Associação Portuguesa de Construção Metálica e Mista. Coimbra, Portugal 21st – 22nd November 2019, 1083-1092;
iv. Simões, R. and Pereira, M. (2019). Vertical shear behaviour of steel-concrete composite slabs. The 14th Nordic Steel Construction Conference. Copenhagen, Denmark, 18th – 20th September 2019;
v. Pereira, M., Simões, R. and Duarte, J. (2017). Análise dos modelos de verificação do esforço transverso em lajes mistas de aço e betão. XI Congresso de Construção Metálica e Mista. CMM – Associação Portuguesa de Construção Metálica e Mista. Coimbra, Portugal 23rd – 24th November 2017, 645-654.

(v) Presentations

i. Pereira, M. (2019). Development of a new reinforcing system for steel-concrete composite slabs. Presentation on "2019 ISISE Day-Out & 9th PhD Workshop", Braga, 24th September 2019;
ii. Pereira, M. (2019). Innovative systems for steel-concrete composite slabs. Presentation on Friday @ ISISE, Coimbra, 17th May 2019;

iii. Simões, R. and Pereira, M. (2018). Composite slabs: Design Models, Innovation and Improvement of the Structural Behaviour. Oral presentation on "Journée Technique Labcom anr B-Hybrid Structures Hybrides Béton-Acier", Rennes, France, 29 March 2018;
iv. Simões, R. and Pereira M. (2016). Composite slabs – ongoing research on structural behaviour and design models. Oral presentation on "The ECCS Open Workshop on Composite Construction", Delft, Netherlands, 20 October 2016.

REFERENCES

Abas, F. M., Gilbert, R. I., Foster, S. J., & Bradford, M. A. (2013). Strength and serviceability of continuous composite slabs with deep trapezoidal steel decking and steel fibre reinforced concrete. *Engineering Structures*, *49*, 866–875. https://doi.org/10.1016/j.engstruct.2012.12.043

Abdullah, R., & Easterling, W. S. (2009). New evaluation and modeling procedure for horizontal shear bond in composite slabs. *Journal of Constructional Steel Research*, *65*(4), 891–899. https://doi.org/10.1016/j.jcsr.2008.10.009

Abdullah, R., Paton-cole, V. P., Easterling, W. S., & Asce, F. (2007). Quasi-Static Analysis of Composite Slab. *Malaysian Journal of Civil Engineering*, *19*(2), 1–13.

ABNT. (2008). *ABNT NBR 8800: Projeto de estruturas de aço e de estruturas mistas de aço e concreto de edifícios*. *Anbt*. https://doi.org/01.080.10; 13.220.99

ABNT. (2010). *ABNT NBR 14762: Dimensionamento de estruturas de aço constituídas por perfis formados a frio*. Rio de Janeiro: Associação brasileira de Normas Técnicas.

Abspoel, R., Stark, J. . W. B., & Prins, H. (2018). The influence of vertical shear on the hogging bending moment resistance of ComFlor composite slabs. In *12th International Conference on Advances in Steel-Concrete Composite Structures* (pp. 183–190). València: ASCCS.

Ackermann, F. P., & Schnell, J. (2008). Steel Fibre Reinforced Continuous Composite Slabs. *International Conference on Composite Construction in Steel and Concrete*, *41142*(January 2008), 125–137. https://doi.org/10.1061/41142(396)11

Ahmed, S. M., Avudaiappan, S., Sheet, I. S., Saavedra Flores, E. I., Pina, J. C., Yanez, S. J., & Guzmán, C. F. (2019). Prediction of longitudinal shear resistance of steel-concrete composite slabs. *Engineering Structures*, *193*(April), 295–300. https://doi.org/10.1016/j.engstruct.2019.05.010

Ali, A. M., Farid, B., & Al-janabi, A. (1990). Stress-Strain Relationship for Concrete in Compression Madel of Local Materials. *JKAU: Eng. Sci*, *2*, 183–194. Retrieved from http://www.kau.edu.sa/Files/135/Researches/54136_24603.pdf

Altoubat, S., Ousmane, H., & Barakat, S. (2015). Effect of fibers and welded-wire reinforcements on the diaphragm behavior of composite deck slabs. *Steel and Composite Structures*, *19*(1), 153–171. https://doi.org/10.12989/scs.2015.19.1.153

An, L. (1993). *Load Bearing Capacity and Behaviour of Composite Slabs with Profiled Steel Sheet*. Chalmers University of Technology.

ANSI. (2007). AISI S100-2007: North American Specification for the Design of Cold-

formed Steel Structural Members. American National Standards Institute; Steel Deck Institute.

ANSI, & SDI. (2012). C-2011 Standard for Composite Steel Floor Deck - Slabs. American National Standards Institute; Steel Deck Institute.

Ansourian, P. (1981). Experiments on continuous composite beams. *Proc. Instn Civ. Engrs Part 2*, *71*, 25–51.

Arrayago, I., Ferrer, M., Marimon, F., Real, E., & Mirambell, E. (2018). Experimental investigation on ferritic stainless steel composite slabs. *Engineering Structures*, *174*(April), 538–547. https://doi.org/10.1016/j.engstruct.2018.07.084

Arrayago, I., Real, E., Mirambell, E., Marimon, F., & Ferrer, M. (2019). Experimental study on ferritic stainless steel trapezoidal decks for composite slabs in construction stage. *Thin-Walled Structures*, *134*(June 2018), 255–267. https://doi.org/10.1016/j.tws.2018.10.012

Attarde, S. (2014). *Nonlinear Finite Element Analysis of Profiled Steel Deck Composite Slab System*. Ryerson University.

Balan, T. A., Spacone, E., & Kwon, M. (2001). A 3D hypoplastic model for cyclic analysis of concrete structures. *Engineering Structures*, *23*(4), 333–342. https://doi.org/10.1016/S0141-0296(00)00048-1

Bažant, Z. P. (2002). Concrete fracture models: Testing and practice. *Engineering Fracture Mechanics*, *69*(2), 165–205. https://doi.org/10.1016/S0013-7944(01)00084-4

Bezerra, L. M., Cavalcante, O. O., Chater, L., & Bonilla, J. (2018). V-shaped shear connector for composite steel-concrete beam. *Journal of Constructional Steel Research*, *150*, 162–174. https://doi.org/10.1016/j.jcsr.2018.07.016

Birtel, V., & Mark, P. (2006). Parameterised Finite Element Modelling of RC Beam Shear Failure. In *ABAQUS Users' Conference* (pp. 95–108).

Blaβ, H. J., & Saal, H. (2006). *Experimentelle Trayfähigkeitsuntersuchung von Stahlblechprofilen COFRADAL 60 PLUS. Fa. PAB Nord Groupe USINOR S.A. Bericht Nr: 993016-a*. Nanterre, France.

Bridge, R. Q., & Patrick, M. (2002). Innovations in composite slabs incorporating profiled steel sheeting. *Advances in Building Technology*, *1*, 191–198. https://doi.org/10.1016/b978-008044100-9/50024-3

Bruedern, A., Mechtcherine, V., Kurz, W., & Jurisch, F. (2012). Self-compacting lightweight aggregate concrete for composite slabs. *Concrete Beton Journal*, *130*, 9–13. https://doi.org/10.1201/b10162-17

BSi. (1994). BS 5950-4. Structural use of steelwork in building - Part4: Code of practice for design of composite slabs with profiled steel sheeting. London, UK: British Standard institution.

Burnet, M. J., & Oehlers, D. J. (2001). Rib shear connectors in composite profiled slabs. *Journal of Constructional Steel Research*, *57*(12), 1267–1287.

https://doi.org/10.1016/S0143-974X(01)00038-4

Calixto, J. M., Lavall, A. C., Melo, C. B., Pimenta, R. J., & Monteiro, R. C. (1998). Behaviour and strength of composite slabs with ribbed decking. *Journal of Constructional Steel Research*, *46*(1–3), 211–212. https://doi.org/10.1016/S0143-974X(98)00127-8

Campista, F. F., & da Silva, J. G. S. (2018). Vibration analysis of steel–concrete composite floors when subjected to rhythmic human activities. *Journal of Civil Structural Health Monitoring*, *8*(5), 737–754. https://doi.org/10.1007/s13349-018-0303-6

Carmona, R. L., Branco, J. C., & Simões, R. (2009). Lajes mistas com chapa colaborante: Soluções para melhorar o seu comportamento. In *VII Congresso de Construção Metálica e Mista* (pp. II-593-II–604). Lisbon, Portugal: CMM - Associação portuguesa de Construção Metálica e Mista.

CEN. (2002a). EN 1990. Eurocode - Basis of structural design. Brussels: European Commitee for Standardization.

CEN. (2002b). EN 1991-1-1. Eurocode 1: Actions on structures - Part 1-1: General actions - Densities, self-weight, imposed loads for buildings. Brussels: European Commitee for Standardization.

CEN. (2002c). EN 1991-1-1. Eurocode 1: Actions on structures - Part 1-1: General actions - Densities, selfweight, imposed loads for buildings. Brussels: European Commitee for Standardization.

CEN. (2004a). EN 1992-1-1. Eurocode 2: Design of concrete structures - Part 1-1-: General rules and rules for buildings. Brussels: European Commitee for Standardization.

CEN. (2004b). EN 1994-1-1. Eurocode 4: Design of Composite Steel and Concrete Structures - Part 1-1: General Rules and Rules for Buildings. Brussels: European Commitee for Standardization.

CEN. (2005a). EN 1991-1-6. Eurocode 1 - Actions on structures; Part 1-6: General actions - Actions during execution. Brussels: European Commitee for Standardization.

CEN. (2005b). EN 1993-1-1. Eurocode 3: Design of steel structures - Part 1-1: General rules and rules for buildings. Brussels: European Commitee for Standardization.

CEN. (2005c). EN 1993-1-8. Eurocode 3: Design of steel structures - Part 1-8: Design of joints. Bruxelas: European Commitee for Standardization.

CEN. (2005d). EN 1994-1-2. Eurocode 4 - Design of composite steel and concrete structures - Part 1-2: General rules - Structural fire design Eurocode. Brussels: European Commitee for Standardization.

CEN. (2006a). EN 1993-1-3. Eurocode 3 - Design of steel structures; Part 1-3: General rules - Supplementary rules for cold-formed members and sheeting Eurocode. Brussels: European Commitee for Standardization.

CEN. (2006b). EN 1993-1-4. Eurocode 3 - Design of steel structures - Part 1-4: General rules - Supplementary rules for stainless steels. Brussels: European Commitee for Standardization. https://doi.org/10.2514/2.2772

CEN. (2006c). EN 1993-1-5. Eurocode 3 - Design of steel structures - Part 1-5: Plated structural elements. Brussels: European Commitee for Standardization.

Chaudhari, S. V., & Chakrabarti, M. A. (2012). Modeling of Concrete for Nonlinear Analysis using Finite Element Code ABAQUS. *International Journal of Computer Applications*, *44*(7), 14–18. https://doi.org/10.5120/6274-8437

Chen, S. (2003). Load carrying capacity of composite slabs with various end constraints. *Journal of Constructional Steel Research*, *59*(3), 385–403. https://doi.org/10.1016/S0143-974X(02)00034-2

Chen, S., Shi, X., & Qiu, Z. (2011). Shear bond failure in composite slabs- A detailed experimental study. *Steel and Composite Structures*, *11*(3), 233–250. https://doi.org/10.12989/scs.2011.11.3.233

Chen, S., Shi, X., & Zhou, Y. (2014). Strength of composite slabs with end-anchorage studs. *Structures & Buildings*, *168*(2), 127–140. https://doi.org/10.1680/stbu.13.00039

Chen, S., Zhang, R., & Zhang, J. (2018). Human-induced vibration of steel-concrete composite floors. *Proceedings of the Institution of Civil Engineers: Structures and Buildings*, *171*(1), 50–63. https://doi.org/10.1680/jstbu.16.00179

Chuan, D. L. Y., Abdullah, R., & Bakar, K. B. (2008). BEHAVIOUR AND LOAD BEARING CAPACITY OF COMPOSITE SLAB ENHANCED WITH SHEAR SCREWS, *8*(6), 501–549.

Cifuentes, H., & Medina, F. (2013). Experimental study on shear bond behavior of composite slabs according to Eurocode 4. *Journal of Constructional Steel Research*, *82*, 99–110. https://doi.org/10.1016/j.jcsr.2012.12.009

Cornellissen, H., Hordijk, D., & Reinhardt, H. (1986). Experimental determination of crack softening characteristics of normal weight and lightweight concrete. *Heron*, *31*(2), 45–56.

Crisinel, M. (1990). Composite Slabs. *IABSE Reports*, *61*, 69–87.

Crisinel, M., & Edder, P. (2006). New method for the design of composite slabs. *Proceedings of the 5th International Conference on Composite Construction in Steel and Concrete V*, *40826*(January), 166–177. https://doi.org/10.1061/40826(186)17

Crisinel, M., Ferrer, M., Marimón, F., & Rossich Verdes, M. (2006). Influence of sheet surface conditions and concrete strength on the longitudinal shear resistance of composite slabs. In *A Forecast of the Future for Steel and Composite Steel-Concrete Structures - Professor Jean-Marie Aribert Retirement Symposium* (pp. 233–244). Rennes, France.

Crisinel, M., & Marimon, F. (2004). A new simplified method for the design of composite slabs. *Journal of Constructional Steel Research*, *60*(3–5), 481–491.

https://doi.org/10.1016/S0143-974X(03)00125-1

Crisinel, M., Schumacher, A., & Lääne, A. (2002). Nouvelle méthode de calcul des dalles mixtes à tôles profilées. *Tracés : Bulletin Technique de La Suisse Romande*, *128*.

Daniels, B. J. (1990). *Comportement et capacité portante des dalles mixtes modélisation mathématique et etude expérimentale*. Ecole Polytechnique Fédérale de Lausanne.

Daniels, B. J., & Crisinel, M. (1993a). Composite Slab Behavior and Strength Analysis. Part I:Calculation Procedure. *Jornal of Structural Engineering*, *119*(1), 16–35.

Daniels, B. J., & Crisinel, M. (1993b). Composite Slab Behavior and Strength Analysis. Part II: Comparisons with test results and parametric analysis, *119*(1), 36–49.

de Andrade, S. A. L., Vellasco, P. C. G. da S., da Silva, J. G. S., & Takey, T. H. (2004). Standardized composite slab systems for building constructions. *Journal of Constructional Steel Research*, *60*(3–5), 493–524. https://doi.org/10.1016/S0143-974X(03)00126-3

Degtyarev, V. V. (2014a). Strength of composite slabs with end anchorages. Part I: Analytical model. *Journal of Constructional Steel Research*, *94*, 150–162. https://doi.org/10.1016/j.jcsr.2013.10.005

Degtyarev, V. V. (2014b). Strength of composite slabs with end anchorages. Part II: Parametric studies. *Journal of Constructional Steel Research*, *94*, 163–175. https://doi.org/10.1016/j.jcsr.2013.10.005

Dere, Y., & Koroglu, M. A. (2017). Nonlinear FE Modeling of Reinforced Concrete. *International Journal of Structural and Civil Engineering Research*, *6*(1), 71–74. https://doi.org/10.18178/ijscer.6.1.71-74

El-sayed, K. M., Nabih, N., & Taha, A. M. (2015). Flexural Behavior of Composite Slab, *5*(3), 1–12. https://doi.org/10.9734/AIR/2015/18847

Feldmann, M., Heinemeyer, C., Butz, C., Caetano, E., Cunha, A., Galanti, F., … Waarts, P. (2009). *Design of floor structures for human induced vibrations* (Vol. 3). JRC Scientific and Technical Reports.

Ferrer, M., & Crisinel, M. (2005). Optimised steel sheet profile for composite slabs - A design optimisation procedure using 3D non-linear finite elements.

Ferrer, M., Marimon, F., & Casafont, M. (2018). An experimental investigation of a new perfect bond technology for composite slabs. *Construction and Building Materials*, *166*, 618–633. https://doi.org/10.1016/j.conbuildmat.2018.01.104

Ferrer, M., Marimon, F., & Crisinel, M. (2006). Designing cold-formed steel sheets for composite slabs: An experimentally validated FEM approach to slip failure mechanics. *Thin-Walled Structures*, *44*(12), 1261–1271. https://doi.org/10.1016/j.tws.2007.01.010

Ferrer, M., Marimon, F., & Roure, F. (2004). Composite Slabs: Parametrical analysis of the longitudinal slide failure mechanics using finite element models. In *3rd International Conference on Advances in Structural Engineering and Mechanics*. Seoul.

Ferrer, M., Marimon, F., Roure, F., & Crisinel, M. (2005). Optimised design of a new profiled steel sheet for composite slabs using 3d non-linear finite elements. In *4th Eurosteel Conference on Steel and Composite Structures*. Maastricht, Netherlands, Netherlands.

Fonseca, A., Marques, B., & Simões, R. (2015). Improvement of the behaviour of composite slabs : A new type of end anchorage. *Steel and Composite Structures*, *19*(6), 1381–1402.

Ganesh, G. M., Upadhyay, A., & Kaushik, S. K. (2005). Simplified Design of Composite Slabs Using Slip Block Test. *Journal of Advanced Concrete Technology*, *3*(3), 403–412. https://doi.org/10.3151/jact.3.403

Genikomsou, A. S., & Polak, M. A. (2015). Finite element analysis of punching shear of concrete slabs using damaged plasticity model in ABAQUS. *Engineering Structures*, *98*, 38–48. https://doi.org/10.1016/j.engstruct.2015.04.016

Gholamhoseini, A. (2018). Experimental and finite element study of ultimate strength of continuous composite concrete slabs with steel decking. *International Journal of Advanced Structural Engineering*, *10*(1), 85–97. https://doi.org/10.1007/s40091-018-0183-3

Gholamhoseini, A., Khanlou, A., MacRae, G., Scott, A., Hicks, S., & Leon, R. (2016). An experimental study on strength and serviceability of reinforced and steel fibre reinforced concrete (SFRC) continuous composite slabs. *Engineering Structures*, *114*, 171–180. https://doi.org/10.1016/j.engstruct.2016.02.010

Gopalaratnam, V. S., & Shah, S. P. (1985). Softening response of plain concrete in direct tension. *J ACI*, *82*, 310–323.

Hamerlinck, R., & Twilt, L. (1995). Fire-Resistance of Composite Concrete Slabs. *Journal of Constructional Steel Research*, *33*(94), 71–85. https://doi.org/10.1007/978-3-642-34393-3_9

Hartmeyer, S., & Kurz, W. (2013). Evaluation of the Shear Force Behaviour of Composite Slabs. In ASCE (Ed.), *Composite Construction in Steel and Concrete VII*. Palm Cove, North Queensland, Australia. https://doi.org/https://ascelibrary.org/doi/10.1061/9780784479735.055

Hechler, O., Feldmann, M., Heinemeyer, C., & Galanti, F. (2008a). Design guide for floor vibrations. In *EUROSTEEL 2008 – 5th European Conference on Steel and Composite Structures – Research – Design – Construction* (pp. 3–5). Graz, Austria.

Hechler, O., Feldmann, M., Heinemeyer, C., & Galanti, F. (2008b). *Design guide for floor vibrations*. Esch-sur-Alzette, Luxembourg.

Hedaoo, Namdeo, Gupta, L., & Ronghe, G. N. (2012). Design of composite slabs with profiled steel decking : A comparison between experimental and analytical studies Design of composite slabs with profiled steel decking : a comparison between experimental and analytical studies. *International Journal of Advanced Structural Engineering*, *3*(1). https://doi.org/10.1186/2008-6695-3-1

Hedaoo, Nemdeo, Raut, N., & Gupta, L. (2015). Composite Concrete Slabs with Profiled

Steel Decking: Comparison Between Experimental and Simulation Study. *American Journal of Civil Engineering*, *3*(5), 157–169. https://doi.org/10.11648/j.ajce.20150305.14

Hicks, S., & Peltonen, S. (2013). Vibration Performance of Composite Floors Using Slim Floor Beams. In *Composite Construction in Steel and Concrete VII* (pp. 185–198).

Hillerborg, A., Modéer, M., & Peterson, P. E. (1976). Analysis of crack formation and crack growth in concrete by means of fracture mechanics and finite elements. *Cement and Concrete Research*, *6*, 773–782. https://doi.org/10.1016/0008-8846(76)90007-7

HIVOSS. (2008). *Vibration Design of Floors: Guideline*. Retrieved from http://www.stb.rwth-aachen.de/projekte/2007/HIVOSS/download.php

Holomek, J., Karásek, R., Bajer, M., & Barnat, J. (2012). Comparison of Methods of Testing Composite Slabs. *International Journal of Mechanical, Aerospace, Industrial, Mechatronic and Manufacturing Engineering*, *6*(7), 1201–1206.

Holomek, Josef, Bajer, M., & Vild, M. (2017). Cast Screws as Shear Anchors for Composite Slabs. *Procedia Engineering*, *195*, 114–119. https://doi.org/10.1016/j.proeng.2017.04.532

Holomek, Josef, Bajera, M., & Vilda, M. (2016). Test Arrangement of Small-scale Shear Tests of Composite Slabs. *Procedia Engineering*, *161*, 716–721. https://doi.org/10.1016/j.proeng.2016.08.749

Hordijk, D. A. (1991). *Local Approach to Fatigue of Concrete*. Delft University of Technology.

Hossain, K. M. A., Attarde, S., & Anwar, M. S. (2019). Finite element modelling of profiled steel deck composite slab system with engineered cementitious composite under monotonic loading. *Engineering Structures*, *186*(January), 13–25. https://doi.org/10.1016/j.engstruct.2019.02.008

Hsu, L. S., & Hsu, C. T. T. (1994). Complete stress - strain behaviour of high-strength concrete under compression. *Magazine of Concrete Research*, *46*(169), 301–312.

ISO. (2009). ISO 6892-1. *Metallic Materials - Tensile Testing - Part 1: Method of Test at Room Temperature*. Switzerland.

Jankowiak, T., & Lodygowski, T. (2005). Identification of parameters of concrete damage plasticity constitutive model. *Foundations of Civil and Environmental Engineering*, (6), 53–69. https://doi.org/10.3390/app6090245

Johnson, R. P. (2018). *Composite Structures of Steel and Concrete: Beams, Slabs, Columns and Frames for Buildings* (4th editio). Oxford, UK: Wiley Blackwell.

Johnson, R. P., & Anderson, D. (2004). Designers' guides to EN 1994-1-1, Eurocode 4: Design of composite steel and concrete structures.

Johnson, R. P., & Shepherd, A. J. (2013). Resistance to longitudinal shear of composite slabs with longitudinal reinforcement. *Journal of Constructional Steel Research*, *82*, 190–194. https://doi.org/10.1016/j.jcsr.2012.12.005

Johnson, R. P., & Yuan, H. (1998). Existing rules and new tests for stud shear connectors in troughs of profiled sheeting. *Proceedings of the Institution of Civil Engineers: Structures and Buildings*, *128*(3), 244–251. https://doi.org/10.1680/istbu.1998.30458

Jolly, C. K., & Lawson, R. M. (1992). End anchorage in composite slabs: an increased loadcarrying capacity. *Structural Engineering*, *70*(11), 202–205.

Kim, B., Wright, H. D., & Cairns, R. (2001). The behaviour of through-deck welded shear connectors: An experimental and numerical study. *Journal of Constructional Steel Research*, *57*(12), 1359–1380. https://doi.org/10.1016/S0143-974X(01)00037-2

Kim Kun-Soo, Han Oneil, Gombosuren Munkhtulga, K. S.-H. (2019). Numerical simulation of Y-type perfobond rib shear connectors using finite element analysis. *Steel and Composite Structures*, *30*(1), 53–67. https://doi.org/DOI: https://doi.org/10.12989/scs.2019.31.1.053

Lauwens, K., Fortan, M., Arrayago, I., Mirambell, E., & Rossi, B. (2018). On the shear resistance of ferritic stainless steel composite slabs. *Construction and Building Materials*, *189*, 728–735. https://doi.org/10.1016/j.conbuildmat.2018.09.003

Lee, J., & Fenves, G. L. (1998). Plastic-Damage Model for Cyclic Loading of Concrete Structures. *Journal of Engineering Mechanics*, *124*(8), 892–900.

Lee, L. H., Quek, S. T., & Ang, K. K. (2001). Moment redistribution in continuous profiled steel-concrete composite slabs. *Magazine of Concrete Research*, *53*(5), 301–309. https://doi.org/10.1680/macr.2001.53.5.301

Leskelä, M. V. (2017). *Shear connections in composite flexural members of steel and concrete* (Technical). ECCS.

Li, X., Zheng, X., Ashraf, M., & Li, H. (2019). The longitudinal shear bond behavior of an innovative laminated fiber reinforced composite slab. *Construction and Building Materials*, *215*, 508–522. https://doi.org/10.1016/j.conbuildmat.2019.04.153

Liang, Q. Q. (2015). *Analysis and Design of Steel and Composite Structures* (CRC Press). Boca Raton, Florida: Taylor & Francis Group.

Liang, Q. Q., Uy, B., Bradford, M. A., & Ronagh, H. R. (2004). Ultimate strength of continuous composite beams in combined bending and shear. *Journal of Constructional Steel Research*, *60*(8), 1109–1128. https://doi.org/10.1016/j.jcsr.2003.12.001

Lloyd, R. M., & Wright, H. D. (1990). Shear connection between composite slabs and steel beams. *Journal of Constructional Steel Research*, *15*(4), 255–285. https://doi.org/10.1016/0143-974X(90)90050-Q

Lopes, E., & Simões, R. (2008). Experimental and analytical behaviour of composite slabs. *Steel and Composite Structures*, *8*(5), 361–388. https://doi.org/10.12989/scs.2008.8.5.361

Lubliner, J., Oliver, J., Oller, S., & Onate, E. (1989). a Plastic-Damage Model. *International Journal of Solids and Structures*, *25*(3), 299–326.

https://doi.org/https://doi.org/10.1016/0020-7683(89)90050-4

Marques, B. (2011). *Sistemas de conexão em lajes mistas aço-betão com cofragem colaborante*.

MHURCPRC. (2015). GB 50010−2010. Code for Design of Concrete Structures. Ministry of Housing and Urban-Rural Construction of the People's Republic of China.

Molkens, T., Dobric, J., & Rossi, B. (2019). Influence of the concrete shear capacity on the failure behaviour of composite decks. In D. Lam, X. Dai, T. Sheehan, J. Yang, & K. Zhou (Eds.), *9th International Conference on Steel and Aluminium Structures (ICSAS19)* (pp. 931–942). Bradford, UK.

Nagy, Z. V, & Szatmári, I. (1998). Composite Slab Design. In *2nd Int. PhD Symposium in Civil Engineering 1998* (pp. 1–8). Budapest, Hungary.

Nayal, R., & Rasheed, H. A. (2006). Tension Stiffening Model for Concrete Beams Reinforced with Steel and FRP Bars. *Journal of Materials in Civil Engineering*, *18*(6), 831. https://doi.org/10.1061/(ASCE)0899-1561(2006)18:6(831)

Nethercot, D. A. (2004). *Composite Construction*. Londres: Spon Press.

Nguyen, N. H., & Whittaker, A. S. (2017). Numerical modelling of steel-plate concrete composite shear walls. *Engineering Structures*, *150*, 1–11. https://doi.org/10.1016/j.engstruct.2017.06.030

Patrick, M. (1993). Testing and design of Bondek II composite slabs for vertical shear. *Steel Construction Journal*, *27*(2), 2–26.

Patrick, M., & Bridge, R. (1993). The slip block test for composite slab shear connection performance. University of Sydney Centre for Advanced Structural Engineerin.

Patrick, M., & Bridge, R. (1994). Partial shear connection design of composite slabs. *Engineering Structures*, *16*(5), 348–362.

Pereira, M., & Simões, R. (2019). Contribution of steel sheeting to the vertical shear capacity of composite slabs. *Journal of Constructional Steel Research*, *161*, 275–284. https://doi.org/10.1016/j.jcsr.2019.07.005

Pereira, M., Simões, R., & Duarte, J. (2017). Analysis of the vertical shear design model for steel-concrete composite slabs. *Ce/Papers - the Online Collection for Conference Papaers in Civil Engineering*, *1*(4), 405–414. https://doi.org/10.1002/cepa.540

Peterson, P. E. (1981). *Tech. Rep. TVBM-1106. Crack growth and development of fracture zones in plain concrete and similar materials.*

Popovics, S. (1973). A numerical approach to the complete stress-strain curve of concrete. *Cement and Concrete Research*, *3*(5), 583–599. https://doi.org/10.1016/0008-8846(73)90096-3

Porter, M L, & Ekberg, J. C. E. (1976). Design recommendatios for steel deck floor slabs. *ASCE Journal Structural Division*, *102*(11), 2121–2136.

Porter, Max L, & Ekberg, C. (1978). Compendium of ISU research conducted on cold-

formed steel-deck-reinforced slab systems. Iowa State University, Ames, Iowa: Engineering Research Institute.

Porter, Max L, & Greimann, L. F. (1984). Shear-bond Strength of Studded Steel Deck Slabs. In *7th International Specialty Conference on Cold-Formed Steel Structures*. St. Louis, Estados Unidos da América.

Qureshi, J., & Lam, D. (2012). Behaviour of headed shear stud in composite beams with profiled metal decking. *Advances in Structural Engineering*, *15*(9), 1547–1558. https://doi.org/10.1260/1369-4332.15.9.1547

Rana, M. M., Uy, B., & Mirza, O. (2015). Experimental and numerical study of end anchorage in composite slabs. *Journal of Constructional Steel Research*, *115*, 362–379. https://doi.org/10.1016/j.jcsr.2015.08.018

Ríos, J. D., Cifuentes, H., Martínez-De La Concha, A., & Medina-Reguera, F. (2017). Numerical modelling of the shear-bond behaviour of composite slabs in four and six-point bending tests. *Engineering Structures*, *133*, 91–104. https://doi.org/10.1016/j.engstruct.2016.12.025

Saenz, L. P. (1964). Discussion of equation for the stress-strain curve of concrete by Desayi and Krishnan. *Journal of American Concrete Institute*, *61*, 1229–1235.

Salonikios, T. N., Sextos, A. G., & Kappos, A. J. (2012). Tests on composite slabs and evaluation of relevant eurocode 4 provisions. *Steel and Composite Structures*, *13*(6), 571–586. https://doi.org/10.12989/scs.2012.13.6.571

Saravanan, M., Marimuthu, V., Prabha, P., Arul Jayachandran, S., & Datta, D. (2012). Experimental investigations on composite slabs to evaluate longitudinal shear strength. *Steel and Composite Structures*, *13*(5), 489–500. https://doi.org/10.12989/scs.2012.13.5.489

Schmeckebier, N., & Kurz, W. (2019). Shear capacity of composite slabs used in building structures. In D. Lam, X. Dai, T. Sheehan, J. Yang, & K. Zhou (Eds.), *9th International Conference on Steel and Aluminium Structures (ICSAS19)* (pp. 894–904). Bradford, UK.

Simões da Silva, L., Rebelo, C., Nethercot, D., Marques, L., Simões, R., & Real, P. M. M. V. (2009). Statistical evaluation of the lateral – torsional buckling resistance of steel I-beams , Part 2 : Variability of steel properties. *Journal of Constructional Steel Research*, *65*(4), 832–849. https://doi.org/10.1016/j.jcsr.2008.07.017

Simões da Silva, L., Tankova, T., Marques, L., & Rebelo, C. (2018). Safety Assessment of EUROCODE 3 Stability Design Rules for the Lateral- torsional Buckling of Prismatic Beams. *Advanced Steel Construction*, *14*(4), 668–693. https://doi.org/10.18057/IJASC.2018.14.9

Simões, R., & Pereira, M. (2019). Vertical shear behaviour of steel-concrete composite slabs. *Ce/Papers - the Online Collection for Conference Papaers in Civil Engineering*, *3*(3–4).

SIMULIA. (2015). ABAQUS CAE. Simulia.

Sinha, B. P., Gerstle, K. H., & Tulin, L. G. (1964). Stress-Strain Relations for Concrete Under Cyclic Loading. *ACI Journal*, *61*(2), 195–212.

Stark, J. W. B., & Brekelmans, J. W. P. M. (1990). Plastic design of continuous composite slabs. *Journal of Constructional Steel Research*, *15*, 23–47. https://doi.org/10.1016/0143-974X(90)90041-E

Sümer, Y., & Aktaş, M. (2015). Defining parameters for concrete damage plasticity model. *Challenge Journal of Structural Mechanics*, *1*(3), 149–155.

Swaminathan, S., Siva, A., Senthil, R., & Prabu, K. (2016). Experimental investigation on shear connectors in steel-concrete composite deck slabs. *Indian Journal of Science and Technology*, *9*(30), 1–8. https://doi.org/10.17485/ijst/2016/v9i30/99216

Szczecina, M., & Winnicki, A. (2015). Calibration of the CDP model parameters in Abaqus. *Advances in Structural Engineering and Mechanics*.

Tao, Y., & Chen, J. F. (2014). Concrete Damage Plasticity Model for Modeling FRP-to-Concrete Bond Behavior. *Journal of Composites for Construction*, *19*(1), 04014026. https://doi.org/10.1061/(asce)cc.1943-5614.0000482

Viest, I. M. (1997). Studies of Composite Construction at Illinois and Lehigh, 1940-1978. In ARCE (Ed.), *Composite Construction in Steel and Concrete III* (pp. 1–14). Irsee.

Wahalathantri, B. L., Thambiratnam, D. P., Chan, T. H. T., & Fawzia, S. (2011). A material model for flexural crack simulation in reinforced concrete elements using ABAQUS. In *First International Conference on Engineering, Designing and Developing the Built Environment for Sustainable Wellbeing* (pp. 260–264).

Xu, X., Liu, Y., & Zuo, Y. (2018). Contribution of perforated steel ribs to load-carrying capacities of steel and concrete composite slabs under negative bending. *Advances in Structural Engineering*, *21*(12), 1879–1894. https://doi.org/10.1177/1369433218758774

Yang, Y., Liu, R., Huo, X., Zhou, X., & Roeder, C. W. (2018). Static Experiment on Mechanical Behavior of Innovative Flat Steel Plate-Concrete Composite Slabs. *International Journal of Steel Structures*, *18*(2), 473–485. https://doi.org/10.1007/s13296-018-0012-3

Annex A

Developed design tool for composite slabs

A.1 Introduction

Typically, steelwork producers of steel sheeting profiles for steel-concrete composite slabs provide design tables to promote their application on the construction industry. Design tables usually provide the (characteristic value of the) maximum load supported by a slab, in function of several established parameters: the length span *L*; the profiled steel sheeting *t*; the height of the slab *h*; the number of spans; materials, among others. To take into account the construction phase, the maximum span length without temporary supports or the minimum number of temporary supports needed is usually given as well. These tables are very useful because provide an easy and fast way to design composite slabs, which promote their application on steel and composite buildings. Fig. A.1 and Fig. A.2 give some examples of design tables of different profiles available in the market: COFRAPLUS 77, H60 and ComFlor 80.

Deflection during construction	L/180	**Deflection of finished floor**	L/300
Concrete covering	25mm	**Concrete class**	NC25/30
End support width	50mm	**Internal support width**	100mm

Number of props during construction | Without prop | 1 prop | 2 props

Single span

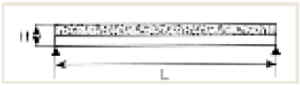

Upper reinforcement		Admissible load (kN/m²) 150x150x6x6										
Rebar in the rib (mm/rib)		0										
Thickness	Slab depth (mm)	Span (m)										
		2,00	2,20	2,40	2,60	2,80	3,00	3,20	3,40	3,60	3,80	4,00
0,75	130	14,5	12,1	10,1	8,6	7,4	6,2	5,6	4,8	4,2	3,6	3,2
	140	14,9	12,4	10,4	8,9	7,6	6,6	5,8	5,0	4,3	3,8	3,3
	150	15,3	12,8	10,7	9,2	7,9	6,8	5,9	5,1	4,5	3,9	3,4
	160	15,7	13,1	11,0	9,4	8,1	7,0	6,1	5,3	4,6	4,0	3,4
	170	16,1	13,4	11,3	9,7	8,3	7,2	6,3	5,4	4,7	4,1	3,5
	180	16,5	13,8	11,6	9,9	8,5	7,4	6,4	5,5	4,8	4,2	3,6
	190	16,9	14,1	11,9	10,2	8,7	7,5	6,5	5,6	4,9	4,2	3,7
	200	17,3	14,5	12,2	10,4	8,9	7,6	6,6	5,7	4,9	4,3	3,7
	210	17,7	14,8	12,5	10,6	9,1	7,8	6,7	5,8	5,0	4,4	3,8
0,88	130	16,6	13,8	11,6	9,9	8,5	7,3	6,2	5,6	4,9	4,3	3,8
	140	17,0	14,1	11,9	10,1	8,7	7,5	6,6	5,7	5,0	4,4	3,9
	150	17,4	14,5	12,2	10,4	8,9	7,7	6,7	5,9	5,2	4,6	4,0
	160	17,8	14,8	12,5	10,6	9,2	7,9	6,9	6,0	5,3	4,7	4,1
	170	18,2	15,2	12,8	10,9	9,4	8,1	7,1	6,2	5,4	4,8	4,2
	180	18,6	15,5	13,1	11,2	9,6	8,3	7,2	6,3	5,5	4,8	4,2
	190	19,0	15,9	13,4	11,4	9,8	8,5	7,4	6,4	5,6	4,9	4,3
	200	19,4	16,2	13,7	11,7	10,0	8,7	7,5	6,5	5,7	4,9	4,3
	210	19,8	16,6	14,0	11,9	10,3	8,8	7,6	6,6	5,8	5,0	4,4
1,00	130	18,6	15,4	12,9	11,0	9,5	8,2	7,1	6,0	5,2	4,9	4,3
	140	19,0	15,7	13,2	11,3	9,7	8,4	7,3	6,2	5,6	5,0	4,4
	150	19,4	16,1	13,5	11,5	9,9	8,6	7,5	6,3	5,8	5,1	4,5
	160	19,8	16,4	13,8	11,8	10,1	8,8	7,6	6,7	5,9	5,2	4,6
	170	20,2	16,8	14,1	12,0	10,4	9,0	7,8	6,8	6,0	5,3	4,7
	180	20,6	17,1	14,4	12,3	10,6	9,2	8,0	7,0	6,1	5,4	4,8
	190	21,0	17,5	14,7	12,6	10,8	9,4	8,1	7,1	6,3	5,5	4,8
	200	21,4	17,8	15,0	12,8	11,0	9,6	8,3	7,3	6,3	5,5	4,9
	210	21,8	18,2	15,3	13,1	11,3	9,7	8,5	7,4	6,4	5,6	4,9

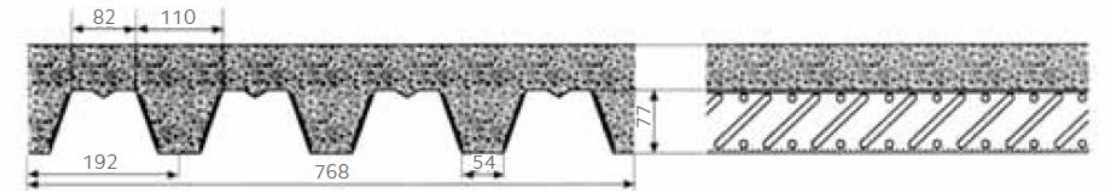

(a) COFRAPLUS 77 (ArcelorMittal)

Fig. A.1 Design tables example

In order to complement the outcome of the present study, a design tool was developed using the software *Excel* from *Microsoft Office* to provide the design tables for composite slabs incorporating the innovative aspects studied and presented on the scope of the

present research work. This tool allows to obtain the design tables for steel-concrete composite slabs with transversal bars intersecting the profiled steel sheeting, using the partial connection method. Other applications, such as those considering different design methods or the fire design according to standard EN 1994-1-2 (CEN, 2005d) were also included in this design tool to make it the most embracing as possible. The design tool is presented over this chapter.

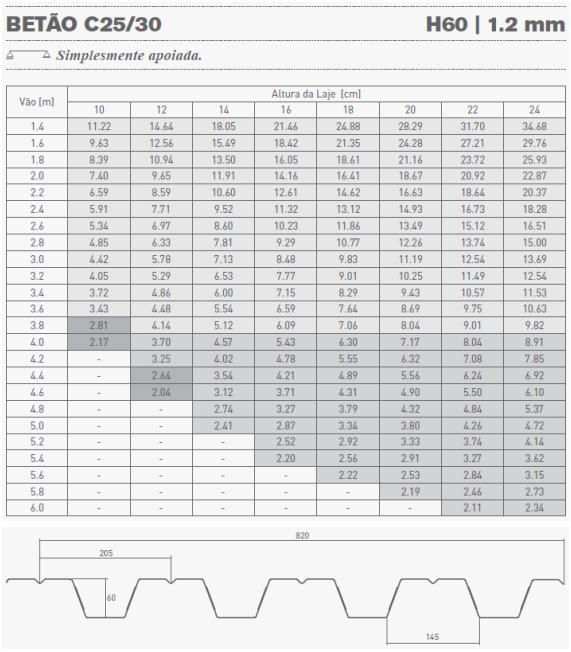

BETÃO C25/30 — **H60 | 1.2 mm**

Simplesmente apoiada.

Vão [m]	Altura da Laje [cm]							
	10	12	14	16	18	20	22	24
1.4	11.22	14.64	18.05	21.46	24.88	28.29	31.70	34.68
1.6	9.63	12.56	15.49	18.42	21.35	24.28	27.21	29.76
1.8	8.39	10.94	13.50	16.05	18.61	21.16	23.72	25.93
2.0	7.40	9.65	11.91	14.16	16.41	18.67	20.92	22.87
2.2	6.59	8.59	10.60	12.61	14.62	16.63	18.64	20.37
2.4	5.91	7.71	9.52	11.32	13.12	14.93	16.73	18.28
2.6	5.34	6.97	8.60	10.23	11.86	13.49	15.12	16.51
2.8	4.85	6.33	7.81	9.29	10.77	12.26	13.74	15.00
3.0	4.42	5.78	7.13	8.48	9.83	11.19	12.54	13.69
3.2	4.05	5.29	6.53	7.77	9.01	10.25	11.49	12.54
3.4	3.72	4.86	6.00	7.15	8.29	9.43	10.57	11.53
3.6	3.43	4.48	5.54	6.59	7.64	8.69	9.75	10.63
3.8	2.81	4.14	5.12	6.09	7.06	8.04	9.01	9.82
4.0	2.17	3.70	4.57	5.43	6.30	7.17	8.04	8.91
4.2	-	3.25	4.02	4.78	5.55	6.32	7.08	7.85
4.4	-	2.64	3.54	4.21	4.89	5.56	6.24	6.92
4.6	-	2.04	3.12	3.71	4.31	4.90	5.50	6.10
4.8	-	-	2.74	3.27	3.79	4.32	4.84	5.37
5.0	-	-	2.41	2.87	3.34	3.80	4.26	4.72
5.2	-	-	-	2.52	2.92	3.33	3.74	4.14
5.4	-	-	-	2.20	2.56	2.91	3.27	3.62
5.6	-	-	-	-	2.22	2.53	2.84	3.15
5.8	-	-	-	-	-	2.19	2.46	2.73
6.0	-	-	-	-	-	-	2.11	2.34

(a) H60 (O Feliz Metalomecânica)

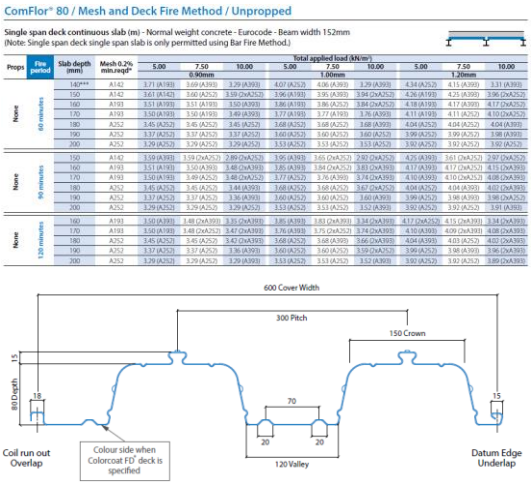

ComFlor® 80 / Mesh and Deck Fire Method / Unpropped

Single span deck continuous slab (m) - Normal weight concrete - Eurocode - Beam width 152mm
(Note: Single span deck single span slab is only permitted using Bar Fire Method.)

Props	Fire period	Slab depth (mm)	Mesh 0.2% min.req'd*	Total applied load (kN/m²) 5.00	7.50	10.00	5.00	7.50	10.00	5.00	7.50	10.00
					0.90mm			1.00mm			1.20mm	
None	60 minutes	140***	A142	3.71 (A193)	3.69 (A393)	3.29 (A393)	4.07 (A252)	4.06 (A393)	3.29 (A393)	4.34 (A252)	4.15 (A393)	3.31 (A393)
		150	A142	3.61 (A142)	3.66 (A252)	3.59 (2xA252)	3.96 (A193)	3.95 (A393)	3.94 (2xA252)	4.26 (A193)	4.25 (A393)	3.96 (2xA252)
		160	A193	3.51 (A193)	3.51 (A193)	3.50 (A393)	3.86 (A193)	3.86 (A252)	3.84 (2xA252)	4.18 (A193)	4.17 (A393)	4.17 (2xA252)
		170	A193	3.50 (A193)	3.50 (A193)	3.49 (A393)	3.77 (A193)	3.77 (A193)	3.76 (A393)	4.11 (A193)	4.11 (A252)	4.10 (2xA252)
		180	A252	3.45 (A252)	3.45 (A252)	3.45 (A252)	3.68 (A252)	3.68 (A252)	3.68 (A393)	4.04 (A252)	4.04 (A252)	4.04 (A393)
		190	A252	3.37 (A252)	3.37 (A252)	3.37 (A252)	3.60 (A252)	3.60 (A252)	3.60 (A252)	3.99 (A252)	3.99 (A252)	3.98 (A393)
		200	A252	3.29 (A252)	3.29 (A252)	3.29 (A252)	3.53 (A252)	3.53 (A252)	3.53 (A252)	3.92 (A252)	3.92 (A252)	3.92 (A252)
None	90 minutes	150	A142	3.59 (A393)	3.59 (2xA252)	2.89 (2xA252)	3.95 (A393)	3.65 (2xA252)	2.92 (2xA252)	4.25 (A393)	3.61 (2xA252)	2.97 (2xA252)
		160	A193	3.51 (A193)	3.50 (A393)	3.48 (2xA393)	3.85 (A393)	3.84 (2xA252)	3.83 (2xA393)	4.17 (A393)	4.17 (2xA252)	4.15 (2xA393)
		170	A193	3.50 (A193)	3.49 (A252)	3.48 (2xA252)	3.77 (A252)	3.76 (A393)	3.74 (2xA393)	4.10 (A393)	4.10 (2xA252)	4.08 (2xA393)
		180	A252	3.45 (A252)	3.45 (A252)	3.44 (A393)	3.68 (A252)	3.68 (A252)	3.67 (2xA252)	4.04 (A252)	4.04 (A393)	4.02 (2xA393)
		190	A252	3.37 (A252)	3.37 (A252)	3.36 (A393)	3.60 (A252)	3.60 (A252)	3.60 (A393)	3.99 (A252)	3.98 (A393)	3.98 (2xA252)
		200	A252	3.29 (A252)	3.29 (A252)	3.29 (A252)	3.53 (A252)	3.53 (A252)	3.52 (A393)	3.92 (A252)	3.92 (A252)	3.91 (A393)
None	120 minutes	160	A193	3.50 (A393)	3.48 (2xA393)	3.35 (2xA393)	3.85 (A393)	3.81 (2xA393)	3.34 (2xA393)	4.17 (2xA252)	4.15 (2xA393)	3.34 (2xA393)
		170	A193	3.50 (A193)	3.48 (2xA252)	3.47 (2xA393)	3.76 (A393)	3.75 (2xA252)	3.74 (2xA393)	4.10 (A393)	4.09 (2xA393)	4.08 (2xA393)
		180	A252	3.45 (A252)	3.45 (A252)	3.42 (2xA393)	3.68 (A252)	3.68 (A393)	3.66 (2xA393)	4.04 (A393)	4.03 (A252)	4.02 (2xA393)
		190	A252	3.37 (A252)	3.37 (A252)	3.36 (A393)	3.60 (A252)	3.60 (A252)	3.59 (2xA252)	3.99 (A252)	3.98 (A393)	3.96 (2xA393)
		200	A252	3.29 (A252)	3.29 (A252)	3.29 (A393)	3.53 (A252)	3.53 (A252)	3.52 (A393)	3.92 (A252)	3.92 (A252)	3.89 (2xA393)

(b) ComFlor 80 (TATA Steel)

Fig. A.2 Design tables examples

A.2 Brief description

The design tool was developed to provide the design tables of steel-concrete composite slabs incorporating the innovative aspects established over this research. Fig. A.3 show the general aspect of the developed design tool. The design tables are developed for simply-supported or continuous (1 span or 2 spans, respectively) steel-concrete composite slabs subjected to a uniformly distributed load. The design tables show, for each pair *L*-*h*, the characteristic value of the maximum load supported by the slab and the colour indicates the mode that governs the design. The design methodology applied in the design tool was described on Chapter 3 of the thesis (Design of steel-concrete composite slabs). The output given by this tool was useful to show the efficiency of the proposed reinforcing system. Some results were presented on Chapter 7 (Assessment of the e) where several comparisons were carried out between conventional steel-concrete composite slabs and slabs with transversal reinforcement.

The design tables are generated based on the several parameters introduced by the user on the general input section (see Fig. A.4): the steel sheet profile; the concrete grade; the steel grade; the profiled steel sheeting thickness; the number of spans; the possibility of account the contribution of the profiled steel sheeting on the vertical shear capacity of the slab; the amount of longitudinal reinforcement; the longitudinal shear design method used – *m-k* or partial connection method (PCM); the maximum deflection values admitted on constructive and definitive phases, for verification of the service condition. When the *m-k* method is used a new section shows up where the user should specify the *m* and *k* values. Currently, the design tool allows to design steel-concrete composite slabs with steel profiles H60 and H120 (or the equivalent profiles LAMI 60+ and LAMI 120+, respectively).

Based on experimental and numerical results obtained on this research it was found that the profiled steel sheeting has an important contribution on the vertical shear resistance of steel-concrete composite slabs. On the general input section, it is possible to take this contribution into account, determining the design value of the vertical shear resistance of the slab as the sum $V_{v,c,Rd} + V_{v,p,Rd}$, as it was proposed at the end of Chapter 6 (Vertical shear capacity of composite slabs).

DESIGN TABLES OF STEEL-CONCRETE COMPOSITE SLABS

Steel profile:	H60
Concrete grade:	C 25/30
Steel grade:	S320 GD+Z
Profiled steel sheeting thickness:	1.2 mm
Number of spans:	1 span
Vertical shear capacity with $V_{v,p,Rd}$?:	Yes
Longitudinal reinforcement:	Yes
Longitudinal shear design model:	PCM
Deflection in the construction phase:	L/ 240
Deflection in the definitive phase:	L/ 300

Partial Connection Method	
Ultimate stress resistance ($\tau_{u,Rd}$)	0.369 MPa
End anchorage device:	No
Transversal reinforcement:	Yes

Transversal reinforcement	
Diameter of the rebars:	8 mm
Spacing between rebars:	200 mm

Longitudinal reinforcement	
Number of rebars per rib:	1 rebar
Diameter of the rebars:	12 mm
Steel grade:	A500 NR
Distance to the bottom flange:	30 mm

Dynamic Table	
Design modes	
ULS: Vertical shear	Sim
ULS: Longitudinal shear	Sim
ULS: Bending	Sim
SLS: Deflection	Sim
Minimum load - $q_{k,min}$ [kN/m²]	
Do not present values under:	2 kN/m²

Characteristic value of the maximum supported load - q_k [kN/m²]

L \ h	100	110	120	130	140	150	160	170	180	190	200	210	220	230	240	250
1.2	119.48	141.69	163.38	165.91	167.94	169.97	172.00	174.04	176.07	178.10	180.13	182.16	184.20	186.23	187.78	188.95
1.4	78.19	103.62	121.95	135.12	143.60	145.30	147.01	148.72	150.43	152.14	153.85	155.56	157.27	158.98	160.28	161.25
1.6	51.81	69.10	82.89	105.67	116.00	126.29	128.27	129.74	131.21	132.68	134.14	135.61	137.08	138.55	139.65	140.47
1.8	35.86	47.94	72.37	85.10	93.73	102.32	110.86	114.97	116.25	117.53	118.81	120.09	121.37	122.65	123.61	124.31
2.0	25.67	34.41	53.17	67.42	77.48	84.80	92.08	99.33	104.29	105.42	106.55	107.68	108.81	109.94	110.78	111.39
2.2	18.85	25.35	39.39	50.03	62.47	71.57	77.88	84.15	90.41	95.51	96.52	97.52	98.53	99.53	100.28	100.81
2.4	14.12	19.07	29.82	37.96	47.48	58.47	66.84	72.35	77.84	83.31	88.15	89.06	89.96	90.86	91.53	92.00
2.6	10.73	14.57	22.98	29.33	36.76	45.35	55.16	62.52	67.84	72.69	77.52	81.90	82.71	83.53	84.12	84.54
2.8	8.24	11.27	17.95	22.98	28.88	35.71	43.51	52.35	58.37	63.27	68.17	72.72	76.50	77.24	77.78	78.15
3.0	6.38	8.79	14.17	18.22	22.97	28.47	34.77	41.91	49.32	54.65	58.89	63.13	67.37	71.61	72.28	72.61
3.2	4.95	6.89	11.28	14.57	18.44	22.93	28.08	33.91	40.47	47.60	51.30	55.00	58.70	62.40	66.10	67.76
3.4	3.83	5.41	9.03	11.73	14.92	18.62	22.87	27.69	33.12	39.18	45.00	48.26	51.51	54.76	58.01	61.26
3.6	2.95	4.24	7.25	9.49	12.13	15.21	18.75	22.78	27.31	32.37	38.00	42.61	45.48	48.36	51.23	54.11
3.8	2.25	3.31	5.83	7.69	9.91	12.49	15.46	18.84	22.66	26.83	31.67	36.31	40.39	42.34	45.50	48.05
4.0	-	2.55	4.68	6.24	8.10	10.28	12.79	15.66	18.89	22.52	26.55	31.00	35.89	38.31	40.60	42.89
4.2	-	-	3.74	5.05	6.62	8.47	10.61	13.05	15.81	18.91	22.35	26.17	30.36	34.33	36.39	38.44
4.4	-	-	2.96	4.07	5.40	6.98	8.80	10.89	13.26	15.92	18.89	22.17	25.79	29.74	32.73	34.58
4.6	-	-	2.31	3.25	4.38	5.73	7.30	9.10	11.14	13.44	16.00	18.84	21.97	25.41	29.15	31.22
4.8	-	-	-	2.56	3.53	4.68	6.03	7.59	9.35	11.35	13.57	16.04	18.77	21.76	25.03	28.27
5.0	-	-	-	-	2.81	3.80	4.96	6.31	7.84	9.58	11.52	13.68	16.06	18.68	21.54	24.65
5.2	-	-	-	-	2.19	3.04	4.05	5.22	6.56	8.07	9.77	11.66	13.75	16.05	18.56	21.30
5.4	-	-	-	-	-	2.40	3.27	4.29	5.45	6.78	8.27	9.93	11.77	13.80	16.01	18.43
5.6	-	-	-	-	-	-	2.60	3.48	4.50	5.66	6.97	8.44	10.06	11.85	13.82	15.96
5.8	-	-	-	-	-	-	2.01	2.78	3.68	4.70	5.85	7.15	8.58	10.17	11.91	13.81
6.0	-	-	-	-	-	-	-	2.18	2.96	3.86	4.88	6.02	7.23	8.70	10.25	11.95

Maximum span length without temporary supports - $L_{u,max}$ (m)

h	100	110	120	130	140	150	160	170	180	190	200	210	220	230	240	250
L_max	2.8	2.8	2.6	2.6	2.6	2.4	2.4	2.4	2.4	2.2	2.2	2.2	2.2	2.2	2.2	2.0

Fig. A.3 Developed design tool for steel-concrete composite slabs

Steel profile	**H60**	
Concrete grade	C 25/30	
Steel grade	S320 GD+Z	
Profiled steel sheeting thickness	1.2	mm
Number of spans	2 spans	
Vertical shear capacity with $V_{p,Rd}$?	Yes	
Longitudinal reinforcement:	Yes	
Longitudinal shear design model:	PCM	
Deflection in the construction phase:	L / 240	
Deflection in the definitive phase:	L / 300	

Fig. A.4 General input section

When the partial connection method (PCM) is used, a new input section shows up (see Fig. A.5(a)) in order to: (i) specify the value of $\tau_{u,Rd}$; (ii) define any end anchorage device or (iii) account for transversal reinforcement if any. Two different end anchorage devices were considered in the design tool, which can be considered on the second field of this section: (i) headed studs welded to the supporting beams through the profiled steel sheeting or (ii) transversal bars intersecting the webs of the profiled steel sheeting in the supporting sections, as proposed by Fonseca *et al.* (2015). When transversal bars are intersecting the profiled steel sheeting distributed over the span the value of $\tau_{u,Rd}$ is automatically replaced by $\tau_{u,Rd}$ and a new input section shows up (see Fig. A.5(b)). The transversal reinforcement input section allows to define the diameter of transversal bars (d) and the spacing between them (l_b).

Partial Connection Method	
Ultimate stress resistance ($\tau_{u,Rd}$)	0.369 MPa
End anchorage device:	No
Transversal reinforcement:	Yes

(a) PCM input section

Transversal reinforcement	
Diameter of the rebars:	8 mm
Spacing between rebars:	200 mm

(b) Transversal reinforcement input section

Fig. A.5 Longitudinal shear input sections

The design tool also allows to design composite slabs with longitudinal reinforcement on the ribs. When the longitudinal reinforcement is considered, a new input section shows up to define this reinforcement (see Fig. A.6(a)). To account for the contribution of the longitudinal reinforcement the user must specify: the number of bars on each rib; the diameter of those bars; the steel grade and; the distance from the centroidal to the bottom flange of the profiled steel sheeting.

When the number of spans is specified as “2 spans” in the general input section (Fig. A.4), the design is developed for continuous slabs and longitudinal reinforcement to resist the tensile forces in the top part of the slab in the support region should be provided. For the design of continuous composite slabs a new input section shows up (see Fig. A.6(b)). On this section is also possible to define the moment redistribution coefficient.

Longitudinal reinforcement	
Number of rebars per rib:	1 rebar
Diameter of the rebars:	12 mm
Steel grade	A500 NR
Distance to the bottom flange:	30 mm

(a) Longitudinal reinforcement input section

Hogging bending reinforcement	
Diameter of the rebars:	10 mm
Spacing between rebars:	150 mm
Steel grade	A500 NR
Concrete coating layer:	25 mm
Moment redistribution	30 %

(b) Longitudinal reinforcement for hogging bending moment input section

Fig. A.6 Longitudinal reinforcement input sections

Fig. A.7 shows an additional section developed to: (i) show the colour meanings of these design tables – each colour refers the mode that governs the design of the slab; (ii) neglect or consider a certain type of failure/design and; (iii) define the minimum value of the load to be considered in design tables – useful, for example, to neglect all cases with solutions out of the range of application.

Dynamic Table	
Design modes	
ULS: Vertical shear	Sim
ULS: Longitudinal shear	Sim
ULS: Bending	Sim
SLS: Deflection	Sim
Minimum load - $q_{k,min}$ [kN/m^2]	
Do not present values under:	2 kN/m^2

Fig. A.7 Condition values

Taking into account all conditions established on these input sections the design tool automatically generates the corresponding design table. One example is shown on Fig. A.8.

Characteristic value of the maximum supported load - q_k [kN/m^2]																
L \ h	100	110	120	130	140	150	160	170	180	190	200	210	220	230	240	250
1.2	119.48	141.69	163.38	165.91	167.94	169.97	172.00	174.04	176.07	178.10	180.13	182.16	184.20	186.23	187.78	188.95
1.4	78.19	103.62	121.95	135.12	143.60	145.30	147.01	148.72	150.43	152.14	153.85	155.56	157.27	158.98	160.28	161.25
1.6	51.81	69.10	92.89	105.67	116.00	126.29	128.27	129.74	131.21	132.68	134.14	135.61	137.08	138.55	139.65	140.47
1.8	35.86	47.94	72.97	85.10	93.73	102.32	110.86	114.97	116.25	117.53	118.81	120.09	121.37	122.65	123.61	124.31
2.0	25.67	34.41	53.17	67.42	77.48	84.80	92.08	99.33	104.29	105.42	106.55	107.68	108.81	109.94	110.78	111.39
2.2	18.85	25.35	39.39	50.03	62.47	71.57	77.88	84.15	90.41	95.51	96.52	97.52	98.53	99.53	100.28	100.81
2.4	14.12	19.07	29.82	37.96	47.48	58.47	66.84	72.35	77.84	83.31	88.15	89.06	89.96	90.86	91.53	92.00
2.6	10.73	14.57	22.98	29.33	36.76	45.35	55.16	62.52	67.84	72.69	77.52	81.90	82.71	83.53	84.12	84.54
2.8	8.24	11.27	17.95	22.98	28.88	35.71	43.51	52.35	58.37	63.27	68.17	72.72	76.50	77.24	77.78	78.15
3.0	6.38	8.79	14.17	18.22	22.97	28.47	34.77	41.91	49.92	54.65	58.89	63.13	67.37	71.61	72.28	72.61
3.2	4.95	6.89	11.28	14.57	18.44	22.93	28.08	33.91	40.47	47.60	51.30	55.00	58.70	62.40	66.10	67.76
3.4	3.83	5.41	9.03	11.73	14.92	18.62	22.87	27.69	33.12	39.18	45.00	48.26	51.51	54.76	58.01	61.26
3.6	2.95	4.24	7.25	9.49	12.13	15.21	18.75	22.78	27.31	32.37	38.00	42.61	45.48	48.36	51.23	54.11
3.8	2.25	3.31	5.83	7.69	9.91	12.49	15.46	18.84	22.66	26.93	31.67	36.91	40.38	42.94	45.50	48.05
4.0	-	2.55	4.68	6.24	8.10	10.28	12.79	15.66	18.89	22.52	26.55	31.00	35.89	38.31	40.60	42.89
4.2	-	-	3.74	5.05	6.62	8.47	10.61	13.05	15.81	18.91	22.35	26.17	30.36	34.33	36.39	38.44
4.4	-	-	2.96	4.07	5.40	6.98	8.80	10.89	13.26	15.92	18.89	22.17	25.79	29.74	32.73	34.58
4.6	-	-	2.31	3.25	4.38	5.73	7.30	9.10	11.14	13.44	16.00	18.84	21.97	25.41	29.15	31.22
4.8	-	-	-	2.56	3.53	4.68	6.03	7.59	9.35	11.35	13.57	16.04	18.77	21.76	25.03	28.27
5.0	-	-	-	-	2.81	3.80	4.96	6.31	7.84	9.58	11.52	13.68	16.06	18.68	21.54	24.65
5.2	-	-	-	-	2.19	3.04	4.05	5.22	6.56	8.07	9.77	11.66	13.75	16.05	18.56	21.30
5.4	-	-	-	-	-	2.40	3.27	4.29	5.45	6.78	8.27	9.93	11.77	13.80	16.01	18.43
5.6	-	-	-	-	-	-	2.60	3.48	4.50	5.66	6.97	8.44	10.06	11.85	13.82	15.96
5.8	-	-	-	-	-	-	2.01	2.78	3.68	4.70	5.85	7.15	8.58	10.17	11.91	13.81
6.0	-	-	-	-	-	-	-	2.18	2.96	3.86	4.88	6.02	7.29	8.70	10.25	11.95

Fig. A.8 Design tables of steel-concrete composite slabs

The maximum span without need of temporary supports (unpropped) $L_{u,\max}$ is also given for each value of h. This information is useful to define the number of props needed during the construction phase. An example of this section is presented on Fig. A.9.

Maximum span length without temporary supports - $L_{u,max}$ (m)																
h	100	110	120	130	140	150	160	170	180	190	200	210	220	230	240	250
$L_{u,max}$	2.8	2.8	2.6	2.6	2.6	2.4	2.4	2.4	2.4	2.2	2.2	2.2	2.2	2.2	2.2	2.0

Fig. A.9 Maximum span length without props

A.3 Fire design

Although the fire design of steel-concrete composite slabs is out of the scope established for this study, in order to complement the output information provided by the design tool, the fire design of steel-concrete composite slabs was implemented on it.

Standard EN 1994-1-2 (CEN, 2005d) provides a simplified method to design steel-concrete composite slabs in a simple and quick way (Hamerlinck and Twilt, 1995). Experimental results showed that due to the heat absorbed by the concrete during a fire the resistance of composite slab without any fire protection is at least 30 minutes. That is why clause 4.3.2(5) of standard EN 1994-1-2 (CEN, 2005d) prescribes that, for slabs successfully designed according to standard EN 1994-1-1 (CEN, 2004b), the R30 grade can be assumed to be verified. Taking this into account, the fire design of steel-concrete composite slabs in accordance with standard EN 1994-1-2 (CEN, 2005d) is also provided by the developed design tool.

Fig. A.10 shows the general aspect of the fire resistance design table developed integrated on the design tool. Taking into account the conditions established on the development of the design tool according to the specifications of standard EN 1994-1-1 (CEN, 2004b) (see previous section) a new design table is developed. Under the same conditions the tool allows to create a table indicating the fire resistance in minutes. For example, R90 means that the slab is stable under fire conditions until 90 minutes. Fig. A.11 shows the same example considered and presented in Fig. A.10 but with addition of longitudinal reinforcement. The comparison between both figures allow to show the significant influence of the longitudinal reinforcement in the fire resistance of steel-concrete composite slabs. For example, as it can be observed, the fire resistance of a simply-supported composite slab, with a span L of 3.40 m and a height h of 150 mm, increases from R30 to R90 just by adding a 12 mm diameter reinforcing bar per concrete rib, placed 30 mm above the bottom flanges of the profiled steel sheeting.

Concerning the criterions E (integrity) and I (thermal insulation) for fire design, the clause 4.3.2(6) of standard EN 1994-1-2 (CEN, 2005d) prescribes that the integrity criterion E is assumed to be satisfied on steel-concrete composite slabs and it is assumed that the conditions for criterion I are fulfilled. Taking this in consideration, design tables are developed just concerning the criterion R (Load bearing).

Category of use:	B
Steel profile	H60
Concrete grade	C 25/30
Steel grade	S320 GD+Z
Profiled steel sheeting thickness	1.2 mm
Number of spans	1 span
Vertical shear capacity with $V_{a,Rd}$?	No
Longitudinal reinforcement	No
Longitudinal shear design model:	m-k
Deflection in the constructio phase:	L / 240
Deflection in the definitive phase:	L / 300
m-k method	
m (MPa) 98.32	k (MPa) 0.08

	Fire resistance															
L \ h	100	110	120	130	140	150	160	170	180	190	200	210	220	230	240	250
1.2	R120	R120	R120	R120	R120	R120	R180	R180	R180	R180	R180	R180	R180	R180	R180	R180
1.4	R120	R120	R120	R120	R120	R120	R120	R120	R120	R120	R120	R120	R120	R120	R120	R120
1.6	R120	R120	R120	R120	R120	R120	R120	R120	R120	R120	R120	R120	R120	R120	R120	R120
1.8	R90	R90	R90	R120	R120	R120	R120	R120	R120	R120	R120	R120	R120	R120	R120	R120
2.0	R60	R90	R90	R90	R90	R90	R90	R120	R120	R120	R120	R120	R120	R120	R120	R120
2.2	R60	R90	R90	R90	R90	R90	R90	R90	R90	R90	R90	R90	R90	R90	R90	R90
2.4	R60	R60	R60	R60	R60	R90	R90	R90	R90	R90	R90	R90	R90	R90	R90	R90
2.6	R60	R60	R60	R60	R60	R60	R60	R60	R60	R60	R60	R60	R90	R90	R90	R90
2.8	R30	R60	R60	R60	R60	R60	R60	R60	R60	R60	R60	R60	R60	R60	R60	R60
3.0	R30	R30	R60	R60	R60	R60	R60	R60	R60	R60	R60	R60	R60	R60	R60	R60
3.2	R30	R30	R30	R30	R30	R60	R60	R60	R60	R60	R60	R60	R60	R60	R60	R60
3.4	R30	R30	R30	R30	R30	R30	R30	R60	R60	R60	R60	R60	R60	R60	R60	R60
3.6	R30	R30	R30	R30	R30	R30	R30	R30	R30	R30	R30	R60	R60	R60	R60	R60
3.8	-	R30	R30	R30	R30	R30	R30	R30	R30	R30	R30	R30	R30	R30	R30	R30
4.0	-	R30	R30	R30	R30	R30	R30	R30	R30	R30	R30	R30	R30	R30	R30	R30
4.2	-	-	R30	R30	R30	R30	R30	R30	R30	R30	R30	R30	R30	R30	R30	R30
4.4	-	-	R30	R30	R30	R30	R30	R30	R30	R30	R30	R30	R30	R30	R30	R30
4.6	-	-	-	R30	R30	R30	R30	R30	R30	R30	R30	R30	R30	R30	R30	R30
4.8	-	-	-	-	R30	R30	R30	R30	R30	R30	R30	R30	R30	R30	R30	R30
5.0	-	-	-	-	-	R30	R30	R30	R30	R30	R30	R30	R30	R30	R30	R30
5.2	-	-	-	-	-	-	-	R30	R30	R30	R30	R30	R30	R30	R30	R30
5.4	-	-	-	-	-	-	-	-	-	-	R30	R30	R30	R30	R30	R30
5.6	-	-	-	-	-	-	-	-	-	-	-	-	R30	R30	R30	R30
5.8	-	-	-	-	-	-	-	-	-	-	-	-	-	-	-	-
6.0	-	-	-	-	-	-	-	-	-	-	-	-	-	-	-	-

Fig. A.10 Fire design of steel-concrete composite slabs (without longitudinal reinforcement)

Category of use:	B
Steel profile	H60
Concrete grade	C 25/30
Steel grade	S320 GD+Z
Profiled steel sheeting thickness	1.2 mm
Number of spans	1 span
Vertical shear capacity with $V_{a,Rd}$?	No
Longitudinal reinforcement	Yes
Longitudinal shear design model:	m-k
Deflection in the constructio phase:	L / 240
Deflection in the definitive phase:	L / 300
m-k method	
m (MPa) 98.32	k (MPa) 0.08

Longitudinal reiforcement	
Number of bars per rib	1 bar(s)
Diameter	12 mm
Steel grade	A500 NR
Height of the reinforcement geometric center	30 mm

	Fire resistance															
L \ h	100	110	120	130	140	150	160	170	180	190	200	210	220	230	240	250
1.2	R180	R180	R180	R180	R180	R180	R180	R180	R180	R180	R180	R180	R180	R180	R180	R180
1.4	R180	R180	R180	R180	R180	R180	R180	R180	R180	R180	R180	R180	R180	R180	R180	R180
1.6	R180	R180	R180	R180	R180	R180	R180	R180	R180	R180	R180	R180	R180	R180	R180	R180
1.8	R120	R120	R120	R180	R180	R180	R180	R180	R180	R180	R180	R180	R180	R180	R180	R180
2.0	R120	R120	R120	R120	R120	R120	R120	R120	R180	R180	R180	R180	R180	R180	R180	R180
2.2	R120	R120	R120	R120	R120	R120	R120	R120	R120	R120	R120	R120	R120	R120	R120	R120
2.4	R120	R120	R120	R120	R120	R120	R120	R120	R120	R120	R120	R120	R120	R120	R120	R120
2.6	R90	R120	R120	R120	R120	R120	R120	R120	R120	R120	R120	R120	R120	R120	R120	R120
2.8	R90	R90	R90	R120	R120	R120	R120	R120	R120	R120	R120	R120	R120	R120	R120	R120
3.0	R60	R90	R90	R90	R90	R90	R120	R120	R120	R120	R120	R120	R120	R120	R120	R120
3.2	R60	R60	R90	R90	R90	R90	R90	R90	R90	R90	R90	R120	R120	R120	R120	R120
3.4	R60	R60	R60	R60	R90	R90	R90	R90	R90	R90	R90	R90	R90	R90	R90	R90
3.6	R60	R60	R60	R60	R60	R60	R60	R90	R90	R90	R90	R90	R90	R90	R90	R90
3.8	R60	R60	R60	R60	R60	R60	R60	R60	R60	R60	R60	R60	R90	R90	R90	R90
4.0	-	R60	R60	R60	R60	R60	R60	R60	R60	R60	R60	R60	R60	R60	R60	R60
4.2	-	-	R60	R60	R60	R60	R60	R60	R60	R60	R60	R60	R60	R60	R60	R60
4.4	-	-	R60	R60	R60	R60	R60	R60	R60	R60	R60	R60	R60	R60	R60	R60
4.6	-	-	R60	R60	R60	R60	R60	R60	R60	R60	R60	R60	R60	R60	R60	R60
4.8	-	-	-	R60	R60	R60	R60	R60	R60	R60	R60	R60	R60	R60	R60	R60
5.0	-	-	-	-	R60	R60	R60	R60	R60	R60	R60	R60	R60	R60	R60	R60
5.2	-	-	-	-	R60	R60	R60	R60	R60	R60	R60	R60	R60	R60	R60	R60
5.4	-	-	-	-	-	-	R60	R60	R60	R60	R60	R60	R60	R60	R60	R60
5.6	-	-	-	-	-	-	-	R60	R60	R60	R60	R60	R60	R60	R60	R60
5.8	-	-	-	-	-	-	-	-	-	-	R60	R60	R60	R60	R60	R60
6.0	-	-	-	-	-	-	-	-	-	-	-	-	R60	R60	R60	R60

Fig. A.11 Fire design of steel-concrete composite slabs (with longitudinal reinforcement 1Ø12/rib)